Bolin Centre for Climate Research

CRUISE REPORT SWERUS-C3 LEG 2

Meddelanden från Stockholms universitets
Bolin Centre for Climate Research No 2

Stockholm University

SMHI

KTH

Printed by SU-AB, Stockholm 2016
Cover Photo courtesy of Björn Eriksson
Oden's bridge, SWERUS expedition
ISBN 978-91-87355-21-9

MEDDELANDEN från STOCKHOLMS UNIVERSITETS
BOLIN CENTRE FOR CLIMATE RESEARCH No 2

The Swedish-Russian-US Arctic Ocean Investigation of Climate-Cryosphere-Carbon Interactions

The SWERUS-C3 2014 Expedition

CRUISE REPORT – LEG 2 (of 2)
The SWERUS Scientific Party

Science and Ship Crew (Leg 2). Foto by Björn Eriksson

Table of Contents

Acknowledgements

Leg 2 scientific party enjoyed superb support from *IB Oden's* crew led by Captain Erik Andersson. Technical support during the expedition was also provided by the Swedish Polar Research Secretariat led by expedition coordinator Magnus Augner. The SWERUS-C3 expedition ship operation was financed by a grant from Knut and Alice Wallenberg Foundation and by the base funding of Swedish Polar Research Secretariat. Financial support for expedition participation has also been provided to individual research groups through countries research councils including The Swedish Research Council (VR), the U.S. National Science Foundation. Stockholm University scientists received financial support from the Bolin Centre for Climate Research.

Participants

Scientific party

Last name	First name	Affiliation	Nationality	E-mail address
Ananyev	Roman	P.P.Shirshov Institute of Oceanology, RAS	Russian Federation	corer@mail.ru
Andersson	Leif	Dept of Chemistry and Molecular Biology, University of Gothenburg,	Sweden	leifand@chem.gu.se
Augner	Magnus	Swedish Polar Research Secretariat	Sweden	magnus.augner@polar.se
Backman	Jan	Dept of Geological Sciences, Stockholm University	Sweden	backman@geo.su.se
Barrientos	Natalia	Dept of Geological Sciences, Stockholm University	Spain	naba2756@student.su.se
Björk	Göran	Dept of Earth Sciences, University of Gothenburg	Sweden	gobj@gvc.gu.se
Brooks	Barbara	National Centre for Atmospheric Science/ Atmospheric Measurement Facility	UK	barbara.brooks@ncas.ac.uk
Bull	Josef	Swedish Polar Research Secretariat	Sweden	info@josefbull.com
Chernykh	Denis	V.I.Il`ichev Pacific Oceanological Institute, RAS	Russian Federation	salomatin@poi.dvo.ru
Cronin	Tomas	US Geological Survey	USA	tcronin@usgs.gov
Drott	Christer	Dept of Surgery, Borås hospital/Swedish Polar Research Secretariat	Sweden	christer.drott@vgregion.se
Edsgren	Caroline	Dept of Earth Sciences, University of Gothenburg	Sweden	carolineedsgren@hotmail.com
Ericsson	Ylva	Dept of Geological Sciences, Stockholm University	Sweden	ylva.ericson82@gmail.com
Eriksson	Björn	Dept of Geological Sciences, Stockholm University	Sweden	bjorn.eriksson@geo.su.se
Flodén	Thomas	Dept of Geological Sciences, Stockholm University	Sweden	tom@geo.su.se
Gemery	Laura	U.S. Geological Survey	USA	lgemery@usgs.gov
Gukov	Aleksandr	Ust-Lensky State Nature Reserve	Russian Federation	sgukov@mail.ru
Gutekunst	Sören	Faculty of Engineering, Kiel University	Germany	sgu@tf.uni-kiel.de
Holby	Ola	Environmental and Energy Systems, Karlstad University	Sweden	Ola.Holby@KaU.se
Jakobsson	Martin	Dept of Geological Sciences, Stockholm University	Sweden	martin.jakobsson@geo.su.se

Jerram	Kevin	Center for Coastal and Ocean Mapping, University of New Hampshire	USA	kjerram@ccom.unh.edu
Johansson	Carina	Dept of Geological Sciences, Stockholm University	Sweden	carina.johansson@geo.su.se
Jutterström	Sara	IVL, Swedish Environmental Institute	Sweden	sara.jutterstrom@ivl.se
Karasti	Markus	Dept of Geological Sciences, Stockholm University	Sweden	m.karasti@gmail.com
Khortov	Alexey	Institute of Oceanology, RAN	Russian Federation	akhortov@mail.ru
Koshurnikov	Andrey	V.I.Il`ichev Pacific Oceanological Institute, RAS	Russian Federation	koshurnikov@msu-geophysics.ru
Kosmach	Denis	V.I.Il`ichev Pacific Oceanological Institute, RAS	Russian Federation	den-kosmach@mail.ru
Lif	Arne	Dept of Geological Sciences, Stockholm University	Sweden	alif@geo.su.se
Lindberg	Amund	Swedish Polar Research Secretariat	Sweden	amund.lindberg@telia.com
Mayer	Lawrence	Center for Coastal and Ocean Mapping, University of New Hampshire	USA	larry@ccom.unh.edu
Miller	Clint	Dept of Earth Science, Rice University	USA	cmm10@rice.edu
Mohammad	Rezwan	Department of Geological Sciences, Stockholm University	Sweden	rezze@geo.su.se
Molin	Mikael	Swedish Polar Research Secretariat	Sweden	mikael.molin@umf.umu.se
Muschitiello	Francesco	Department of Geological Sciences, Stockholm University	Italy	francesco.muschitiello@geo.su.se
Nilsson	Johan	Department of Meteorology, Stockholm University	Sweden	nilsson@misu.su.se
O'Reagan	Matthew	Stockholm University	Canada	matt.oregan@geo.su.se
Parsson	Ola	CIRES , University of Colorado	USA/ Sweden	ola.persson@colorado.edu
Preto Ferreira da Costa	Pedro	Department of Geological Sciences, Stockholm University	Portugal	pedropreto@gmail.com
Prytherch	John	University of Leeds	UK	earjpr@see.leeds.ac.uk
Salyuk	Anatoly	V.I.Il`ichev Pacific Oceanological Institute, RAS	Russian Federation	san@poi.dvo.ru
Sotiropoulou	Georgia	Department of Meteorology, Stockholm University	Greece	georgia@misu.su.se
Stranne	Christian	Departemnet of Geology, Stockholm University	Sweden	christian.stranne@geo.su.se
Stöven	Tim	GEOMAR, Helmholtz Centre for Ocean Research	Germany	tstoeven@geomar.de
Ulfsbo	Adam	Department of Chemistry and Molecular Biology, University of Gothenburg	Sweden	ulfsbo@chem.gu.se
Wolfe	Daniel	Cooperative Institute for Research in Environmental Science, University of Colorado	USA	daniel.wolfe@noaa.gov
Zemlyak	Frank	(Retired)	Canada	tidesreach@ns.sympatico.ca

Crew

Last name	First name	Position	Nationality
Andersson	Erik	Master	Swedish
Öström	Ivan	Chief Officer	Swedish
Johansson	Patrik	2:nd Officer	Swedish
Nordström	Kristian	2:nd Officer	Swedish

Grundberg	Lars	2:nd Officer	Swedish
Hansson	Mats	Bosun	Swedish
Sjöbom	Einar	Night Bosun	Swedish
Nilsson	Jan	AB	Swedish
Nilsson	Kenneth	AB	Swedish
Björklund	Ralph	AB	Swedish
Brorsson	Jonas	Chief Engineer	Swedish
Q Hall	Alexander	1:st Engineer	Swedish
Persson	Johan	2:nd Engineer	Swedish
Leth	Aron	2:nd Engineer	Swedish
Wie	Robin	Oiler	Swedish
Groop	Christoffer	Oiler	Swedish
Pettersson	Lennart	Oiler	Swedish
Andersson	Lars	Chief Cook	Swedish
Fredin	Maria	Cook	Swedish
Hålldin	Ann-Katrin	Messman	Swedish
Pettersson	Kristel	Messman	Swedish
Ax	Jan	Electric Engineer	Swedish
Karlsson	Bengt	Fitter	Swedish
Buckley	Christopher	IT/Logistic	British

Context, scientific objectives and summary

Introduction and context

The Swedish-Russian-US Investigation of Climate, Cryosphere and Carbon interaction (SWERUS-C3) program was initiated as a Knut and Alice Wallenberg funded research project. The project was developed into a multi-disciplinary international research program focused on investigating the historical functioning of the Climate-Cryosphere-Carbon (C3) system of the East Siberian Arctic Ocean (ESAO) (Fig. 1). A two-leg expedition with the Swedish research icebreaker *Oden* constitutes the central part of SWERUS-C3.

Leg 2 departed from Barrow, Alaska, August 21 after rotation of both science and ship crew. Leg 1 had started July 5 from Tromsö Norway and worked along the Siberian continental shelf towards the point of Leg1/2 rotation in Barrow. Leg 2 complements Leg 1 by bringing the expedition further out from the Siberian continental shelf and slope into the deep central Arctic Ocean. While the main part of Leg 2 was carried out in international waters, 10 days of the 45-day long leg involved research within the Russian Exclusive Economic Zone (EEZ). This required a permission for scientific investigations. An application was submitted and the SWERUS-C3 expedition was granted permit to carry out research within the requested study polygons by the Russian Ministry of Education and Science (permit nr 51). This permit was issued, per our application/Zayavka, to the Pacific Oceanological Institute (POI, Febras, Vladivostok) as the lead organization of the Russian-international collaboration. Consequently, for the work performed within the Russian EEZ, the SWERUS-C3 expedition is a Russian-led international expedition, with chief scientist Andrey Koshurnikov in charge of execution and fulfillment of Leg 2 and Igor Semiletov of Leg 1.

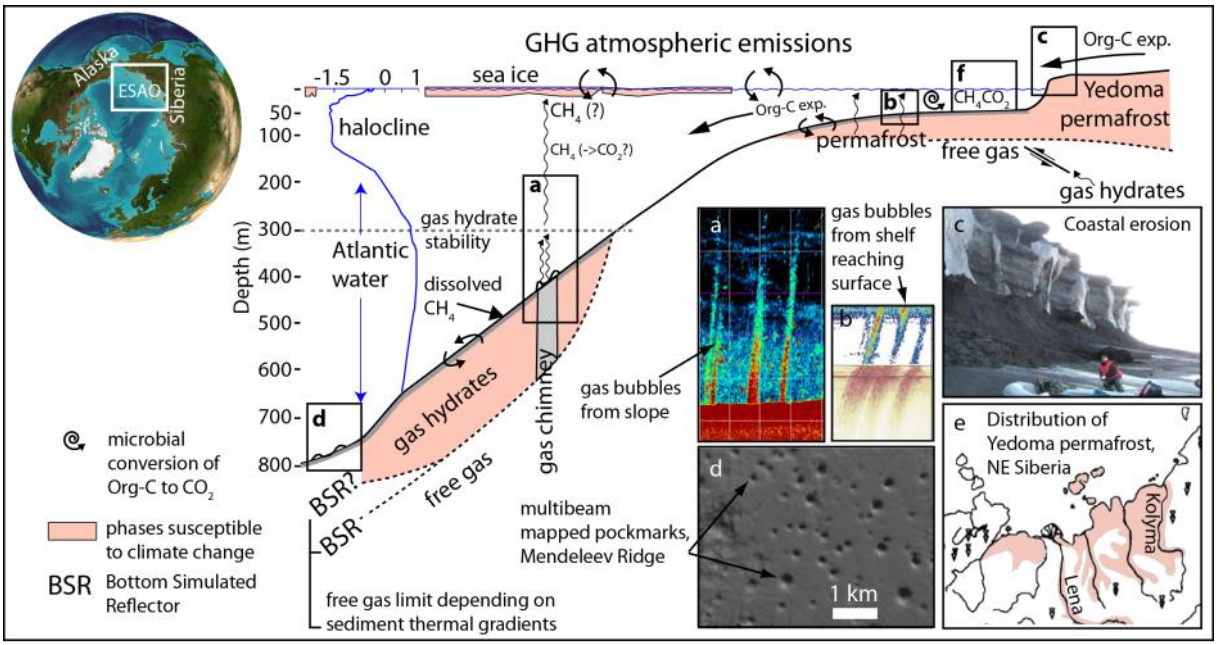

Figure. 1. *Schematics of key components of the Arctic climate-cryosphere-carbon (C3) system that are addressed by the SWERUS-C3 program. The insets* ***a-f*** *illustrates the Arctic C3-system in focus for the SWERUS-C3 two-leg expedition.* ***a,b)*** *Sonar images of gas flares in the water column caused by sea floor venting of methane (****a****: slope west of Svalbard (Westbrook et al., 2009);* ***b****: ESAO (Shakhova et al., 2010).* ***c)*** *Coastal erosion of organic-rich Yedoma permafrost, Muostoh Island, SE Laptev Sea. d) Multibeam image showing pockmarks from gas venting off the East Siberian shelf. e) Distribution of Yedoma permafrost in NE Siberia. f) Multiple transport, conversion, and venting processes of released permafrost organic matter, CH_4 and CO_2.*

In order to begin the collection of scientific data from departure of the leg in Barrow, Alaska, a so called RATS application (Application for Consent to Conduct Marine Scientific Research) was submitted to United States Department of State (application U2014-023) to work in the US EEZ. Permission was granted.

The objective of this Leg 2 cruise report is to provide an overview of the expedition organization and execution, participants, data collected and collection methods, shipboard processing as well as preliminary results obtained from the initial shipboard data analyses. This cruise report was written by Work Package (WP) leaders onboard *IB Oden* toward the end of Leg 2 with contributions by many scientists. Additional information of the SWERUS-C3 program may be found at (http://swerus-c3.geo.su.se/), some of the additional common documents include a Scope of Work for the expedition and a pre-departure cruise plan. A cruise report and corresponding documents also exist for Leg 1 of the SWERUS-C3 2014 expedition.

SWERUS-C3 Leg 2 scientific objectives

To address the SWERUS-C3 general scientific objectives, Leg 1 and 2 of the 2014 *Oden* expedition were designed to focus on somewhat different specific scientific objectives. Leg 2 is specifically designed to investigate:

1. **CH_4 release from subsea permafrost, continental slopes and deep sea**

   Geophysical mapping using multibeam, chirp and reflection seismic, and acoustic water column imaging, to characterize gas and gas hydrate related features on the continental shelf, along the continental slope and in the deep sea. Determine the activity of deep sea pockmarks; what is the proportion of relict pockmarks and active pockmarks? Are there gas hydrates present along the Siberian continental slope? If so, how thick is the Gas Hydrate Stability Zone (GHSZ)?

2. **Past and present bottom and sub-bottom temperatures of the continental shelf, along the continental slopes and deep sea and their importance for the GHSZ and release of CH_4**

   Characterize the present Atlantic water flow along the Siberian margin and the inflow of Pacific water from the Bering Strait through Herald Canyon with oceanographic sections. Collect sediment cores for paleoceanographic studies of bottom water temperature history as influenced via Atlantic and Pacific water inflows. Determine sub-bottom temperature gradients on the shallow shelf along the Siberian continental slope, and adjacent ridges and deep basins. Determine variations in sediment physical properties and thermal conductivity. Determine the CH_4 concentration in the water column along the continental margin.

3. **Re-sequestration of carbon released from thawing coastal permafrost into the shelf seas with subsequent off-shelf export to deeper basins**

   Water sampling for marine chemistry and coring to acquire undisturbed surface sediments. Determine the distribution of chemical parameters (dissolved inorganic carbon, nutrients, oxygen) in the water column along the continental margins. Determine the particulate carbon export from the surface sediment record. Determine the "age" of the waters from CFC and SF_6 concentrations.

4. **History of Arctic sea ice and its impact on carbon fluxes**

Coring to acquire high resolution sedimentary archives for studies of paleo-proxies (e.g., IP25, microfossils, carbon and oxygen isotopes).

5. **The role of Arctic Ocean glaciation for stored carbon on shelves and slopes**

   Geophysical mapping of shelves and bathymetric highs to determine past glacial activities, and collection of sediment cores for determination of past accumulation of carbon and timing of glacial activity.

6. **Air-sea exchange of and the effects on clouds in different sea ice conditions**

   Continuously monitor the atmospheric conditions to determine the flux across the air-ocean interface, from direct eddy-correlation flux measurements of momentum, heat, water and trace gases, to low clouds and their properties, and to the vertical structure of the lower atmosphere including clouds and boundary-layer structures. Continuous determination of surface water pCO_2.

Summary of the execution of SWERUS-C3 Leg 2

Leg 2 managed to accomplish more than anticipated in the cruise plan. High quality data were collected in all planned research areas, defined as Boxes 1-4 (see below). Ice conditions were very light during the entire cruise and several of the target areas were only covered by 20-50% sea ice and some even sea ice free (Boxes 1 and 4). The main challenge was gale-force winds and an open sea over larges areas resulting in long fetches and built up swell. Since *IB Oden* lacks a dynamic positioning system, drifting while carrying out station work in strong winds was a challenge during large portions of Leg 2. On the other hand, the generally light sea ice conditions permitted much faster transit times between the research areas. Instead of the planned transits at ca 3 knots, transit could often be carried out with a speed of around 9 knots. Another advantage of the light sea ice conditions was that multibeam/sub-bottom profiling surveys could be carried out along optimal survey lines rather than in between ice flows. This resulted in much higher quality seafloor mapping data being collected in several areas than during any previous expedition to the central Arctic Ocean with *IB Oden*. Overall, the light sea ice conditions allowed the work research in Boxes 1-4 to be completed about one week earlier than planned. This permitted Leg 2 to extend its work further north along the Lomonosov Ridge. A new "Box 5" was defined at about 84°30'N where a comprehensive geophysical mapping, geological coring and oceanographic station campaign was completed. This further improved one of the SWERUS-C3 goals; to connect continental shelf and slope environmental records with the deep central Arctic Ocean.

Cruise track and stations

Leg 2 cruise map

The expedition closely following the cruise plan based on the outlined working areas (Boxes 1-4) with the different research objectives requiring investigations involving geophysical surveys and sampling programs (Figs. 2 and 3). Entrance/exit times in/out of the Russian Exclusive Economic Zone (EEZ) are provided in Table 1.

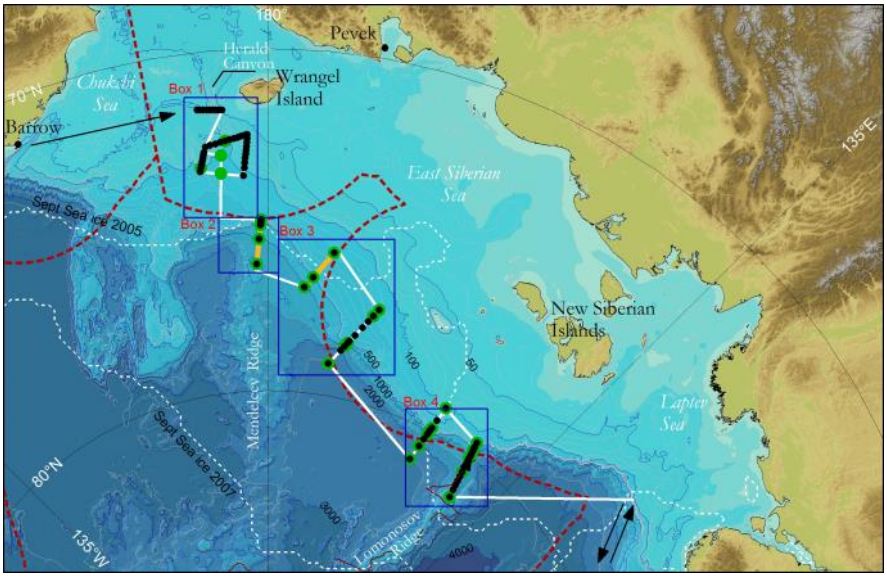

Figure 2. *Map from the original Leg 2 cruise plan. Planned coring stations are shown with green circles, CTD stations with black dots, and seismic reflection lines with orange lines.*

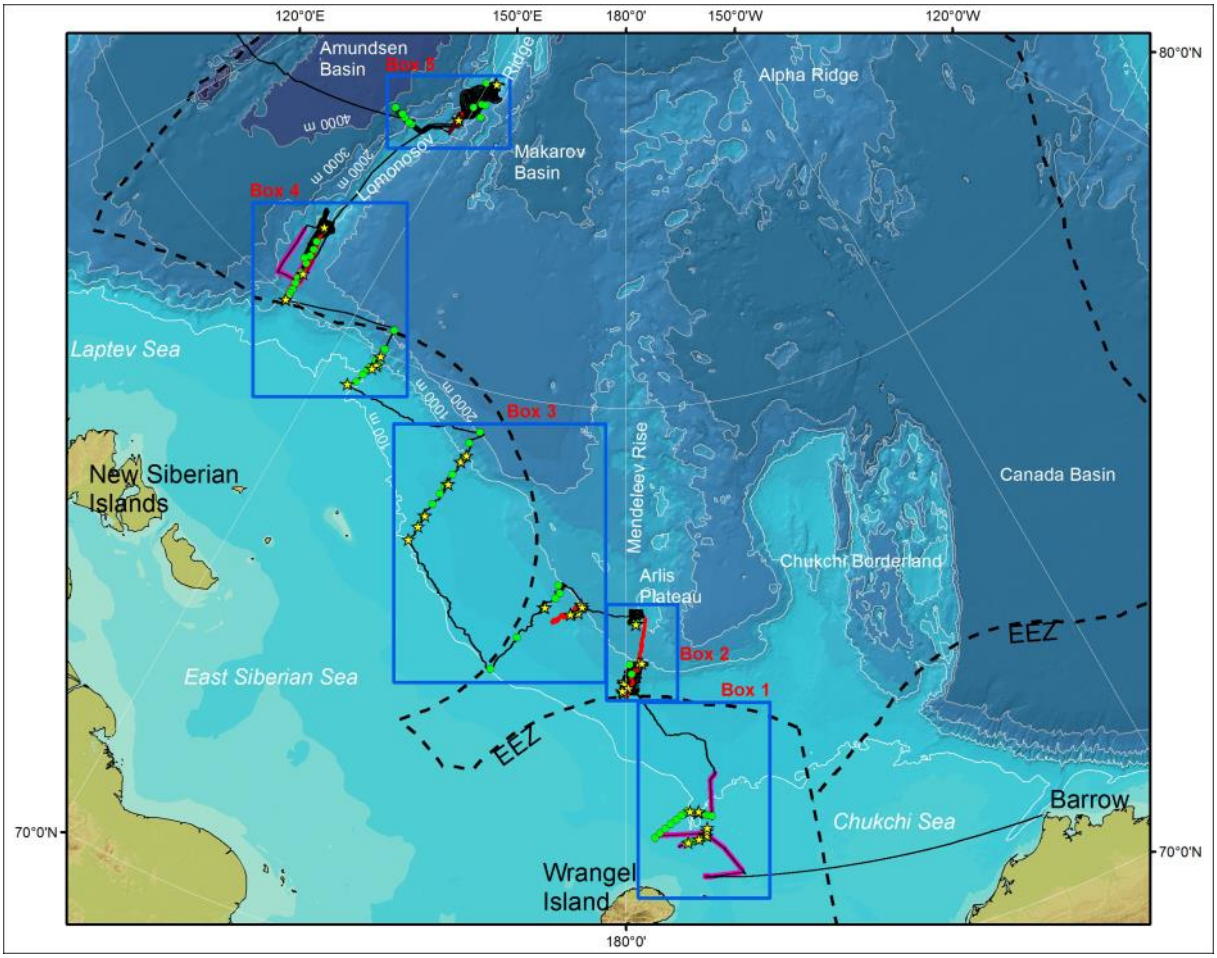

Figure 3: *Overview map of Leg 2 cruise track starting August 21 from Barrow, Alaska. The cruise ended in Tromsö, Norway, August 4. Working Boxes 1-5 are outlined with blue boxes. Red lines=Seismic reflection profiles; purple lines=Electromagnetic profiles; yellow stars=coring stations; green dots=CTD stations (some also included water sampling).*

Table 1: *Entrance/exit times in/out of the Russian Exclusive Economic Zone (EEZ). Positions for each entrance/exit are provided to the nearest minute with reference to WGS 84.*

Russian EEZ: Entrance and exit	Date and Time (UTC)	Longitude	Latitude
Entrance from US-EEZ	2014-08-22 19:09	168°58'W	71°35'N
Exit western Chukchi slope	2014-08-27 19:59	179°8'W	74°56'N
Entrance East Siberian Shelf	2014-09-07 03:12	170°19'E	75°14'N
Exit East Siberian Shelf	2014-09-12 15:00	154°30'E	80°25'N

On positions of stations, observations and sampling

Descriptions of naming conventions of sampling stations, subsamples and geophysical surveys are found in the sections dedicated to each Work Package (WP). These WP sections also contain detailed maps showing locations of sampling stations and survey lines. All geographic positions throughout Leg 2 of the SWERUS-C3 expedition are given with reference to the vertical datum WGS84. All depths are referenced to mean sea level. Times for sampling stations are provided in UTC. The local ship time adopted from Barrow, Alaska, was UTC-12, until September 28, when a change over to UTC+1 was carried out.

Methods – sampling, observations and shipboard analyses

Coordination and organization

The SWERUS-C3 expedition organization is based on the Work Package (WP) leaders that each is responsible for a research area. These WP are described below. Prior to the expedition, the WP leaders jointly developed the cruise plan in coordination with Leg 1 co-chief scientists and WP leaders. The overall shipboard coordination was carried out by the two co-chief scientists and the captain with support from the expedition coordinator from the Swedish Polar Research Secretariat (see Expedition management).

Work packages

Each WP has two leaders. In some cases, the co-leader was shore based and thus primarily helped organizing the shipboard work prior to the expedition. Some of the WP worked with scheduled shift systems, for example the GM, WC, CO, and PO WPs. This further described under respective WP.

Overview list of work packages

Work Package	WP Lead	WP Co-Leader
Coordination - Cruise leadership	M. Jakobsson A. Koshurnikov	O. Dudarev (shore based)
GM: Geophysical Mapping	M. Jakobsson	L. Mayer
WC: Water Column Imaging	L. Mayer	T. Weber (shore based)
SC: Sediment coring	M. Jakobsson	M. O'Regan
SP: Sediment physical properties	M. O'Regan	
CP: Sediment chemical properties	C. Miller	M. Mörth (shore based)
MB: Micropaleontology and Biostratigraphy	J. Backman	T. Cronin
CO: Chemical oceanography	L. Anderson	
PO: Physical oceanography	G. Björk	J. Nilsson
BLM: Boundary layer meteorology	O. Persson	M. Tjernström (shore based)

Manning of the individual Work Packages

GM: Geophysical Mapping		
Name	Institution	WP Responsibility
M. Jakobsson	SU	WP Leader
L. Mayer	CCOM/UNH	WP Co-Leader/Seafloor mapping

B. Eriksson	SU	Seafloor mapping (multibeam/chirp)
R. Mohammad	SU	Seafloor mapping (multibeam/chirp)
K. Jerram	CCOM/UNH	Seafloor mapping (multibeam/chirp)
T. Flodén	SU	WP Co-Leader, seismic reflection
A. Lif	SU	Seismic reflection
A. Koshurnikov	Moscow State Univ	Electromagnetics
D. Chernykh	POI	Seafloor mapping (multibeam/chirp)
A. Khortov	Shirshov IO	Seismic reflection
R. Ananiev	Shirshov IO	Seafloor mapping (multibeam/chirp) Seismic reflection, electromagnetics

WC: Water Column Mapping		
Name	Institution	WP Responsibility
L. Mayer	CCOM/UNH	WP Leader
K. Jerram	CCOM/UNH	Water column imaging
D. Chernykh	POI	Water column imaging
R. Mohammad	SU	Water column imaging

SC: Sediment Coring		
Name	Institution	WP Responsibility
M. Jakobsson	SU	WP Leader
M. O'Regan	SU	WP Co-Leader
M. Karasti	SU	Piston/Gravity/Multi coring
J. Backman	SU	Piston/Gravity/Multi coring
T. Cronin	SU	Piston/Gravity/Multi coring
C. Johansson	SU	Core curation
A. Gukov	Ust . Lendsky Nat.	Multi coring
N. Barrientos	SU	Multi coring
F. Muschitiello	SU	Multi coring

SP: Sediment Physical Properties		
Name	Institution	WP Responsibility
M. O'Regan	SU	WP Leader
P. Preto	SU	Sediment physical properties (Core logger/temp probes/conductivity)
C. Johansson	SU	Sample curation

CP: Sediment Chemical Properties

Name	Institution	WP Responsibility
C. Miller	Rice Univ	Sediment chemical properties (pore water sampling and analyses)
C. Johansson	SU	Lab support
F. Muschitiello	SU	Lab support

MB: Micropaleontology and Biostratigraphy		
Name	Institution	WP Responsibility
J. Backman	SU	WP Leader, micropaleontology
Thomas M. Cronin	SU	WP Co-Leader, visual core description, micropaleontology
Laura Gemery	USGS	Sample curation and preparation, visual core description
Natalia Barrientos	SU	Sampling and sample preparation (sieving), micropaleontology
Carina Johansson	SU	Sampling and sample preparation, core and sample curation

CO: Chemical Oceanography		
Name	Institution	Responsibility
L. Anderson	GU	WP Leader
S. Gutekunst	Christian-Albrechts-University of Kiel	Determining CFCs and SF_6
T. Stöven	GEOMAR	Determining CFCs and SF_6
F. Zemlyak	GU	Determining oxygen
A. Ulfsbo	GU	Determining the inorganic carbon system
O. Holby	GU	Water sampling
Y. Ericson	GU	Determining nutrients
S. Jutterström	GU	Determining the inorganic carbon system
D. Kosmach	POI	Ocean Methane program

PO: Physical Oceanography		
Name	Institution	Responsibility
G. Björk	GU	WP Leader
J. Nilsson	SU	WP Co-Leader
C. Stranne	SU	CTD
C. Edsgren	GU	CTD
		CTD

BLM: Boundary Layer Meteorology		
Name	Institution	Responsibility

Ola Persson	NOAA	WP Leader, overall BLM science oversight, CIRES/NOAA systems responsible, soundings, met diagnostics
Dan Wolfe	NOAA	CIRES/NOAA systems maintenance, soundings, data collection support
John Prytherch	SU	Leeds' systems maintenance, soundings, data collection support, met diagnostics
Georgia Sotiropoulou	SU	Stockholm systems maintenance, soundings
Barbara Brooks	Leeds Univ	Leeds' systems responsible, incl. soundings; systems maintenance; Stockholm systems support
Anatoly Salyuk	POI	Noble gas isotopes; tending Cavity-ring down lasers for continuous CH4 and CO2 (sys of Humborg and Crill)

Expedition management

Erik Andersson served as Master of *IB Oden* for Leg 2. Martin Jakobsson and Andrey Koshurnikov served as co-chief scientists for Leg 2. Andrey Koshurnikov was chief scientist with Martin Jakobsson serving as deputy chief scientists for the work within the Russian EEZ. Magnus Augner of the Swedish Polar Research Secretariat served as expedition coordinator for Leg 2. These four held a daily briefing at the bridge 07:00 together with the Chief Officer and the meteorologist. Before each working area (Boxes 1-5) the WP leaders and co-chiefs held a joint meeting to develop a detailed survey and sampling plan along with an estimated time schedule. For each working box, a latest departure time was set in order to transit to the next box. The work on deck was organized by the WP leaders. Chief Officer (Ivan Öström) carried out detailed "Toolbox" meetings on deck for each sampling activity to ensure proper safety methods.

Information about the daily activates was spread to all cruise participants through the WP-leaders and through the ship's information system. A seminar series open to both crew and scientists was run throughout the. Finally, the common server "vdata" was used to share information and data between participants.

Methods – sampling, observations and shipboard analyses

WP GM (Geophysical Mapping)

The SWERUS-C3 Leg 2 geophysical mapping program aimed to continuously map the seafloor and uppermost, ca 50-100 m of sediment stratigraphy along the entire cruise track using *IB Oden's* 12 kHz hull-mounted multibeam echo sounder and integrated 3-7 kHz chirp sub-bottom profiler. In addition, detailed seafloor mapping was planned to be carried out to select coring sites, in areas of specific interest for the glacial history and in areas where gas related features were indicated on the geophysical mapping data. Furthermore, two seismic reflection profiles were planned to be acquired from the shallow continental shelf slope to its base. Both these profiles were located outside of the Russian EEZ. The purpose of the seismic reflection profiles was to investigate the sediment stratigraphy deeper than the imaging capacity of the chirp sub-bottom profiler. Stockholm University's 6.4 m long geophysical survey boat *RV Skidbladner* was brought onboard *IB Oden* in case the opportunity to map in shallow areas of the continental shelf during calm and ice free conditions would arise. *RV Skidbladner* is equipped with a 200-400 kHz high resolution multibeam echo sounder and a 15 kHz sub-bottom profiler that complements *Oden's* deep water systems. *RV Skidbladner* is capable of mapping in water depth shallower than approximately 500 m.

Equipment

Multibeam and sub-bottom profiling system

The hull-mounted multibeam echo sounder installed in *IB Oden* is a Kongsberg EM122 1°x1° 12 kHz full ocean depth multibeam echo sounder including the capability of logging acoustic data in the water column (see WP WC: Water Column Imaging). The sonar transmitting array is 8 x 1 m (resulting in a 1°-wide transmit pulse), mounted along-ship in the so-called "ice knife", which forms the deepest part of *Oden's* hull (Fig. GM-1). This array is protected from ice impact by poleuterane plates reinforced by titanium bars. Due to the ice protection of the transceivers, the useable angular coverage is reduced to less than 2 × 65°; with typical swath widths of three to four times the water depth. The receiving array measures 8 x 1 m (resulting in a 1°-wide receive beam) and is mounted across-ship. This array is protected by a solid titanium plate. The multibeam system includes a Seatex Seapath 320 for navigation using GLONASS/GPS and motion sensor logging (roll, pitch and heave). The motion sensor unit is a Seatex MRU5. A Seapath 200 is carried on board as a spare unit.

A Kongsberg SBP120 3°x3° chirp subbottom profiler is hull-mounted in *IB Oden* and integrated with the multibeam system. This system operates with a frequency range of 3-7 kHz and has an approximate resolution of 0.35 ms (~70 cm). The penetration is typically 50-200 m in clayey ocean sediments.

Corrections for sound speed changes in the water column come from data generated at oceanographic stations using a standard SeaBird911 CTD (see WP PO: Physical Oceanography). In addition, XBTs (eXpendable BathyThermographs) were used when necessary. The setup of the entire multibeam system including sub-bottom profiler is illustrated in Figure GM-2. Table GM-1 lists the technical specifications of the multibeam and integrated chirp sub-bottom profiling system. Table GM-2 includes the measured offsets between key multibeam components.

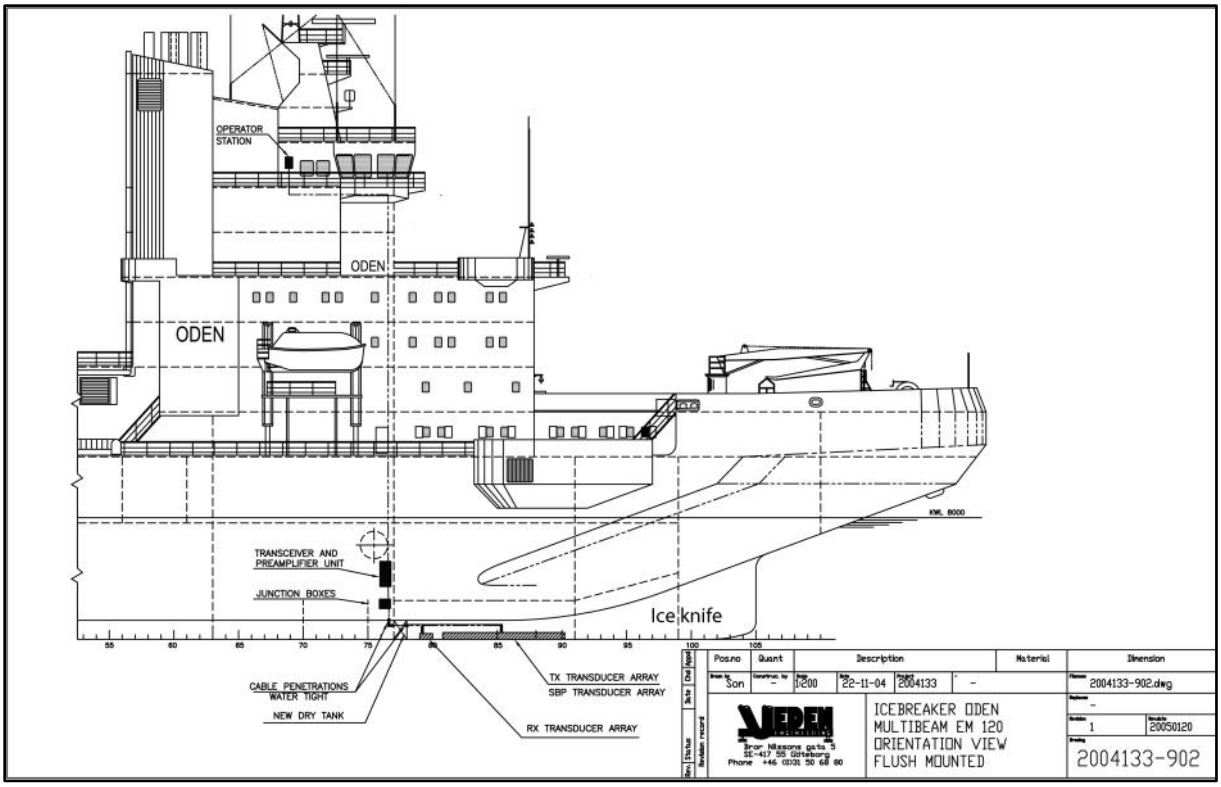

***Figure GM-1**: Drawing of the EM122/SBP120 system installed on the IB Oden.*

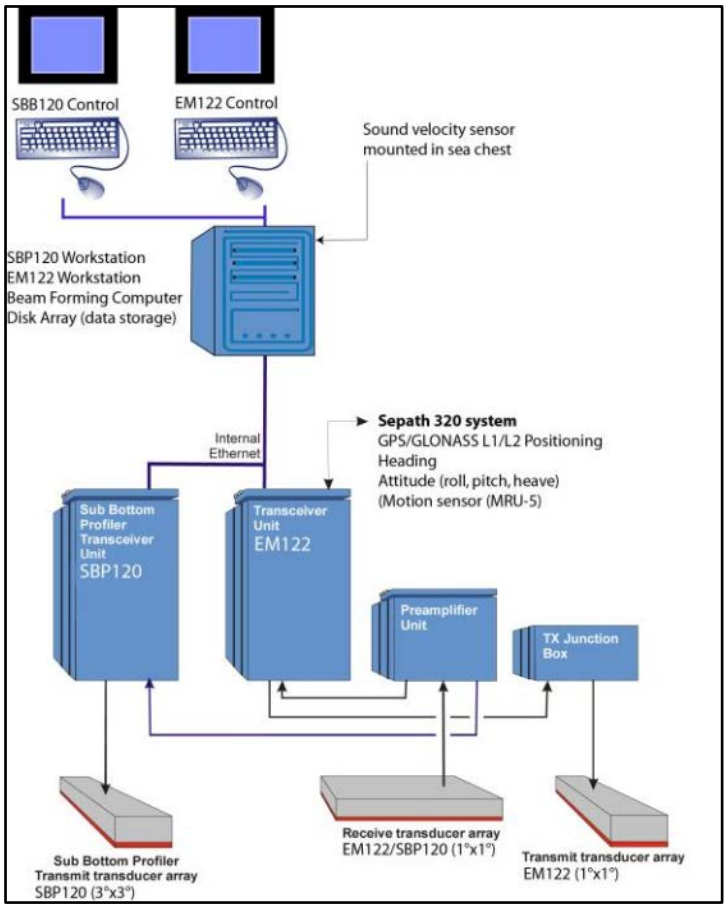

***Figure GM-2**: Schematic illustration of the EM122/SBP120 system installed on the IB Oden. The illustration is a modified version of Kongsberg's original.*

Table GM-1.*Technical specifications of IB Oden's multibeam and integrated sub-bottom profiling system.*

Component	***Technical specification***	***Serial numbers***
Kongsberg EM122 multibeam	*Main operation frequency: 12 kHz* *Beam widths: 1°X 1°* *Number of beams/swath: 288* *No of soundings/swath: 432* *Depth range: 20 to 11 000 m* *Coverage sector: Up to 75°, Oden's ice protection windows limit the coverage to ~65°* *Pulse forms; 2.5 and 15 ms CW and FM chirp (BT=40)*	*Operator station MP8300 (upgraded 2014): CZC3407HBM* *TRU: 110* *PreAmp: 106* *TX JB1: 150* *TX JB2: 151* *Software: SIS Version 4.1.3, build 14*
Seatex MRU5 motion sensor	*See output result for Seapath*	*MRU5: 4603*
Seapath 320 GPS/GLONASS navigation system	*Heading accuracy: 0.05° RMS (4 m baseline)* *Roll and pitch accuracy: 0.02° for ±5° amplitude* *Heave accuracy: 2 cm or 2%, whichever is highest.* *Velocity accuracy: 0.03 m/s RMS or 0.07 m/s (95 % CEP) with DGPS* *Positional accuracy with DGPS: 0.15 m, no DGPS available in the central Arctic Ocean, accuracy is reduced to ~2 to 10 m.* *GLONASS in addition to GPS*	*Processing unit (installed 2014): SP320-CA31NS2050*
Seapath 200 GPS navigation system (spare unit)	*Heading accuracy: 0.05° RMS (4 m baseline)* *Roll and pitch accuracy: 0.03° RMS for ±5° amplitude* *Heave accuracy: 5 cm or 5%, whichever is highest.* *Velocity accuracy: 0.03 m/s RMS or 0.07 m/s (95 % CEP) with DGPS* *Positional accuracy with DGPS: 0.15 m, no DGPS available in the central Arctic Ocean, accuracy is reduced to ~2-10 m.*	*Processing unit: 7148*
SBP120 chirp sonar sub-bottom profiler	*Operation frequency: 2.5 to 7 kHz* *Number of beams per ping: 11* *Beam width: 3° x 3°* *Pulse length: 0.4 to 100 ms* *(navigational data is received from the Seapath system)*	*Operator station MP8300 (upgraded 2014): CZC3407HBZ* *TRU: 105* *TX/RX JB: 104* *CCU1: 119; CCU2: 120; CCU3: 123; CCU4: 124* *Software: SBP/Topas 1.5.3 (2011.12.05)*
SeaBird 911 CTD	*Depth rating: 6800 m* *Temperature: certified stability of 0.001 °C in six months after calibration*	*CTD sensor: 859* *Electronic unit: 11P45395-0750*
Valeport Mini SVS/T Sound velocity sensor mounted in the sea chest		*Sensor: 25509*

Table GM-2.*Offsets between sensors entered into the multibeam sonar acquisition software SIS. Length measurements are in meters. The MRU is set to be the ship XYZ reference point. X: PosFwd; Y Pos STB; Z: PosDwn; Roll Pos STB Dwn; Pitch: Pos bow up; Heading: Pos clock wise.*

	X	**Y**	**Z**	**Roll**	**Pitch**	**Heading**
Reference point, MRU	0	0	0	0.023	-0.057	0.298
EM 120 TX Transducer	17.590	-2.374	9.459	-0.207°	-0.001°	0.033°
EM 120 RX Transducer	12.242	-0.880	9.482	0.021°	0.189°	0.022°
SBP120	17.240	0.619	9.464	0.180°	0.022°	0.018°
GPS Antenna 1	3.973	-3.050	-33,152			
GPS Antenna 2	6.473	-3.010	-33,069			
Ref. point ->Waterline			1,30			

Figure GM-3: *RV Skidbladner with the EM2040 bow mounted multibeam in operation in the Chukchi Sea. The multibeam and sub-bottom profiler can be hoisted up for fast transit if required. Photo: Arne Lif.*

Figure GM-4: *RV Skidbladner stored onboard IB Oden. Photo: Martin Jakobsson*

Figure GM-5*: Launching of RV Skidbladner using IB Odens crane. Photo Arne Lif.*

High-resolution multibeam system

RV Skidbladner is an Arronet 20.5 cs aluminum boat, 6.4 m long, 2.4 wide, weighing about 1.8-1.9 ton with all geophysical equipment onboard (Figs. GM-3,4,5). *RV Skidbladner* has a Honda 150 Hp outboard motor and is equipped with a Garmin 7012 GPS-navigation plotter, radar system, AES, and

radio. The fuel is 95 octane unleaded standard gasoline and the tank is 157 liters. *RV Skidbladner* has a top speed of 32 knots, when all equipment are hoisted up for transit, but typical survey speed with the equipment in the water is 5-6 knots. Fuel consumption during a survey at 6 knots is approximately 10 liters/hour. All equipment is supplied with electricity from a Honda 20i 2kW generator. This generator consumes about 1 liter/hour gasoline (alkylade petrol is recommended).

A Kongsberg EM2040, 200-400 kHz 1°x1° multibeam is installed on *RV Skidbladner* with a bow mounted pole that can be hoisted up for transit (Fig. GM-6). This multibeam is capable of mapping the seafloor down to approximately 500 m water depth. The motion sensor consists of a Seatex MRU5+ mounted in a subsea bottle on the EM2040 transducer casing. Heading is acquired using two VS101 Hemisphere GPS compasses mounted 0.8 m apart. The main positioning is acquired with a Hemisphere R320 GPS/GLONASS receiver mounted in between the VS101 antennas. Sound speed correction data is acquired using a velocimeter (SV) manufactured by Applied Microsystems Limited (AML), that is mounted on the EM2040 transducer casing for continuous readings. An additional velocimeter by Valeport is used for measuring the sound velocity profile in the water column. A Kongsberg EA 600, 15 kHz, sub-bottom profiler is mounted on a pole that can be hoisted up for fast transit (Fig. GM-6). Table GM-3 lists technical specifications of the multibeam and integrated chirp sub-bottom profiling system.

Table GM-3.*Technical specifications of RV Skidbladner's multibeam and sub-bottom profiling system.*

Component	***Technical specification***	***Serial numbers***
Kongsberg EM2040 multibeam	*Main operation frequency: 200,300, 400 kHz* *Beam widths: 1°X 1°* *Number of soundings/swath: Max 800 for 200/300/400 KHz* *CW Pulse lengths:* *200kHz/200 and 600 µs* *300 kHz/70, 200 and 600 µs* *400 kHz/20, 35, and 100 µs* *FM Pulse lengths:* *200 kHz/12 ms; 300 kHz/6 ms; 400 kHz N/A* *Depth range in ocean water: 0.5 to 400 m* *Coverage sector: Up to 70°* *Pulse forms; 2.5 and 15 ms CW and FM chirp (BT=40)*	*TX: 110* *RX: 110*
Seatex MRU5+ motion sensor mounted in sub-sea bottle		*MRU5+: MRU-E-JB-2*
Hemisphere R320 GPS/GLONASS antenna	*GPS with RTK and SBAS correction capability that also receives GLONASS. Neither RTK nor SBAS correction could be used during the expedition since there is no correction information at these high latitudes.*	*Antenna: BB1111-A52S005*
Hemisphere VS101 GPS compass	*Antennas mounted 0.8 m apart*	*Antenna 1: A2120100714187* *Antenna 2:A2120100714188*
Kongsberg EA600 sub-bottom profiler	*Operation frequency: 15 kHz, 2 kW* *Circular beam width: -3 dB 17°/: -6 dB 23°*	*Transducer: 099-133981* *GPT transceiver: 305121*

Valeport sound velocity probe	*With memory for operation without cable, max depth rating 500 m*	*5107*
AML SVsound velocity sensor mounted near transducer face, and AML SVP sound velocity/pressure sensor used for depth profiling of sound velocity at stations	*Max depth rating: 200 m*	*SV-probe:4646* *SVP-probe: 5107*

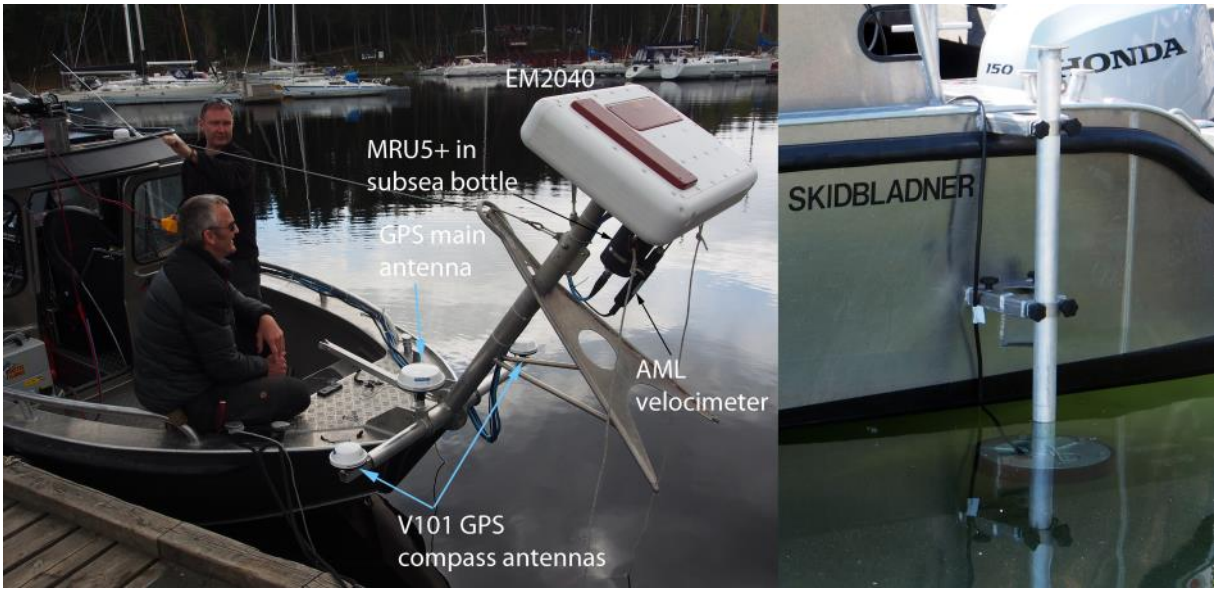

Figure GM-6*:Multibeam setup on RV Skidbladner.*

Seismic reflection profiling

A single channel seismic reflection profiling system was used to acquire the planned seismic profiles. The setup of this system and how the seismic source and receiver was towed behind *IB Oden* is illustrated in Figure GM-7. The expected sea ice conditions required the instruments to be towed closely behind the icebreaker, preferably below the propeller stream. Using an ordinary depressor device for the cables was not an option as it would twist and coil the entire cable system when lowered through the propeller wash. Instead, a 60 kg weight at the end of a 25 m plastic hose was used as the towing point. This arrangement was not sufficient to keep the transmitter/receiver totally below the propeller stream, the actual towing depth was estimated to be 10 m at a profiling speed of ca 6 knots. A positive aspect of this arrangement was that air-bubbles in the water created by the propellers prevented disturbing echoes from the sea surface.

Four compressors were operated simultaneously to supply compressed air to the seismic source consisting of an airgun. The capacity of the compressors, two Bauer and two Compair, is ca 270 liters/minute free air each. The compressors were stored and run inside a 10’ container placed on the aft-deck (Fig.GM-8). A PAR-1600 airgun equipped with a 40 cubic inch (~0.66 liter) chamber was used as seismic source (Fig. GM-9).The maximum allowed pressure to this airgun is 140 kilos (2000 psi). The compressors were regulated to operate slightly below this maximum pressure, which permitted shooting at an interval of 3 seconds. Longer shot intervals, up to 5 seconds, were occasionally used during compressor maintenance periods. Navigation was acquired with a

Hemisphere A100 GPS smart antenna setup specifically for the seismic system adjacent to *Oden's* helicopter platform. This antenna was setup because we encountered problems with providing navigation from the Seapath 320 GPS/GLONASS navigation system to the container on the aft-deck where the seismic operations were carried out. The hydrophone streamer contains 100 hydrophone elements connected in parallel (Fig. GM-10).The total length of this streamer including tow and signal cable sections is 72.5 m. In addition, a low noise pre-amplifier was contained in the streamer. The geometry of the instrument locations was measured relative to the recording container in order to automatically recalculate successive positions to the location of the transmitter/recorder in the x/y/z space using the Polar stereographic projection specified in Table GM-4.

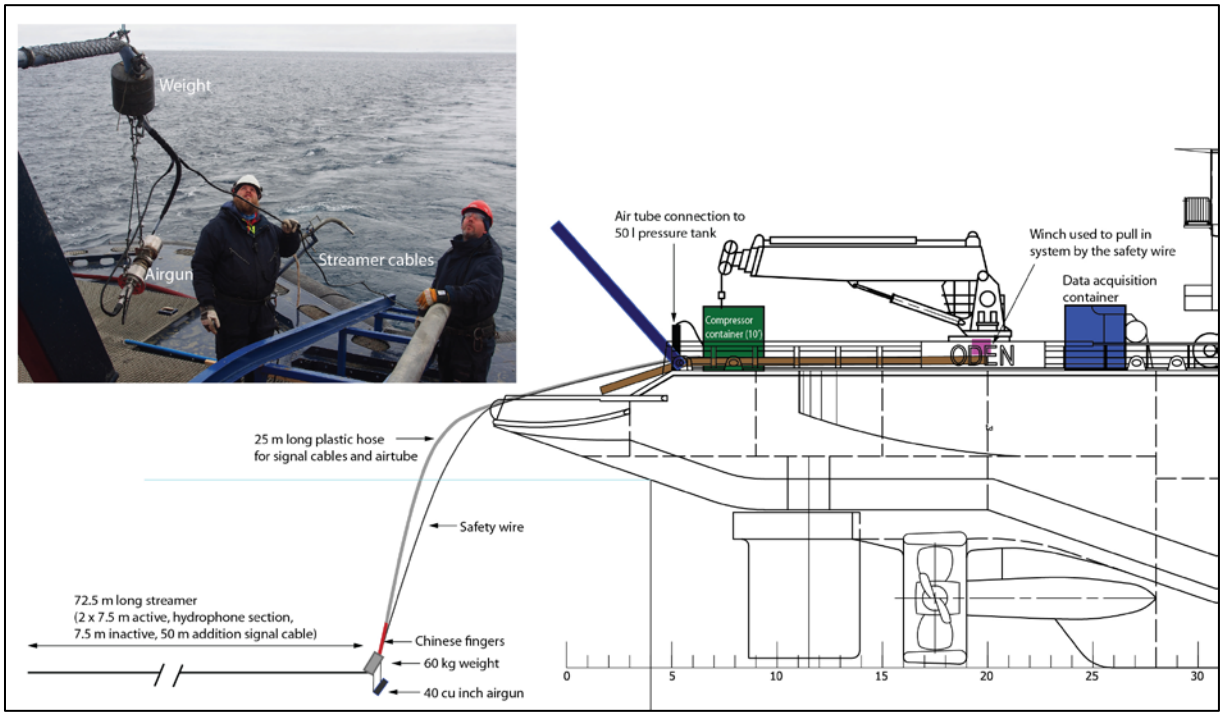

***Figure GM-7**: Setup of seismic reflection profiling system.*

Figure GM-8: *Air compressor used for air-supply to the seismic airgun.*

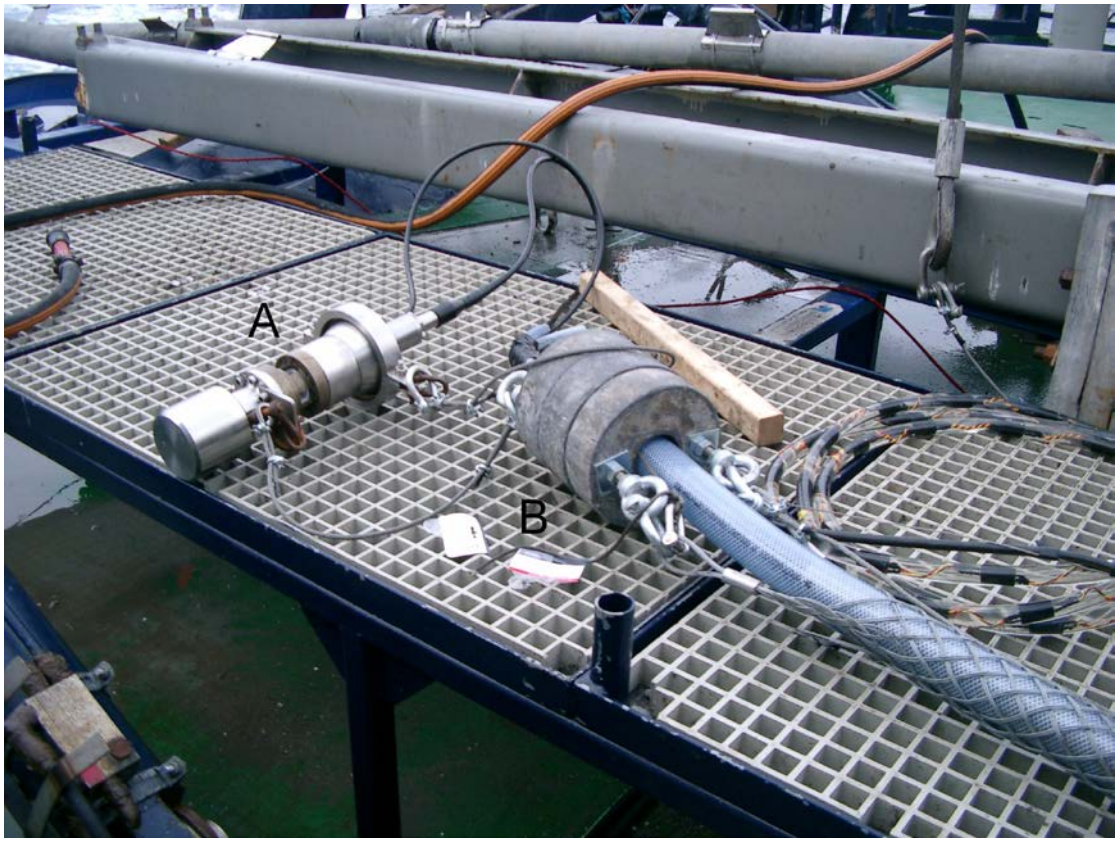

GM-9: *The PAR-1600 airgun equipped with a 40 cubic inch (~0.66 liter) chamber used as seismic source (A) and the depressor weight (B) at the lower end of a plastic hose used to protect signal cables and air hose.*

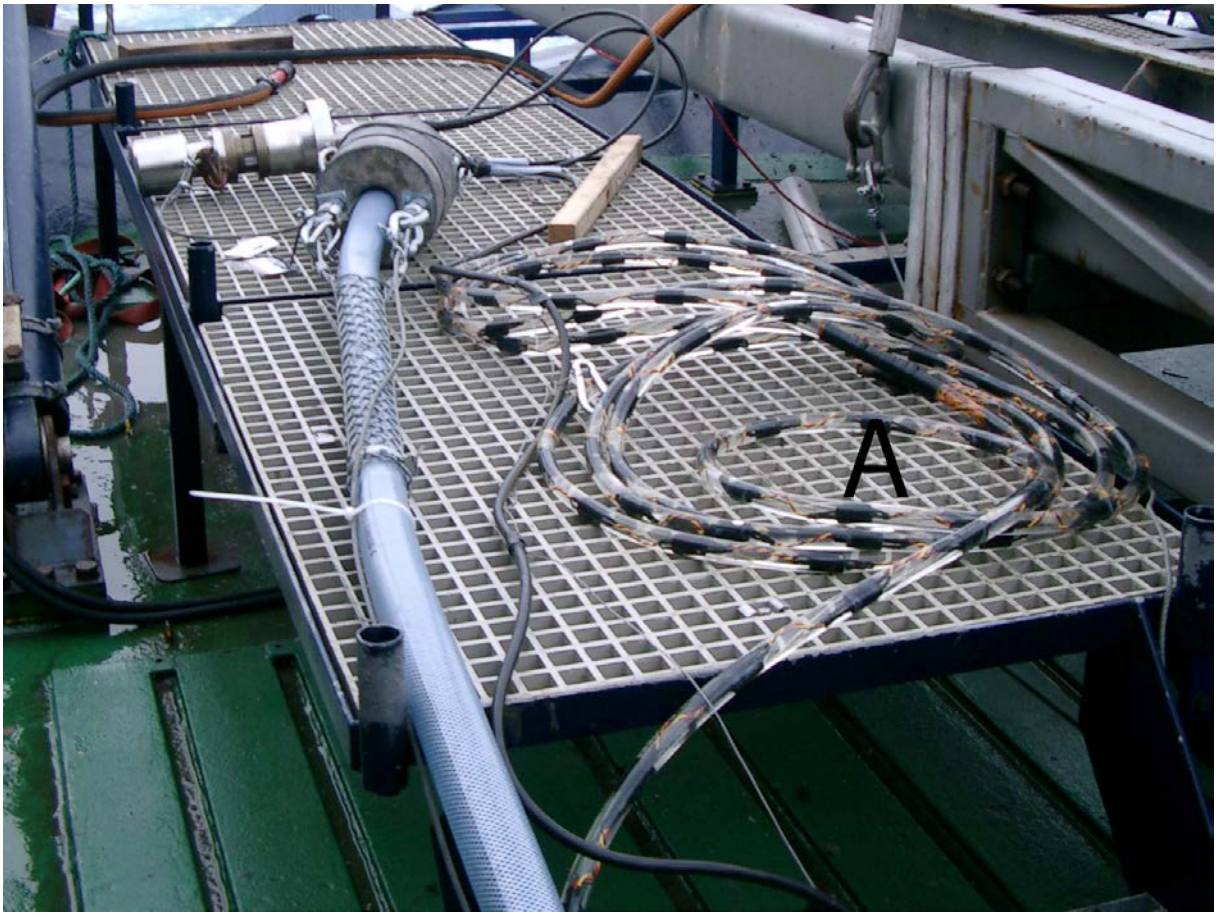

GM-10: *Hydrophone streamer consisting of 100 elements of type Aquadyne AQ-1.*

Electromagnetic system

Electromagnetic soundings were carried out using TEM-technology (time-domain). TEM- technology is based on using variable electromagnetic fields in the time domain. On the sea surface, a primary electromagnetic field is created. This field is spread through the water column and sub-bottom. When the transmitted primary variable electromagnetic field reaches a conductive layer, a secondary current is formed according to Faradays' Law. This current generates a secondary electromagnetic field, according to the Maxwell law. The secondary electromagnetic field spreads extensively and eventually reaches the sea surface where it is registered by a towed receiver line (Fig. GM-12). The secondary field depends on the conductivity of the media, in our case marine sediments, on which it is spread. Therefore it is possible to model a geoelectric cross-section (cross-section of resistivity), if the secondary field is known. If the electromagnetic wave has a large time period, it extends to deep sub-bottom depths, implying that if we measure electromagnetic waves with large time periods, we receive resistivity information about deep geological layers. On the contrary, if we measure electromagnetic waves with small periods, we receive resistivity information about the near-surface geology. This makes it possible to apply TEM sounding in order to record resistivity information about geologic layers at different depths. The primary electromagnetic field was created by transmission of impulses of a direct current in a generator line (Fig. GM-11).

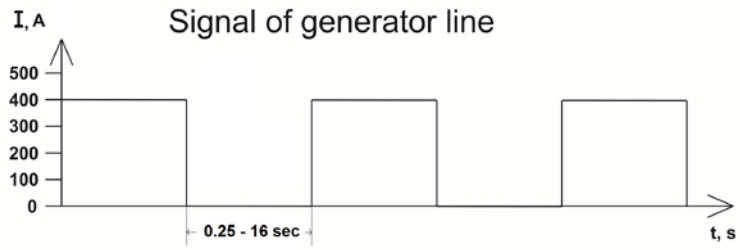

***Figure GM-11**: Signal of generator line.*

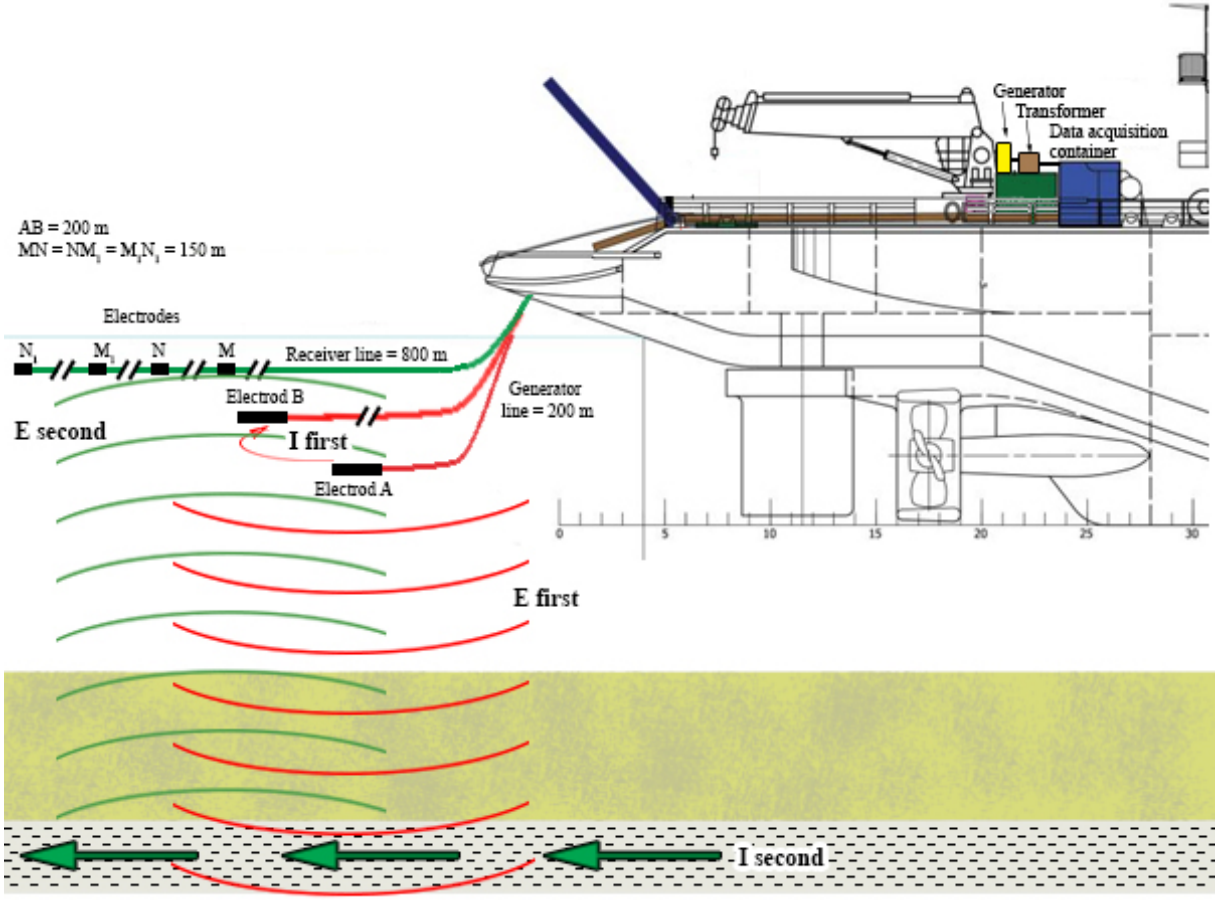

***Figure GM-12**: Setup of EM system.*

According to the law of Faraday, change of a current strength in a conductor (the moment of insert and lockout) generates a variable electromagnetic field. Transmitter Telss-3 E was used to create impulses of a direct current circuit (Fig. GM-13 B).Technical parameters of EM equipment TELSS-3-E are given in Table GM-4.

***Table GM-4:** Technical parameters EM equipment TELSS-3-E*

Technical parameters of the TELSS-3-E receiver	
Number of channels	3

Word length ADC, bit	32
Dynamic range, dB	130
Preliminary amplifier amplification constant, dB	0; 12; 24; 36; 48
Sample period, msc	0,25;0,5;1;2;4;8;16
The peak length of record, readout on the channel	16384
The peak input signal at the underload amplification, V	±2,5
The noise level given in an inlet in a strip 0 - 125 Hz, mkV	0,08
Coefficient of nonlinear distortions,%	0,0005
Cross influences between channels, dB	130
Coefficient of inhibition of an in-phase signal, dB	120
Power supply system: an electrochemical battery, V	12
Power consumption, the V/channel	1
Service conditions, ^{0}C	– 40 to +70
Mass, kg	1,9
Overall dimensions, mm	406 x 330 x 174

Technical parameters of the TELSS-3-E current transmitter	
Amount of phases of an input voltage	3
Value of the rectified current	A – 400
Output voltage type	Unipolar

The transmitter power supply was from a diesel generator “Atlas Copco 100” through a reducing transformer (Fig. 14).

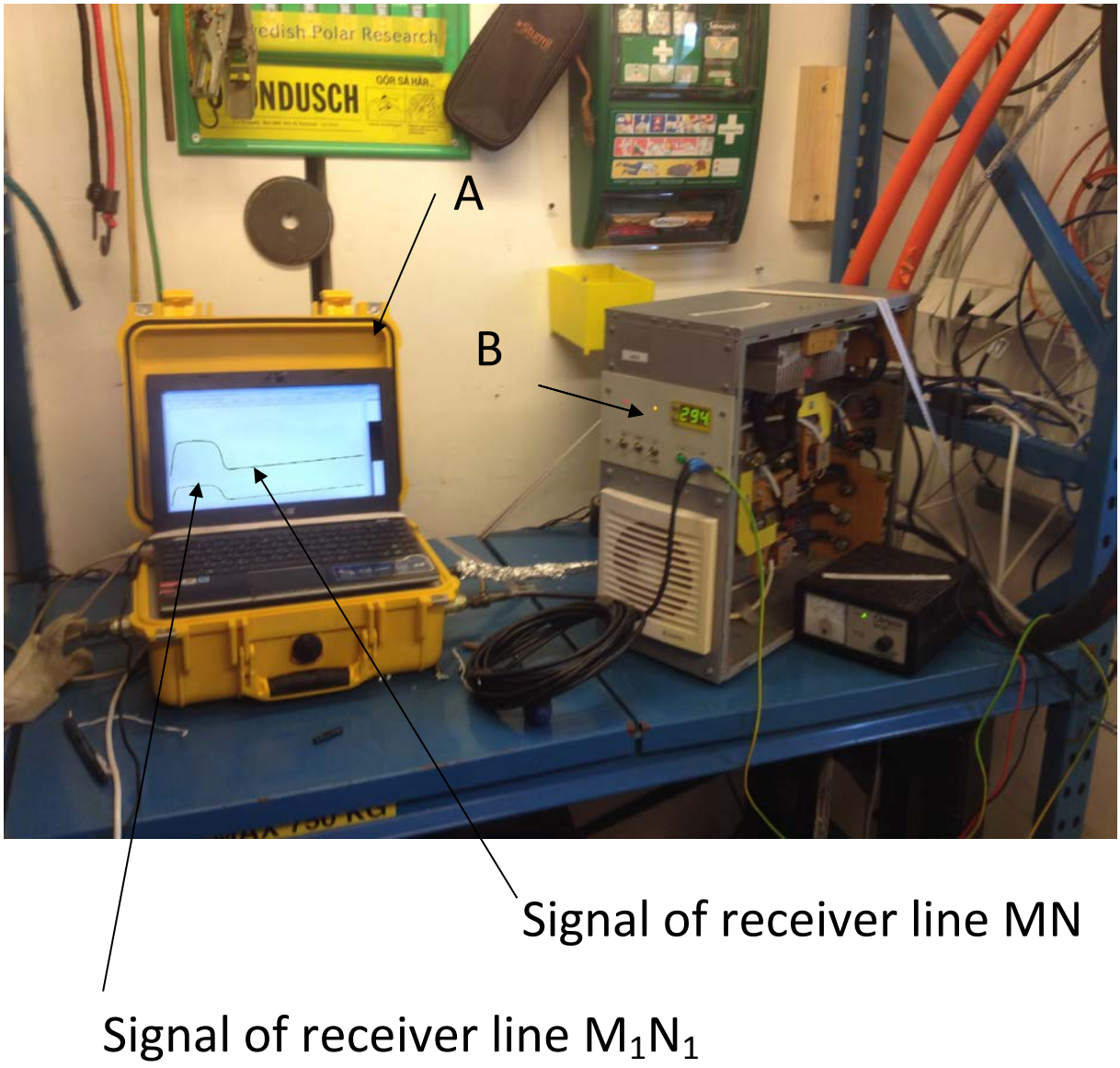

Figure GM-13: *TELSS-3 receiver (A) and transmitter (B) of electromagnetic field.*

Figure GM-14: *Generator (A) and transformer (B) of electromagnetic field*

The primary electromagnetic field was formed in water using a generating line (Fig. GM-15). The secondary electromagnetic field was measured by means of a receiving line (Fig. GM-15B). During data acquisition the operator watched that receiving and transmitting lines were parallel. (Fig. 16).

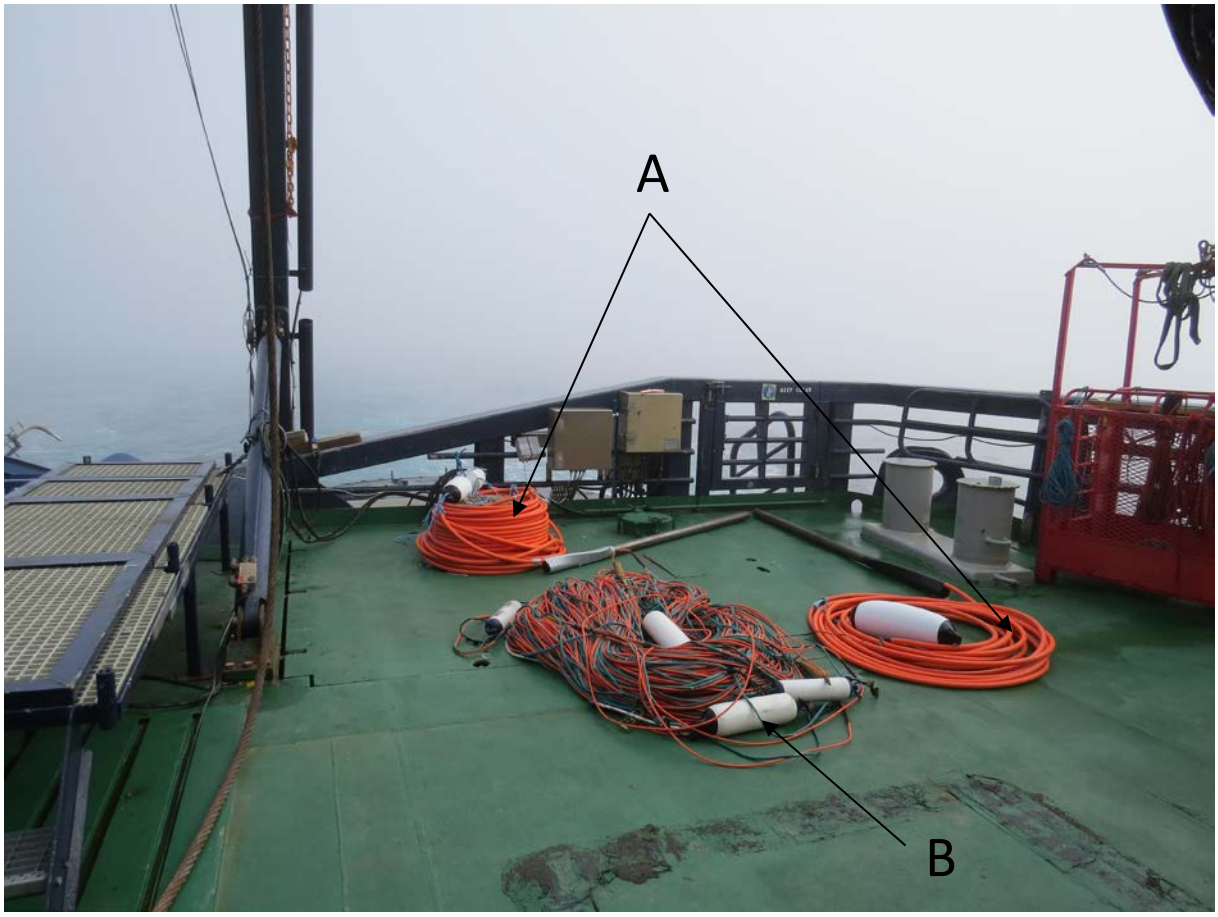

Figure GM-15: *Generator (A) and receiver (B) lines.*

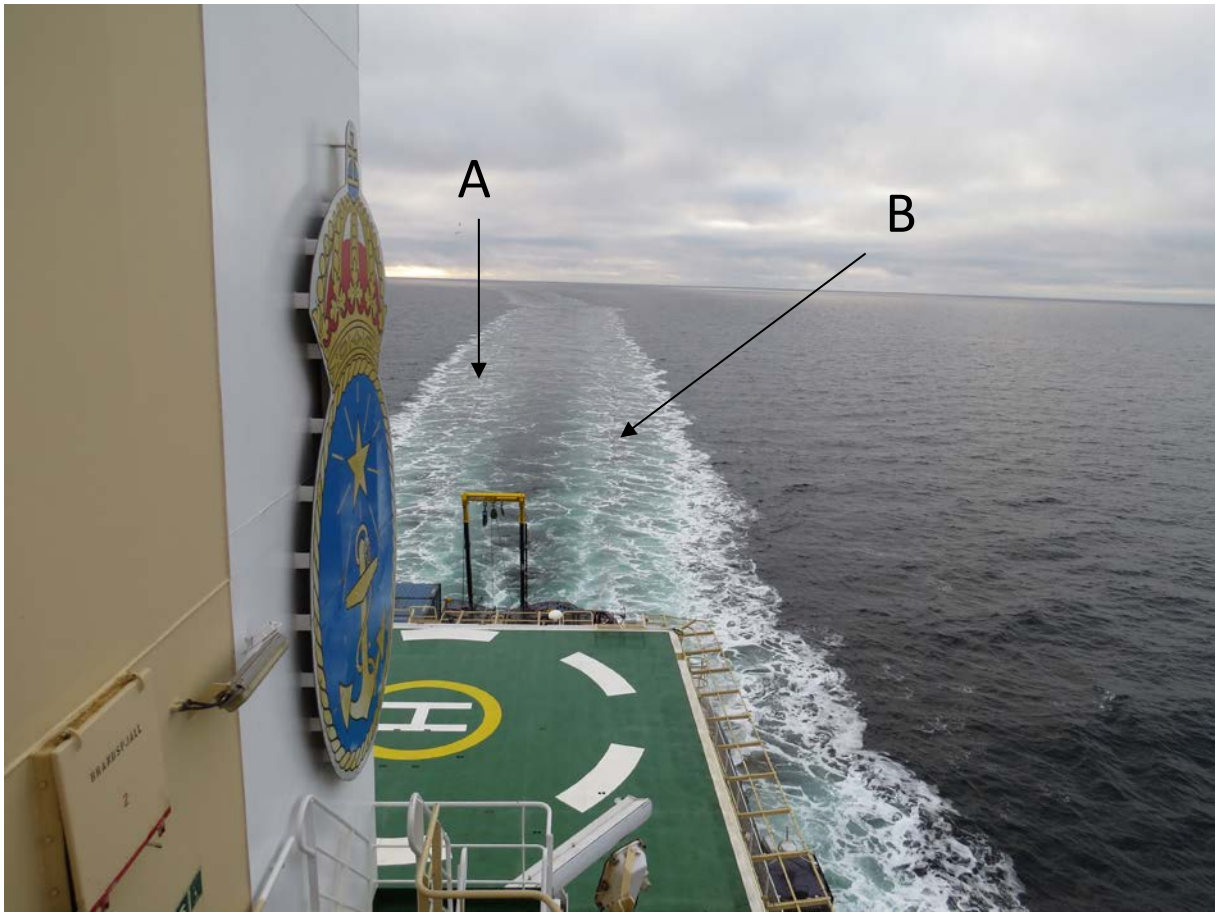

Figure GM-16: *Location of receiver line (A) and generator line (B) towed behind IB Oden during data acquisition.*

Operation

A 24-hour per day operation of the multibeam, including data post-processing, was achieved by six operators divided into three teams for four hours shifts (Table GM-5). Seafloor mapping with *RV Skidbladner* required two people while the seismic data acquisition required two people and additional assistance during launch and recovery of the streamer/airguns. The operation of the EK 80 mid-water sonar system (see WP-WC) was also carried out by the teams listed in Table GM-5. The EM system required one operator on each shift.

Table GM-5: *Multibeam watch standing and data processing teams.*

Team 1 (0-4, 12-16)	Björn Eriksson and Dennis Chernykh
Team 2 (4-8, 16-20)	Rezwan Mohammad and Kevin Jerram
Team 3 (8-12, 20-24)	Larry Mayer and Roman Ananiev
*RV Skidbladner*mapping	Martin Jakobsson and Tom Flodén
Seismic data acquisition	Tom Flodén, Arne Lif assisted by Alexey Khortov, *IB Oden* crew, and technicians from Swedish Polar Research Secretariat (Mikael Molin and Amund Lindberg)

Shipboard post-processing

Multibeam

Multibeam data were acquired on board *Oden* using Kongsberg Maritime's SIS Ver. 4.1.3 system control and acquisition software. The Kongsberg raw.all files were then processed onboard using a combination of CARIS HIPS/SIPS Ver. 8.1 and Fledermaus, Ver. 7.4.1. Data sets were divided into field sheets for cleaning in CARIS and generally cleaned through the application of the CUBE algorithm for initial cleaning in either CARIS or Fledermaus, followed by manual editing using the CARIS swath-editor or the Fledermaus 3-D editor. Cleaned data were then gridded at a resolution commensurate with the water depth (ranging from 5 m grids for shallow water sites to 40-50 m grids for deepest sites) and brought into Fledermaus for 3-D visualization and exploration. Gridded bathymetric products along with all track and sample data (CTDs, XBTs, core stations) were brought into a Geographical Information System (ArcMap 10.2.1) and viewed within the context of the IBCAO Ver. 3. Arctic bathymetry (Jakobsson *et al.,* 2012). All data were processed using a Polar Stereographic projection with a true scale at 75°N and horizontal datum of WGS 84 (Figure GM-17).

While the quality of most of the multibeam sonar data acquired was high, some data quality problems were encountered. The two most serious issues were "punch-through" or over-penetration of the nadir beams in shallow water and the appearance of "horns" (positive features that parallel the track on either side of the nadir beam). These issues will be discussed further in the section titled "Multibeam Data Quality Issues." Aside from these issues, there was the expected degradation of data quality while surveying in ice or at high speed.

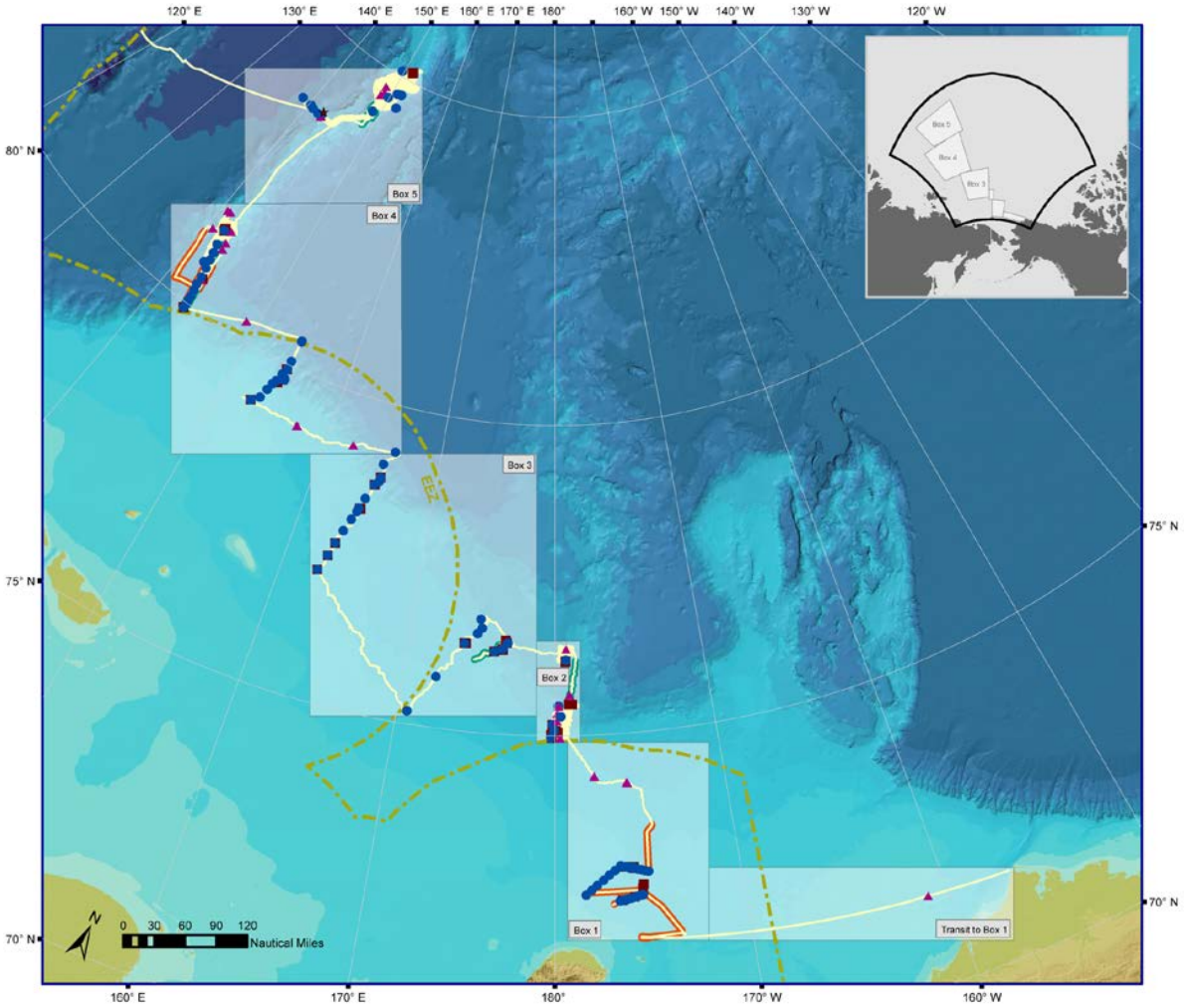

***Figure GM-17**: Overview of SWERUS-C3 Leg 2 track, departing Barrow 21 August 2014 until crossing into Russian EEZ enroute to Tromsö 27 Sept. 2014. Oden arrived Tromsö 3 October 2014. Multibeam sonar, high-resolution sub-bottom profiles and EK80 water column mapping was done along entire track. Location of airgun seismic (green lines) and EM profiles (orange lines) are marked. CTD (blue dots), XBT (purple triangles) and coring stations (brown squares) are also displayed.*

Sound velocity corrections

The multibeam sonar requires a detailed knowledge of the speed of sound in seawater to convert the travel-time measurements it makes into true depths, to calculate ray bending due to refraction in the water column (and thus calculate the proper location of the measurement on the seafloor) and to properly calculate the steering angle of the beam at transmit. For the most part, sound speed profile information for SWERUS-C3 Leg 2 was provided to the EM122 through the data collected by CTD measurements supplemented by eXpendable BathyThermograph (XBT) drops (see the WP PO section for a description of the CTD system and measurements made). The sound speed of the water at the transducer head was monitored continuously by an Applied Micro Systems LTD sound velocity probe located within the sea-water intake in the ship's hull. During Leg 2 a total of 88 CTD stations were occupied (see WP PO). When the real-time display of the SIS indicated a problem with the sound speed profile (either noticeable refraction in the profile or a discrepancy of more than 10 m/sec between the upper values of the sound speed profile collected with the CTD and the sound speed

from the AMS probe) an eXpendable BathyThermograph (XBT) was typically launched to provide updated profile information. Salinity from the nearest (or most appropriate CTD) was used to supplement the XBT data and generate a sound speed profile. Additionally, the temperature and salinity of the intake water was displayed in real-time in the ArcMap GIS providing useful guidance for when the sound speed profile should be updated. During Leg 2 XBT measurements were made using T-5 probes in deep water and T-6 probes in shallow water. In all cases (CTD and XBT) the sound speed had to be calculated from measured temperature, salinity and depth data. The sound speed formula used for this conversion is that provided by UNESCO (Fofonoff and Millard, 1983). A Python script does this conversion, bins and thins the data, and then extends the profile to 12000 m depth as required by the SIS system.

Sub-bottom profiles

High-resolution subbottom profile data were collected with the SBP-120 subbottom system using Kongsberg Maritime's SBP/Topas Ver. 1.5.3 system control and acquisition software. The Topas software was further used to automatically convert the raw SBP120 data files into the industry standard SEG-y data format for further processing. On board the SEG-Y files were imported into the NRCAN SEGyJP2 software package authored by Bob Courtney of Natural Resources Canada. This software package also allows for some gain adjustments during conversion and also allows lines to be combined (or segmented) for ease of interpretation. It also provides a JP2 viewing tool that offers further opportunities to enhance the image produced (e.g. Figure GM-18). The output of this process was then used for core site selection, initial interpretation and for combining with seafloor bathymetry and water column imagery (see discussion in WP WC).

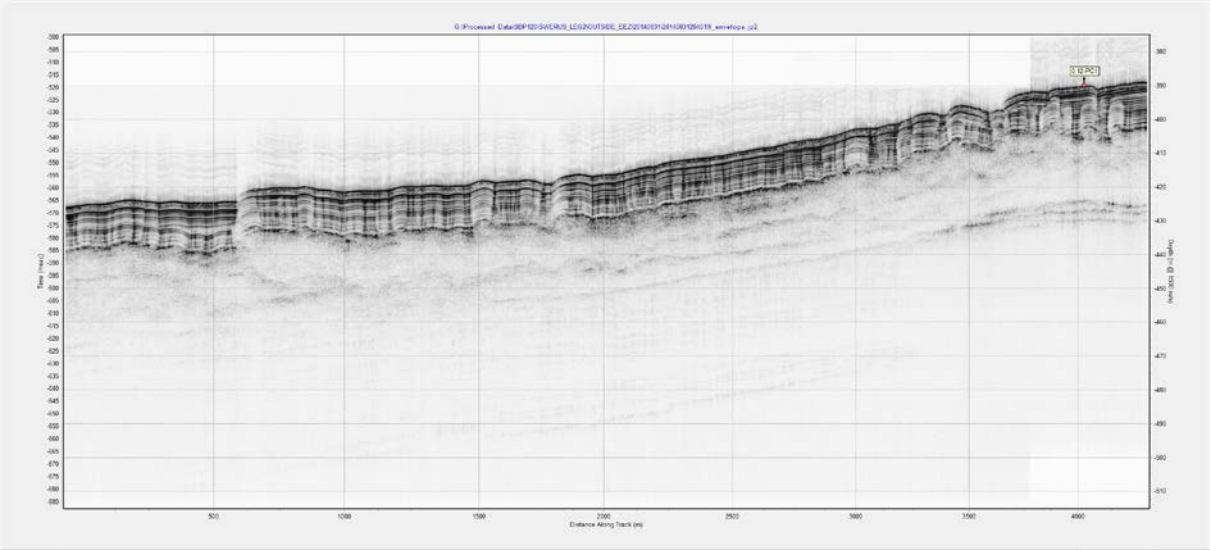

Figure GM-18*: Example of shipboard processing of SBP-120 high-resolution profiler data.*

Seismic reflection profiles

The Meridata acquision system MDCS ver. 5.2 was used for data acquisition and storage of seismic profiler data. The reflection seismic data was recorded in the Meridata native file system. All recorded seismic profiles were also converted to standard SEG-Y format. Data were collected and stored in a Polar Stereographic projection (Table GM-6).

Table GM-6. *Polar stereographic projection parameters used in the Meridata acquisition system MDCS ver. 5.2.*

Projection: North Polar Stereographic
Latitude of origin: 0
Longitude of origin: 0
Latitude of true scale: 75°N
False X: 0; False Y: 0
Scale reduction factor at the pole: 0.982966757777337
Horizontal datum: WGS84

Electromagnetic

Along with the electromagnetic soundings time was recorded permitting synchronization with navigation. The accuracy of time synchronization between the EM system and the GPS is on the order of 1 second. In total, 535 628 electromagnetic soundings were acquired over the Herald Canyon and Lomonosov Ridge. Preliminary analysis of the EM data was made in the software "Test". The dependences E (t) are converted in dependences Ro (t) on this step, where E (t) – curve of dependence of the signal in an receiver line from time for each point of sounding, and Ro (t) - curve of dependence of the apparent resistivity from time for each point of sounding. Only typical curves of apparent resistivity have been converted during the expedition The result of converting of typical curves of apparent resistivity is shown on Figure GM-19.

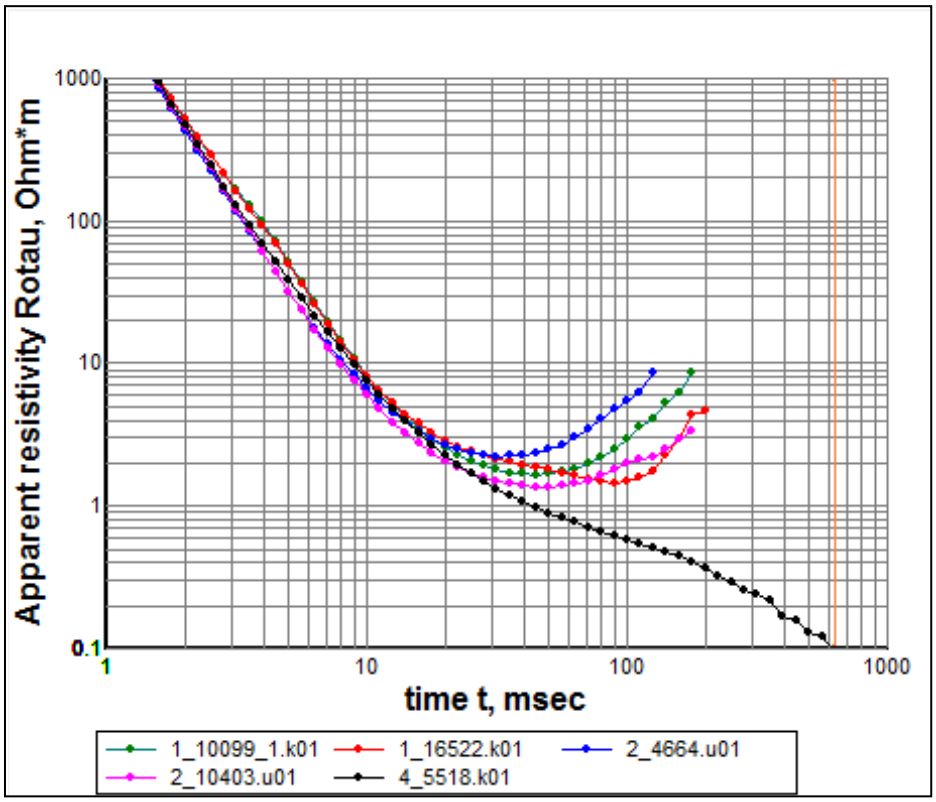

Figure GM-19: *Typical curves Ro (t) for Herald Canyon.*

WP WC (Water Column Mapping)

The Water Column Mapping program on Leg 2 has been designed to address the SWERUS-C3 objectives through mapping the spatial distribution and geologic context of gas seeps in the East Siberian Arctic Ocean as well as attempting an new approach that may enhance the estimates of the flux of gas emanating from the seeps by providing acoustic information related to bubble size distribution. The Water Column Mapping team used an array of tools to address these objectives including the EM122 multibeam sonar, the SBP 120 high-resolution subbottom profiler and an EK80 broad-band split-beam sonar. The EM122 on the *Oden*, described in detail in the Geophysical Mapping section has, in addition to its seafloor mapping capabilities, the ability to also map acoustic targets in the water column. Natural gas seeps have been shown to be very strong acoustic targets that can often be identified in multibeam sonar water column imagery. From these data the areal distribution and density of natural seeps can be mapped directly in the context of seafloor bathymetry. Additionally, data from the SBP120 high-resolution sub-bottom profiling system (as well as data from data from single channel seismic reflection profiling system) will be integrated with the midwater data to better understand the relationship of gas in the sediment column to gas seeps observed in the water column.

The EK60 and the EK80 were calibrated on Leg 2 with a calibration sphere (see details below). The calibration process makes it possible to quantify the acoustic target strength of gas bubbles within an ensonified volume such as a plume of gas bubbles rising from a seep.

These observations can be used to examine the spatial (and temporal, for seeps observed multiple times) variability of gas seep 'strength'. With knowledge of bubble size distribution, these target strength observations can then be used to make quantitative estimates of gas flux. The EK80 provides broadband information that should provide higher resolution detection of targets and most importantly, allow for estimation of bubble size distribution. Gas seep target strength measurements made across a wide range of frequencies can be inverted for estimates of bubble size distribution and, subsequently, estimates of free gas within the plume. Frequency-dependent changes in the target strengths of gas bubbles rising through the water column may also help constrain models for the evolution and fate of gas bubbles as they rise to the surface and will help determine what fraction of gas exiting the seafloor is capable of reaching the atmosphere.

Specific tasks of the Leg 2 Water Column Mapping Work Package include:

1) Mapping the areal distribution and density of natural gas seeps along the full cruise track, using the EM122 and EK80.
2) Determining the relationship of the distribution of gas seeps with the distribution of gas seen in the sediment column through seismic profiling (low and high-frequency)
3) Making quantitative measurements of acoustic target strength from gas seeps using the EK80.
4) Quantify absolute (EK80) and relative (EM122 and SBP120) depth dependent changes in seep target strength, in order to constrain changes in bubble size distribution for gas rising through the water column, and ultimately attempt to estimate gas flux rates.

Equipment

Multibeam, sub-bottom profiling, and seismic profiling systems

(Described in the Geophysical Mapping Work Package Section)

EK60 Echosounder

The EK60 echosounder on the *Oden* is a split-beam scientific echosounder produced by Kongsberg Maritime that is typically used for fish stock assessment and can be coupled with a number of different frequency transducers. On *Oden*, the EK60 is coupled with a Simrad ES18-11 transducer with a nominal -3 dB beamwidth of 11° at 18 kHz. The ES18-11 transducer is mounted on the ice keel at Frame 93, 60 cm starboard of the center line (Fig. WC-1). The EK60 transceiver (General Purpose Transceiver or GPT) is mounted in a rack in the "tween deck" accessible through the hatch in the gym at approximately Frame 83 (Fig. WC-1). The server that runs the EK60 is located in the "Apparatrum" on the fifth deck.

The EK60 echosounder has a maximum bottom detection range of approximately 7000m at 2000W of transmit power and a pulse length of 8.21 msec. The split-beam capability allows for phase measurements on individual targets and thus positioning of targets with mechanical angle resolution of approximately 0.1° within the beam. This positioning capability allows the target strengths of individual targets to be compensated for their positions relative to the main response axis and, thus, recorded target strengths can be used to compare the relative strength of individual targets. The EK60 can also be calibrated using a calibration sphere (see details below) allowing the acoustic returns from targets to be expressed as absolute target strength values. The EK60 was used extensively on SWERUS-C3 Leg 1; a description of its use can be found in the Leg 1 cruise report.

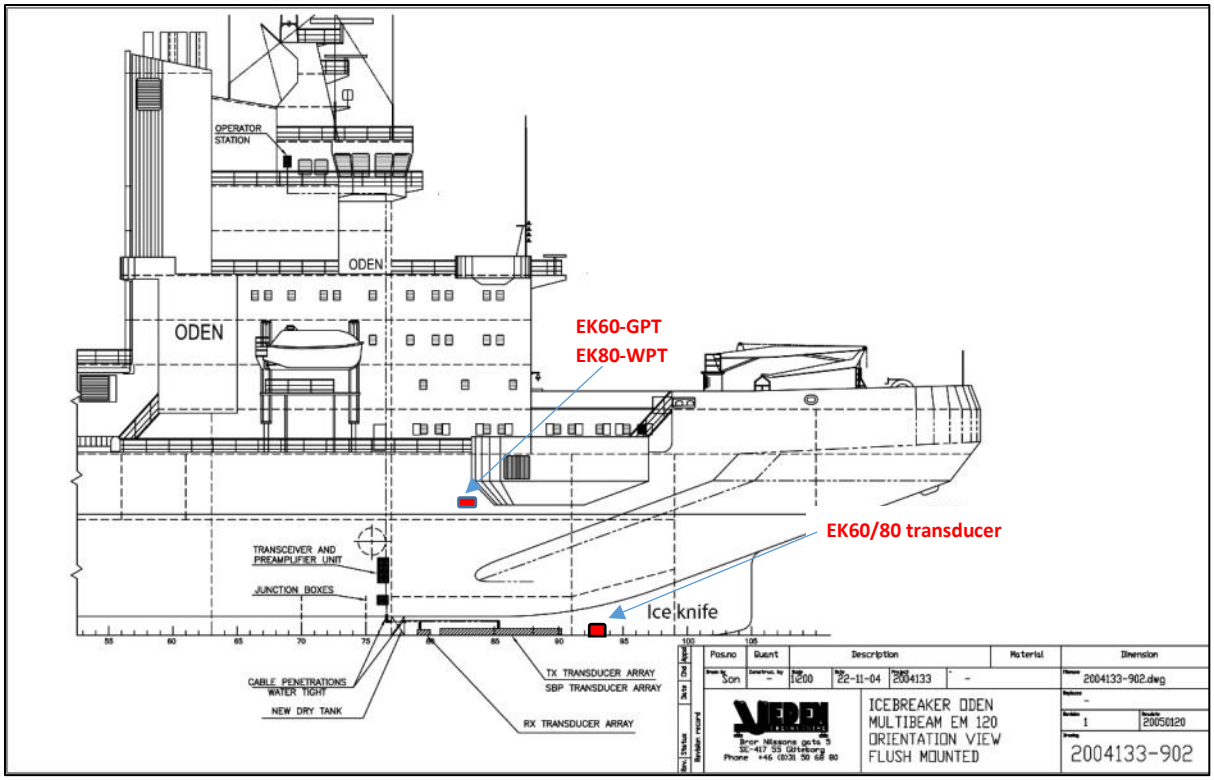

Figure WC-1: *Location of EK60/80 transducer on Oden hull and the EK60 GPT and EK80 WBT in the tween deck space.*

EK80 Echosounder:

For SWERUS Leg 2, the transceiver of the the split-beam echosounding system was upgraded to operate in a broadband mode. In this mode the ES18-11 transducer on the *Oden* can operate over a much broader range of frequencies. In it original mode, the system on the *Oden*, is capable of

transmitting and receiving narrow band (250-1000 Hz) pulses only at the transducer center frequency (18 kHz). The new wideband transceiver (WBT) is designed to achieve a frequency range of approximately an octave but was meant for use with composite transducers at frequencies of 70 kHz and above. Nonetheless, tests of the new WBT demonstrated that significant bandwidth could be achieved at lower frequencies with traditional (Tonpilz) transducers like those used with the ES18-11 on the *Oden.*

The prototype WBT was interfaced to an ES18-11 transducer in the UNH test tanks and used to transmit linear frequency modulated acoustic pulses between 10-30 kHz as the ES18-11 was rotated from -90° to +90° along its equator. The tests demonstrated that the main beam behaved as expected, with a 1-way -3 dB beamwidth that varies smoothly from 6° near 30 kHz to 19° at 10 kHz, with maximum sidelobe levels of -18 dB near the design frequency (close to a theoretically predicted value of -17 dB). Above 22 kHz, increased sidelobes (or suppressed grating lobes) that are likely due to the echosounder construction (44 individual Tonpilz transducer elements) appear, but these sidelobe levels are still lower than -15 dB (1-way).

The tests also revealed that the frequency-dependent figure of merit (combined transmit and receiving response, Figure WC-2) for the ES18-11 is relatively flat between 16-22 kHz. Field trials conducted by the Leg 2 Water Column team at the University of New Hampshire just before the departure of Leg 2 demonstrated that the WBT was capable of producing an optimal response from a target sphere between approximately 15 and 30 kHz and this was the band chosen for operations on SWERUS Leg 2.

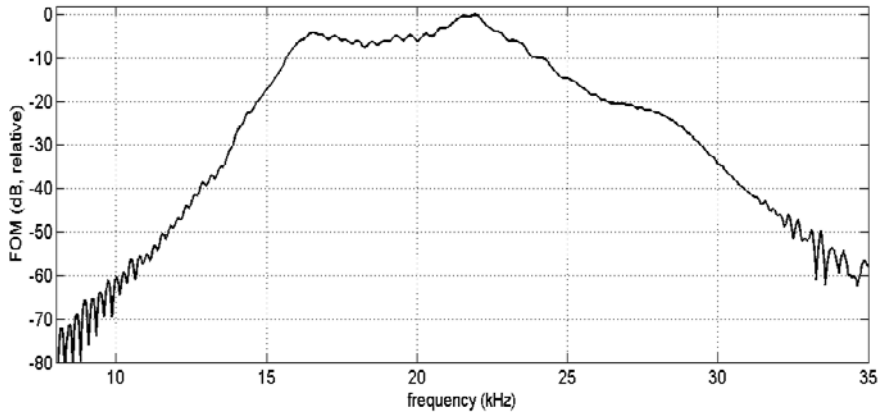

Figure WC-2: *Figure of merit (combined transmit/receive response) of ES18 using WBT in decibels, relative to its peak value.*

Installation of EK80

The WBT was installed in the same rack as the EK60 GPT (in the tween deck at about Frame 83) with the GPT shifted to a lower position in the rack and the WBT mounted on a specially constructed mounting plate above the GPT (Fig. WC-3).

Figure WC-3: *EK80 WBT installed in rack with EK60 GPT in tween deck below gym. Left – front view of rack with front door open – GPT is behind gray panel on bottom. Right – back view with back door open – GPT on lower level – WBT on upper level.*

Conveniently, the wiring of the ES18-11 transducer to the WBT is the same as for the GPT so the swap between the two units simply involved powering off, swapping the large Amphenol connector and Ethernet connectors and powering the other unit back on. We initially had concern that the long run of CAT-5A cable between the WBT and the server (located in the Apparatrum on the 05 deck) would not support the bandwidth of the WBT. Fortunately, this was not a problem, enabling us to use the same wiring and servers for the EK80 as for the EK60.

Given the bandwidth of the EK80, we deemed it essential to synchronize the EK80 with the EM122 and SBP120. This was accomplished by connecting a spare cable that had been run from the EM122 transceiver in the engine room (Fig. WC-1) to the server rack in the Apparatrum. The synch out signal (5V TTL) was found on the EM122 connector plate (pins 1 and 2) and the spare cable connected to this. On the other end of the cable a serial port was wired in and connected to the EK60/80 server providing the necessary EM122 synch pulse for the EK60/80 to run in 'slave' mode.

The prototype EK80 software was installed on the EK60 acquisition computer in the Apparatrum. This software is still in development and has a number of known problems but we have work-arounds for most of them. Throughout the cruise, the EK80 software was run and monitored from the multibeam sonar watch-standers' station on the bridge. The hardware performed flawlessly throughout the 45 day program with only one hard restart required; the software experienced infrequent crashes (particularly when crossing the International Dateline) but was easily restarted and with minimal data loss.

The EK80 collects a very large amount of data (typically about 3 GB per hour); to store these data a dedicated Netgear NAS device with approximately 10.9 TB of storage capacity was placed in the Apparatrum next to the server rack and connected to the EK60/80 through the shipboard network.

Operation

The wideband EK80 data collection was monitored by the underway geophysical watch team (see WP-MG for details). The watch team changed recording range as depth changed and monitored the records for evidence of gas seeps or other midwater targets. For most of the survey the EK80 was run in frequency-modulated (FM) mode with maximum pulse length (8.192 msec), and maximum power (1975W) and a start frequency of 15 kHz, stop frequency of 30 kHz, and fast ramping. In

shallower water the pulse width was occasionally lowered to 4.096 msec and the power level decreased to 987.5W. All pulse length and power setting changes are automatically logged with the data files and should be noted in the electronic log kept by the watch standers.

Calibration of the EK60/80

Overview

As discussed earlier, one of the advantages of using the EK60/80 for mapping gas seeps is the fact that the system can be calibrated so that absolute values of acoustic backscatter and target strength can be calculated for ensonified targets. The calibration process for the EK60/80 is not simple on a vessel the size of the *Oden* but was carried out successfully twice during SWERUS Leg 2, once in shallow water while at anchor off Barrow and again, on 12 September 2014, in deeper water while drifting. Below we provide an overview of the calibration process; Appendix WC-1 provides a detailed description of the procedures undertaken on the *Oden,* so that they can be repeated if necessary.

The acoustic estimate of gas flux from a seep depends primarily on the distribution of bubble sizes and the acoustic scattering strength ('target strength', or TS) of a bubble at each size in the distribution. To maximize utility of the EK60 and EK80 gas seep observations from both legs, target strength calibration data were collected for both systems using a 64 mm copper sphere suspended on high-strength line in the echosounder field of view (FOV) on the main response axis (MRA). Differences between the theoretical and observed TS of the sphere throughout the echosounder FOV will provide a basis for beam pattern corrections during later data analysis. The details of the procedures and equipment used for calibration of the EK60/80 on the *Oden* for SWERUS Leg 2 can be found in the document *"Sphere Deployment for EK60/80 Target Strength Calibration,"* Appendix WC-1 of this report.

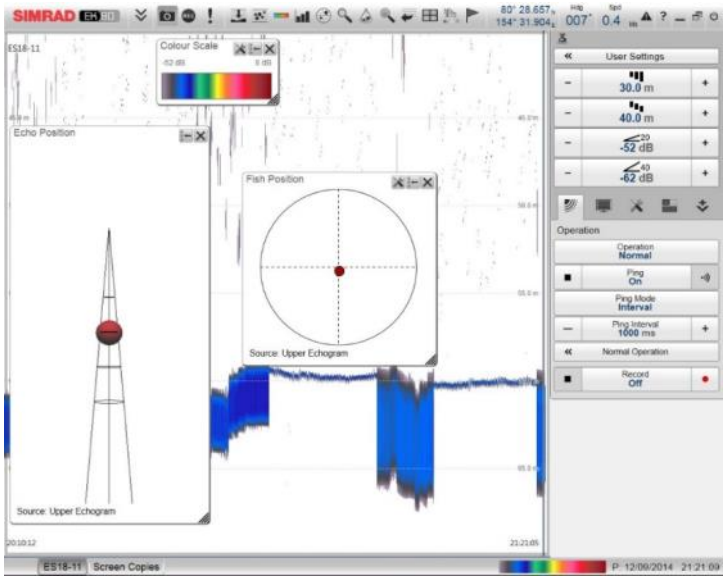

Figure WC-4: *Example of calibration sphere being ensonified at Maximum Response Axis (MRA) under the Oden. This example is from calibration carried out on Oden on 12 Sept. 2014. Note that the sphere size in the software image is indicative of acoustic scattering strength, not the physical sphere size. The EK80 WBT installed in a rack with the EK60 GPT in the 'tween deck' area below the gym.*

The first calibration was carried out under calm conditions on 21 August 2014 at anchor off Barrow, Alaska, prior to getting underway for the Leg 2. A current of approximately 1 knot severely complicated sphere deployment and control in the echosounder field of view, resulting in damage to two outrigger rods used to provide line clearance from the hull. Additionally, the sphere depth was limited by the bathymetry and current.

After discussion with Tom Weber (UNH CCOM), it was decided to prioritize collection of sphere data on the MRA over providing coverage throughout the FOV. The second calibration was performed while drifting on 12 September 2014; swell height was approximately 1 m and current relative to the ship was less than 0.5 kt, providing substantially more favorable conditions for sphere positioning compared to the Barrow calibration. Table WC-1 provides an overview of the EK60 and EK80 operational settings for which sphere data were collected during both calibrations.

Table WC-1. *Split-beam echosounder settings used during target strength calibration*

Date	System	Frequency (kHz)	Power (W)	Pulse Length (μs)	Ramping
21 Aug 2014	EK60	18	1000	512	-
		18	1000	1024	-
	EK80	15-30	987.5	2048	Fast
		15-30	987.5	4096	Fast
		15-30	987.5	8192	Fast
12 Sept 2014	EK80	15-30	987.5	4096	Fast
		15-30	1975	4096	Fast
		15-30	987.5	8192	Fast
		15-30	1975	8192	Fast

An example of uncalibrated target strength for the sphere and its split-beam (phase difference) position within the echosounder FOV are shown in Figs. WC-5 and WC-6 for one configuration over one data collection period. Conductivity-temperature-depth (CTD) profile data collected immediately before each deployment will be used to calculate sound speed and acoustic absorption profiles as well as the theoretical acoustic scattering strength of the sphere under environmental parameters at its depth and frequency of ensonification during each data collection period. The observed sphere scattering strength will be corrected for range and acoustic absorption and then compared to its theoretical value to provide target strength corrections near the MRA. Finally, a transducer model will be applied to incorporate TS offsets on the MRA and provide target strength corrections across the entire echosounder FOV for each configuration. Similar calibrations of a Simrad ES18-11 transducer using EK60 and EK80 transceivers under more controlled conditions may be coordinated at the UNH acoustic test tank if additional laboratory data will be useful for transducer model application to *Oden* field data. The details of the procedures and equipment used to calibrate the EK60/80 on the *Oden* for Leg 2 can be found in Appendix WC-1.

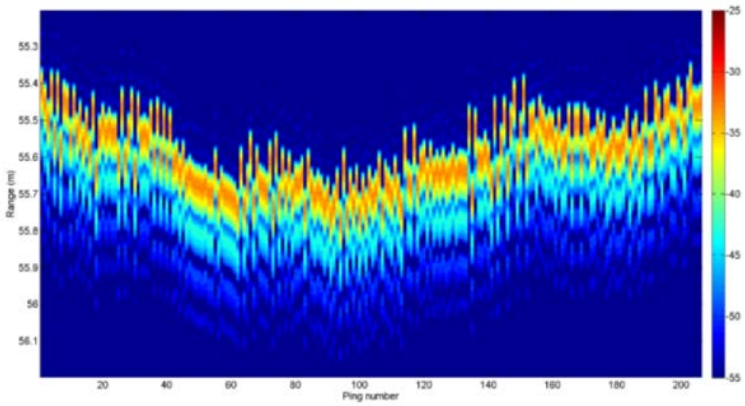

Figure WC-5: *Uncalibrated target strength (dB) for the sphere over one data collection period. Low-frequency fluctuation of the sphere range is due to drifting near the MRA, whereas high-frequency fluctuation of the sphere range is due to sea surface swell and accompanying stresses on the sphere support lines.*

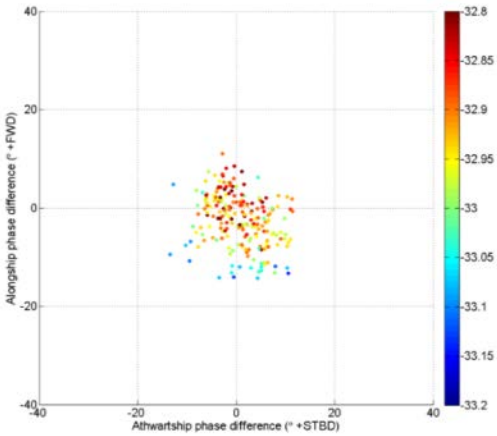

Figure WC-6. *Observed target strengths for sphere detections near the MRA over the data collection period represented in Figure WC-5. Phase difference is converted to target mechanical angle along each axis through the split-aperture relationship using sound speed at the transducer face; for reference, a 40° phase difference corresponds to a mechanic angle of approximately 3°.*

Initial Testing of EK80

Inasmuch as the EK80 is a prototype system that has never been operated with the EM122, we spent considerable time after installation evaluating the performance of the EK80 using different power and pulse length settings, background noise levels, and the potential of interference from the EM122 and the SB120 systems. As part of this exercise data were collected at all power settings and all pulse lengths at the first coring station between 0335Z and 0514Z on 25 August 2014) while the vessel was drifting and the EM122 and SBP 120 secured. Each combination of pulse length (0.512, 1.024, 2.048, 4.096, and 8.192 ms) and power (197.5, 395, 592.5, 790, 987.5, 1185, 1382, 1580, 1777.5, and 1975 W) was recorded for several minutes with the EK80 operating in stand-alone mode using a frequency range of 15-30 kHz with fast ramping.

In addition to these tests, EK80 data were recorded using CW and FM modes as well as with and without the EM122 and SBP120 and with and without synchronization. The purpose of these tests

were to better understand the performance of the EK80 as well as to ensure that it was not impacting the performance of the EM122 and SBP120 (or vice versa).

CW vs FM Mode and Effect of Pulse Length

During the testing phase data were collected in both the CW and FM modes of the EK80 (e.g., Figure WC-7). The comparison indicates the clear advantage that the broadband mode offers with respect to target resolution and discrimination (in this case biological scatterers). However, it was also noted that in broadband mode there was a strong pre-cursor to the bottom (blue area above red bottom on left side of Figure WC-7 and right side of Figure WC-8). This problem is exacerbated as pulse length increases (Figure WC-8). Despite this pre-cursor, the actual detected bottom (small black ticks above red zone of bottom) remained correct for the FM mode (Figure WC-7).

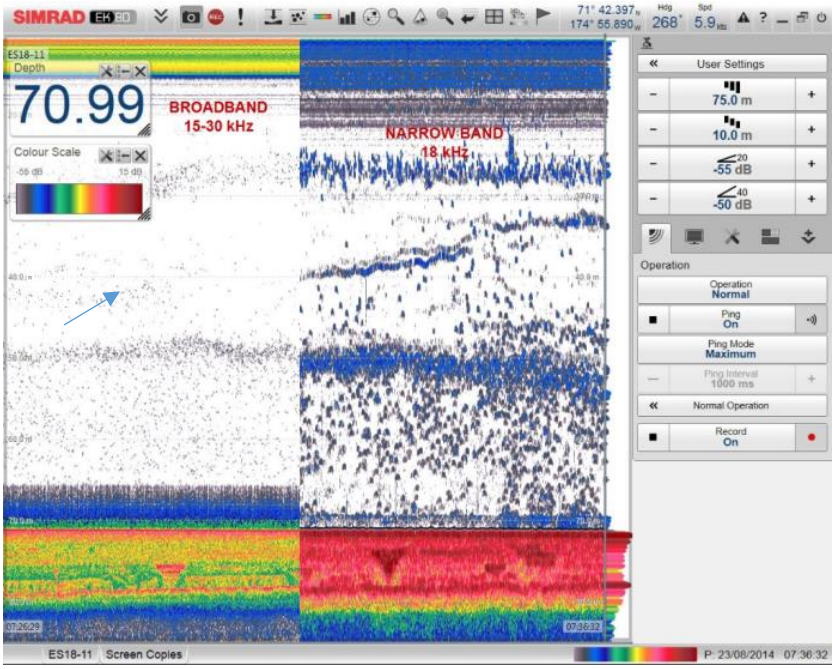

Figure WC-7: *Comparison of EK80 in broadband (15-30 kHz) mode (left) with EK80 in CW mode (18 kHz) with approximately 400 Hz of bandwidth. Note much higher resolution of individual scatterers with broadband mode.*

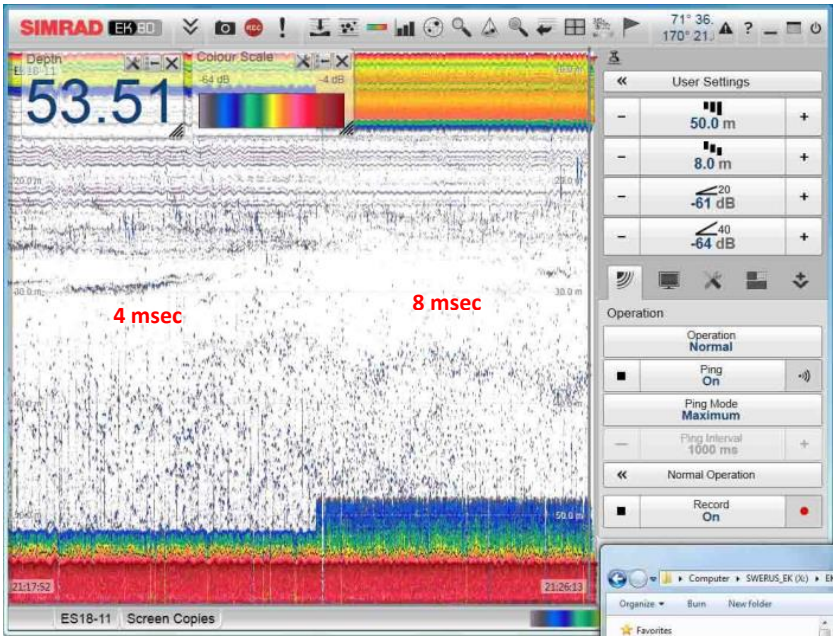

Figure WC-8: *Effect of pulse length on display of bottom on EK80.*

Interference between EK80 and EM122/SBP120:

A series of tests were run to better understand the interaction of the EK80 with the EM122 and SBP120. On 28 August 2014, between 2123Z and 2351Z, while drifting at a CTD station, data were recorded with and without synchronization and with the systems sequentially turned on and off. During these tests we were also able to examine the impact of the water jets on the EK80. Figure WC-9 shows the clear impact of synchronization (EK80 slaved to the EM122) on the EK80 with the multibeam signal randomly moving through the EK80 signal without synchronization (right side of figure). With synchronization, the multibeam return comes in at the seafloor level with the EK80 return (left side of figure). Figure WC-10 captures the impact of securing the EM122 and SB120 as well as the impact of the water jets which were turned on to help hold station during the CTD deployment. The test started with all systems (EK80, EM122 and SBP120) running in the normal modes with the EM122 acting as master synchronizing the transmit pulse of both the SBP120 and the EK80 (left on Figure WC-10). Removal of the synch (letting the EK80 run in standalone mode) resulted in increased noise in the EK80 but no apparent impact on the EM122 or SBP120. The EK80 was placed in passive mode (listening only) and it became clear that the apparent subbottom returns on the EK80 were actually the reception of the EM122 return by the EK80. The impact of the EK80 transmit on the EM122 is examined in the Geophysical Mapping section; at no time during normal survey operations did we see any impact of the EK80 on the EM122 or the SBP120.

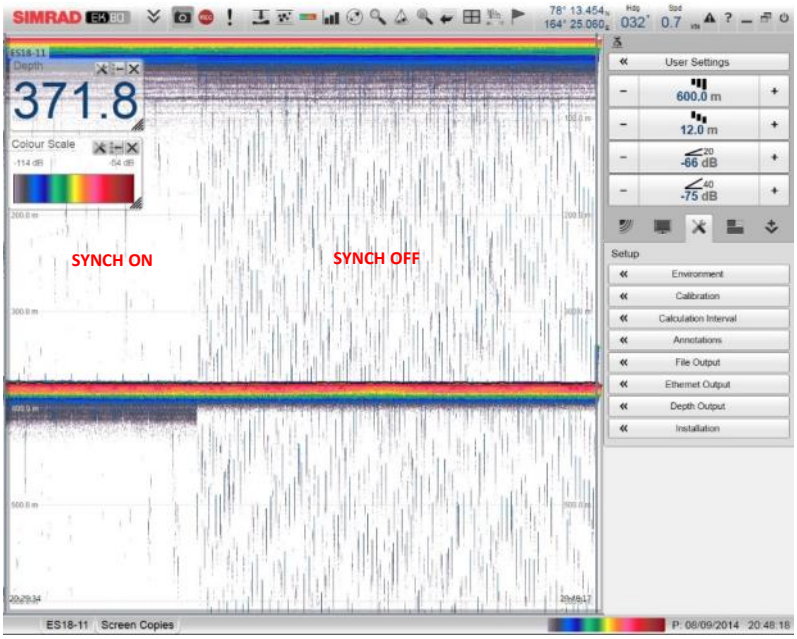

Figure WC-9: *Impact of removal of synchronization (EK80 slaved to EM122) on EK80 record.*

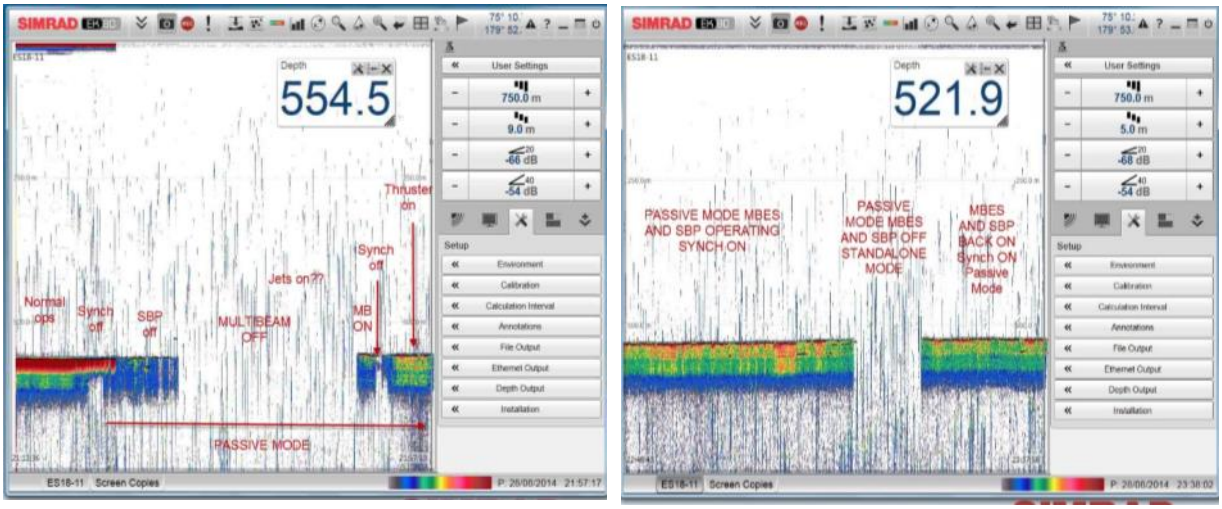

Figure WC-10: *Interference tests for EM122, SPB120 and EK80. Note high background noise levels that were result of water jets running*

Other sources of noise on the EK80

We also examined other sources of noise on the EK80 through operation in passive mode with the EM122, the SBP120 and the ship's echo-sounder secured (the ship's echo-sounder remained secured throughout Leg 2). These tests clearly indicated that in rough seas, at speeds greater than about 8 knots, there is significant hull noise on the EK80, most likely caused by bubble sweep past the transducer. It was noted that during turns (with no reduction of speed) this noise was greatly reduced probably the result of bubbles being diverted away from the transducer during the turn (Fig. WC-11). In smooth seas or with the vessel drifting, there is still a low level noise source throughout the EK80 record (left side of Fig. WC-9). Based on the frequency of occurrence (about 80 times per minute) and the spectral characteristics of the noise, we believe this noise source is the result of "steam hammers" originating in the steam valves that are warming the bunker fuel. This banging is clearly heard on the mess level of the *Oden*. Discussions with the chief engineer suggest that there is not an easy remedy for this.

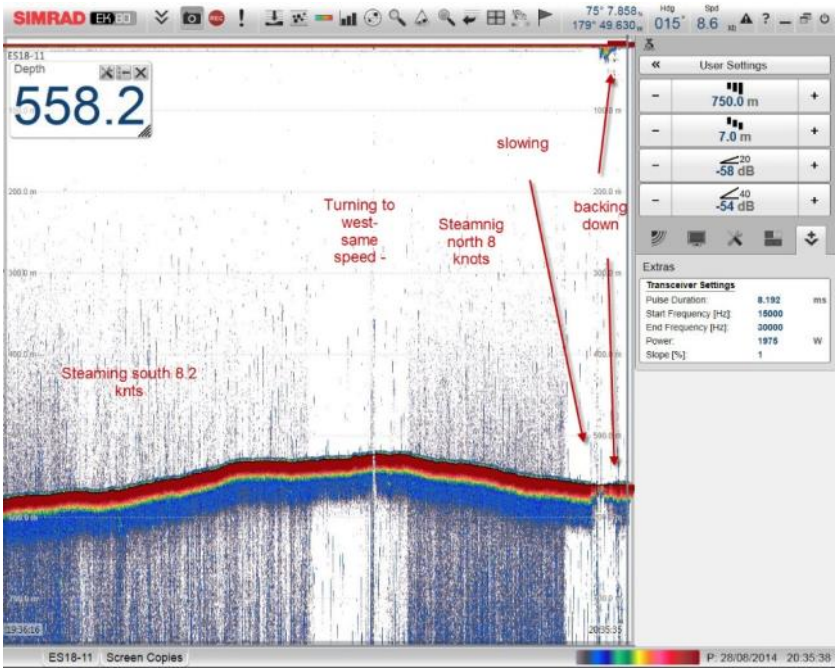

Figure WC-11: *Rough seas and speeds above 8 knots generate significant background noise on EK80, this noise disappears during turns indicating it is related to bubbles being diverted away from transducer during turn.*

Shipboard post-processing

EK80

The EK80 clearly showed the presence (or absence) of seeps without post-processing (e.g. Fig. WC-12). Some post-processing (using UNH Matlab code) was done on the EK80 calibration data and other sections of EK80 data to check that data were being collected appropriately. These steps showed that the calibration and normal survey data appear to have been collected successfully, but no further analysis has been performed on board. Because the EK80 is a prototype with no established processing code available, the UNH Matlab code used to parse the EK80 files is in an early stage of development. Parsing errors were encountered in several files, though it is believed the error stems from the parser and not a corruption of the file. These issues will require closer scrutiny and further parser development before major post-processing of EK80 data may begin. Furthermore, it is expected that commercially available post-processing software (e.g., Fledermaus FMMidwater) will accommodate EK80 data formats in future releases.

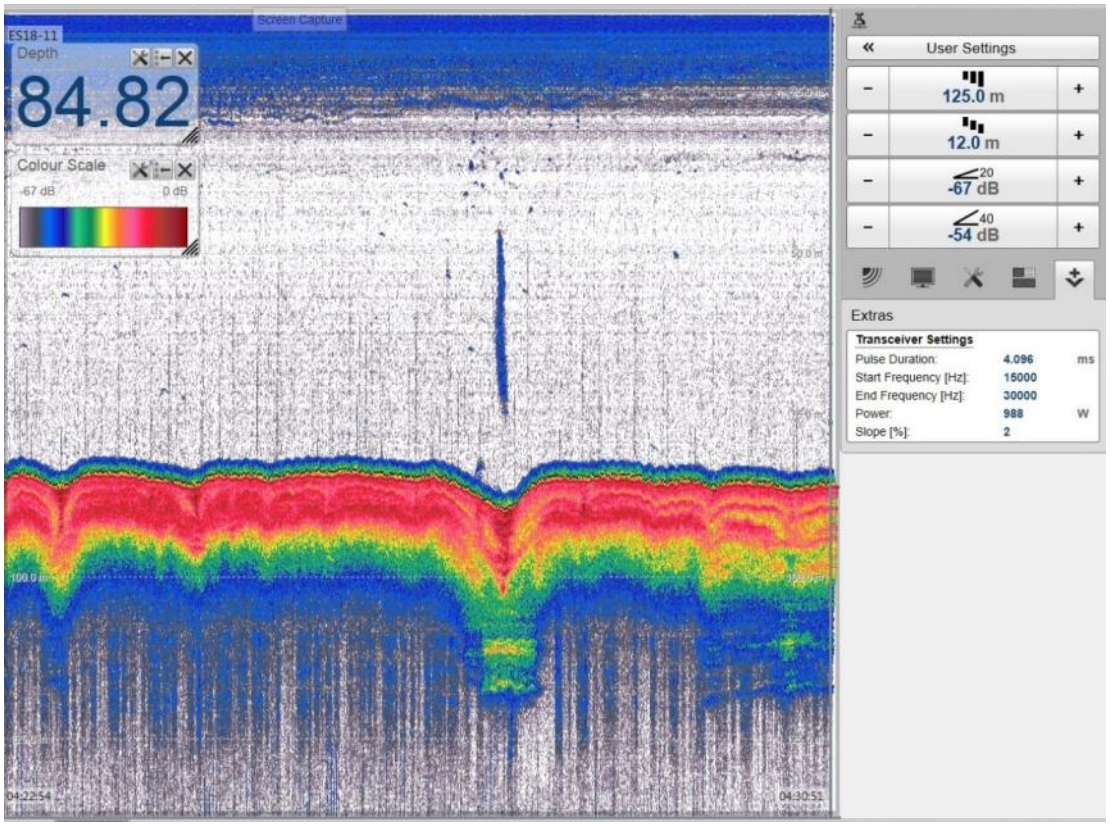

Figure WC-12. ***Example of gas seep as seen on EK80***

EM122 Water Column Data

The EK80 provided the primary tool for the identification of midwater targets. In those few areas where seeps were found (mostly Herald Canyon) and in areas where other interesting midwater targets were observed, EM122 data were brought into the QPS Fledermaus Midwater tool for extraction and subsequent placement of the target within the context of seafloor bathymetry (using

gridded bathymetry and the Fledermaus 3-D visualization tool (e.g. Fig. WC-16). The raw EM122 .all files were brought into QPS DMagic and a PFM and CUBE surface created for the seafloor bathymetry. Data were cleaned both automatically (with CUBE) and with additional editing with the QPS 3-D editor. Inasmuch as most of the seep data were collected in very shallow water (less than 100 m) the performance of the 12 kHz EM122 is not optimal in these water depths and significant data editing was required. Problems encountered included penetration below the seafloor of the nadir beam ("punch-through") and the appearance of "horns" (parallel elevated tracks) to either side of nadir. A discussion of these and other issues found with the multibeam bathymetry data can be found in the Marine Geophysics Work Package result section of the cruise report.

At the target sites identified by the EK80, EM122 water column data was brought into QPS-FMMidwater tool kit for extraction of midwater targets. Upon examination of the water column data it became apparent that the dual pulse mode used for most of the bathymetric survey work created problems in the identification of midwater target (there appeared to be leakage of the dual pings into each other creating a very noisy water column display – Fig. WC-13 top). The issue was addressed by using only the first ping of the dual swath mode for water column processing (Fig WC-13 bottom). This is a less than ideal solution because it cuts the along-track data density rate over targets in half.

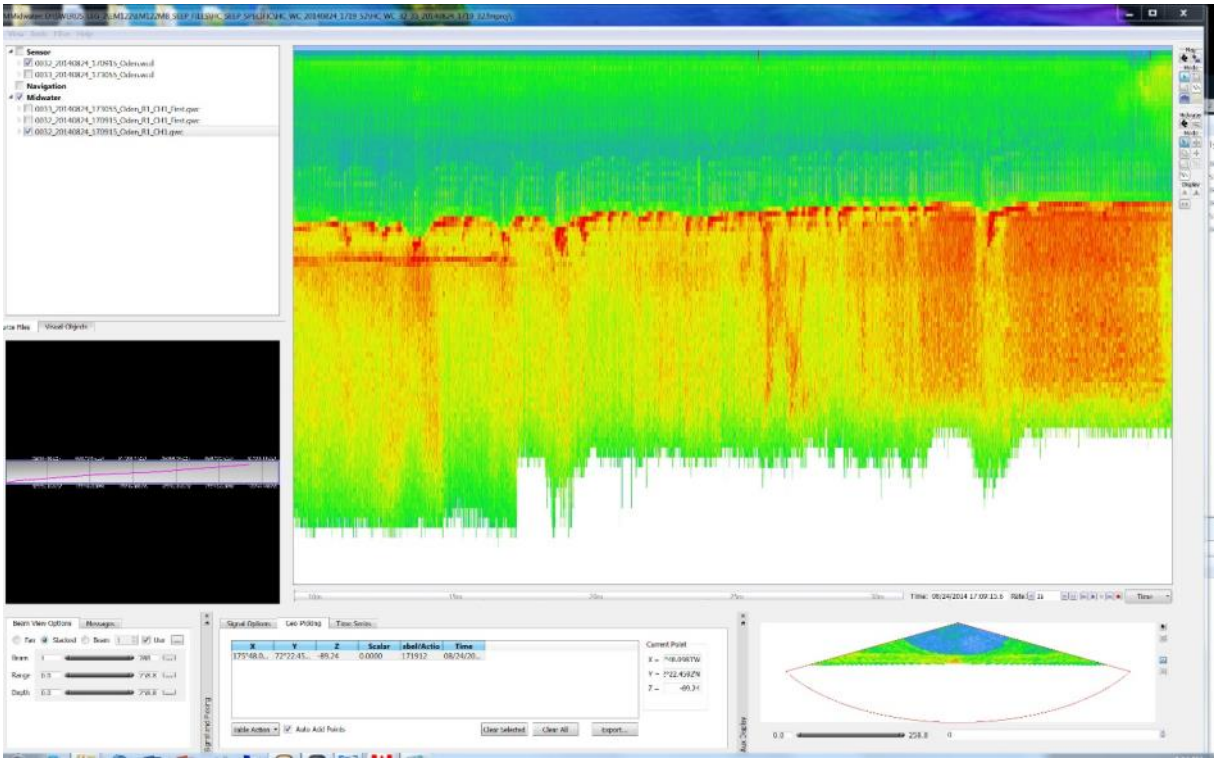

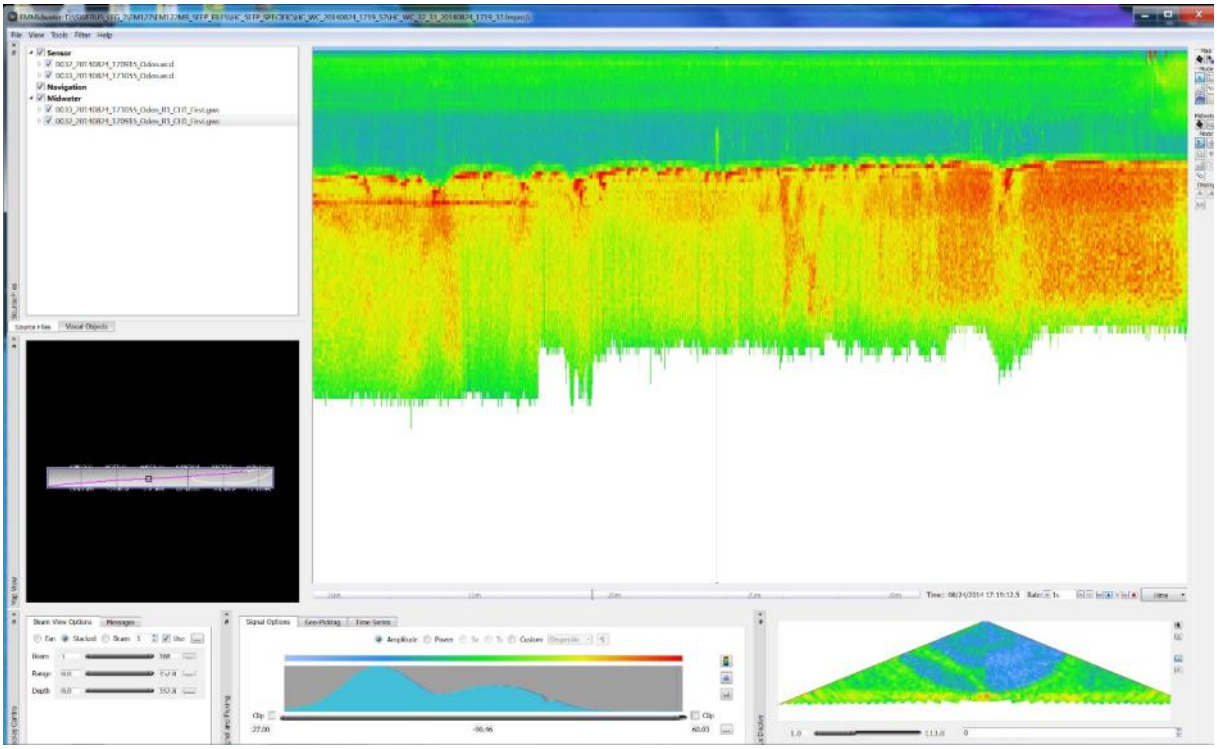

Figure WC-13. *Display of stacked water column data. Upper image is of both pings in dual swath mode- note high level of noise on alternative pings. Lower image is same data set processed using only single ping – water column targets are much more easily discernable in this mode.*

In addition to standard QPS-FM processing, UNH-Matlab code (written by Tom Weber) was run on water column data to further remove background noise and isolate midwater targets. Once targets were isolated they were exported as 3-D point clouds to be brought into the 3-D bathymetric scene.

For those lines that displayed midwater targets, the SBP120 high-resolution subbottom profiler data were brought into the Natural Resources Canada (Bob Courtney) SEGYJP2 software package and converted the JP2 images. The segment of these images corresponding to the bathymetric line that contained the midwater targets was extracted, georeferenced and also brought into the 3-D scene. Examples of this process will be shown in the results section below.

WP SC (Sediment Coring)

The SWERUS-C3 sediment coring program retrieved sediment cores at sites determined by geophysical mapping and along a set of depth transects. The main objectives of the Leg 2 coring program can be summarized in four main points:

1. Retrieve undisturbed sediment records for studies of Arctic Ocean paleoceanography, including the histories of bottom water temperature and sea ice distribution.
2. Retrieve sediment cores along depth transects from the continental shelf to approximately 1500 m down slope for studies of sediment physical properties, heat flow, and chemical properties of sediment and pore water to study the stability and presence of gas hydrates in slope sediments.
3. Retrieve sediment cores from areas subjected to grounding of deep drafting icebergs and/or ice shelves to date the ice grounding events.
4. Retrieve sediment cores from the shallow shelf to investigate the presence of gas.

The coring equipment used during Leg 2 involved two different diameter piston/gravity corers, a kasten corer and a multicorer.

Equipment

Piston/gravity corer

The Stockholm University piston/gravity coring system was used during the SWERUS-C3 expedition. The first version of this coring system was built 1996 for the *Arctic Ocean 96* expedition with *IB Oden* to take up to 12 m long sediment cores from the aft deck. The corer itself is capable of taking longer cores, but because this device is operated across *Oden's* fantail, the limited space between the winch container placed on the aft deck and the fantail limits the length of the corer that can be deployed. The corer has standard metric dimensions of barrel, screws and couplings. It has been upgraded several times since initially built. The latest upgrade was made in preparation for the SWERUS C3 2014 expedition. This recent upgrade makes it possible to switch between two different dimensions of the core barrel/liner system. The change between dimensions requires changing core barrel, couplings, liner and piston. In addition, the piston stop was redesigned as a part of the upgrade so it could be loosened in order to make it possible to push out the core liner using a metal rod. This feature makes the retrieval of sediment filled liners after each coring much easier.

The core head and the release arm remains the same between the two setups. The original liner dimension has an inner/outer diameter of 80/88 mm while the new wider diameter setup takes a liner dimension with an inner/outer diameter of 110/100 mm. Transparent polycarbonate liners were used for the smaller diameter while standard dimension PVC pipes were used for the larger during the SWERUS-C3 expedition. The core head can be loaded with lead weights of up to 1360 kg. The standard release arm is designed so that a trigger weight of 1/10 of the main core head weight is recommended. Hydrostatic safety releases are used to secure the release arm from triggering prematurely. However, in waters shallower than 300 m a safety pin that it is pulled just before the corer is lowered below the water surface used.

Two complete setups of the large diameter piston/gravity corer were brought onboard *IB Oden* for the SWERUS-C3 expedition and two setups of the "old" smaller diameter version. The piston/coring equipment was stored in a 20' container placed on the aft deck next to the launching cradle described below (Figure SC-1). Lead weights and liners were stored in other storage places on *IB Oden*. The piston corer in its launching cradle is seen if Figure SC-2. This support "cradle", was built

1996. A rail that launches the cradle was constructed and manufactured for the Lomonosov Ridge of Greenland (LOMROG) expedition 2007 to improve the safety of the coring procedure. The cradle with the corer is moving along the rail on nylon wheels. When the cradle reaches the end of the fantail it pivots and places the corer in a vertical position ready to be launched. The trigger weight corer is always launched before the cradle is brought to the position where it pivots. When the corer is in upright position it is lifted out of the cradle with a wire from the main coring winch that runs through a block in the A-frame. There were several problems with the coring winches and the A-frame block during SWERUS-C3. Figure SC-3 shows the different steps to launch the corer.

In addition to the main coring winch, a small winch is required to launch and recover the corer (Figure SC-4). However, this winch broke down at an early stage of Leg 2. It was replaced with a small battery driven winch (Figure SC-4), which normally is used to pull out the cradle on the rail. During Leg 2, the cradle was pushed out manually until it pivoted.

Figure SC-1*: Container with the piston/gravity corer stored. Four complete setups were stored in this 20' contain except for the lead weights and liners. The liners were made in 6 m long lengths to fit a multiple of 3 m, which is the length of each core barrel. This made the liners slightly too long to fit in a 20' container.*

Figure SC-2: *Stockholm University large diameter piston corer (center) resting in the deployment cradle. This large diameter corer can also be rigged as a gravity corer, seen to the right. The standard setup during Leg 2 of the SWERUS C3 cruise was to have both a gravity corer and a piston corer rigged and ready for deployment. In addition, the smaller diameter corer is seen to the left in this photo with a blue core head top. This smaller corer was only used once during Leg 2 to take a gravity corer at 1665 m water depth because the winch used could not handle the large diameter and heavier corer at depths deeper than approximately 1500 m (see winches).*

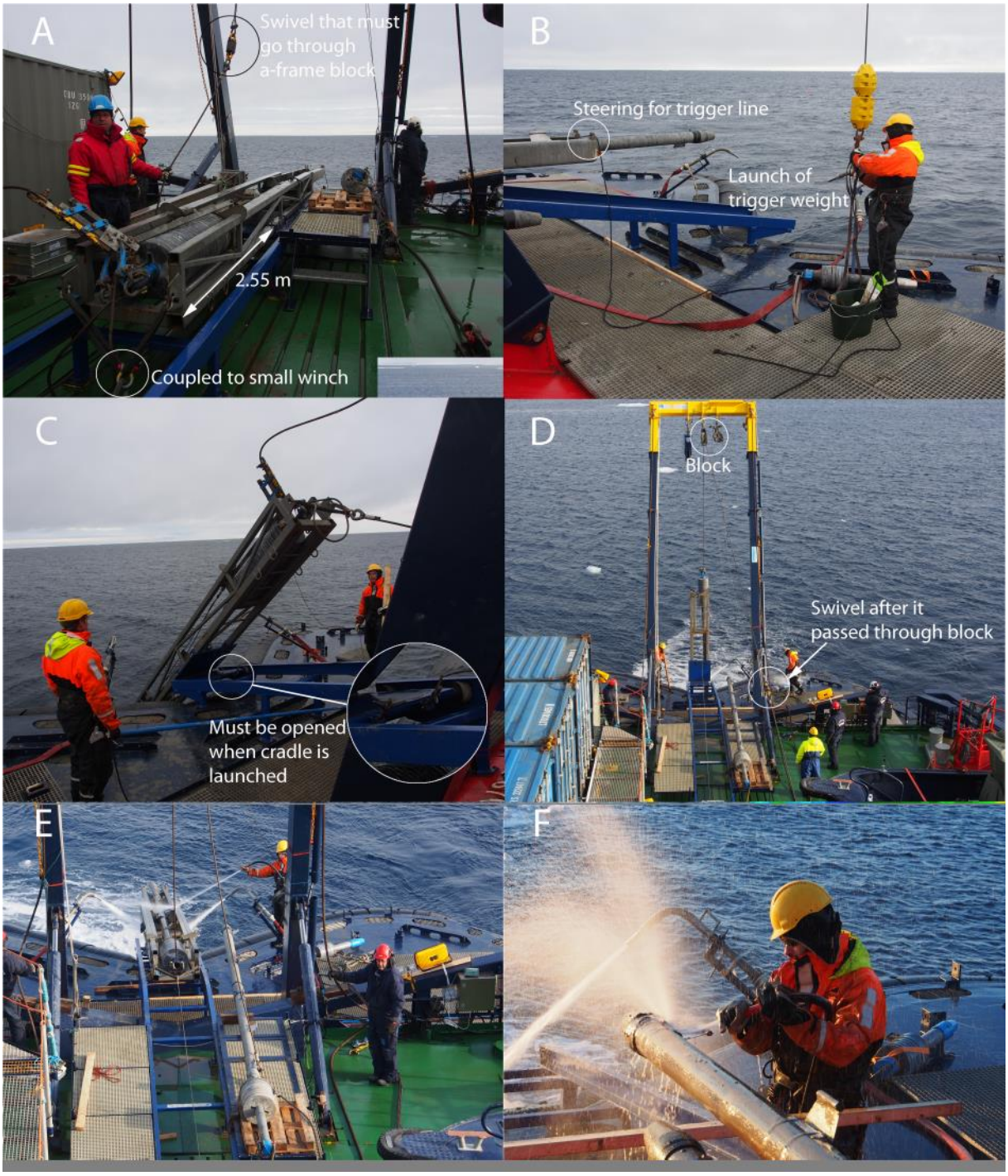

Figure SC-3: *A-F shows the main steps of launch and recovery of the piston corer. A) The piston corer fully rigged to be launched using the cradle. The cradle was manually pushed until it pivots into an upright position. The balance of the cradle should be adjusted for a soft pivoting. During SWERUS C3 the balance was set for a 9 m long corer and 1215 kg lead weight on the core head. The distance from the cradle top and the pivot part for this balance is marked in the figure. For the 9 m used corer with 1215 kg weight it is 2.55 m, and for a 12 m corer with the same weight it is 1.77 m. B) Launch of the trigger weight corer. This is done before the cradle is pushed to the pivot position. A separate lifting rope is used that can be pulled away from the trigger weight corer before launch. C) The cradle during pivoting. Note the two screws that must be listened before the cradle is push out to pivot. The screws are only tightened during transit to stabilize the cradle. D) The corer on its way to be docked in the cradle after a core has been taken. Note that the release wire now is longer, which requires that the*

swivel must be pulled through the block to lift the corer. E) The corer is pulled up on deck using the small battery driven winch shown in Figure SC-4. F) The sediment filled liners are retrieved on the fantail of IB Oden.

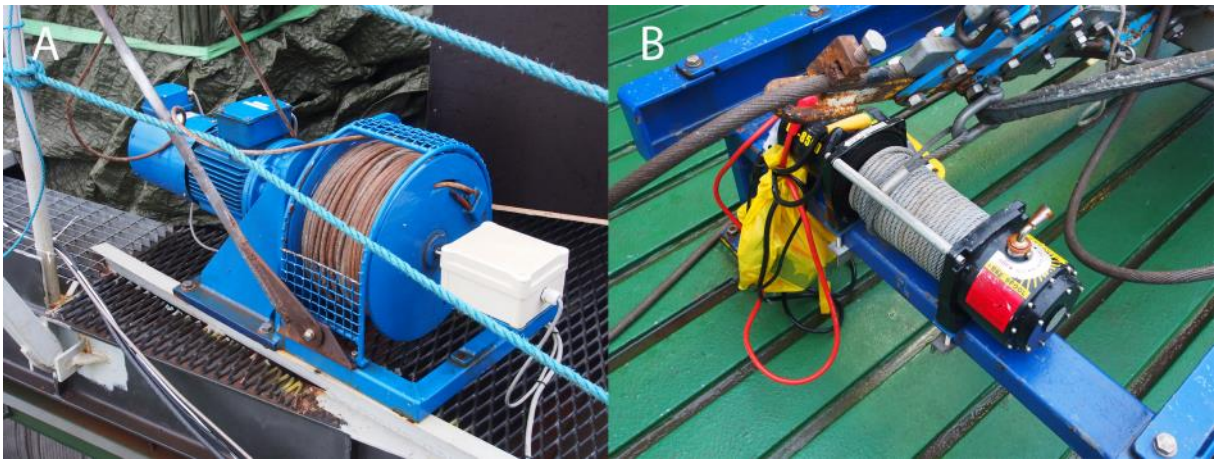

Figure SC-4: *Small winch mounted on the roof of the NorthSea coring winch container to pull the piston core cradle with (A). This winch broke down at the beginning of Leg 2 and was replaced with a small battery driven winch (B) mounted directly on the rail that guides the cradle.*

Multicorer and mounted camera

The multicorer used during SWERUS-C3 was an 8-tube corer made by Oktopus GmbH (Germany). It has been developed to collect samples of the seabed with an undisturbed sediment-water interface (Fig. SC-5). The liners are made of polycarbonate and are 60 cm long with a 10 cm diameter. The multicorer was deployed with full weight (head weight about 500 kg). The winch speed should be low, ~0.5 m/s, when the corer reaches the seabed. This was however difficult to fully accommodate during bad weather conditions with large waves and fast drift speed of *IB Oden*. In addition, the used coring winch manufactured by NorthSea was not easy to operate at low speeds. To increase the sediment recovery, the multicorer was left to sit, usually 30 seconds to 1 minute, on the seafloor.

A GoPro Hero3+ camera was mounted on the multicorer frame which permitted filming the corer's impact with the seabed (Figure SC-6). The Iphone app made by GoPro was used to start and stop the GoPro camera once it was mounted in the underwater housing manufactured by the US Company Group B. The underwater housing, model ScoutPro H3, is capable of protecting the GoPro camera down to 2750 m water depth. The light and its underwater housing were also manufactured by Group B; model Nautilux underwater video light and GPH-1250 general purpose underwater housing. The housing for the light sustains a water depth of 1250 m.

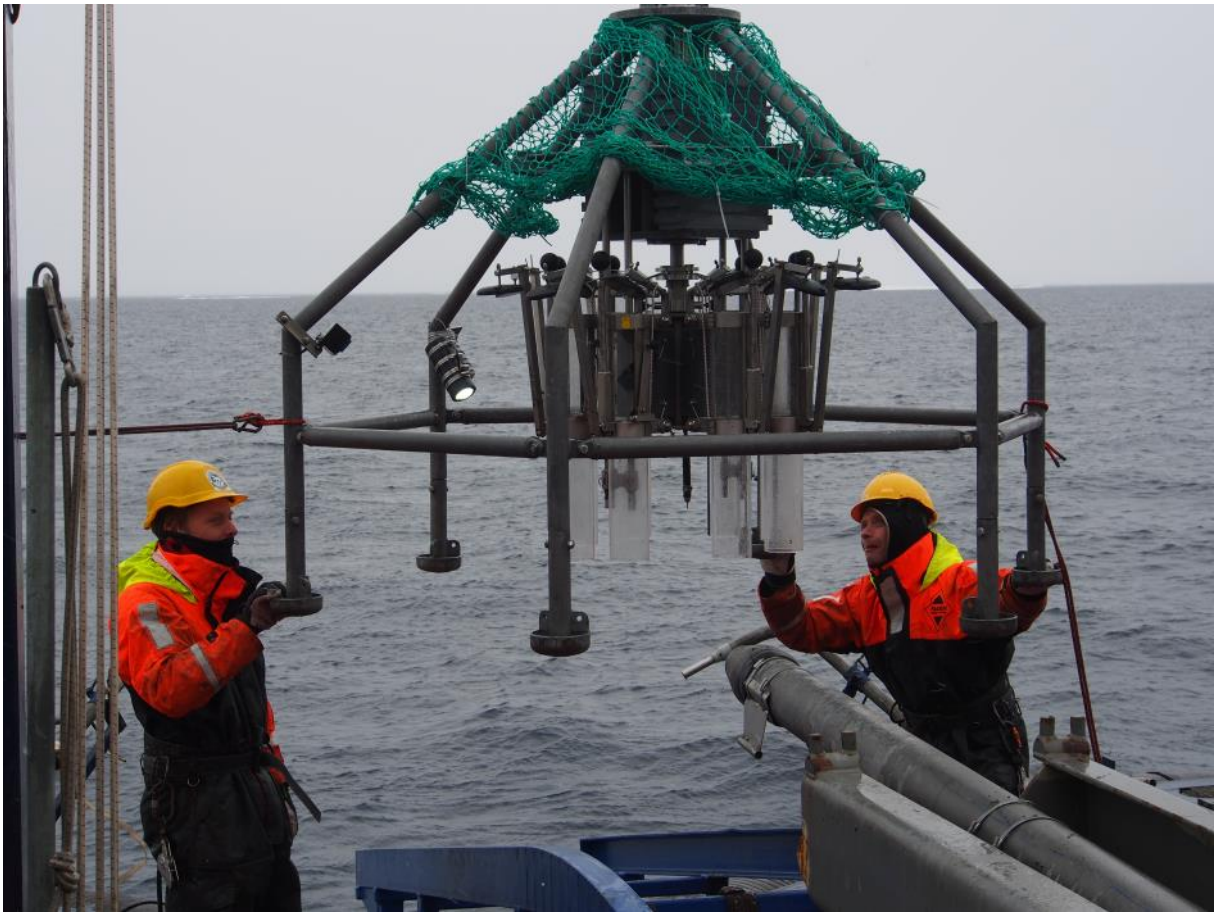

Figure SC-5. *The multicorer during deployment over IB Oden's fantail. Note the mounted GoPro camera and light.*

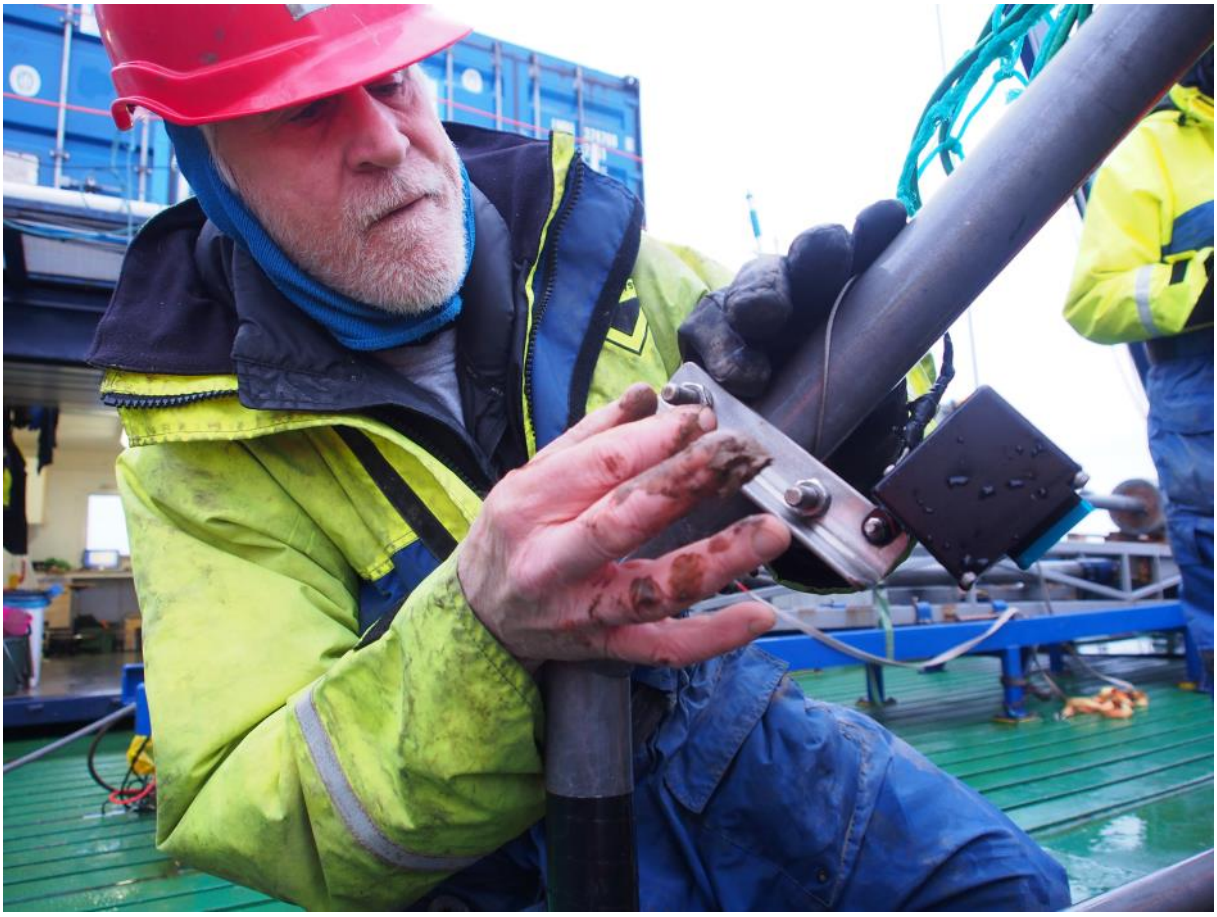

Figure SC-6: *The GoPro Hero3+ camera mounted on the multicorer frame in the ScoutPro H3 housing*.

Kasten corer

The Kasten corer has a 3 meter long 15x15 cm barrel made of stainless steel. The core head can be loaded with a maximum of 18 lead weights of 32 kg/weight. It was used at the first two coring sites during Leg 2, with nine lead weights (Fig. SC-7).

Figure SC-7: *Kasten corer.*

Coring winches

The Swedish Polar Research Secretariat provided two large coring winches that were brought onboard *IB Oden* to be used during the SWERUS C3 expedition. They are both stored in custom made containers. The older of the two winches is manufactured by MacArtney. It was purchased in 2012. It is a traction winch equipped with an 8000 m long 14 mm diameter Dyneema synthetic rope. It is capable of pulling 8 tons at the bottom layer and 6 tons at the first layers of rope. The winch broke down after a few coring stations during Leg 2. The MacArtney winch has generally of poor quality with several details not dimensioned for Arctic conditions and icebreaking, which implies heavy

motions at times. The winch electronics began falling apart already during Leg 1. It was not possible to repair implying that the second large coring winch had to be used. This winch is manufactured by NorthSea and was purchased just before the SWERUS-C3 expedition. It has a 20 mm diameter steel wire (Fig. SC-8). The wire is heavy and largely over-dimensioned for our coring operations, implying that the capacity of the winch does not permit operations of our large diameter piston corer, weighing ca 1.6 ton, at water depths exceeding approximately 1500 m. This was a severe limitation for SWERUS-C3 coring operations.

An important component of the coring operations is a reader for the lenght of wire out and registration of pull out force. A remote display provided these parameters from the NorthSea winch (Figure SC-9).

Figure SC-8: *Coring winch manufactured by NorthSea.*

Figure SC-9: *Remote display showing load and wire out of the NorthSea winch.*

Shipboard post-processing

The shipboard processing of the sediment cores are described under WP-MB, -SP and -SCh.

Labeling of sediment cores and samples

Individual sediment cores are identified using the expedition label SWERUS-C3 Leg 2. This is shortened to SWERUS-L2 on core and sample labels. The next identifiers are the station number, the type of coring deviced used, and the number of cores taken at a single station using a specific coring device. Five coring devices were used during Leg 2 of SWERUS-C3, namely Gravity Corer (GC), Multi Corer (MC), Piston Corer (PC), Trigger Weight Corer (TWC) and Kasten Lot (KL; deployed only during the first two coring stations). For example, a single piston corer was taken at coring station number eight (8). Its unique identification, or Core ID, hence is: SWERUS-L2-8-PC1. This translates into Expedition-Leg number-Station number-Coring device (piston corer in this example). The number 1 after PC (PC1) implies that this was piston core #1 taken at Station 8. The trigger weight core that was taken together with this piston core at Station 8 is labeled SWERUS-L2-8-TWC1. If a second piston core had been taken at Station 8, this would be labeled SWERUS-L2-8-PC2, and its trigger weight core SWERUS-L2-8-TWC2.

Retrieved gravity and piston cores are extruded from the base of the corer, that is, from the maximum depth of penetration in the sediment column. The nose cone holds the Core Catcher and the core catcher sample, labeled CC. The extruded core liners with their content of sediments are cut into 150 cm long sections. The base of the first section extruded from the corer is labeled A and its

top B, the next section C (base) and D (top), etc. Sections were subsequently labeled 1, 2, etc., starting with Section 1 at the top of the core (Figure SC-10), normally at the water-sediment interface.

A full curatorial identifier for a sample consists of the Core ID with the addition of Section number and centimeter depth from the top of the Section. A sample taken 75-77 cm from the top of Section 3 of the piston core at Station 8 (see example above) is labeled: SWERUS-L2-8-PC1-4, 75-77 cm. This Sample ID is easily converted to absolute core depth with knowledge of the lengths of Sections 1, 2 and 3. If Sections 1, 2 and 3 each is 150 cm long, the sample is located 520-522 cm (150+150+150+75/77) below the top of the core.

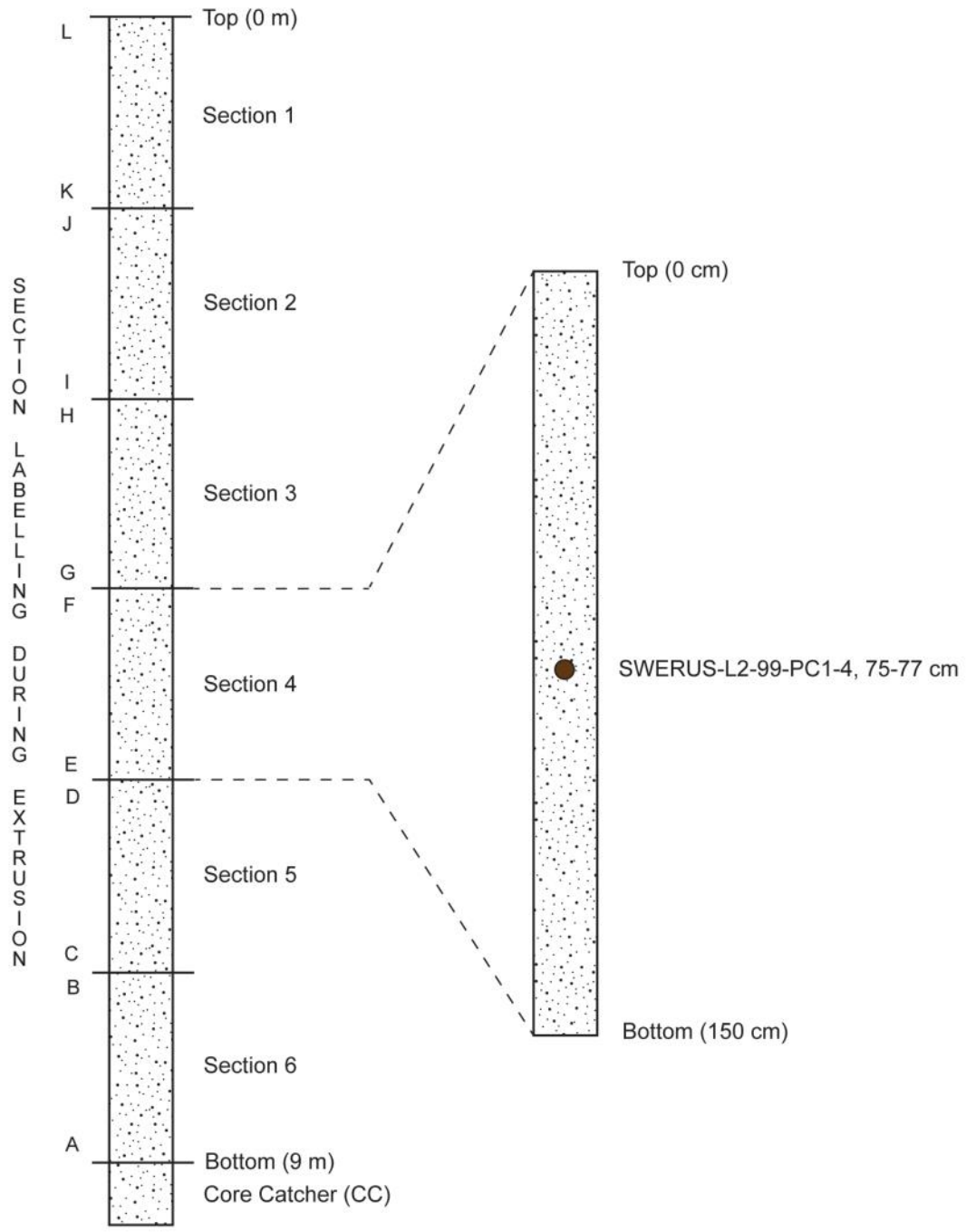

Figure SC-10: *Section labeling (left) of a 9 m long piston core. Labeling (right) of a 2 cm thick stratigraphic sample taken 75-77 cm below the top of Section 4 at Coring Station 99: SWERUS-L2-99-PC1-4, 75-77 cm.*

WP SP (Sediment Physical Properties)

The measurement program for shipboard analyses of sediment physical properties was designed to:

1) Provide a basis for making initial stratigraphic interpretations, inter-core correlation and facilitate post-cruise subsampling planning.
2) Collect data on the shear strength and engineering properties of sediments at the time of core opening.
3) Collect in-situ temperature, and laboratory measurements of sediment thermal properties, to determine the heat flow at coring sites.

Unsplit sediment cores in PVC liners were logged on the Multi-Sensor Core Logger (MSCL) to obtain measurements of the bulk density, compressional wave velocity and magnetic susceptibility. After opening, the cores were scanned on the MSCL to provide high-resolution digital images.

Shear strength (fall cone) and index property (moisture content and grain density) measurements, were made on many of the split cores. These measurements were made on the working half of the cores. Sediment thermal properties (thermal conductivity, diffusivity and specific heat capacity) were measured on the archived halves, but at the same position as the index property and shear strength measurements.

In-situ temperature measurements at most coring sites were obtained using miniature outrigger probes attached to either the gravity or piston core barrels. Combined with the sediment thermal properties, these measurements will be used to determine heat flow at the coring sites, and investigate the subsurface thermal regime.

A summary of all the shipboard physical property measurements conducted during leg 2 of SWERUS is presented in Table PP-1.

Core ID	Opened	MSCL	Imaging	Full Core	Thermal Prop.	Moisture Content	Grain Density	In-Situ temp
SWERUS-L2-2-PC1	X	X	X	X	X	X	X	X
SWERUS-L2-2-TWC1	X							
SWERUS-L2-4-PC1	X	X	X	X	X	X	X	X
SWERUS-L2-4-TWC1	X		X	X	X	X		
SWERUS-L2-5-GC1	X	X	X	X	X	X		
SWERUS-L2-6-GC1		X						X
SWERUS-L2-7-GC1	X	X	X	X	X	X		X
SWERUS-L2-8-GC1		X						X
SWERUS-L2-8-PC1	X	X	X	X	X	X		X
SWERUS-L2-8-TWC1								
SWERUS-L2-9-GC1	X		X	X	X	X		X
SWERUS-L2-10-GC1	X	X	X	X	X	X	X	X
SWERUS-L2-11-GC1	X	X	X	X	X	X		X
SWERUS-L2-12-PC1	X	X	X	X	X	X	X	X
SWERUS-L2-12-TWC1								
SWERUS-L2-13-GC1		X						X
SWERUS-L2-13-PC1	X	X	X	X	X	X		X
SWERUS-L2-13-TWC1								
SWERUS-L2-14-GC1	X	X	X	X	X	X		X
SWERUS-L2-15-GC1	X	X	X	X	X	X		X
SWERUS-L2-16-GC1	X	X	X	X	X	X		X
SWERUS-L2-17-PC1	X	X	X	X	X	X		X
SWERUS-L2-17-TWC1	X							
SWERUS-L2-18-GC1	X	X	X	X	X	X		X
SWERUS-L2-18-GC2		X						X
SWERUS-L2-20-GC1	X	X	X	X	X	X		X
SWERUS-L2-22-GC1		X						X
SWERUS-L2-22-PC1	X	X	X	X	X	X		X
SWERUS-L2-22-TWC1	X		X					
SWERUS-L2-23-GC1	X	X	X	X	X			X
SWERUS-L2-24-GC1	X	X	X	X	X			X
SWERUS-L2-26-PC1	X	X	X	X	X			X
SWERUS-L2-26-TWC1	X		X					
SWERUS-L2-28-GC1	X	X	X	X	X			X
SWERUS-L2-29-GC1	X	X	X	X	X			X
SWERUS-L2-29-PC1	X	X	X					X
SWERUS-L2-29-TWC1	X		X					
SWERUS-L2-30-SGC1		X						X
SWERUS-L2-31-PC1	X	X	X	X	X			X
SWERUS-L2-31-TWC1								
SWERUS-L2-32-GC1		X						X
SWERUS-L2-32-GC2	X	X	X	X	X			X
SWERUS-L2-33-GC1		X						X
SWERUS-L2-33-PC1	X	X	X	X	X			X
SWERUS-L2-33-TWC1	X		X					

Table PP-1: *Physical property measurements performed on cores from Leg 2 of SWERUS.*

Equipment

GEOTEK Multi-Sensor Core Logger

The Geotek Multi-Sensor Core Logger (MSCL) from Stockholm University was set-up in the main lab on the foredeck of the Oden (Figure PP-1). Sensors were oriented in the horizontal direction for whole-core logging. Measurements of the gamma ray derived bulk density, compressional wave velocity (p-wave) and magnetic susceptibility were acquired at a down core resolution of 1 cm.

Gamma-ray attenuation was measured using a ^{137}Cs source with a 5 mm collimator and a 10 s count time. Calibration of the system was usually done daily using a machined piece of aluminum that was fit within a section of core liner. The aluminum calibration piece has 5 different thicknesses of aluminum with diameters of 1.8, 2.8, 3.8, 4.8, and 5.8 cm.

The liner was then filled with distilled water from the Milli-Q system, and left to equilibrate with room temperature (≈20^{o}C). The calibration piece and liner were then placed in front of the ^{137}Cs source. The number of gamma rays passing through each section over a course of 60 s, as well as through an interval containing only water, was logged. The relationship between the measured counts per s [ln(cps)] and the known bulk density of the aluminum/water mixture at each step was determined using a 2nd order polynomial. Throughout the expedition the gamma ray source was left open, with the calibration piece used to shield the gamma ray detector from excess radiation while not in use.

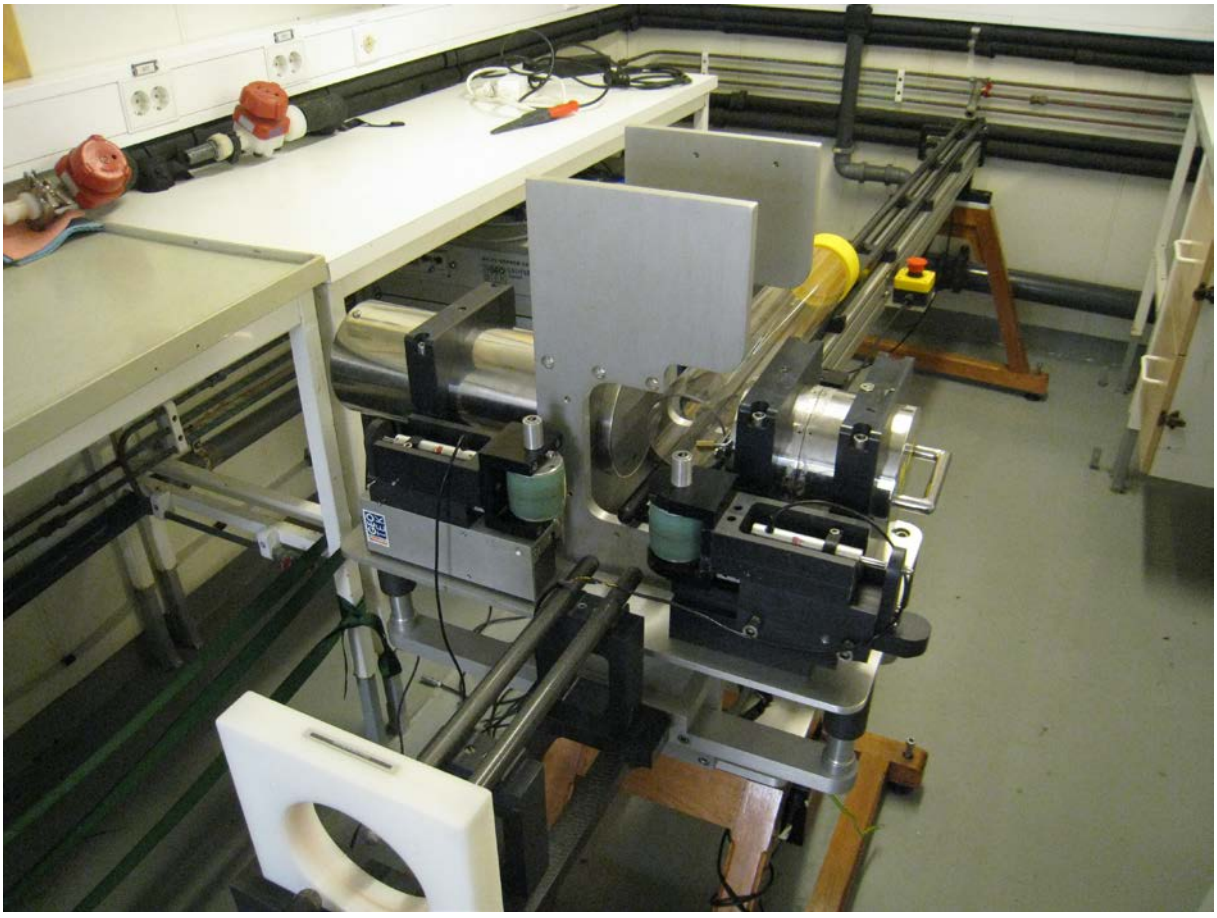

Figure PP-1: *The Multi-Sensor Core Logger being installed in the main lab during mobilization. The computer and electronics rack are stored under the counter on the top left of the picture. The digital line camera has not been attached in this photo.*

Compressional (p-wave) velocity measurements were made on the MSCL by a pair of automated spring loaded rolling transducers. The travel time of the p-wave between the send and receive transducer is logged. Conversion of the travel time into a p-wave velocity requires calibration to account for delays introduced by the electronic circuitry and those associated with the passage of the p-wave through the liner.

Calibration is performed by measuring the travel time through a water-filled core liner at a known temperature. The temperature and thickness of the water is used to calculate a theoretical travel time (TT) through the water inside the core liner. The difference between the logged total travel time (TOT) and theoretical travel time (TT) is the offset time (PTO).

A 40 μs gate and 30 μs delay was used for calibration and logging. A digital oscilloscope was run during all core logging to monitor the strength of the p-wave signal and to ensure that it arrived within the defined gate interval. Occasionally, distilled water was sprayed on the outside of the core liner to improve the acoustic coupling between the sensors and the core.

Magnetic susceptibility was acquired with a 125 mm Bartington loop sensor using a 1 s acquisition time. This provided a spatially integrated susceptibility signal that encompasses the entire diameter of the core, with an effective sensor length of generally 4-6 cm. No mass or volume corrections were made to the Magnetic susceptibility measurements.

During logging, small variations in core thickness were also measured and logged using the displacement transducers attached to the p-wave housings. Variations in core thickness, usually more pronounced at the taped and capped core ends, were automatically incorporated into the processed calibrated measurements of p-wave velocity and bulk density.

Thermal properties of sediments

The thermal properties of sediments were measured using a TPS 500 thermal constants analyzer, manufactured by K-analysis in Uppsala, Sweden. The TPS 500 measures the thermal conductivity, thermal diffusivity and specific heat capacity. The HotDisk TPS 500 sensors are made from a thin nickel double spiral that is electrically insulated by two layers of Kapton (polymide). The sensors are mechanically stable and suitable for both transient heating and precise temperature readings. The Kapton material allows isotropic, anisotropic, slab, one-dimensional and structural probe measurements across a large temperature range (from -196 °C up to 300 °C). The measurement range of the HotDisk TPS 500 is 0.03 to 100 W/mK for thermal conductivity, 0.02 to 40 mm^2/s for thermal diffusivity and 0.10 to 4.5 MJ/m^3K for specific heat capacity measurements.

The TPS 500 can be used for 1-sided or 2-sided measurements of sediment thermal properties. During a typical 2-sided test, the sensor is placed between the surfaces of two pieces of sample. A current passes through the Nickel spiral and creates an increase in temperature. The heat generated dissipates through the sample on either side at a rate dependent on the thermal transport characteristics of the material. By recording the temperature versus time response in the sensor, the samples thermal characteristics are calculated. For shipboard measurements, the 1-sided measurement technique was used, where the sensor was placed on the surface of a split core, and a piece of Styrofoam (expanded polystyrene (EPS) form) was used as a backing material. EPS has thermal conductivity values typically ranging from 0.032 to 0.038 W/mK, but it can depend on the density of the EPS itself (the higher the density, the lowest the value of the thermal conductivity). The thermal properties of the Styrofoam were determined using a 2-sided test at the beginning of the cruise and were 0.3586 W/mK, 1.161 mm^2/s and 0.0309 MJ/m^3K for thermal conductivity, thermal diffusivity and specific heat capacity, respectively.

A 5 cm diameter, 2 cm tall and 100 g weight was placed on top of the Styrofoam to ensure that the sensor was pressed into the sediment surface and remained in place during the measurement period. Measurements were usually conducted using an 80 s heating period with power of 0.5 watts. In sandy and silty sediments, it was necessary to reduce the measurement time to 40 ss in order to obtain accurate values.

Index properties

Index property samples, commonly used to directly determine the bulk density, porosity, water content and grain density of sediments, were taken at a resolution of 1-2 samples per section. These samples were taken using 20 cm^3 sample scoops, and were not constant volume samples. Therefore, no wet volume measurement was made, and bulk density was not determined. Instead, the wet mass and dry mass of the sample was used to calculate the water content.

$$Water\ contentent\ (\%) = \frac{m(wet\ sample) - m(dry\ sample)}{m(wet\ sample)} \times 100$$

Dry masses were measured after the samples had spent at least 24 hours in the oven at a temperature of 95^{o}C.

Motion of the ship was problematic for the balance. All wet and dry masses were determined during periods when the ship was either on station in the ice, or on very calm days. Even under optimal conditions, measurement accuracy was ≈0.01 g. Wet sample weights ranged between 12.39 and 30.39 g for the wet samples.

Grain density measurements were conducted on some of the dry samples using a Micrometrics helium displacement pycnometer (Accupyc1340). After drying, the samples were crushed in a mortar to a fine powder. The powder was inserted into the 10 cm^3 chamber insert of the pycnometer and weighed. Three to five measurements of the sample volume were made on the pycnometer. The average volume was used with the dry mass of the sample to calculate the grain density.

The time required to run the pycnometer at sea made it difficult to keep these measurements in pace with the opening of the cores. A computer malfunction in the last 2 weeks also made the pycnometer unavailable. Samples not analysed on the ship will be processed and measured at Stockholm University.

Shear Strength

The *Undrained Shear Strength* (S_U) of the sediments was measured using a CONTROLS-group liquid limit penetrometer (fall cone). The fall cone test was performed according to ISO-TS-17892-6 (Swedish standards institute) at a downcore resolution of approximately 30 cm. For most measurements a 60°/82g cone was used, but it some instances a heavier weight (60º/112g) or narrower cone (30º/62g) was used to achieve penetration depths of ≈4-20 mm.

From the fall cone tests, S_U (kPa) was calculated by,

$$S_U = Kg \cdot \frac{Q}{h^2}$$

where *K* is a cone dependent constant (0.8 for the 30° cone and 0.27 for the 60° cone) (ISO-TS-17892-6), *Q* is the cone weight (g) and *h* the cone penetration (mm). No correction was applied to the calculated shear strength to account for variations in the liquid limit of sediments.

In-Situ Temperature Measurements

In-situ temperature measurements were obtained using ANTARES miniature temperature probes attached to the outside of the gravity or piston core barrel. Each stainless steel temperature logger is 16 cm long and 1.5 cm in diameter. They have an operational range of -5 to 50 °C, 100 MPa, and a resolution of 0.001°C.

The probes were inserted into stainless steel fins attached to the core barrels using large diameter hose clamps (126-147 mm) (Figure PP-2). The fins protected the temperature probes and kept them 10 cm away from the core barrel. This offset distance reduced the effects of frictional heating from the core barrel as it entered into the sediments.

Figure PP-2. *Stainless steel outrigger fins to attach the temperature probes to the core barrel.*

The probes were programmed and downloaded in the coring container before and after each deployment. A 2-s sampling interval was used on most deployments. At the last 4 stations on the Lomonosov Ridge, a sampling time of 30 s was used. Between 3 and 6 temperature probes were used on each deployment to ensure that the thermal gradient in the sediments could be resolved (Figure PP-3). Spacing was usually between 0.75 and 2 m, but the distance varied slightly between deployments. Details of sensor spacing are found on the Individual logs sheets for each deployment (Appendix PP-1).

During the temperature measurements, the core barrel was left in the sediments for anywhere between 1.5 to 3.5 minutes. The amount of time depended on the water depth and drift speed of the ship, which in some circumstances was >1 knot.

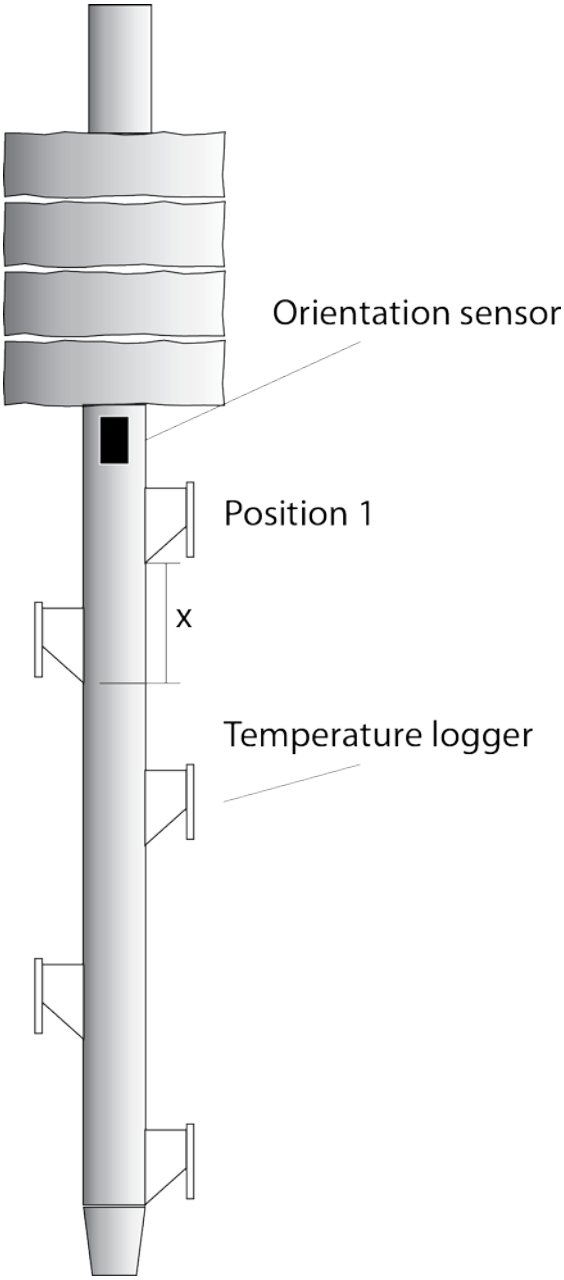

Figure PP-3: *Schematic illustration of temperature and orientation sensor set-up on the gravity/piston core barrel. Between 3-6 temperature loggers were used on each deployment. On the log sheets in Appendix PP-1, position 1 is at the top of the core barrel. Distances (x) between each temperature sensor are recorded from the base of 1 fin to the base of the next.*

Figure PP-4: *Star Oddi DSC magnetic sensor and casing attached to the core barrel.*

Figure PP-5: *Position of the DSC magnetic sensor on the core barrel.*

To monitor the angle of the core barrel while embedded in the sediments, a Star Oddi DST magnetic orientation sensor was used (Figure PP-4). The sensor records the temperature, pressure (depth), ambient magnetic field strength, tilt (in 3 directions), and the azimuth. The DST magnetic was programmed and downloaded in the coring container. A 2 s sampling time was used throughout the expedition. These sensors were attached to the core barrels using hose clamps. They were strapped

to the barrels below the weights on the gravity cores and piston core (Figure PP-5). While in the water column and sediments, the sensor should record a Z-axis tilt of ≈0^{o} if it is in the vertical direction.

WP CP (Sediment Chemical Properties)

The goal of this work package is to understand the complex pore water geochemistry of arctic sediments. The pore water profiles generated in this investigation will be used to understand a range of processes including: microbial reactions, mineral diagenesis, subsurface fluid flow, glacial/interglacial changes, gas hydrate dissolution, and methane flux. Sediment pore water profiles yield smooth curves that are defined by diffusion gradients of dissolved species. By studying these profiles the geochemical processes can be measured and quantified.

Sampling of the pore water for this project was carried out via rhizon sampling. Rhizon samplers are small hydrophilic polymer tubes which can be used to extract filtered (<0.18 µm) pore water from sediment (See Figure CP-1). The rhizons are inserted into the piston, gravity, and multicores by drilling 3mm holes in the liner and pushing the tube into the sediment. The rhizons are then attached to syringes by flexible hoses and pulled to create negative pressure which generally causes water to flow <10 mL h^{-1}. Due to the slow rate of collection the syringes are propped open with spacers and allowed to sit up to 12 hours. Shipboard exigencies prevented workers from analyzing the core density and magnetic susceptibility prior to pore water sampling. Pore water extraction decreases the efficacy of physical properties measurements; therefore the spacing of the rhizons differed between coring locations in order to best accommodate these measurements. Upon collection, each sample was divided into multiple aliquots.

Poor water analyses

Metals and Sulfur

The first sample aliquot was set aside for metals and sulfur analysis. These measurements will be performed in Houston, Texas at Rice University following the expedition. Metals include but are not limited to: Al, Ba, Ca, Fe, Mg, Mn, P, Si, and Sr. These analytes are heavily involved in bacterial mediated reactions as well as precipitation/dissolution reactions with the solid phase sediment. Sulfur, as sulfate (SO_4^{2-}), is one of the primary electron acceptors in the oxidation of organic matter in the sediment as well as upward migrating methane from gas hydrates. Immediately following pore water extraction 3 mL were placed in acid washed cryovials for metals and sulfur analyses. The vials were acid washed prior to the expedition. After sampling, 10 µL of ultrapure HNO_3 preservative were pipetted into the cryovials. The vials were placed in refrigerated boxes until the end of the expedition.

Hydrogen sulfide and sulfur isotopes

The second sample aliquot was set aside for HS^- and sulfur isotope analyses. These measurements will be performed in Houston, Texas at Rice University following the expedition. Sulfide is produced during the anaerobic oxidation of methane (AOM) along with bicarbonate (HCO_3^-) and water. This reaction consumes methane and produces characteristic profiles of sulfide and sulfur isotopes which can be used to describe methane behavior in the sediments. Immediately following the first aliquot, 2 mL of pore water were placed in cryovials and reacted with 200 µL of Zn-acetate ($Zn(C_2H_3O_2)_2$) preservative. The vials were placed in refrigerated boxes until the end of the expedition.

***Figure CP-1**: Rhizon samplers collecting pore water from a gravity core. The spacing of the Rhizons varied between coring locations from 6 to 30 cm. Photo Pedro Preto*

***Figure CP-2**: Rhizon samplers under negative pressure sampling water from a gravity core. The rate of sampling varied between Rhizons. The sampling times are given in Table CP-1. Photo Pedro Preto*

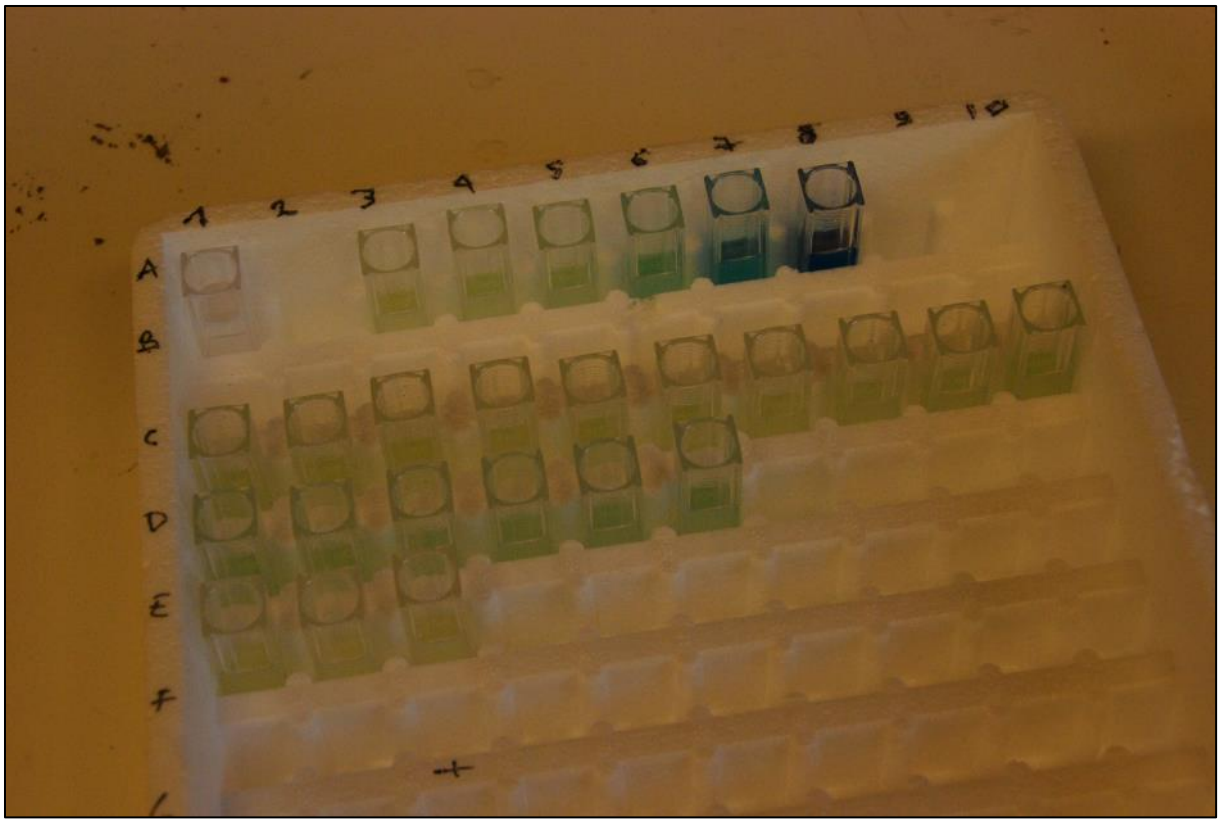

Figure CP-3: *Ammonia color analysis. The standards are at the top. Photo Clint Miller*

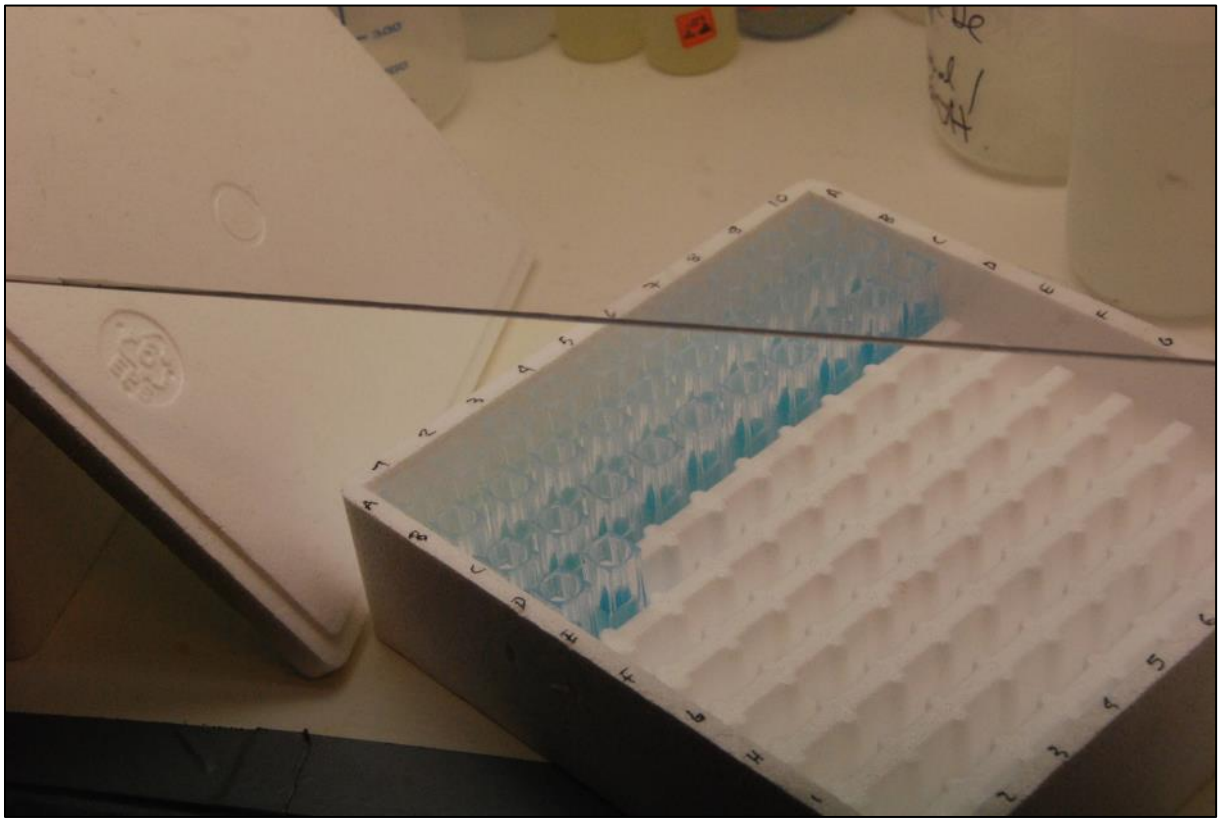

Figure CP-4: *Ammonia pore water analysis. The concentration is measured via absorbance. Photo Franscesco Muschitiello*

***Figure CP-5**: Spectrophotometer used for phosphate and ammonia analyses. Photo Clint Miller.*

Alkalinity

The third aliquot was used to measure pore water alkalinity. Alkalinity is the measure of how much acid is consumed while lowering the pH of a water sample enough to convert all bicarbonate (HCO_3^-) and carbonate (CO_3^{2-}) to carbonic acid (H_2CO_3). Total alkalinity is equal to the stoichiometric sum of all bases in solution, but alkalinity is generally dominated by carbonates in seawater. Therefore, the alkalinity of these near surface pore water samples is approximately equal to the sum of bicarbonate and carbonate. The alkalinity was measured onboard the Oden with a Mettler Toledo titrator. 2 mL of pore water were diluted to approximately 40 mL with milli-Q water and autotitrated with 0.005 M hydrochloric acid (HCl) from the original pH to a pH of 5.4.

δ13C of DIC

The fourth aliquot will be used to measure the δ13C of dissolved inorganic carbon (DIC) in the pore water. The isotopic composition of DIC is used to determine the source (and flux) of diffusing carbon. This analysis will be performed at the University of Stockholm after the expedition. Septum-sealed glass vials prepared with 100 uL of 85% phosphoric acid, and flushed with Helium, were brought on board. Suitable volumes of pore water was injected into the vials, after determination of the concentration of bicarbonate in the water (determined by aliquot 3). The δ13C of DIC analyses will be performed with a Gasbench II coupled to a MAT 253 mass spectrometer (both from Thermo Scientific). From these measurements the reproducibility should be better than 0.1‰.

Ammonia

The fifth aliquot was used to measure ammonia in the pore water. Ammonia is a terminal electron acceptor in nitrification that is commonly used as a biogeochemical indicator of the pore water

environment. This analysis was carried out onboard the Oden during the expedition via spectrophotometry on a Hitachi U-1100 spectrophotometer (see Figure CP-5). A set volume (100 µL) of pore water was pipetted into 1 cm plastic cuvettes, diluted with 900 µL of milli-Q water, and introduced to two reagents. Reagent A was 35 g of trisodium citrate, 2.7 g of phenol, and 0.06 g of sodium nitroprusside dissolved in 100 mL of milli-Q water. Reagent B was prepared by dissolving 1.36 g of sodium hydroxide in 100 mL of milli-Q water and adding 3mL sodium hypochlorite solution. After preparing samples 100 µL of Reagent A and Reagent B were added, mixed, and allowed to react for at least 6 but not more than 24 hours. The solution turned cloudy to blue or purple (see Figure CP-3 and CP-4), and the original concentration was given by the absorbance of the solution at 630 nm.

Phosphate

The sixth aliquot was used to measure phosphate. Phosphate is a nutrient that is commonly used as a biogeochemical indicator. This analysis was also carried out via spectrophotometry on a Hitachi U-1100 spectrophotometer. For phosphate, the remainder of the pore water sample was added to milli-Q water to a sum of 10 mL. Generally, this was between 1 and 3 mL of pore water. Two reagents were then added to the solution to react with phosphate. Reagent A was prepared by adding 8 g of ammonium molybdate to 80 mL milli-Q water, 50 mL concentrated sulfuric acid in 150 mL milli-Q water, and 0.01 g potassium antimonyl tartrat in 10 mL milli-Q water. Then, 30 mL of the ammonium molybdate solution were added to 90 mL of the sulfuric acid solution, and 5 mL potassium antimonyl tartrate solution was added dropwise. Reagent B was created by dissolving 10 g of ascorbic acid in 50 mL milli-Q water. After the samples were prepared, 200 µL of Reagent A and Reagent B were added, mixed, and allowed to react for 10 but not more than 30 minutes. The absorbance at 880 nm was then measured on the Hitachi U-1100 spectrophotometer.

Methane measurements in sediments

Headspace extraction of gases in sediments

Headspace extraction of gases for concentration analysis was performed directly in the 20 (22.5) mL glass serum bottles. The volume was adjusted to 5 mL for sediment sample and 18.5 mL for air. The bottles with samples were degassed (headspace extracted) in the ultrasonic bath for 1 min, and were left for additional 30 min for headspace equilibration (temperature was 22 C). 5 ml of headspace was taken by 5 ml syringe from the serum bottle and then injected directly to the GC.

Concentration analysis of gases in sediments using gas chromatography

A SRI – 8610C series gas chromatograph equipped with flame ionization detector (FID) and methanator was used for the analysis of CH4, CO, CO2 and C2-C5 hydrocarbons. The instrument also had a helium ionization detector (HID; for H2, O2, N2, CH4) and a thermal conductivity detector (TCD; for O2, N2, CH4). For the SRI GC, 1+1 mL of sample was injected to the instrument using a 2 sample-loop system held at 130 C (total injected volume was 5 mL). Separation prior to FID was performed on a HaysepD packed column (1/8” diameter, 2 m) using helium as the carrier gas at 25 mL/min. Separation to TCD - HID was performed on a Mol Sieve 13x packed column (1/8” diameter, 2 m) using helium as the carrier gas at 25 mL/min. The sediment concentration profile was obtained with a temperature program according to [40 C for 5 min, ramp 7 C/min to 210 C and hold 7.7 min]. The FID was in all cases heated to 300 C, HID to 300 C and the TCD to 150 C (25 mL/min hydrogen from the hydrogen generator, 250 mL/min air, 25/40+10/25 mL/min helium). The detection limit for methane was 1 ppm.

Operation

Pore water sampling was carried out on gravity, piston, and multi-cores. After coring operations, the sediment cores were immediately brought to the chemical properties laboratory for sampling. The time when the sediment coring took place was recorded. The environment on the ship deck and especially inside the work package laboratory was drastically different from the ocean bottom environment. Therefore, all sampling activities were undertaken as quickly as possible to minimize biogeochemical changes in the sediment and pore water. The Rhizon holes were drilled with a power drill, and the Rhizons were immediately placed inside the cores. The syringes were pulled and blocked with spacers to apply constant negative pressure. The time when sampling began was recorded. The microporous polymer on the Rhizon works best when it is wet. For this reason, the Rhizons were placed in milli-Q water for 30 minutes before use. The first 0.5 mL of sample was discarded to avoid dilution of the water sample. The pore water sampling time varied due to porosity, water saturation, and environmental factors such as temperature. A synopsis of the Rhizon sampling times is given in Table CP-1. Occasionally, the Rhizon sampler did not work. When this occurred the Rhizon was removed and another was put in its place. The new starting time was recorded. The average time from ocean bottom to completed sampling for the multicores was 1.89 hours. The average time for gravity and piston cores was 13.68 hours.

Sediment sampling of the multicores for methane measurements were performed using 5 mL plastic syringes with fronts cut off. At each 4 cm depth from a pre-drilled multicorer PVC liner, 5 mL samples were taken. Out of the 6 mL samples, 5 mL was ejected into the 20 ml serum bottles with air headspace. The serum bottles were sealed subsequently.

Table CP-1: *Rhizon Efficacy*

Station	Core Type	Rhizon Extraction Time		Coring to Sampling Time	
		Average (Hrs)	Range (Hrs)	Average (Hrs)	Range (Hrs)
2	MC	0.57	(0.25 - 1.38)	1.99	(1.67 - 2.80)
3	MC	1.77	(0.17 - 2.83)	2.57	(0.97 - 3.63)
4	MC	0.27	(0.25 - 0.42)	1.84	(1.82 - 1.98)
8	MC	0.47	(0.08 - 1.20)	0.92	(0.57 - 1.15)
13	MC	0.40	(0.20 - 0.68)	1.40	(1.20 - 1.68)
14	MC	1.76	(0.08 - 3.67)	2.51	(0.83 - 4.42)
16	MC	1.44	(0.50 - 2.33)	2.81	(1.87 - 3.70)
18	MC	1.21	(0.42 - 1.78)	2.11	(1.32 - 2.68)
21	MC	0.73	(0.17 - 1.08)	4.02	(3.45 - 4.37)
22	MC	0.38	(0.33 - 0.40)	0.73	(0.68 - 0.75)
23	MC	1.24	(0.35 - 1.85)	1.48	(0.67 - 1.93)
24	MC	1.34	(0.52 - 1.67)	1.79	(0.85 - 2.18)
25	MC	0.63	(0.50 - 0.83)	0.97	(0.83 - 1.17)
26	MC	1.53	(0.50 - 2.50)	1.83	(0.80 - 2.80)
27	MC	1.30	(1.00 - 1.83)	1.65	(1.35 - 2.18)
28	MC	1.10	(0.42 - 1.83)	1.53	(0.85 - 2.27)
29	MC	1.17	(0.67 - 1.67)	1.55	(1.05 - 2.05)

31	MC	2.08	(1.50 - 3.08)	2.38	(1.80 - 3.38)
32	MC	3.33	(1.33 - 4.00)	4.38	(2.38 - 5.05)
Multicore Average		1.20	(0.08 - 4.00)	1.89	(0.57 - 5.05)
10	GC	10.31	(1.83 - 11.83)	11.01	(3.38 - 12.38)
14	GC	9.00	(5.22 - 10.0)	14.58	(6.55 - 17.0)
18	GC	6.40	(1.73 - 12.92)	7.72	(3.0 - 14.37)
24	GC	5.89	(4.83 - 7.42)	12.25	(10.94 - 14.19)
29	GC	13.38	(4.72 - 14.0)	17.43	(9.25 - 18.02)
33	GC	8.55	(5.92 - 15.42)	12.20	(9.57 - 19.07)
2	PC	2.37	(1.00 - 3.50)	5.79	(4.42 - 6.92)
4	PC	3.63	(0.33 - 8.00)	8.16	(3.76 - 14.43)
8	PC	15.22	(1.78 - 17.5)	18.56	(4.80 - 20.85)
12	PC	17.95	(16.42 - 19.15)	21.44	(20.27 - 21.77)
17	PC	16.58	(15.08 - 16.58)	19.62	(18.12 - 19.62)
22	PC	17.71	(11.42 - 23.08)	19.79	(13.5 - 25.17)
31	PC	9.25	(1.33 - 15.5)	11.95	(3.90 - 18.07)
33	PC	9.48	(5.92 - 16.25)	11.06	(7.55 - 17.88)
Gravity/Piston Average		10.41	(0.33 - 23.08)	13.68	(3.00 - 25.17)

WP MB (Micropaleontology and Biostratigraphy)

The general objective of the Micropaleontology and Biostratigraphy (MB) group is to study the geologic temperature history along chosen sediment coring transects from the continental shelf and along the continental slopes and selected deep sea settings. An overarching goal is to decipher the importance of these temperature histories for the Gas Hydrate Stability Zone and potential release of CH_4 to the water and air masses. The aims hence focus on determining the Atlantic water flow along the eastern Siberian margin and the inflow of Pacific water from the Bering Strait through Herald Canyon as a function of geologic time. Sediment cores were also acquired from the Arlis Plateau and the southeastern portion of the Lomonosov Ridge. Two other key goals were included in the work of the Micropaleontology and Biostratigraphy group, namely (1) determination of sediment age relationships via biostratigraphy and biochronology and (2) to use microfossils to determine the distribution of sea ice cover through geologic time. Several microfossil groups will be employed to accomplish these goals, primarily benthic and planktic foraminifers, ostracodes, calcareous nannofossils and diatoms. Other microfossil groups may be added during the shore-based phase of these investigations. Onboard, WP MB also pursued the visual core descriptions and lithostratigraphic characterization of the sediment cores, and the sampling of all cores for subsequent shore-based work. Studies by the MB group were coordinated closely with the geophysical mapping (GM), sediment physical properties (SP), and sediment chemistry (SC) groups.
Shipboard micropaleontological investigations were performed by Jan Backman, Natalia Barrientos, Thomas Cronin and Laura Gemery. Personnel from several WPs were involved in core handling tasks, including curation and splitting, visual core descriptions and sampling, as listed in Table MB-1. The WP MB cruise report chapter is jointly written by Jan Backman, Natalia Barrientos, Thomas Cronin, Laura Gemery and Carina Johansson.

Table MB-1: *Distribution of key tasks (persons in alphabetical order)*

Core curation	Laura Gemery, Carina Johansson, Matt O'Regan, Pedro Preto
Core splitting	Natalia Barrientos, Laura Gemery, Carina Johansson, Pedro Preto
Visual core description, lithostratigraphy	Thomas Cronin, Laura Gemery
Sampling, piston and gravity cores	Natalia Barrientos, Laura Gemery, Carina Johansson
Sampling, multicores	Natalia Barrientos, Alexandr Gukov, Denis Kosmach, Francesco Muschitiello
Sampling, calcareous nannofossils	Jan Backman

Core handling and storage

Basic core handling flow

Gravity cores and piston cores were cut in 1.5 m long core sections and labeled on the aft deck where the coring operation took place. One of *Oden's* two rooms in the main laboratory was dedicated to geology, including macroscopic core description, sampling and sediment physical properties analysis; the other room was set up for oceanography. A separate core splitting facility was placed outside the main laboratory in a weather protected tent. After core sections had been logged on the multi sensor core logger (WP Sediment Physical Properties), these were split and

divided into an Archive half and a Work half. The latter was described macroscopically with respect to lithostratigraphic properties and digitally photographed on the multi sensor core logger (WP Sediment Physical Properties). A few selected cores were not split onboard for shore- based analyses such as optically stimulated luminescence dating (OSL). A few core sections were analyzed for pore water pH changes over time (24-48 hours) to examine potential dissolution of biogenic carbonate.

Micropaleontology

Discrete samples were processed and analyzed in the micropaleontology laboratory, equipped with a refrigerator and a freezer for sample storage, sink and distilled water for sediment processing. This included washing bulk sediment samples over 63 µm sieves and drying at ≤50°C prior to placing the coarse fraction in labeled glass vials. Conventional smear-slides were made for calcareous nannofossil studies. Three binocular stereomicroscopes were used for determination of foraminifers, ostracodes, mollusks and other sediment coarse fraction characteristics. A polarizing microscope was used for determination of calcareous nannofossils. In addition, a digital Arctic micropaleontology library and microfaunal reference slides were was brought on board for species identification.

Sediment sample storage containers

The *Oden* carried a freezer (-18°C) container in which samples taken for shore-based work on IP25 biomarkers, benthic foraminifera, calcareous nannofossil and diatoms are stored. Three tubes of each successful multicore deployment were also stored in the freezer container. The Archive and Working halves were sealed in plastic, placed in labeled D-tubes and stored in a refrigerated (+4°C) container together with discrete samples for planktic foraminifers and ostracodes.

WP CO (Chemical Oceanography)

This WP aims at increasing our understanding of the feedbacks among components of the Arctic Ocean carbon system with a focus on the continental margin boundary current in the Laptev - East Siberian – Chukchi Seas region. We address processes relative to environmental variability regarding questions like: To what degree is the interaction with the shelves impacting the chemical signature of the waters in the deep ocean and in what region is this of most importance? Is there a ventilation of shelf waters to deeper layers? Is methane leaking out to the overlying water along the continental margin?

These studies include the assessment of biogeochemical carbon transformation in the water column and air-sea exchange of CO_2in the outer shelf and slope areas as well as the exchange with the deep central basins, when the sea ice coverage is absent during the productive summer season. A decrease in summer sea ice coverage likely affects the magnitude of primary production and resulting export of marine produced organic matter to the underlying waters. A summer sea ice-free Arctic Ocean will also result in more brine formation through an enhanced sea ice production during the winter season. This might on the shelves contribute to formation of high salinity bottom water that leads to increased deep water ventilation. Both changes in export production and ventilation of the deep waters impact the sequestration of anthropogenic CO_2. Moreover, a warmer climate may impact the temperature of the Atlantic Layer that follows the continental margin and thus deepen the upper level of the methane stabilization horizon. Finally we also aim at assessing the natural ocean acidification, i.e. that caused by biogeochemical processes, in relation to that originating from uptake of anthropogenic CO_2.

In this work package we addressed the above questions by the study of the water column biogeochemistry along the outer Siberian Shelf and slope. Constituents that were determined includes the inorganic carbon system (DIC, TA, pH, CH_4), oxygen and nutrients (O_2, N, P, Si), transient tracer distribution (^{3}H, He, SF_6, CFC-12) and stable isotopes (^{13}C, ^{18}O). Seawater samples for the analyses that have been or will be performed within this WP were collected from Niskin type bottles on a rosette attached to a Seabird® CTD. In total some 52 (to stn 142) distinct stations over the entire transect have been visited and over 800 samples at different depth of the water column has been analysed.

Sampling strategy

Water samples were collected using a rosette system equipped with 24 bottles of Niskin type each having a volume of ~7 L. The bottles were closed at predefined depth during the return of the CTD-rosette package from the bottom to the surface. The latter was typically 10 m as the Oden mixes the water down to approximately this depth when drifting on the stations. On most stations we focused on the surface waters down to 300 m depths in order to have a high resolution in the layers where water exchange from the shelves to the interior basins. However, all depths down to the bottom were sampled with a depth resolution of no less than 500 m. Pressure, salinity and temperature were recorded at the closing of the bottles and stored in a CTD bottle file. This data together with notation of the depth where different constituents were sampled are noted in deck sheets (see appendix CO1). Quality control of the reliability at what depth the bottles were closed, as well as to assure the specific salinity of the water sampled in strong salinity gradients, were assured by determination of the salinity in the individual Niskin samples. This work was done by the physical oceanography group. Water samples for all constituents were drawn soon after the rosette was secured in the CTD container. The order of sampling was determined by the risk of contamination, i.e. CFC/SF_6, O_2, He, ^{3}H, CH_4, CH_4-isotops, DIC, pH/TA, nutrients, stable isotopes (^{13}C, ^{18}O), salt.

Inorganic carbon, oxygen,and nutrients(DIC, TA, pH,O_2, N, P, Si)

Methods for sampling, storage and analysis / oxygen, total alkalinity and pH

Oxygen samples were drawn from the Niskin bottles into Winkler flasks,equipped with glass stoppers, using silicon tubing and filled from below in order to avoid bubbles. The volume of the bottles was approximately 150 mL and they were overfilled with about one flask volumes. The oxygen was directly fixated by the addition of 1 mL each of concentrated manganese sulphate and basic iodide solutions to form $MnO(OH)_2$(s). Samples for the determination of DIC, pH and total alkalinity were collected as soon as possible as atmospheric CO_2 can impact the former. Two 250 mL Pyrex© bottles having tight plastic stoppers were filled to the rim in order to minimize contamination. All samples were stored at temperatures between 10 and 15 ^{o}C before analysis within hours of collection.

Analytical methods

Oxygen was measured using an automatic Winkler titration with UV detection. Before each titration session the system blanks were determined by addition of reagents to MilliQ water. The titrations were performed in the same flasks as the used for the collection of the samples from the rosette after the $MnO(OH)_2$ was dissolved by sulphuric acid. A sodium thiosulphate solution was used for the titration and its concentration was calibrated each day using pre-weighted KIO_3 standard. Precision was determined using replicates from the same depth and was better than 0.5 µmol/kg.

DIC was determined one of the 250 mL Pyrex© bottles collected from the Niskin flask using a coulometer titration method based on Johnson et al.(1987). A known volume of seawater, using a pipette having a volume of 15.250 mL at 25 ^{o}C, was added to a stripping cell containing 0.5 mL 10% phosphoric acid. Pure N_2 gas was extracting the CO_2formed from the DIC and transferred it to a coulometer cell. The gas is bubbled through a reagent containing ethanolamine, which reacts with the carbon dioxide to produce hydroxyethylcarbamic acid. The latter is coulometrically titrated by the hydroxide ions generated at the cathode and the pH in the reagent solution is monitored coulometrically through the indicator thymolphthalein. At the anode silver is oxidised. The amount of electrons produced corresponds to the amount of CO_2in the sample and can thus be converted to concentration by dividing by the sample volume. During leg 2 the precision was typically around 2 µmol kg^{-1}, with the accuracy set by calibration against certified reference materials (CRM), supplied by A. Dickson, Scripps Institution of Oceanography (USA).

The determination of **pH** was done on the total scale applying a spectrophotometric method using the indicator m-Creosol Purple (mCP). Pure mCP was purchased from the laboratory of Bob Byrne, Univ. South Florida, USA. A 0.2 mM indicator solution was prepared by dissolving pre-weighted mCP indicator in 0.5 L filtered seawater of about 34 salinity. The indicator was adjusted to a pH in the same range as the samples, approximately ± 0.2 pH units, by adding a small volume of concentrated HCl or NaOH. Before running a set of samples, the pH of the indicator was measured using a 0.02 cm cuvette. The measurements were performed on board within hours of sampling. An automatic system was used where the sample and indicator was mixed in a syringe (Klohnen) before injected to

a 1 cm cuvette of a diode array spectrophotometer (Agilent 8453), where the absorbance was measured at wavelengths 434 and 578 nm. Indicator corrections were made according to the recommendations from Chierici et al. (1999). The pH values are corrected to 15°C on the total scale.

The accuracy is determined by the pureness of the indicator and was also checked by the determination of reference water certified for total alkalinity and total dissolved inorganic carbon. The latter measurements indicate that it should be well below 0.01 pH unit. The precision as determined by replicates from the same sample bottle was in the range of ±0.001 pH unit.

Total Alkalinity (TA) was measured after pH from the same Pyrex© bottle. It was determined using an open cell potentiometric titration method using a GRAN point determination (Haraldsson et al., 1997). The system measures alkalinity in µmol/L using the nominal acid concentration of 0.05 mol/L. Certified reference material (CRM) as supplied by A. Dickson, Scripps Institution of Oceanography was used to determined accuracy. For all samples and CRM analysis the alkalinity in µmol/kg was calculated using the salinity (from the CTD bottle file and the certified salinity, respectively) and the temperature measured at the beginning of the titration. Sample results were then multiplied with the factor determined from the CRM measurements at each individual station, and the correction was always below 0.5%.

The given precisions were computed as standard deviations of duplicate analyses preformed continually during the cruise. Duplicates were run from the same sample bottle since total alkalinity is not sensitive to atmospheric contamination with the results typically not deviating more than 2 µmol/kg.

Methods for sampling, storage and analysis / N, P, Si

Nutrient samples were retrieved directly from the Niskin bottles into 100 mL HDPE-bottles (Kautex). The bottles were rinsed with sample water 2-3 times before completely filled and closed with a plastic cap. Samples were kept cold (4 °C) and dark until analysis, typically taking place the same day or the day after samples were taken. The bottles and caps were machine washed (70 °C) and rinsed with deionized water prior to the cruise.

Analytical method

Nutrients (PO_4, NO_2 + NO_2, NH_4, and SiO_4) were determined colorimetrically on board using a four-channel continuous flow analyser (QuAAtro system from SEAL Analytical). Each analysis run were preceded by running standards prepared from stock solutions of K_2HPO_4, KNO_3, NH_4Cl, and a commercial stable silica-compound solution. If analytical problems occurred, manifested as abnormal peaks, the sample batch was reanalysed immediately after the problem was located and fixed.

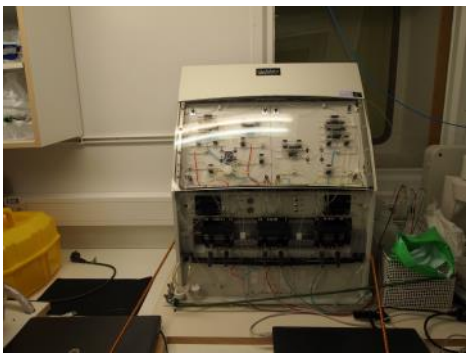

Continuous flow analyser QuAAtro from SEAL Analytical in the clean lab on ODEN. The instrument was used for continual on board measurements of nutrients in water throughout Leg 2.

Methane (CH_4, concentrations and isotopes)

Methods for sampling, storage and analysis / CH_4, concentrations and isotopes

Samples were collected both for CH_4 concentration as well as for its ^{13}C stable isotopes. The sample containers and procedures for different sample types were:

- Determination of CH_4, CO_2, and C_2H_6 at sea

60 mL luer-lock plastic syringes (centric hole), with rubber-gasket plungers. A three-way valve was fitted on the luer-lock fitting for efficient sampling and manipulation of headspace. The syringes were connected to the Niskin bottle using silicon tubing. 5 mL of sample was aspirated and ejected three times to rinse and remove any bubbles from the syringe. 45-50 mL of sample was then aspirated for analysis in the shipboard laboratory.

- Determination of CH_4, CO_2, and C_2H_6 back at shore

A 50 mL clear serum bottles were rinsed with seawater and then filled from the bottom by insertion of the tubing, overflowing for 3 seconds. 0.5 mL of $ZnCl_2$ preservative solution (2000 g $ZnCl_2$/L) was added to the bottle at mid height using a plastic syringe with long hypodermic needle. Pressing down a rubber stopper sealed the bottle immediately, using a hypodermic needle through it to displace sample water. The bottle was then crimp capped for further storage in the +4 ^{o}C cooler container.

- Determination of stable isotopes in CH_4, CO_2, and C_2H_6 back at shore

Two 120 mL amber serum bottles were filled, preserved and stored according to the same protocol as for the 50 mL clear serum bottles.

Analytical methods

For measurements of dissolved methane in water was used headspace equilibration method. Headspace extraction of gases for concentration analysis was performed directly in the 60 mL plastic syringes. The volume was adjusted to 50 mL and 10 mL of helium was aspirated. The syringes were shaken in a horizontal position for 15 min, and left still for an additional 15 min. After this, 10 mL gas sample injected in GC. Separation prior to FID was performed on a HaysepD packed column (1/8" diameter, 2 m) using helium as the carrier gas at 25 mL/min. Separation to TCD - HID was performed on a Mol Sieve 13x packed column (1/8" diameter, 2 m) using helium as the carrier gas at 25 mL/min. The water concentration profile was obtained with a temperature program [40 C isothermal, duration 7 min]. The FID was in all cases heated to 300 C, HID to 300 C and the TCD to 150 C (25 mL/min hydrogen from the hydrogen generator, 250 mL/min air, 20/40+10/20 mL/min helium). The detection limit for methane was 1 ppm.

Transient tracers (^{3}H, He, SF_6, CFC-12)

Methods for sampling, storage and analysis / ^{3}H, He, SF_6, CFC-12

Samples were collected using the following containers and protocols for different constituents:

- Determination of SF_6 and CFC-12

Water samples for CFC-12 and SF_6 measurements were collected with 250 ml TOMOPAL glass syringes from Niskin bottles with gas-tight connections to exclude atmospheric contamination. The syringes were stored in a water bath, flushed by surface seawater to prevent warming and outgassing of the samples during storage time.

- Determination of helium isotopes

Preliminary before sampling a 50 cm of 3/8"copper tubing was temporarily connected a 5 cm length of silicon tubing over each end into which the plunger from a 3 mL plastic syringe can be inserted as a stopper. Degassed water was filled from the bottom and overflowed enough to reject any bubbles inside copper tube. Then copper tube was temporally closed without bubbles by plungers from both sides and permanently closed at the middle by custom crimp clamp, allowing sampling about 10 cm^3 of water from each end of the tube.

At sampling site upper plunger was opened and a thin tube without bubbles was inserted to the bottom end of the one half of the copper tube to fill it from the bottom up and replace degassed water by sample. The tube was allowed to overflow before being temporarily closed using the syringe plunger. Permanent closing was performed within 30 min of the sampling using custom crimp clamps, which were screwed down tightly over the copper tube.

- Determination of tritium
Samples for the determination of tritium were collected in Coca-Cola bottles, preliminary rinsed with tap water and dried. A thin tubing was connected to the Niskin bottle and positioned at the bottom of the PET flask, which was filled and then allowed to overflow before closing.

Analytical methods

- CFC-12 and SF_6 were measured simultaneously by using a custom made purge and trap gas chromatographic system equipped with an Electron Capture Detector (Stöven and Tanhua 2014). Standardization was performed by injecting small volumes of a gaseous working standard containing SF_6 and CFC-12 which was prepared by the company Deuste-Steiniger (Germany). The CFC-12 and SF_6 concentrations in the standard have been calibrated vs. a reference standard obtained from R.F Weiss group at SIO. The CFC-12 data are reported on the SIO98 scale and SF_6 on the NOAA-2000 scale. Another calibration of the working standard will take place in the lab after the cruise, to determine any possible drift in the working standard. Calibration curves were measured every few days, depending on work load and system performance, to determine the non-linearity of the detector. Point calibrations were always performed between stations to determine the short term drift in the detector.

- The determination of ^{3}He, ^{4}He and tritium will be done back in the laboratory in POI, Vladivostok, after the cruise using stable isotope mass spectrometry. Tritium will be determined by measuring accumulated ^{3}He using ^{3}He ingrowth mass spectrometry method.

Stable isotopes (^{13}C, ^{18}O)

Methods for sampling, storage and analysis / ^{13}C, ^{18}O

Seawater for the determination of ^{13}C and ^{18}O was sampled at up to 10 depths per station into serum bottles. Subsamples were drawn from these into 1 mL syringes and injected into sealed test tubes filled with inert gas and to which acid had been added before the cruise. Three syringes were sampled per depth.

Analytical methods

The determination of ^{13}C and ^{18}O will be done back in the laboratory after the cruise using stable isotope mass spectrometry.

Equipment

Collection of water samples were relying on the CTD/rosette system that was handled by the physical oceanography WP. Analytical equipment utilized includes, for:

Carbon system

For determination of pH a system was used where an Angilent spectrophotometer was connected to a syringe for mixing of seawater and indicator, all controlled and evaluated by a PC computer. For the determination of TA a custom made titration system was used and for the determination of DIC a custom made extraction system connected to a UIC coulometer was used.

Nutrients

QuAAtro system from SEAL Analytical.

Methane

A SRI – 8610C series gas chromatograph equipped with flame ionization detector (FID) and methanator was used for the analysis of CH_4, CO, CO_2 and C2-C5 hydrocarbons. The instrument also had a helium ionization detector (HID; for H_2, O_2, N_2, CH_4) and a thermal conductivity detector (TCD; for O_2, N_2, CH_4).

CFC-12 and SF_6

The measurement system consisted of a Shimadzu GC 2014 (Gas Chromatograph) and a custom made purge and trap system.

Helium, tritium

Thermo Scientific HELIX SFT. A new dedicated Split Flight Tube static vacuum Noble Gas Mass Spectrometer is designed for the most precise isotopic analysis of small samples of Helium by simultaneous collection of its two isotopes with masses 3 and 4. It has a magnetic sector analyzer with 35 cm, 120-degree extended geometry bright ion optics with two-direction focusing and high dispersion. HELIX SFT can be used for precise isotopic analysis of all Noble gases.

WP PO (Physical Oceanography)

The physical oceanography program during Leg 2 involved CTD and Niskin water bottle sampling at 88 stations. The stations where mainly located over the continental slope and shelf, but with a few deeper stations in the Makarov and Amudsen Basins as well as several stations along the Lomonosov Ridge. Overall objectives were to characterize water masses in terms of salinity and temperature, vertical stratification, surface mixed layer, near bottom temperatures and bottom boundary layers. Specific objectives were to examine the circulation and development of the Atlantic Water layer and shelf-basin exchange. Also the distribution and flow of the upper low salinity water, derived from river and Pacific inputs and ice melt. Upward and downward looking ADCPs were mounted on the rosette for measuring the ocean currents during each cast. Salinity samples were drawn from the same bottles that were analyzed by the chemical water sampling program. These salinity samples were analyzed onboard with a lab salinometer, and were used for calibration and quality control of CDT derived salinities.

Equipment

CTD and rosette sampling system

The rosette included 24 Niskin bottles (7 liters) and was equipped with the following sensor packages:

- SeaBird 911 CTD
- Dual SeaBird temperature (SBE 3), conductivity (SBE 04C) and oxygen sensors (SBE 43)
- Turbidity sensor: Wetlabs ECO NTU S/N NTURTD-126
- Altimeter: BENTHOS ALTIMETER PSA-916D
- One upward and one downward looking Teledyne RD instruments WH 300kHz Monitor LADCP

Figure PO-1 gives an overview of the rosette setup.

Salinity samples were analyzed using a Guildline Autosal instrument which was kept in a well isolated lab container with relatively constant temperature. The salinometer was calibrated using one standard sea water ampule (IAPSO standard sea water from OSIL Environmental Instruments and Systems) before each batch of 24 samples.

Figure PO-1*: The rosette setup with the upward and downward looking ADCPs (yellow casing).*

Operation

The CTD/Rosette system was operated by two persons from the PO team working in 12 hour watches. During deployment and recovery of the rosette from the CTD container and into the water we had help by one extra person from the water chemistry group. At deep stations the rosette was typically lowered with 0.5 ms^{-1} over the upper 200 meters and with 1 ms^{-1} from 200 m down to bottom. The rosette was normally lowered to about 2 m above the bottom when we had good conditions with low drift speed of the ship and relatively flat bottom. Otherwise it was kept at a larger distance above bottom (3-5 m). The bottles were tripped after a 30 seconds equilibration at constant depth. The CTD was operated from the bow at Oden and most of the CTD casts were made with the ship in free drift with the wind. This is because Oden´s engines are not constructed for running at low power, implying the ship cannot be held at a steady position for more than about 15 min. The CTD operations with free drift worked well during conditions up to about 10 m/s wind speed, although the drift speed during stations were often more than one knot. It appeared that the upper limit for the free-drift CTD operations was at a wind speed around 12 m/s as the wire angle from the vertical became really large (>45 deg).

Shipboard post-processing

The CTD data files were post processed with standard SeaBird data processing software including the steps Data conversion, Filter, AlignCTD, Cell thermal mass, Loop edit, Derive, Bin average, Ascii Out, and Bottle summary.

The despiking was made manually by first visually identifying spikes and then interpolating across the spike in the .cnv file from the raw data conversion. For this purpose a series of Matlab scripts were developed.

The alignment parameter was tuned for each sensor pack following the suggested method described in the SeaBird Data Processing manual.

Salinities were compared with bottle salinites analyzed with the Autosal lab salinometer. The analyses revealed a systematic offset of conductivity sensor 1, from station 16 and onward, corresponding to about 0.002 PSU higher salinities compared to the salinometer and to conductivity sensor 2. A conductivity slope correction was calculated and the raw data conversion was redone with the slope correction put into three configuration files representing the different hardware set-ups used for stations 16-155. The converted files were then despiked. The rest of the processing steps were then performed on the, for some stations, corrected conductivity and despiked raw data converted cnv-files. The final CTD data product is available in full resolution (25 scans per second) and in 1 m bin average versions.

WP BLM (Boundary Layer Meteorology)

The overriding goal of the Arctic Clouds in Summer Experiment (ACSE), also SWERUS WP I, is to better understand Arctic clouds and their role in regulating the surface energy balance. Another related objective is to understand how processes that modulate the surface energy balance are themselves affected by the transitions between open water and ice-covered areas in summer and early autumn. Clouds are known to have a profound influence on climate, reflecting solar radiation back to space and trapping infrared radiation near the surface. In the Arctic the surface energy balance is dominated by processes relating to low clouds, and hence these have an important impact on the freezing and melting of the sea ice. The structure and stability of the Arctic atmospheric boundary layer likely differs over sea ice compared to over open water, and this difference greatly impacts the various components of the surface energy budget, including those related to clouds.

Low clouds and fog are abundant in the Arctic, climatologically cover the surface 60-100% of the time, more in summer than in winter. In the summer Arctic where the sun is low but above the horizon most of the time, the effects of low clouds can vary greatly from over open-ocean to areas covered by sea ice because of the difference in surface albedo, and their effect is different from similar clouds over other world oceans. In short, while low clouds reflect solar radiation and hence limit the available energy at the surface, they absorb longwave radiation from the surface but also emit longwave radiation back to the surface, thus increasing the available energy at the surface. With a high surface albedo as over the sea ice, the longwave ("greenhouse") effect often dominates at all times except in the middle of summer, and the surface is heated by low clouds. In such areas and times, the surface temperature often falls when it becomes clear. Over the open ocean where the albedo is low, solar radiation dominates to an even greater extent during mid-summer, and its dominance persists longer into the autumn. These radiative effects also depend on and interact with the dynamics of the system, both the local cloud and boundary-layer dynamics and the larger-scale motions of the atmosphere which bring air of differing origins to a given location.

Low clouds that have a layer of liquid water are efficient at emitting longwave radiation, thus heating the surface but also cooling the cloud top. The latter destabilizes the vertical column of air and drives buoyant vertical motions – turbulence – that may mix to the surface depending on the stability of the lowest layers of the atmosphere known as the boundary layer. Furthermore, the downwelling longwave radiation depends on the temperature of these clouds, with warmer clouds enhancing the downwelling radiation. If the cloud top temperature is below zero, precipitation may form as ice crystals in the super cooled liquid layer, producing so called mixed-phase clouds. Such clouds are common in the Arctic but the interplay between thermal advection, radiation, turbulence, cloud microphysics and precipitation is poorly understood. Hence, the representation in models of the physics involved is inadequate, and hence weather and climate models struggle to get this right.

The large-scale atmospheric flow may bring warm and moist air from south or cold, dry and clean air from north. These new air masses are gradually brought into balance with the local surface, whether sea ice or open water, through energy fluxes. These energy fluxes likely differ significantly over melting sea ice (where the surface temperature is locked to near freezing), freezing sea ice with a varying surface temperature, and warmer open water. These advective processes also affect the properties of the clouds, and hence the surface energy balance.

The goal of ACSE is to understand these processes better, and to do so necessitates simultaneous measurements of the vertical structure of the atmosphere in general, cloud properties in particular and also the surface energy fluxes and characteristics. These measurements need to be carried out over the open water, near the marginal ice zone, and within the pack ice of the Arctic Ocean. During

Leg 1, summer melting conditions were encountered on a fairly extensive pack ice area (Fig. BLM1), while during Leg 2 melting conditions were initially encountered (Fig. BLM-2a) but some initial freeze-up conditions were also measured towards the end of this leg (Fig. BLM-2b).

To make these measurements on a moving ship is a challenge. We accomplish this by making continuous observations through the whole expedition of the primary parameters, regardless of station or transit between stations, starting and ending in Tromsø, Norway, with an exchange of science crew in Barrow, Alaska (which also marked the transition between Leg 1 and Leg 2). Only the wave buoy measurements depended on stations. Though the cruise track was determined by the other SWERUS objectives, the track included extensive periods of open water and pack ice conditions, and numerous crossing of the Marginal Ice Zone (MIZ). Such mixed conditions allow the above objectives to be met.

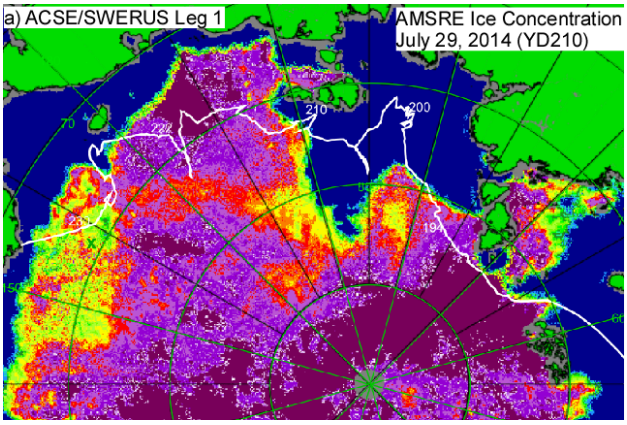

Figure BLM-1: *The ACSE/SWERUS track for Leg 1. The Year Day is at times shown on the track corresponding to the Oden location on that day.*

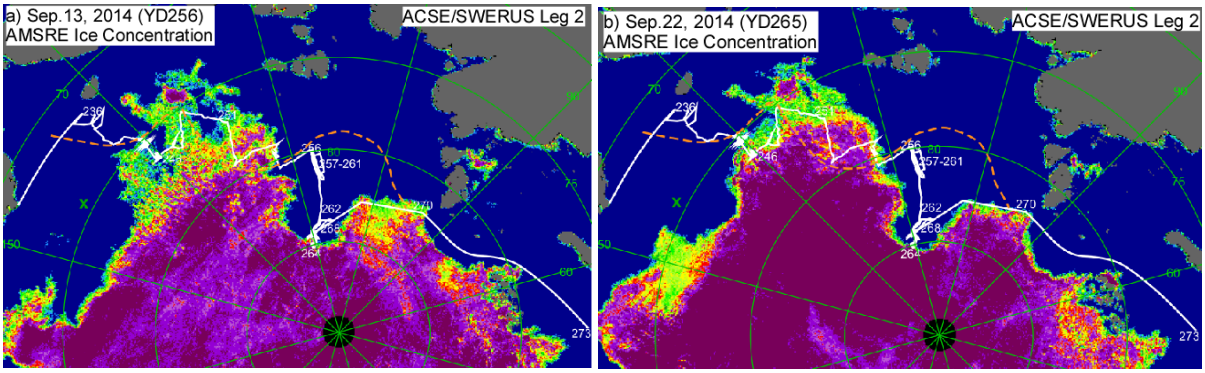

Figure BLM-2: *The ACSE/SWERUS track for Leg 2 showing sea-ice concentrations on a) Sep 13, the approximate minimum sea ice extent, and b) Sep 26. The Sep 26 ice concentration shows an increase within the exisiting ice areas and an increase in extent in some regions (e.g., the Beaufort Sea). The Year Day is at times shown on the track corresponding to the Oden location on that day. The approximate location of the Russian Exclusive Economic Zone is shown as a brown dashed line.*

Three main types of instrumentation systems were used and are described below, as are the involved technology and methods.

Equipment

General meteorology observations

The general meteorology observations provide context to the more specialized observations described below. This program has two main components (total amount of data is 4GB for the weather station and 5GB for the soundings):

1) Weather station: This consists of a combination of instruments located on and in front of the railing in the forward center of the 7th deck of Oden, logged on a common logger all sampled at 1Hz:
   a. Wind speed and direction with a Gill 2D Ultrasonic anemometer
   b. Position and horizontal motions with a Garmin GPS
   c. Temperature and relative humidity with a platinum resistor thermometer and a capacitive hygrometer, respectively
   d. Local atmospheric pressure with an electronic barometer.
   e. Incoming short and longwave radiation are measured with Eppley pyrano- and pyrgeometers, respectively, mounted on a gimbaled platform. The gimbal for the pyranometer (pyrgeometer) was immobilized at 01:40 UTC (01:50 UTC) on Sep. 2 because relative winds from the bow of 6-9 m/s or more caused a tilt of up to 15-20 degrees.
   f. Additional to this, but logged separately at one minute intervals and sampled as one minute averages, are a visibility sensor and a cloud base lidar (so called ceilometer). Both are based on lidar technology.

   All these instruments, with the exception of the GPS system and the ultrasonic anemometer, are from Vaisala Oy.

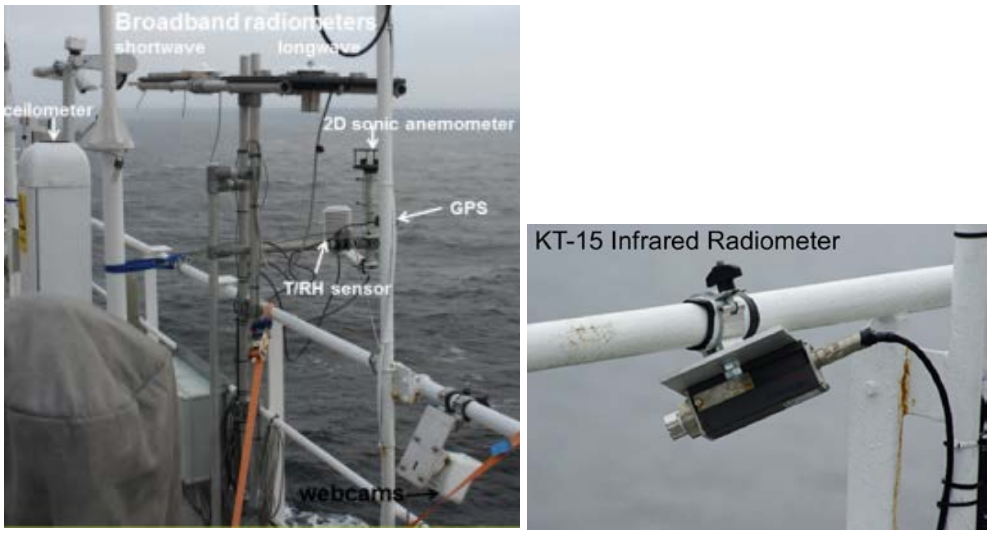

Figure BLM-3: Meteorological instruments deployed on the 7th deck of the Oden and discussed in the text.

2) Rawinsondes: Soundings through the entire troposphere and into the stratosphere are performed with free-flying helium-filled balloons carrying Vaisala RSG92 rawinsondes (sonde); soundings are released every 6 hours from the helideck of Oden (Fig. BLM-4). The receiving station for the system is located on the 7th deck, in the port side container. Each sonde carries a barometer, thermometer and a hygrometer providing profiles of the state of the atmosphere; the techniques used are similar to instruments on the weather station but less expensive since they are expendable. Additionally, a GPS sensor on the sonde measures the track of the sonde; this is the same as the wind, so the sonde also provide profiles of wind speed and direction.

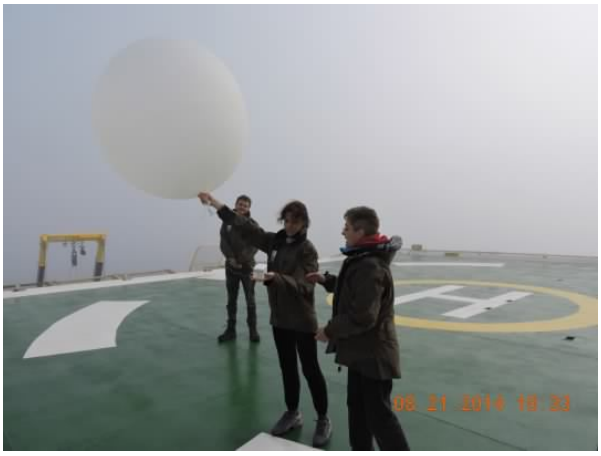

Figure BLM-4: *Launch of a rawinsonde weather balloon during Leg 2.*

Surface flux observations

Near surface atmospheric turbulence and the associated turbulent exchange of momentum, heat, water vapor and aerosol particles were made through the cruise, using so-called eddy-covariance technique. The system consists of several instruments installed at the top of the foremast.

1) At the top of the mast (total amount of data for leg 2 is 70GB):
   a. One heated Metek sonic anemometer (BLM-5a) measures the 3-dimensional turbulent velocity of the air flow at 20Hz. Along with this an XSens MTi-G-700 inertial motion unit that provides 3D accelerations, rotation rates, and GPS position at 40Hz. The frame of reference is aligned with that of the sonic anemometer. The measurements are combined with those from the ship's navigation system (heading, speed and course over ground) to correct the turbulent wind measurements for ship motion. An example of partially processed data is given in Fig. BLM6.
   b. One Licor LI-7500 open path gas analyzer – water vapor concentration also at 20Hz (Fig. BLM5a); when combined with the vertical velocities from the Metek it provides turbulence fluxes of water vapor.
   c. One CLASP aerosol spectrometer sampled at 10Hz. This provides particle size spectra for the size range $0.25 < R < 18.5\mu m$, with 16 logarithmically spaced size bins.
   d. Temperature and relative humidity sampled at 1Hz from instruments mounted in a fan-aspirated and radiation protected shield.
2) One third down the mast (Leg 2 data amount est. 18 GB):
   a. One CSAT-3 sonic anemometer (Fig. BLM-5b) mounted on a 1.5 m boom directed forward measures the 3-dimensional turbulent velocity of the air flow at 20Hz. On the same boom as the CSAT, an XSens MTi-G-700 inertial motion unit provides 3D accelerations, rotation rates, and GPS position at 40Hz. This will be used to process the sonic data.
   b. Temperature and relative humidity sampled at 1Hz from instruments mounted in a fan-aspirated and radiation protected shield.
   c. In addition to this flux system we sampled the high-rate data from Patrick Crill's LGR mass spectrometer system on the mast platform, drawing its sample from the top of the mast. This will enable turbulent fluxes of methane and carbon dioxide to be estimated.

Figure BLM-5: *Photos of the turbulence/surface flux instruments with (left) the top Metek/Licor/CLASP instrumentation with its motion sensor, and (right) the CSAT sonic on its retractable boom with the motion sensor mounted.*

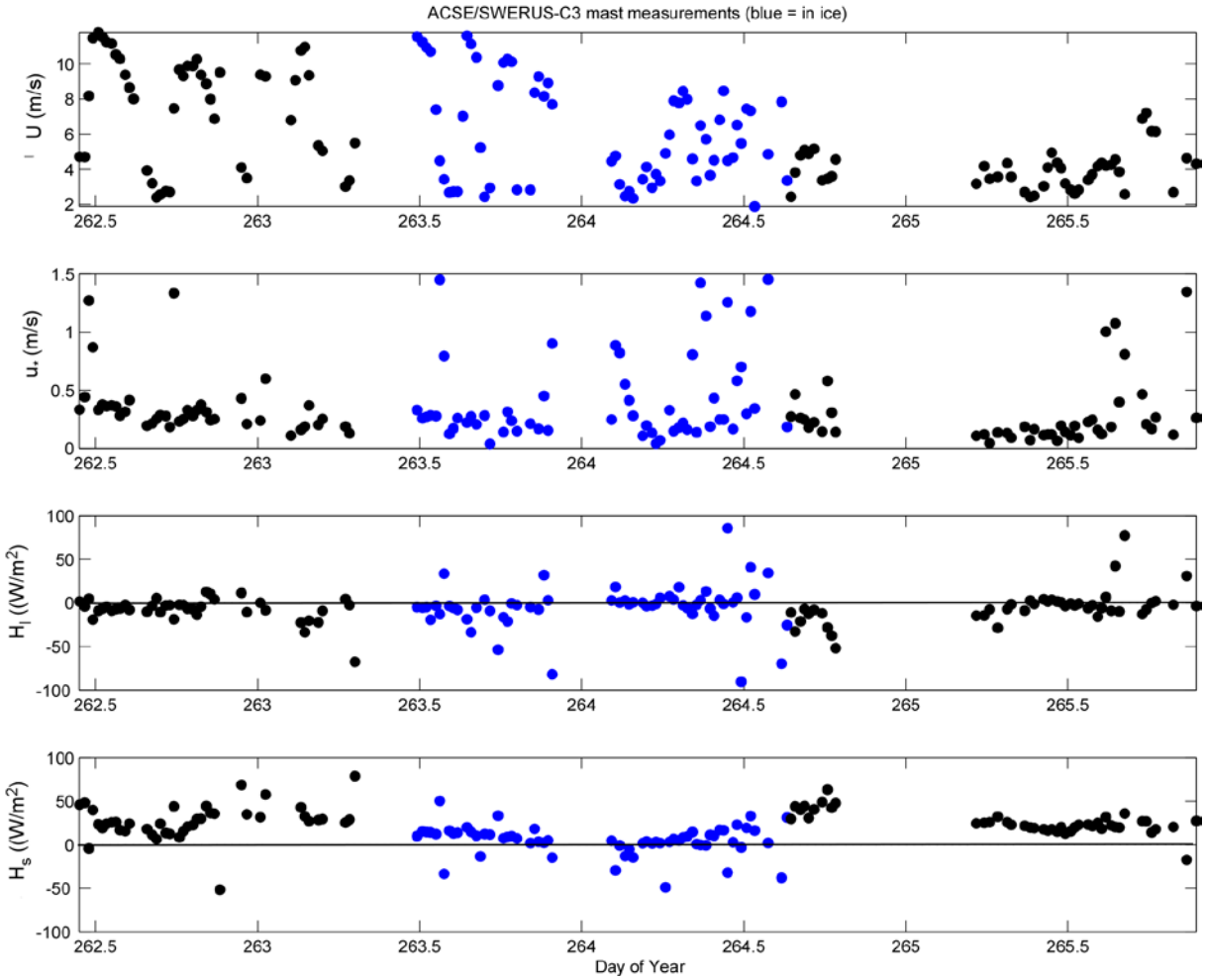

Figure BLM-6: *Plots of very preliminary (a) wind speed, b) friction velocity (momentum flux), c) latent heat flux, and d) sensible heat flux from the Metek sonic anemometer using eddy covariance techniques for Sep 19-22 (YD262-265). Ship distortion corrections have not been applied, but correction for ship motion has been. Blue (black) points are in ice (open water).*

Surface based remote sensing

Surface based remote sensing relies on either active instruments (radar or lidar) or passive instruments (microwave radiometers). The former transmit energy and senses both the strength of the returned signal and its Doppler shift, while the latter senses naturally emitted radiation from the atmosphere at different wavelength, emitted by different atmospheric constituents according to their temperature. We have deployed several such instruments.

1) W-band Cloud Radar**:** This is a NOAA-built cloud radar that was operated from the sea container in position 11 on the roof of Oden's foredeck lab (Fig. BLM-7a). The system operates at 94-GHz and nominally points vertically. It is operated on a motion stabilizing platform designed to maintain the radar level in spite of ship's pitch and roll motions. Measurements include profiles of the full Doppler spectrum that results from backscatter of transmitted signals from hydrometeors in the vertical column. From the spectrum, standard radar moments are derived, including the reflectivity, mean Doppler velocity, and Doppler spectrum width. The system has operated near-continuously for the duration of Leg 2. Many files are produced each day including hourly raw Doppler spectra, Doppler moments, instrument health messages, and output from the positioning system for the motion stabilized platform. Total data volume for Leg #2 is: 60 GB (moments); 900 GB (spectra); 9 GB (logs).

2) 449-MHz Wind Profiler**.** The wind profiler design was originally built at NOAA and is a phased-array Doppler radar operating with 5 fixed beams. The antenna is mounted above the containers placed on top of Oden's main lab (Fig. BLM-7a). It has two operational modes with vertical resolutions of 62 m and 400 m. Transmitted pulses reflect off of radial gradients in the atmospheric refractive index. Using Fourier transform techniques, the system converts raw reflected signals into averaged Doppler spectra that are then analyzed to produce information about the radial velocities and backscatter magnitude. These data are used to estimate hourly profiles of wind speed and direction. The 449 MHz radar operates continuously, and has been very reliable during the cruise but continues to have issues with so-called ground clutter; effects on the so-called side lobes of the instrument by the ocean surface especially as it passes by when the ship is moving. The system produces two daily raw files and two daily, first-estimate wind profile files. Total data volume for Leg 2: 46 GB.

3) LIDAR: A Halo Photonics scanning Doppler lidar was installed on the roof of the CTD winch container (Fig. BLM-7a). The lidar measures the intensity of backscatter laser light, providing a measure of atmospheric particle loading and along-beam Doppler wind speed. Cross-polarization provides additional information on particle shape allowing cloud droplets and ice crystals to be distinguished. The lidar operated in multiple scan modes. Most of its time is spent staring vertically upwards to measure boundary layer structure and cloud. Every 10 minutes a 5-point wind profile is measured (vertical + 4 off-vertical (70° elevation) beams at azimuths of 0,90,180,270 allow a single wind profile to be estimated), every hour 0-90° elevation scans were undertaken forward over the bow and 30° either side, along with a single horizontal scan at an elevation of 0°. To keep the lidar pointing in the correct attitude it was mounted within a motion stabilized platform that keeps it within about 0.1° of the horizontal most of the time. The residual linear velocity of the platform (heave and ship horizontal motion) is monitored and can be used to correct the lidar Doppler velocity for ship motion. Data volume is approximately 1GB per day (processed output) + 19GB per day (raw binary data files) (840 GB for Leg 2). The lidar data will be used to provide boundary layer wind profiles, information on vertical structure and mixing,

turbulence intensity throughout the depth of the boundary layer, and information on cloud phase.

4) HATPRO Scanning Microwave Radiometer: The HATPRO scanning radiometer mounted on the roof of the 4th deck triple-container lab makes a scan from 0-90° elevation over the bow, measuring the microwave brightness temperature at multiple wavelengths. Given an initial best guess of the vertical profile of temperature and humidity, high temporal resolution (5 minute) profiles of temperature and humidity, along with integrated precipitable water vapor and liquid water path can be retrieved. During the cruise the initial best guess profile is provided by a climatological profile for the Arctic. In post processing the radiosonde profiles will be used. Cruise retrievals are available immediately while reprocessed data will be available in approximately 6 months. Approximate data volume: 123MB per day, 5.7GB total.

5) Radiometrics Scanning Microwave Radiometer (MWR)**:** A scanning Radiometrics MP-3000 multi-channel microwave radiometer was installed on the corner block of the CTD winch container in position 10 on Oden. It measures downwelling sky brightness temperatures in the range of 20-30 GHz, to derive the integrated liquid water and water vapor in the atmosphere (e.g., see Fig. BLM-11b), and in the range of 50-60GHz, to derive profiles of atmospheric temperature and moisture. First-estimate geophysical parameters are derived operationally with a default retrieval algorithm that has been applied during the cruise. Best-estimate geophysical parameters will be

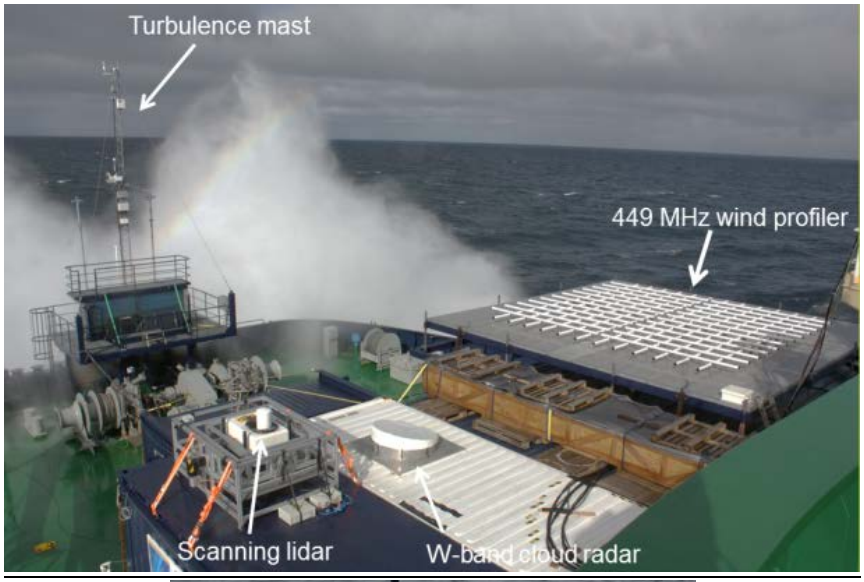

Figure BLM-7: *Photo of remote sensing instruments on Oden's foredeck (top) and the HATPRO scanning radiometer (bottom). Hidden from view are the MWR radiometer, on same container as the lidar, and the ceilometer behind the radar container. The turbulence mast is also shown.*

derived post facto using input from rawinsonde measurements of temperature and moisture structure during the cruise itself. Operations during leg #2 of the cruise have been fairly clean with minimal interruption. Data are provided in a suite of 5 ASCII files (lv0, lv1, lv2, tip, ser), all containing header information that describes the fields, measurement units, operational modes, etc. "ser" files are instrument logs, "tip" files contain calibration information, "lv0" files contain raw voltage measurements, "lv1" files contain brightness temperature measurements, and "lv2" files contain the first-estimated retrievals of geophysical parameters. Total data volume for leg 2: 750 MB.

6) Ceilometer**:** A Vaisala CT-31 ceilometer was installed to the rear of the sea container in position 11. It uses a near-infrared laser to derive the atmospheric backscatter and specifically to derive information on the cloud base height (see Figure X) and vertical visibility height. Cloud base height estimates for up to 3 layers, as well as the depth of penetration into low-level fogs, are derived operationally by the Vaisala software. Operations during leg #2 of the cruise have been continuous. Other than correcting the height measurements for the height of the ceilometer relative to the sea surface the raw measured data set will likely be the final data set. A single daily ASCII file is typically produced in standard Vaisala formats with naming convention CYMMDDhh.DAT, where Y is the last digit of the current year, MM is the month, DD is the day, hh is the hour. Total data volume for leg 2: 1 GB.

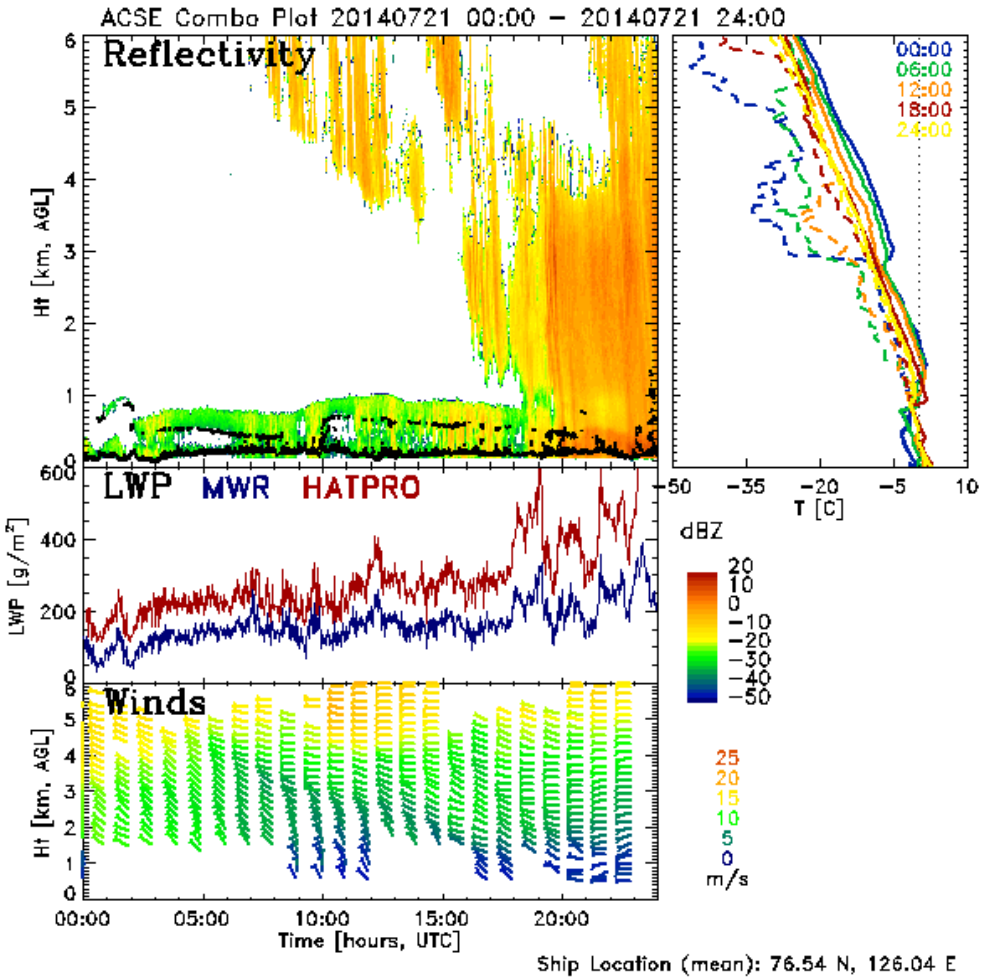

Figure BLM-8: *Example of results showing measurements on 21 July 2014, including time-height color contour of W-band radar reflectivity including ceilometer cloud base height (black dots) in top panel; derived cloud liquid water path from microwave radiometer and HATPRO in middle panel; derived profiles of wind speed and direction from the 449-MHz wind profiler in the bottom panel; and radiosonde temperature profiles in the panel to the right for context.*

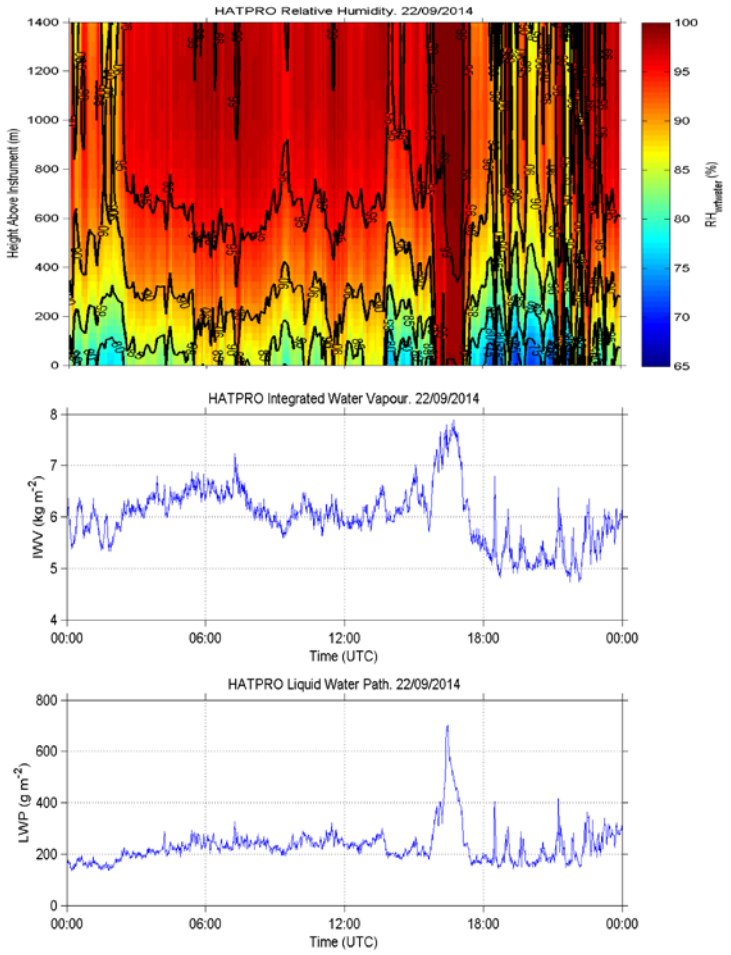

Figure BLM-9: *Example of some of the data from the HATPRO scanning radiometer: Time-height cross-section of temperature to 1400 m height (top), vertically-integrated water vapor (middle), and liquid water path (bottom) as observed by the HATPRO radiometer for Sep. 22, 2014 (YD 265).*

Miscellaneous observations

Some complementary observations were also made, in support of the main observations:

1. Surface skin temperature: Infrared surface temperature estimates were made with two Heitronics KT15.85 IR temperature sensors. Both are mounted on the starboard rail of the 7th deck (Fig. BLM-3), one pointing about 45° forward and one 45° aft. Both are angled out to measure outside the ship wake in open water. Data is available immediately, however, a refined and quality controlled data set will be available within about 6 months. Data volume: 12MB per day (500 MB for Leg 2).
2. Surface imagery: Three webcams were installed on the rail on 7th deck (Fig BLM3), pointing forward, port and starboard. Each camera has a 90° field of view and records one image per minute. Imagery will be used to provide a visual record of the surface conditions through the cruise, and potentially estimates of local ice fraction. Data volume: approximately 250GB for Leg 2.
3. Surface waves: Datawell DWR-4-G Waverider buoy was deployed, tethered to the ship on a 200-m line. The waverider measures the 3-dimensional velocity of the buoy, integrating to obtain the displacements, from which directional wave spectra and basic wave statistics can be derived: significant wave height, wave periods (zero crossing, period of spectral peak, 'energy' period, etc.). For Leg 2, Waverider measurements were obtained on numerous occasions during coring and/or CTD stations outside the pack ice and in large open-water areas within the pack ice (Fig. BLM-10). Twenty-two stations obtained wave data for 30-198 minutes (see Table BL-1). Over 38

hours of good data was obtained, with over 30 hours of those occurring during Leg 2. Local fetch information associated with the buoy deployment is obtained from photographs of the ship's navigation X-band radar screen during pack-ice deployments. Three deployments were done in the Russian EEZ; one of these acquired no useful data because it did not drift away from the ship. (1 MB data for Leg 2)

Table BL-1: *Times, locations and notes of the waverider buoy deployments during ACSE. Those done in the Russian EEZ are marked in red.*

Number	Date	DoY	Lat	Lon	In	Undist.	Recovery	Good Dur.
			deg N	deg E	Water	Waves	Begins	min
1L1	7/18/2014	YD199	76.774	125.830	13:18	-	15:00	0
2L1	7/19/2014	YD200	76.893	127.798	12:50	13:00	18:29	329
3L1	8/14/2014	YD226	74.322	-171.444	22:25	22:27	23:50	83
4L1	8/15/2014	YD227	74.398	-169.671	3:24	3:26	4:30	64
1L2	8/26/2014	YD238	72.821	-175.486	6:30	-	-	0
2L2	8/28/2014	YD240	75.172	179.875	21:10	21:25	22:55	90
3L2	8/28/2014	YD240	75.143	179.862	22:50	22:52	23:30	38
4L2	8/29/2014	YD241	75.475	-179.757	20:27	20:34	21:55	81
5L2	8/30/2014	YD242	75.304	-179.627	6:50	7:00	7:45	45
6L2	8/30/2014	YD242	75.079	-179.988	21:38	21:52	23:54	122
7L2	8/31/2014	YD243	75.505	-179.092	7:58	8:05	8:40	35
8L2	8/31/2014	YD243	75.025	179.833	20:45	20:55	22:55	120
9L2	9/4/2014	YD247	76.4672	176.7894	1:00	1:10	2:00	50
10L2	9/4/2014	YD247	76.3642	176.4383	4:02	4:10	5:38	88
11L2	9/4/2014	YD247	76.3209	175.8902	8:02	8:13	9:27	74
12L2	9/6/2014	YD249	76.4074	173.9226	7:05	7:15	8:32	77
13L2	9/12/2014	YD255	79.8183	154.1786	3:22	3:25	3:56	31
14L2	9/12/2014	YD255	79.9228	154.3826	6:36	6:41	8:54	133
15L2	9/14/2014	YD257	81.3290	141.7355	3:20	3:25	5:40	121*
16L2	9/14/2014	YD257	81.0630	142.1099	9:00	9:03	10:05	62
17L2	9/14/2014	YD257	80.4743	142.9158	22:20	22:23	0:43	140
18L2	9/17/2014	YD260	80.7008	142.1143	6:35	6:39	8:11	92
19L2	9/20/2014	YD263	84.5113	151.9179	2:08	2:15	5:33	198
20L2	9/20/2014	YD263	85.1343	151.5701	21:33	23:01	0:43	102
21L2	9/22/2014	YD265	84.2690	148.7352	2:19	2:21	3:19	58
22L2	9/24/2014	YD267	84.7222	150.9535	22:45	22:55	0:07	72

Figure BLM-10: *Waverider buoy deployment on Sep. 17 and a close-up photograph of the buoy.*

Shipboard post-processing

Post-processing at sea of this data is limited to preliminary quality control analyses, producing quick-look images, and organizing/cataloging of the large amounts of data. Some preliminary correction for ship heading and speed over ground is done for the quicklook products involving wind data (e.g., the lidar and wind profiler; see Figs. BLM-15 and BLM-17 in result section). These same corrections and the corrections for the higher-frequency ship motion, such as heave, pitch, and roll, will be done in post-processing during the coming year for any data set measuring atmospheric motions, which include the lidar, turbulence, cloud radar, and wind profiler. Care is taken that all metadata is saved necessary to understand when, where, and under what conditions the various measurements were obtained, and that ancillary measurements necessary for post-processing corrections of the primary measurements is obtained. For example, measurements of the ship motion are made continuously that will be used to place the turbulence and remote sensor data into a fixed geophysical coordinate system rather than one moving with the ship. Other impacts on the data due to the shipboard nature of the measurements, such as shading of the radiometers by ship superstructure, must be estimated in order to correct the data. Because it is crucial to combine the various parameters measured during the analysis, care is also taken to carefully synchronize timestamps on the various data sets, generally to one second or better.

Also, processing on board has focused on comparing atmospheric structures as obtained by the different instrumentation systems to help guide later analyses. As an example, the radiometer relative humidity fields for a three day period as measured by the Radiometrics radiometer and the radiosondes are compared in Figure BLM-11, showing that the radiometer tends to smooth and vertically elongate the vertical structures found in the radiosondes, and can be in error at higher altitudes. However, especially at lower altitudes, the radiometer is much better able to capture the temporal evolution of the humidity features, since these often have time scales of a few hours.

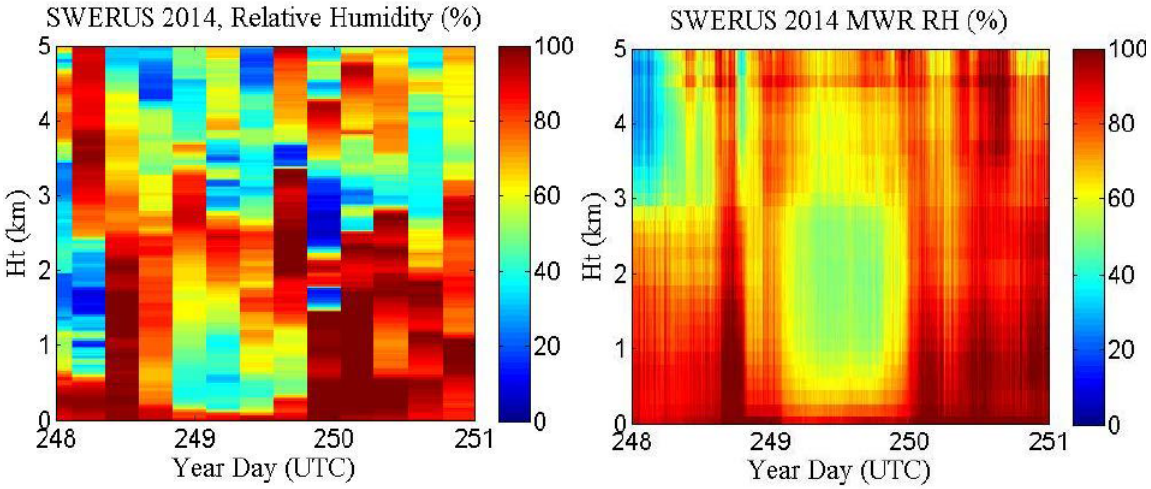

***Figure BLM-11**: Comparison of the relative humidity field from the surface to 5 km height for three days (Sep. 5-7) as observed by the 6-hourly rawinsondes (left) and the higher temporal resolution Radiometrics radiometer. Clearly, the vertical details that the radiosondes capture are greatly smoothed in the radiometer data, especially at upper levels, while the radiometer data provides better temporal resolution of the humidity features, which can often have time scales of a few hours or less.*

Results – metadata, data, and samples collected

WP GM Geophysical Mapping

Multibeam

Data Structure and Organization

EM122 multibeam sonar data were written directly to disk in the "Raw Data" directory of the "multibeam2" computer on the shipboard network. On this disk raw EM122 and SBP120 data from both SWERUS Legs 1 and 2 are stored. Within the EM122/SWERUS Leg2 directory, data were further separated into directories representing data acquired within the Russian Exclusive Economic Zone and those data collected outside the Russian EEZ. This was done in order to be able to fulfill conditions outlined in the Russian research permit. Within both the INSIDE_EEZ and OUTSIDE_EEZ directories the data are further subdivided into sub-directories for each day labelled 2014MMDD. The individual raw data files within each day file are then labelled LNNU_2014MMDD-Thhmmss_Oden.all for bathymetry and LNNU_2014MMDD-Thhmmss_Oden.wcd for water column imagery. LNNU is a four digit line number set by the SIS control system and MM is month, DD day, hh hour, mm minutes, and ss seconds (Fig. GM-20). Backups of the raw data were made throughout the expedition.

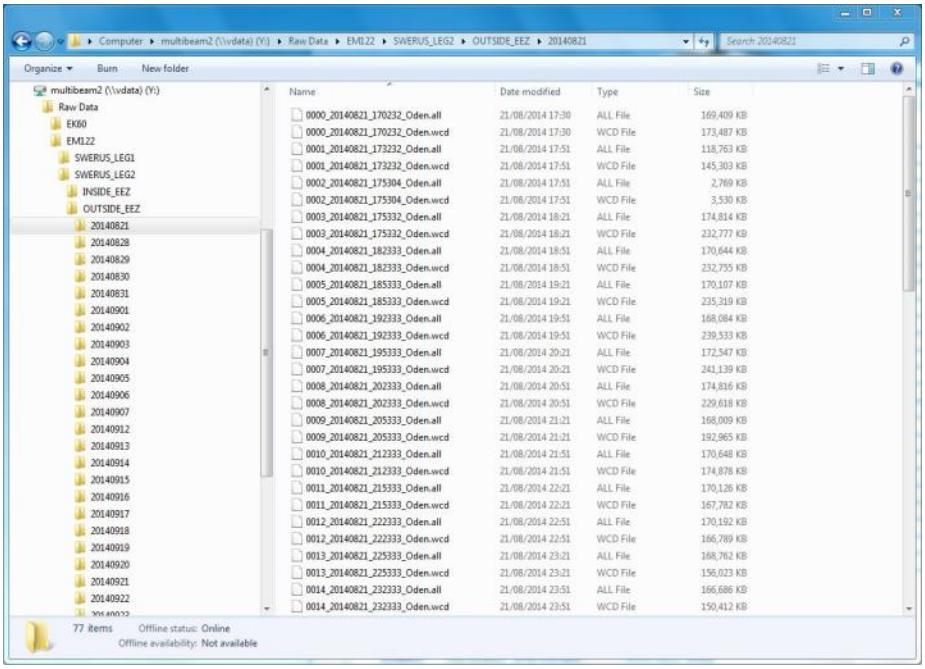

Figure GM-20*: Data storage file structure for EM122 data on SWERUS-C3 Leg 2.*

Multibeam Results

The EM122 data collected on SWERUS-C3 Leg 2 represent a remarkable addition to high Arctic mapping that not only fills critical gaps in our knowledge of Arctic bathymetry but directly addresses a number of the key questions posed by the SWERUS-C3 program including the history and distribution of glaciers and the constraints on deep ocean circulation in the Arctic Ocean. The system operated continuously for the entire leg with more than 10747 line km of multibeam of multibeam sonar data acquired representing a very rough estimate of 14.5 million square km of seafloor mapped. The surveys were divided into 5 main study areas labeled Boxes 1 through 5 with work taking place both within and outside of the Russian Exclusive Economic Zone (Figure GM-17). Logging stopped when we reached the Russian EEZ during the final transit to Tromsö, Norway.

Box 1 (Fig GM-21) was entirely within the Russian EEZ and focused on the Herald Canyon region, an area known to be the locus of numerous gas seeps. Mapping was done more in transect mode (long individual lines rather than concentrated regions of overlapping coverage) in order to find optimal locations for core sites (see WP Sediment Coring section) and to collect both seismic and EM lines to better characterize the geophysical setting of the gas seeps. This region was also an area of intense focus by the Water Column Imaging team (see WP Water Column Imaging section).

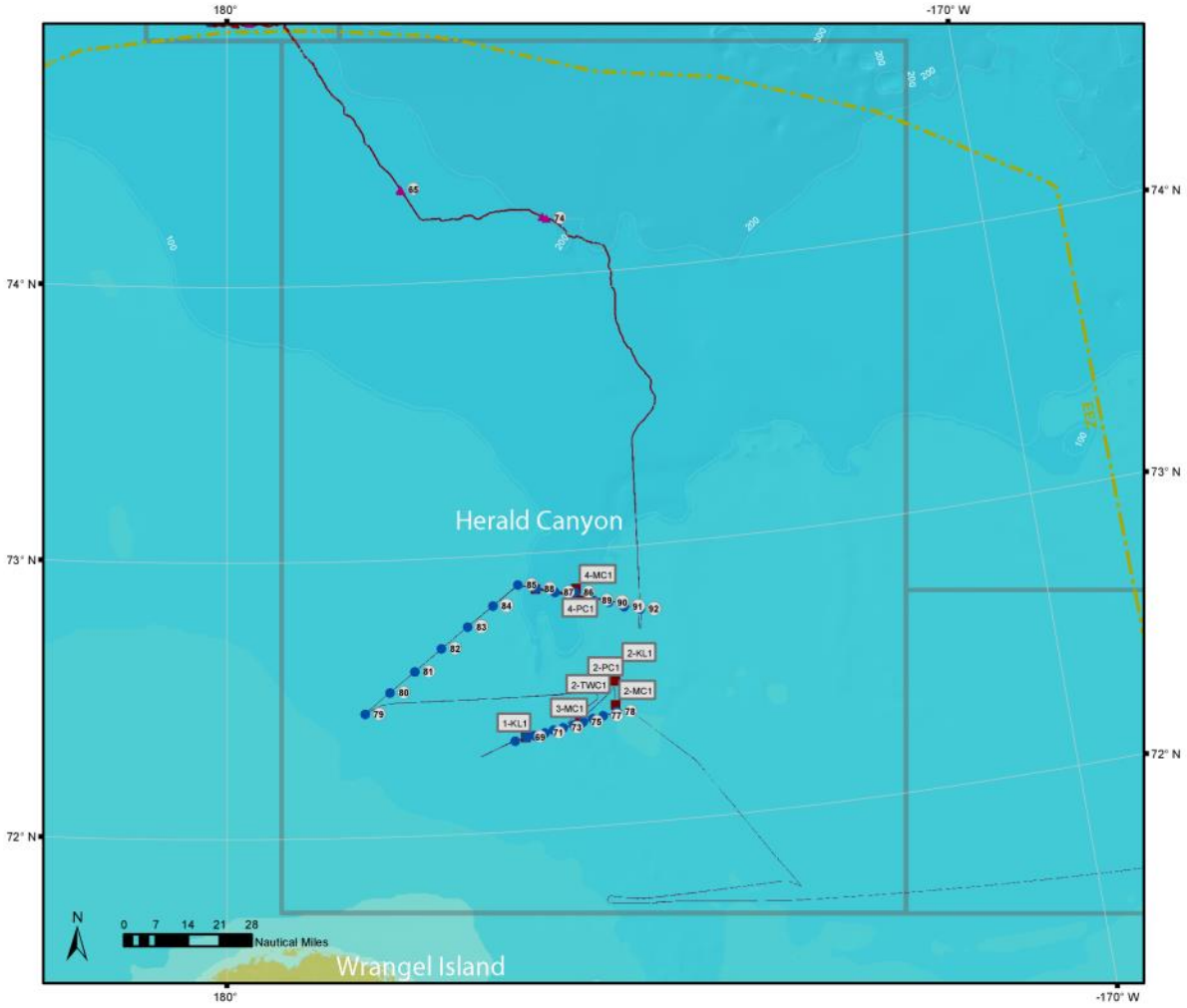

Figure GM-21*: Box 1 encompassing the Herald Canyon area inside the Russian EEZ. Coring stations are marked with purple boxes along with the station name written in the white boxes. All coring stations has the prefix "SWERUS-L2-" omitted on the map (see WP SC). CTD stations are marked with blue dots along with their station number in white circles (See WP PO). The purple triangles show XBT stations.*

Box 2 (Figure GM-22) is on the southern end of the Mendeleev Rise, just beyond the Russian EEZ. Here mapping focused on two areas: 1) the slope region from the Siberian Shelf down to about 1000 m depth, and then after crossing a deeper saddle to the north between the slope and the Mendeleev Ridge; 2) the southwestern flank of a feature known as Arlis Plateau between about 900 and 1200 m depth. In both cases the surveying was designed to document the impact of glacier ice on the seafloor in order to better understand the glacial history of the region and to find appropriate coring

sites to better understand thermal and physical property gradients through the shelf-slope transition.

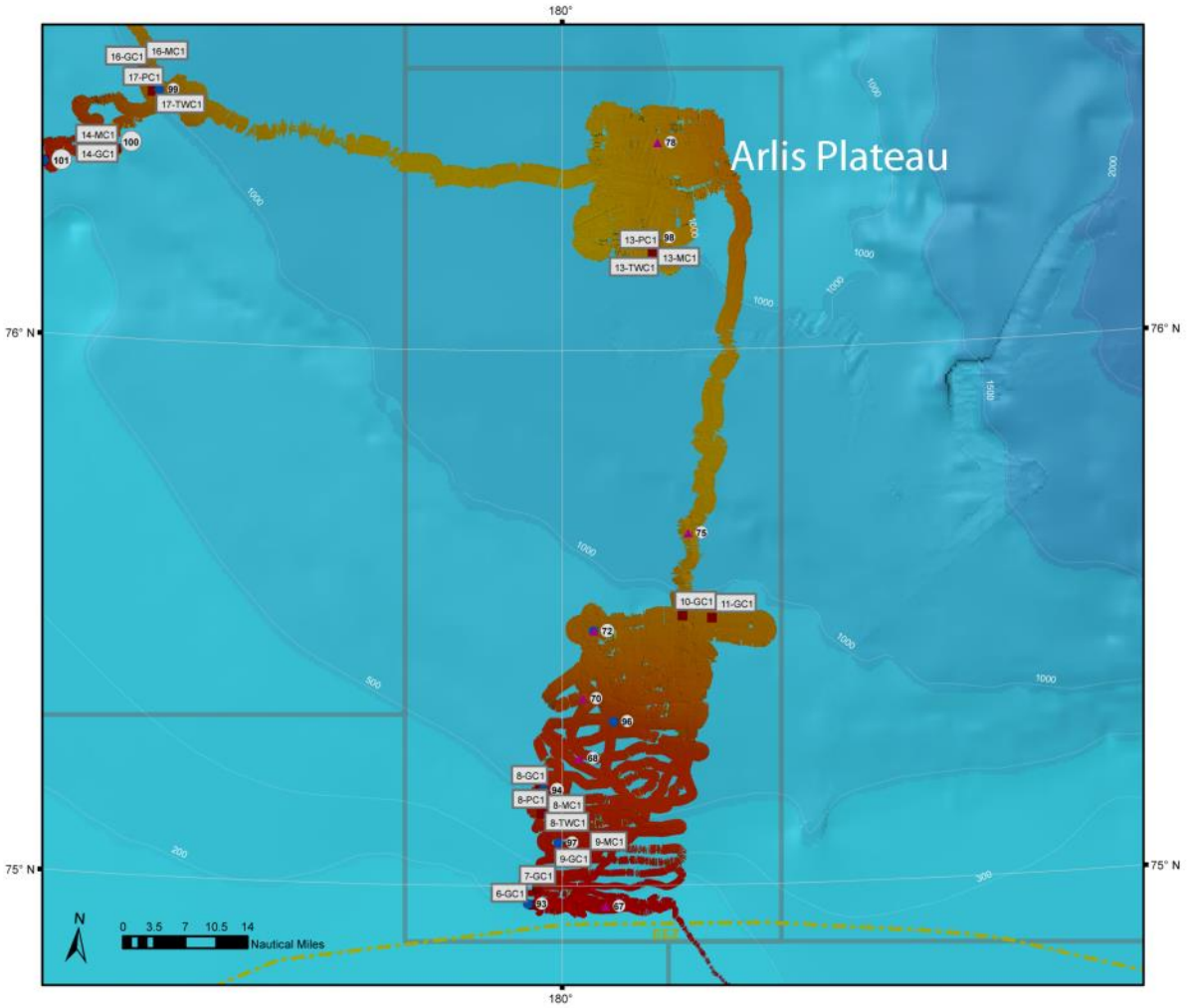

Figure GM-22*: Box 2 located north of Herald Canyon and outside of the Russian EEZ. See Figure GM-21 for description of symbols.*

The Box 3 survey area, represented two long shelf-to-slope transects, one beginning about 170^{o} 45’ E and located entirely out of the Russian EEZ and the second, starting at about 162^{o} 45’E, entirely within the Russian EEZ (Figure GM-25).

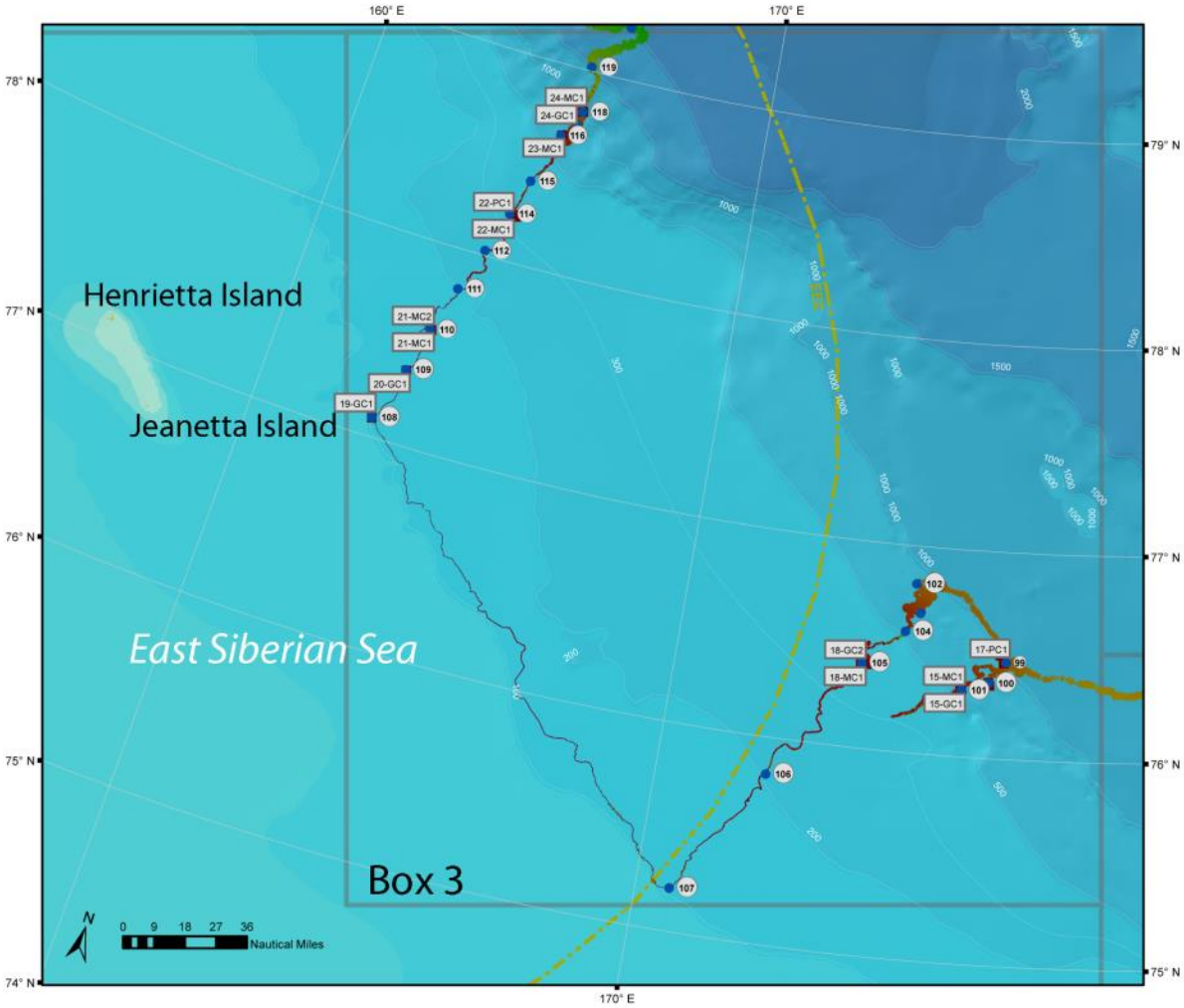

***Figure GM-23**: Box 3. See Figure GM-21 for description of symbols.*

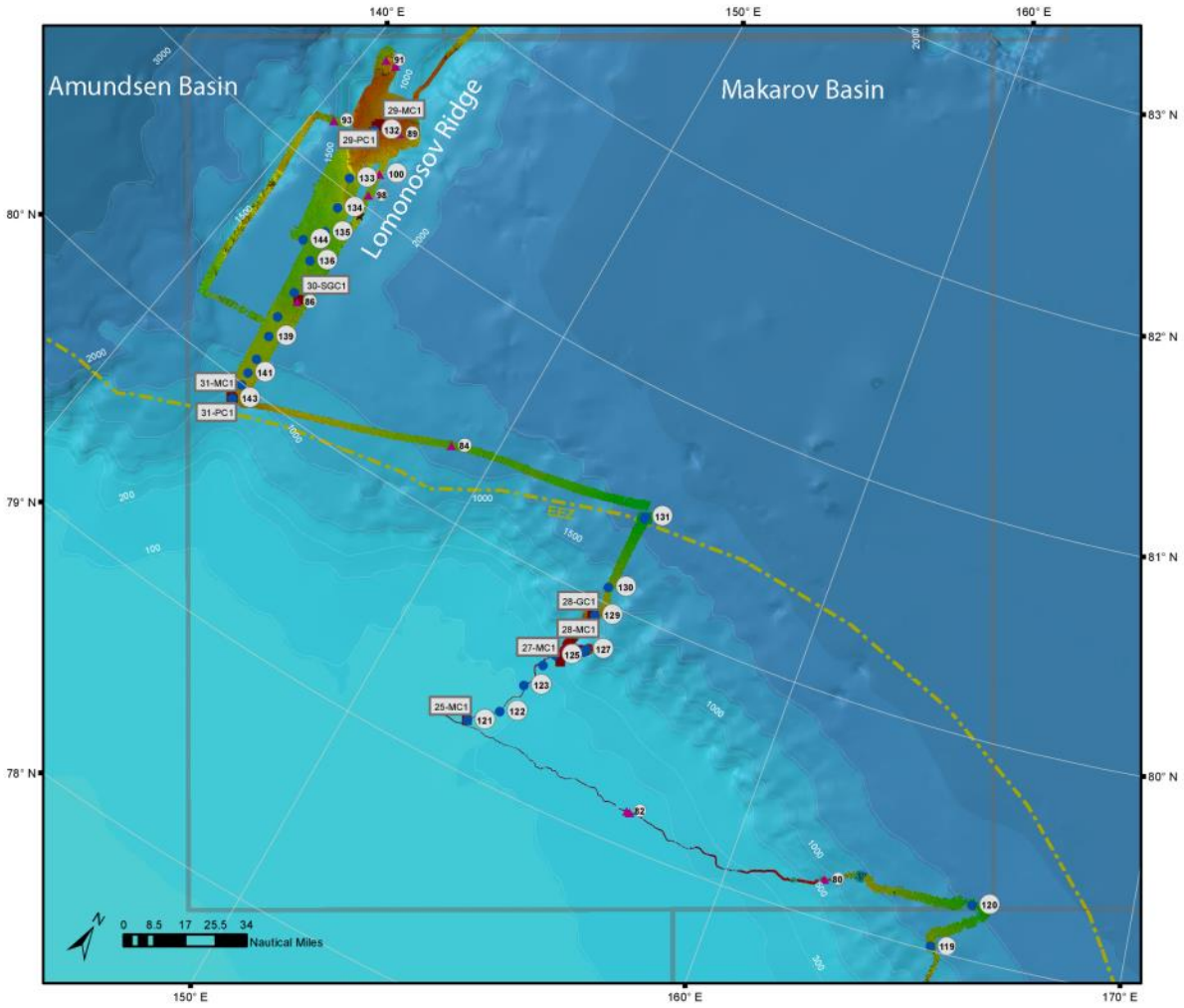

***Figure GM-24**: Box 4. See Figure GM-21 for description of symbols.*

Box 4 consisted of a short shelf slope transect starting at about 152°E and located entirely within the Russian EEZ and a long transect from mid-slope on the Siberian margin (about 800 m water depth) across a saddle and then up on to the southern end of the Lomonosov Ridge (Figure GM-24). Here the surveys were designed to support very closely spaced CTD measurements to document the path of Atlantic water flow into the Arctic (see WP Physical Oceanography section) as well as to look for evidence of the impact of ice on the seafloor and subsurface. Such impact was clearly found in the form of large scale furrows resembling mega-scale glacial lineation, ice-berg scours, and evidence of grounding lines.

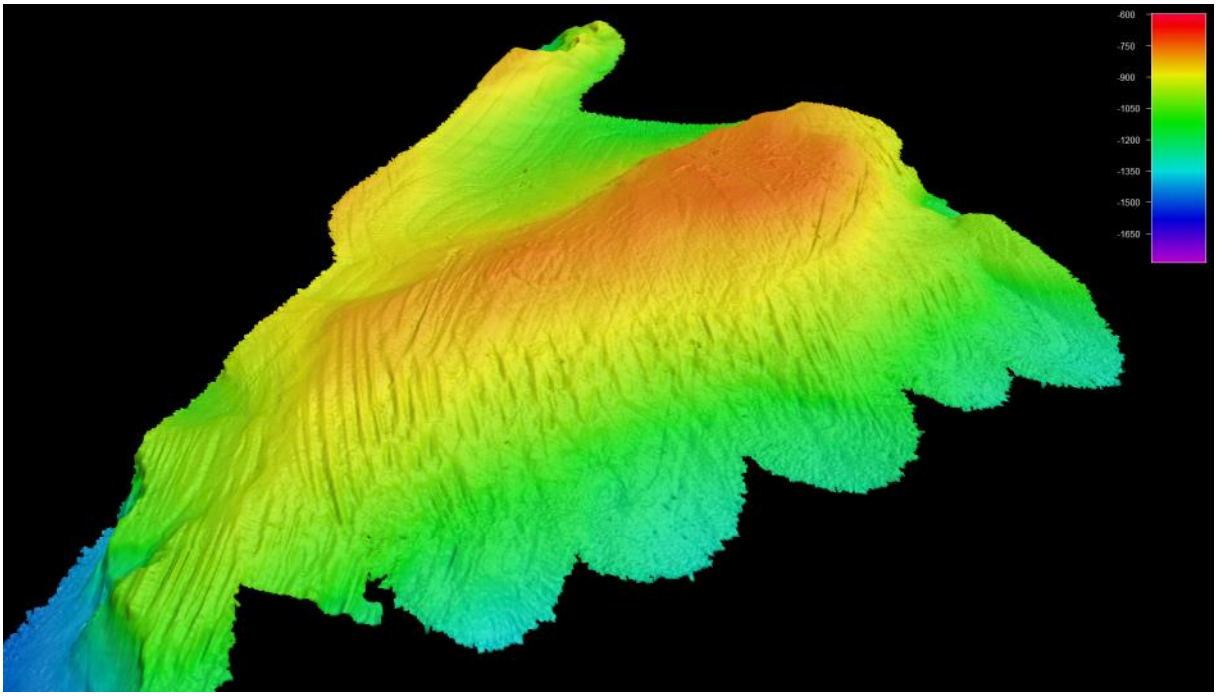

Figure GM-25*: 3-D view of southern portion of Lomonosov Ridge surveyed as part of Box 4. Large scale furrows created from ice grounding and resembling mega-scale glacial lineations are clearly seen.*

Finally, Box 5 included a long transect up the spine of the Lomonosov Ridge, and then a detailed survey of the region between about 84°N and 85° 30'N where the Ridge shoals to less than 800 m water depth as well as transect down the western flank of the ridge at about 83° 45'N. The detailed surveys in the north were focused on a region where pockmarks were seen in the subbottom profiler and the EK80 (see Subbottom Profiler Results section below) and on mapping the interaction of ice with the shallower portions of the ridge. The northernmost part of the survey was also focused on determining minimum sill depths for understanding the flow of deep waters between the Amundsen and Makarov Basins (see WP Physical Oceanography for discussion of this).

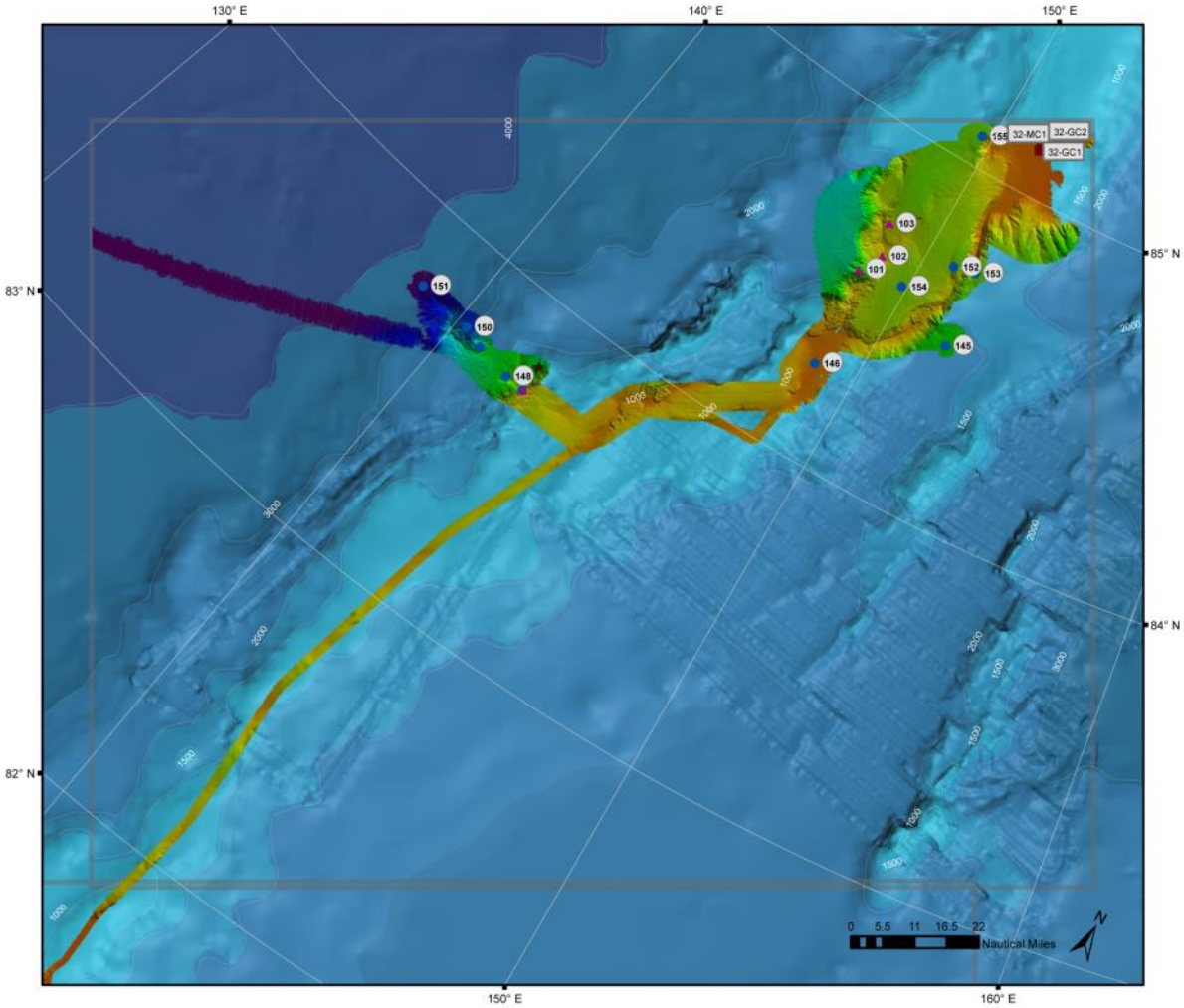

Figure GM-26*: Box 5 on the Lomonosov Ridge. See Figure GM-21 for description of symbols.*

Multibeam Data Quality Issues

As mentioned earlier the EM122 data was, for the most part, of high quality except for the expected degradation when operating in the ice and at high speed. Nonetheless, there were some concerning issues with respect to EM122 data quality – in particular apparent "punch-through" at nadir (Fig. GM-27) and the problem of "horns" – elevated soundings on either side of the nadir beam (Fig. GM-28). It is quite likely that these two issues are interrelated. In order to better understand the cause of these problems we attempted several experiments designed to isolate the potential source. These experiments were typically conducted while the ship was drifting at a CTD or coring station.

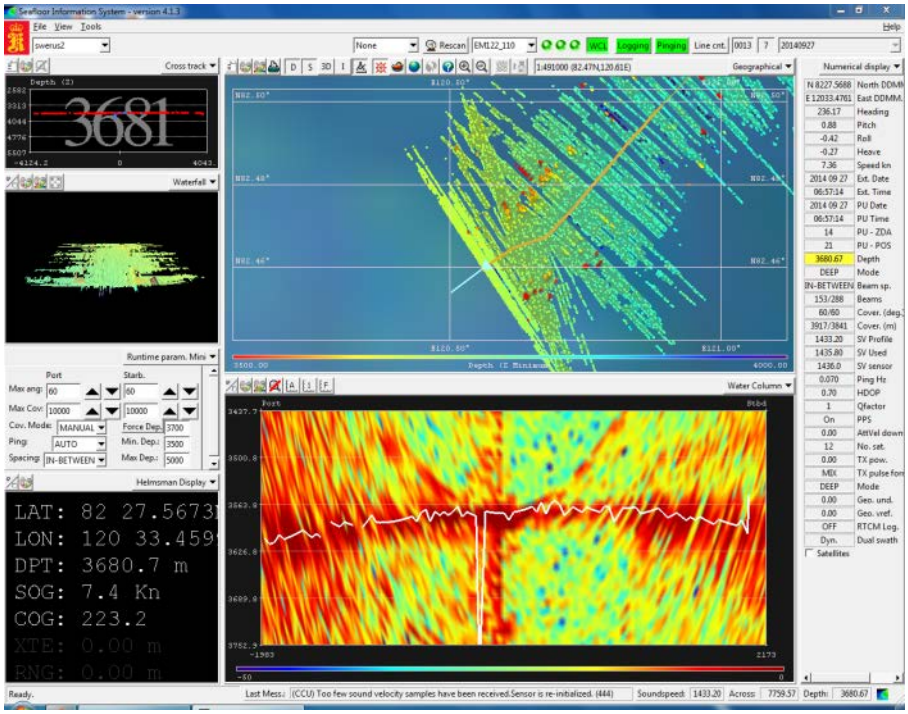

***Figure GM-27**: Example of "punch-through" – deep bottom detect near nadir*

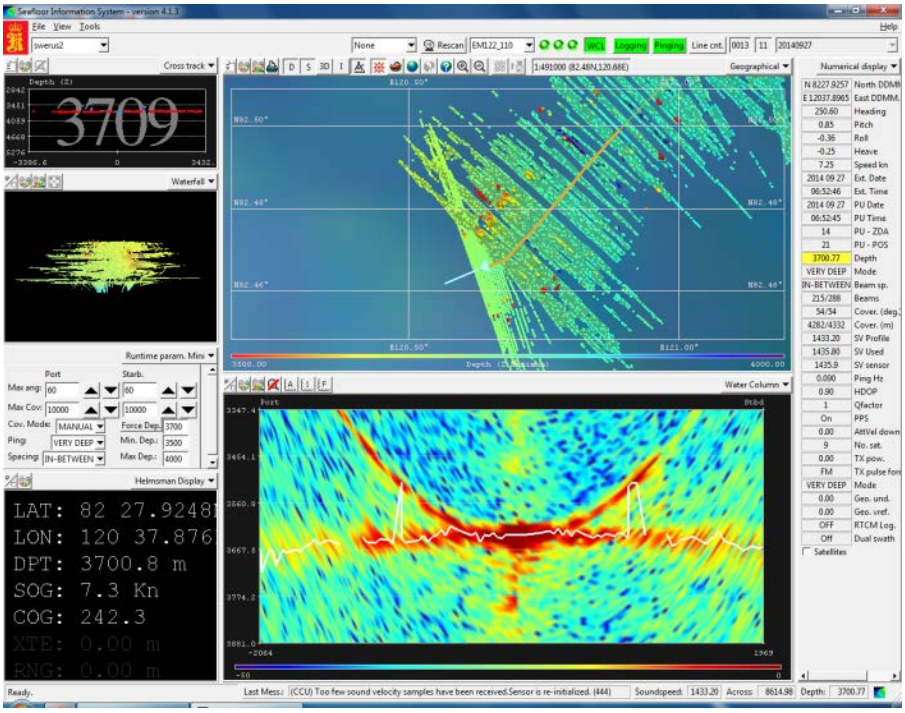

***Figure GM-28**: Example of horns being created from bottom detection on nadir ring.*

Effect of EK80 on EM122

One of the first possible causes investigated was the potential that the EK80, with the lower end of its band (15kHz) approaching the 12kHz center frequency of the EM122, was causing problems with

the EM122 (particularly the horns). To evaluate this, a series of tests were conducted on 8 Sept 2014 looking at the effect of EK80 acoustic interference on EM122 water column data. During these tests *Oden* was drifting at a CTD and coring site with engines secured and the EM122 acting initially as the master for synching of EM122, SBP120, and EK80 transmission. The EM122 was configured to operate in Shallow (CW), Dual Swath – Dynamic mode with a pulse length of 3.5 msec, along-track TX tilt of 10° forward (to reduce nadir 'punch-through'), and HD Equidistant RX beam spacing. EM122 Runtime Parameters for Interference, Aeration, Sector Tracking, Slope, Spike, and Penetration Filters were set to 'Off.' No EM122 or SBP120 parameters were modified during the interference tests. Only TX synchronization and TX bandwidth of the EK80 were adjusted (Table GM-7) for evaluating interference with EM122 water column data.

Table GM-7: *EK80-EM122 interference test parameters and EM122 file numbers.*

Time UTC	EM122 Line	EK80 TX	EK80 Synch	EK80 Bandwidth
19:53	49	Off	On	-
20:18	50	On	On	15-30 kHz
20:37	51	On	Off	15-30 kHz
21:00	52	On	On	18-30 kHz
21:15	53	On	Off	18-30 kHz
21:30	54	On	On	15-30 kHz

These tests indicate that EK80 transmissions over the frequency ranges 15-30 kHz and 18-30 kHz are readily observed in the EM122 when the two echosounders are not synched, demonstrating the importance of transmission synchronization for these two systems. Figure GM-29 includes a 'stacked' view (looking across the swath from starboard) of EM122 water column data for each file and an example 'fan' view (looking ahead through the swath) of the second swath (in Dual Swath – Dynamic mode) showing the effects of EK80 synchronization with the EM122. Interference of the first EM swath return is present in all second swaths and marked for distinction from EK interference. Though not clear in the stacked view, the un-synched EK80 transmissions appear clearly in fan view and have slightly higher amplitude to port of nadir. This difference across the fan view is likely rooted in the different center frequencies used in EM sectors (CW mode), with the sectors to port of nadir employing frequencies more similar to the EK80 transmission than sectors to starboard. Most importantly with respect to the problems found in the EM122, securing the EK80 did not cause the "horns" on the EM122 to go away. Thus while the EK80 can clearly impact the EM122, as long as the systems are synched, the EK80 should not be the cause of the observed problems with the EM122 and the EK80 does not seem to be the source of the "horns".

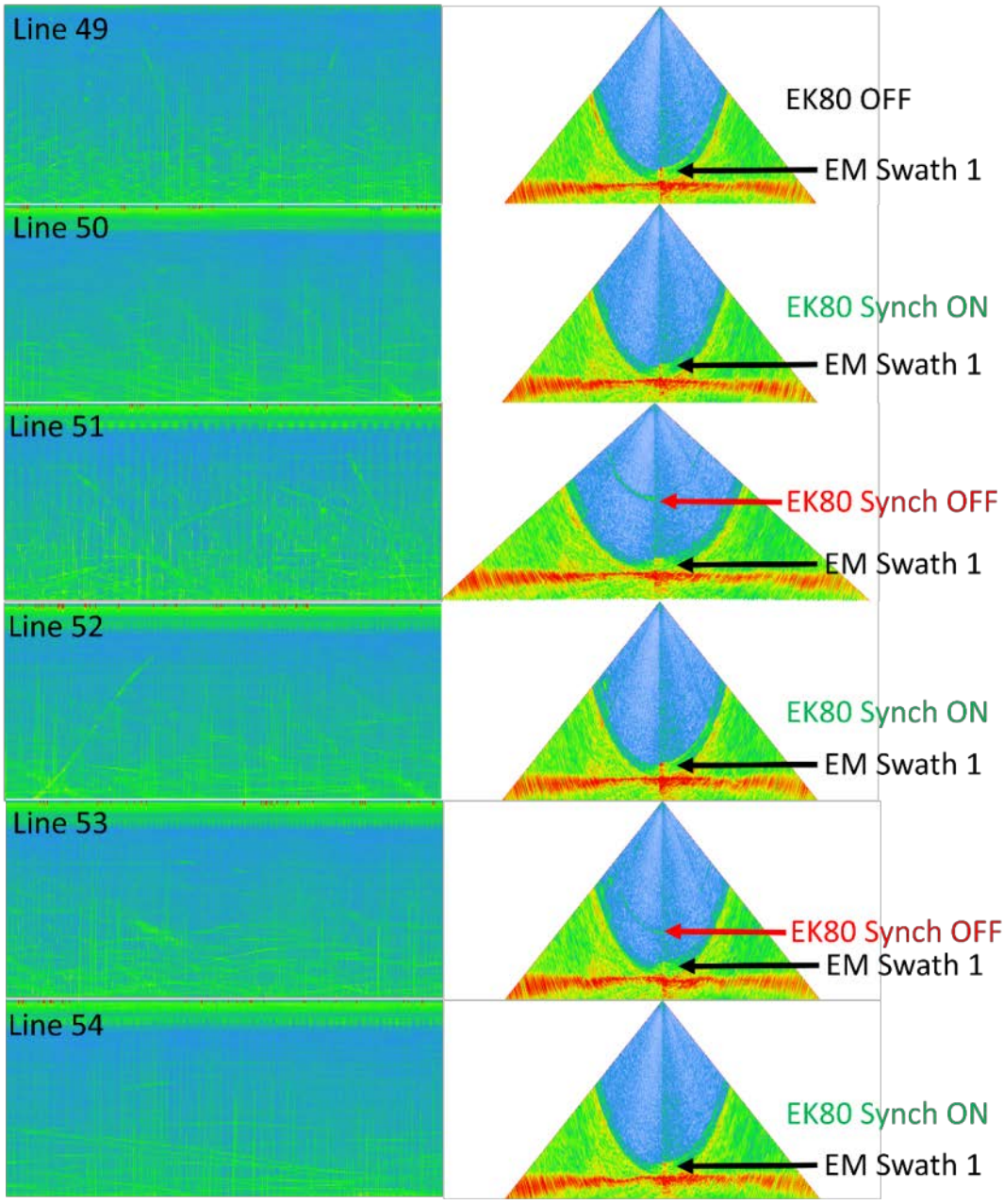

***Figure GM-29**: Testing of EK80 acoustic interference with the EM122. The constant-range rings apparent in lines 51 and 53 are due to EK80 transmissions having frequency ranges that are not completely filtered by the EM122. Across the swath, port sectors appear to show greatest susceptibility to the EK80 frequency ranges of 15-30 kHz (line 51) and 18-30 kHz (line 53). These results demonstrate the importance of synching transmissions between the two systems.*

Bottom detection artifacts related to pulse thickness (The "Horns")

Throughout Leg 2, an EM122 bottom detection artifact appeared as a set of symmetric 'spikes' near nadir, which were persistent in the along-track direction. Sometimes these spikes were also associated with punch-through or over-penetration at nadir. Closer inspection of bottom detections between the spikes in 'water column' view in SIS (Figure GM-30) revealed an apparent relationship to the curvature of the transmission pulse. This curvature follows the 'nadir ring' which is evident throughout the swath (first returns in range that are apparent in side lobes across all beams).

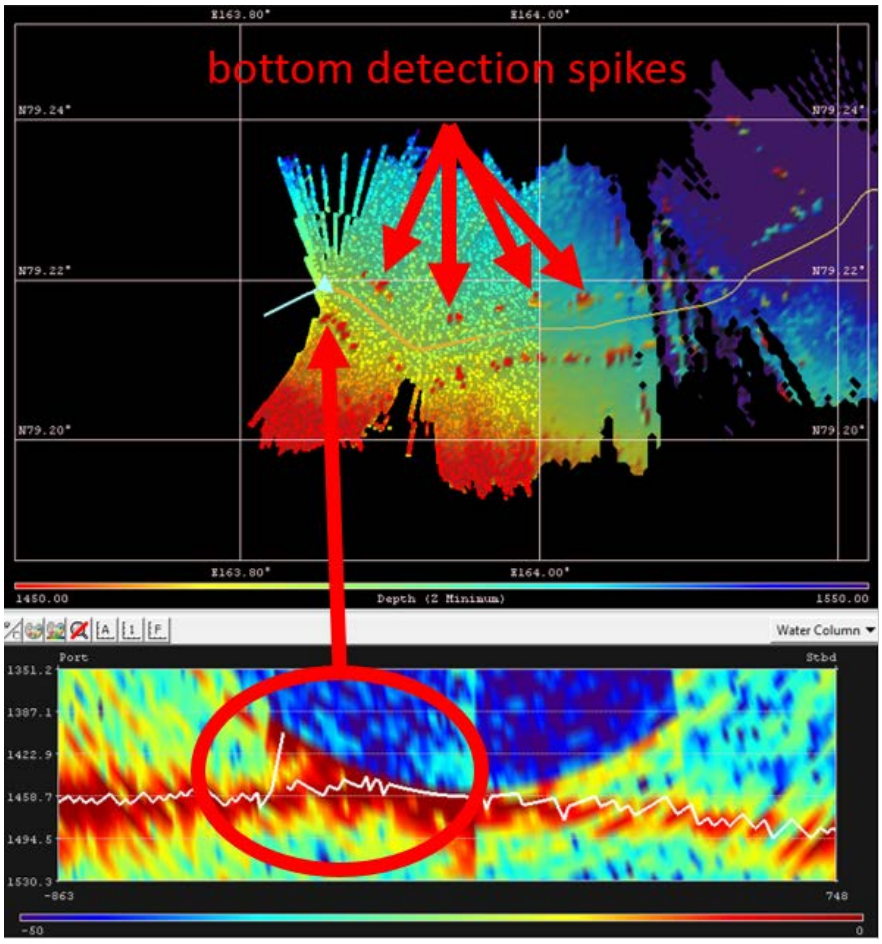

Figure GM-30. *Example of bottom detection artifacts. Spikes are clearly seen to port and starboard in the SIS grid. A single artifact is visible to port in this example water column view. The nadir ring diminishes in amplitude beyond the first sector boundary to each side of nadir. In the most egregious cases of bottom detections along the nadir ring, the resulting spikes occurred at the sector boundaries; in most cases, spikes were located closer to nadir within the first sector. In this figure, the EM122 was operating in Deep, Dual Swath – Dynamic, with HD Equidistant beam spacing and along-track tilt of 0°.*

In general, bottom detections between the spikes follow the curvature of the nadir ring outward from nadir. In this region near nadir, the geometry of transmission pulse intersection with the seafloor yields a broad area of initial ensonification (before the intersecting pulse takes on an annulus shape spreading along the seafloor). This further complicates distinction between the nadir side lobe return and the true seafloor return for beams near nadir.

From frequent observation in SIS 'water column' view, it is believed that the edges of the spikes generally occur at the first outward beam where the true seafloor return detected on the main lobe is sufficiently distinct in time from the nadir return detected on a sidelobe. This results in a sharp break in bottom detections at the spike on each side of nadir, where the range abruptly changes from nadir range to the range of 'true' bottom detection. Figure GM-30 shows a slightly different and less frequent case, in which a spike results from a single beam tracking the nadir ring away; this figure also shows the artifact only on the port side, whereas the spikes were observed to appear equally on the port and starboard sides (as evidenced in the SIS grid).

Several tests were conducted to try to establish a link between presence of the spikes and EM122 runtime parameters, including depth mode, swath mode, and beam spacing. It was observed that spikes would frequently appear and disappear while operating in all water depths and without any changes to EM122 Runtime Parameters (Figure GM-31). While no conclusions were drawn regarding depth, swath, and beam modes, the spikes were observed to change amplitude in some cases based on along-track TX tilt with shallower grazing angles (i.e., angles of arrival smaller than 90° to the plane of the seafloor at nadir) producing a smaller spike artifact. Based on these observations, the most significant factors are likely to be seafloor slope and surficial sediment type. Sediment types are currently unknown but a relationship may be established after the analysis of core samples. These suggestions are supported in Figure GM-31 by changes in spike behavior observed between regions of different slope (and possibly different sediment types) when an along-track tilt angle of 5° was applied to reduce penetration at nadir. Figure GM-31 indicates that the along-track tilt greatly reduces artifacts on the shallow slope but yields large artifacts when moving up-slope (presenting a more perpendicular intersection of the transmit pulse with the seafloor near nadir).

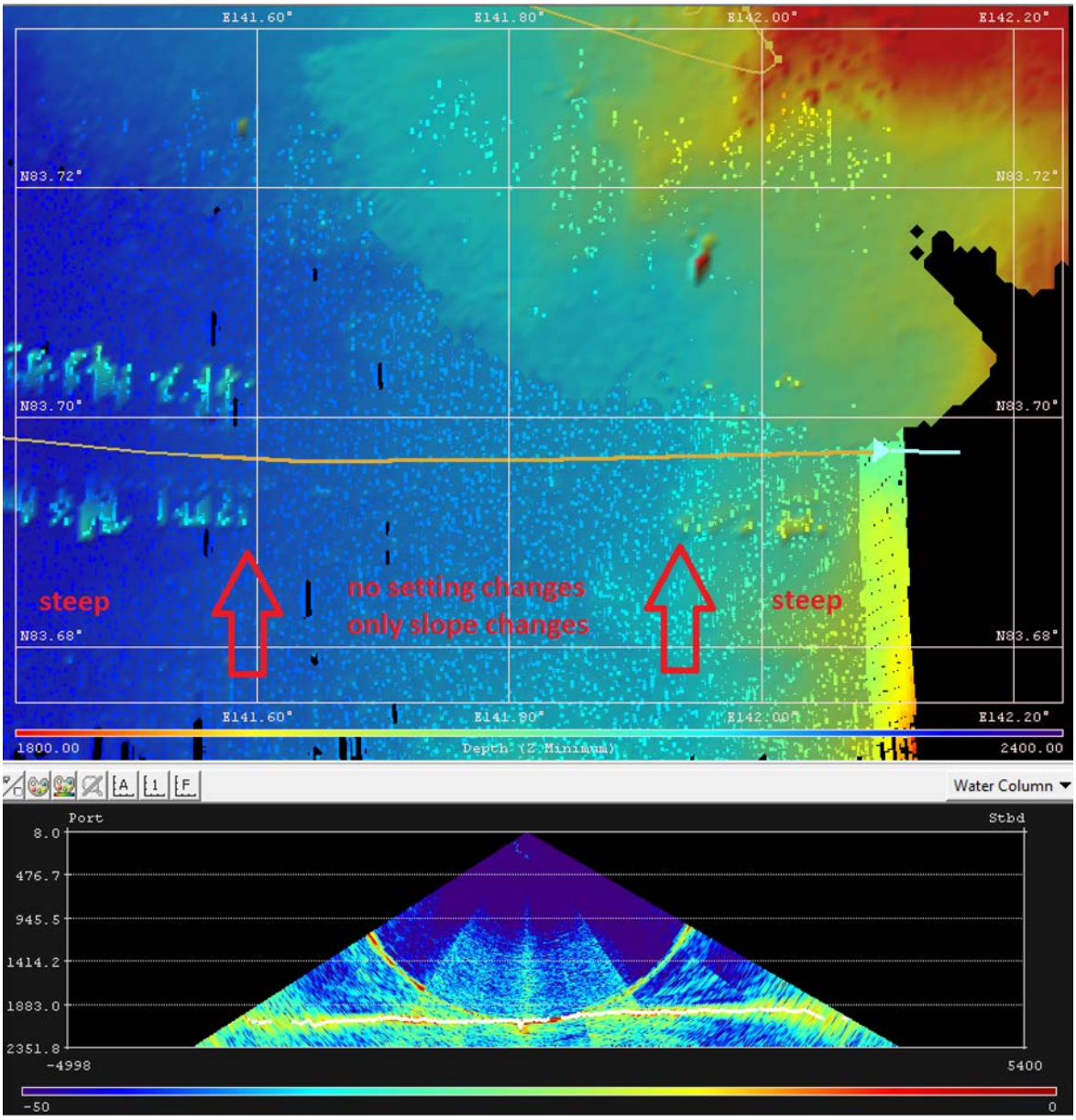

Figure GM-31. *EM122 grid and water column view showing significant change in bottom detection spikes without any changes to operating parameters. Spikes appear to be correlated to slope, with steeper slopes to west and east yielding larger spikes and the middle, shallow slope region yielding no detectable artifact. In this figure, the EM122 was operating in Deep, Single Swath, with In-Between beam spacing and an alongtrack transmission tilt of 5°.*

Sub-bottom profiles

Data Structure and Organization

SBP data were written directly to disk in the "Raw Data" directory of the "multibeam2" computer on the shipboard network. On this disk raw SBP120 and EM122 data from both SWERUS Legs 1 and 2 are stored. Within the SBP120/SWERUS Leg2 directory, data were further separated into directories representing data acquired within the Russian Exclusive Economic Zone and those data collected outside the Russian EEZ. This was done in order to be able to fulfill conditions outlined in the Russian research permit. Within both the INSIDE_EEZ and OUTSIDE_EEZ directories the data are further subdivided into RAW and SEGY directories and within each of these directories are sub-directories for each day labelled 2014MMDD. The individual raw data files within each day file are then labelled

LNNU_2014MMDD-Thhmmss.seg (or .raw for raw files). LNNU is a four digit line number set by the SIS control system and MM is month, DD day, hh hour, mm minutes, and ss seconds (Fig. GM-32). Numerous backups of the raw data have been made.

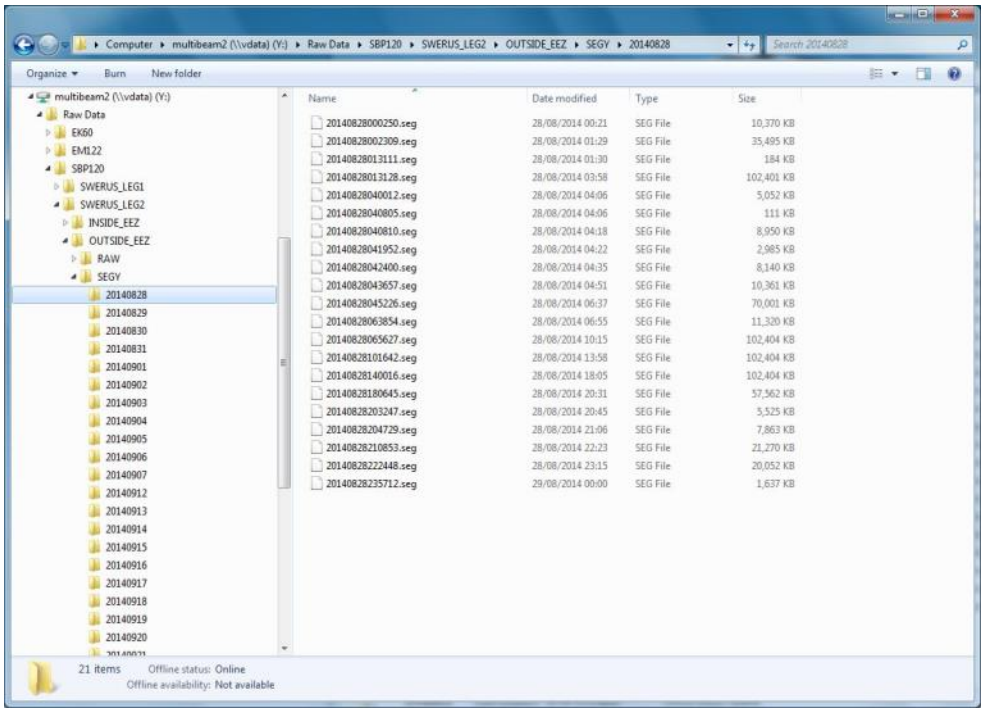

***Figure GM-32**: Data storage file structure for SBP120 data on SWERUS-C3 Leg 2.*

Sub-bottom profile results

The SBP120 subbottom profiling system performed nearly flawlessly throughout the 45 day SWERUS-C3 Leg 2 expedition, providing a detailed picture of the structure of the upper 30 to 150 m below the seafloor. High-resolution subbottom profiler data were acquired continuously on SWERUS-C3 Leg 2 resulting in the collection of more than 10747 line km of SBP120 data (Fig. GM 17). Penetration in the seafloor varied with water depth and sediment type ranging from a minimum of about 30 meters in the sandy, gas-charged sediments of the upper shelf (Fig. GM-33) to nearly 150 meters in the highly stratified sediments of the Lomonosov Ridge (Fig GM-34).

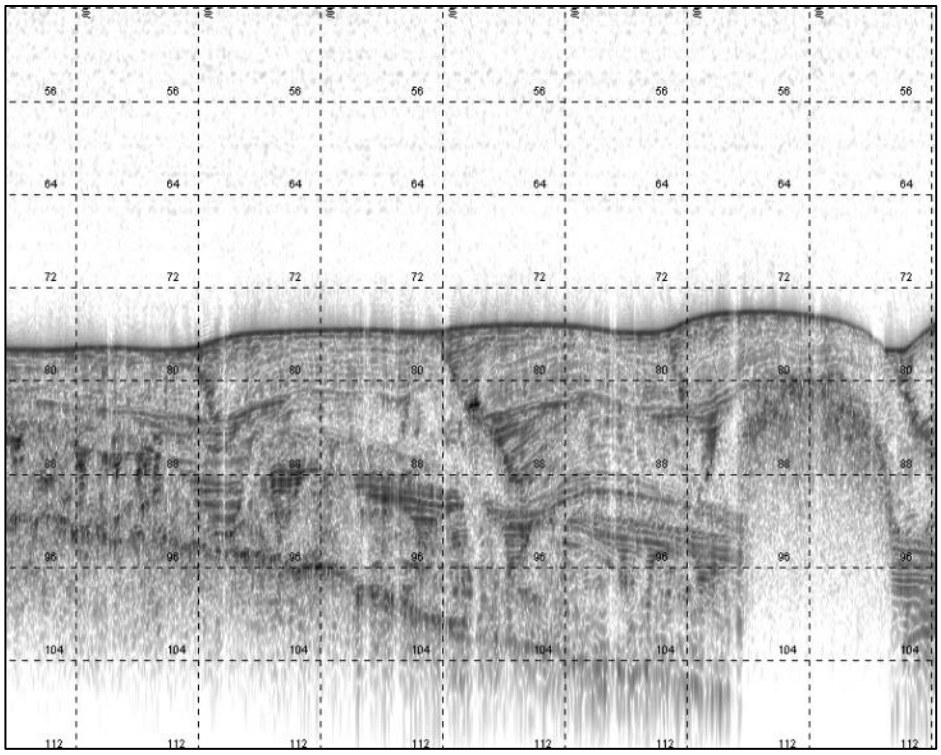

Figure GM-33*: Unprocessed example of high-resolution sub-bottom profile in Herald Canyon area. Complex structure and blank zone to right probably related to gas in the sediment. Vertical scale in meters below seafloor assuming sound speed in water column of 1500 m/sec*

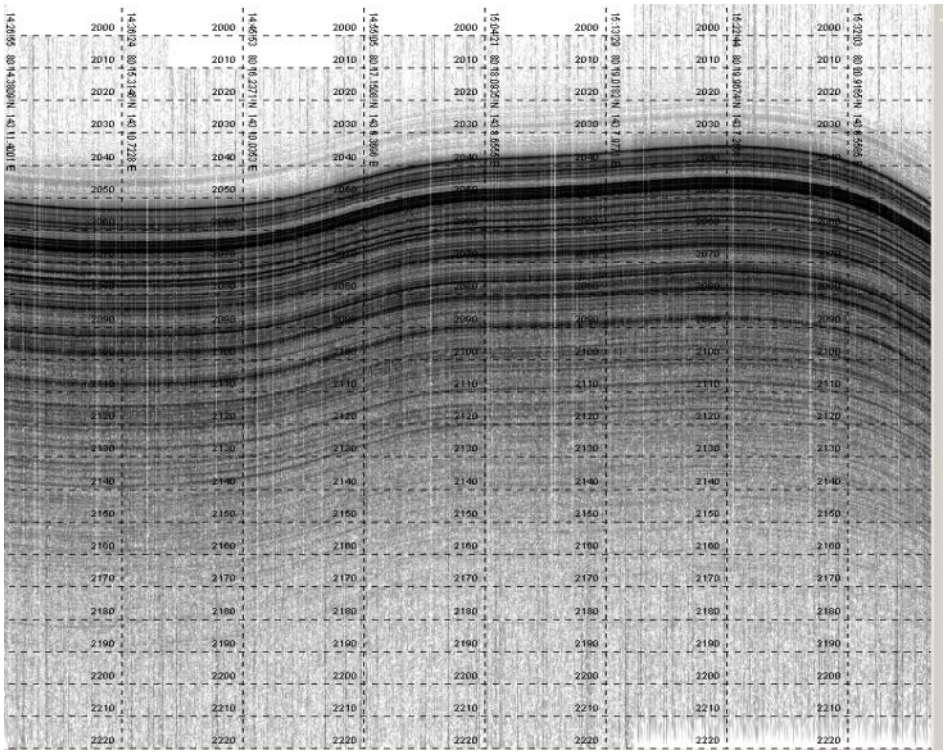

Figure GM-34*: Unprocessed example of high-resolution sub-bottom profile showing highly stratified undisturbed sediments on the southern end of Lomonosov Ridge. Vertical scale in msec below seafloor; water depth is approximately 1520 m. Seismic penetration here is approximately 130 m below seafloor. This section was target for coring.*

The high-resolution sub-bottom profiler was also one of the best indicators of disruption of the seafloor or the near surface and the relation of this disruption to the subsurface. One of the more enigmatic high-resolution sub-bottom sections was that crossing a series of seafloor pockmarks. These features were typically 200 to 300 m across but only about 5 m deep making them difficult to see in real-time with either the EK80 or the EM122, but the intriguing subsurface structure associated with the pockmarks made them very noticeable on the SBP-120 record (Figure GM-35).

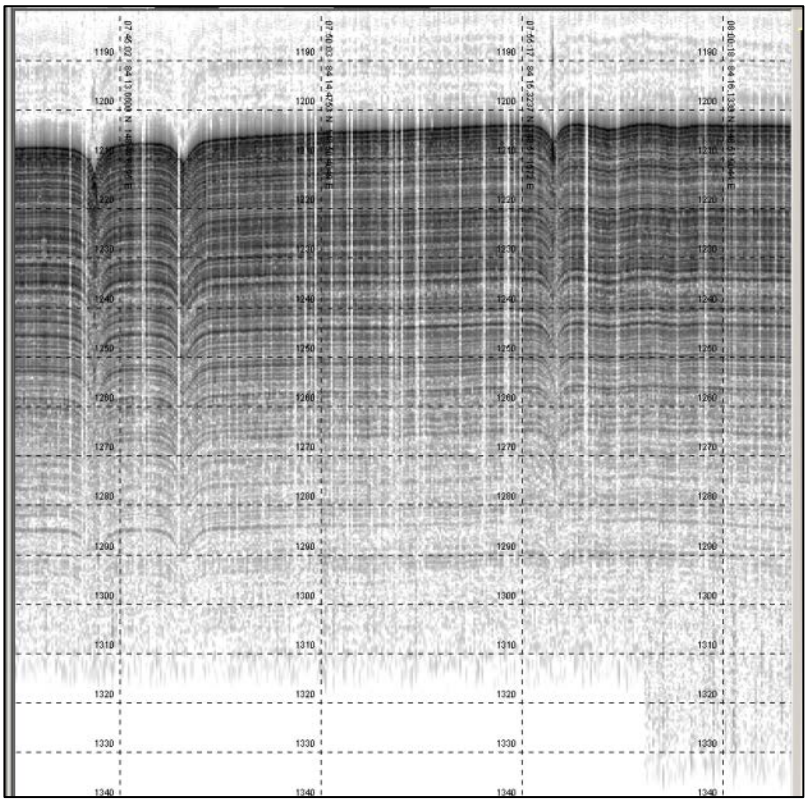

Figure GM-35*: Unprocessed example of high-resolution sub-bottom profile showing three pockmarks on the crest of the Lomonosov Ridge. Ridge. Vertical scale in msec below seafloor; water depth is approximately 900 m. Seismic penetration here is approximately 100 m below seafloor. This section was target for several cores.*

The high-resolution sub-bottom profiler is also an ideal tool for looking at the impact of ice on the seafloor as well as the subsurface. Figures GM-36 and GM-37 clearly show the impressive impact of ice on the Lomonsov Ridge with iceberg scours and a thin deformed zone overlying a sharp angular unconformity (Figure GM-36) and a huge pile of deformed sediment pushed over the side of the ridge by ice (Figure GM-37).

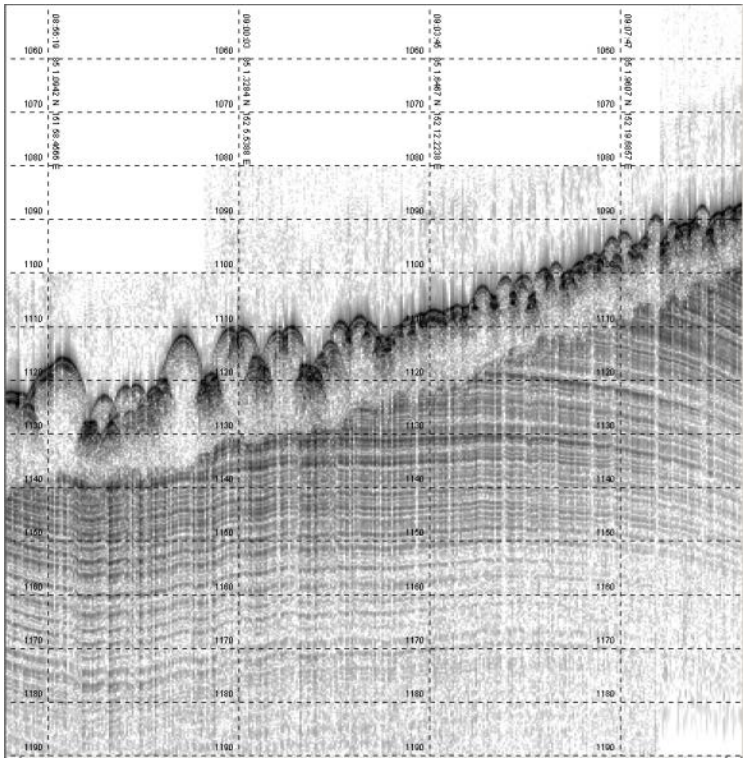

***Figure GM-36**: Unprocessed example of high-resolution sub-bottom profile showing clear impact of ice on the Lomonosov Ridge. Here iceberg scours and lineations in a deformed surficial layer overlie a sharp angular uncomformity. Vertical scale in msec below seafloor; water depth is approximately 825 m. Seismic penetration here is approximately 80 m below the seafloor.*

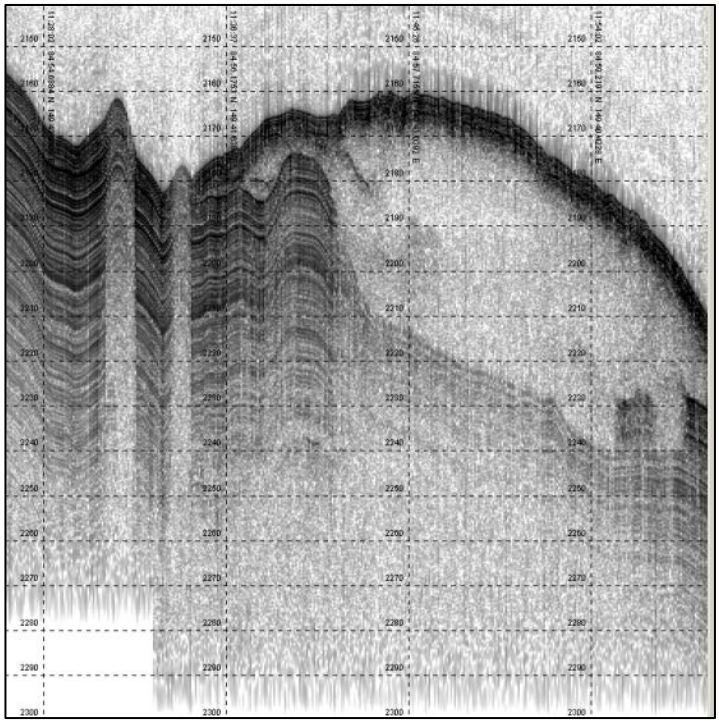

***Figure GM-37**: Unprocessed example of high-resolution sub-bottom profile showing clear impact of ice on the Lomonosov Ridge. Here a thick pile of deformed sediment has been pushed over side of ridge by ice. Vertical scale in msec below seafloor; water depth is approximately 1635m. Seismic penetration here is approximately 100 m below the seafloor.*

Seismic reflection profiles

The performance of a seismic reflection system is to a great extent depending on the towing arrangement of the seismic source and hydrophone streamer. The normal procedure is to arrange a tow point some 3-5 meters off the side of the ship and to optimize the towing point lengthwise by recording the noise level of the ship and propeller. At least for smaller vessels, a tow point near the stern of a ship is normally optimal. The optimal tow depth for a seismic source and hydrophone is ¼ of the wavelength of the peak frequency of the source, ca. 4-5 m in the case of the airgun used during Leg 2 of SWERUS-C3. On *IB Oden*, optimal towing conditions could not be met due to the huge propellers, the high noise and strong turbulence they cause behind the ship and the risk of catching sea ice off the side of the main wake.

Towing the seismic equipment in the propeller stream resulted in disturbing noise levels in a wide frequency band that was equal to, or sometimes even higher in level, than the received echoes from the seafloor and sediment layers. Frequency filtering using unusually narrow pass bands proved necessary in order to bring out the sub-bottom information contained in the raw digital recordings. A great number of filter settings were tested in order to enhance the seismic signal versus the high noise level. The optimal filter settings proved different between the seismic lines, partly due to different power output and thus changing noise levels and frequency spectra, from the ship, and partly due to changing reflectivity patterns in the sediment column. Thus, a low frequency filtering around 50 Hz was found optimal for the ice covered shelf areas north of Wrangel Island outside of the Russian Exclusive Economic Zone. Higher filter settings, around 150 Hz, were applied to enhance the sediment structures on the southern Lomonosov Ridge, profiled in open water. This higher filter setting also results in a higher resolution records. A hardware problem with the seismic registration system (mal functioning SCSI-card) prevented registration of more than 1.2 sec of each shot.

Seismic lines 1 and 2 (Full name SWERUS-L2-SEIS_Line1/Line2) were acquired downslope the East Siberian Shelf north of Wrangel Island (Fig. GM-38). Line 1 has a total length of 170 km and features a maximum penetration into the bottom sediments of about 1200 m (Fig. GM-39).Line 2 has a length of 74 km and a maximum penetration of approximately 1000 m (Fig. GM-40). The penetration depths are in both cases based on an assumed average sound propagation velocity in the sediments of 2300 m/s.

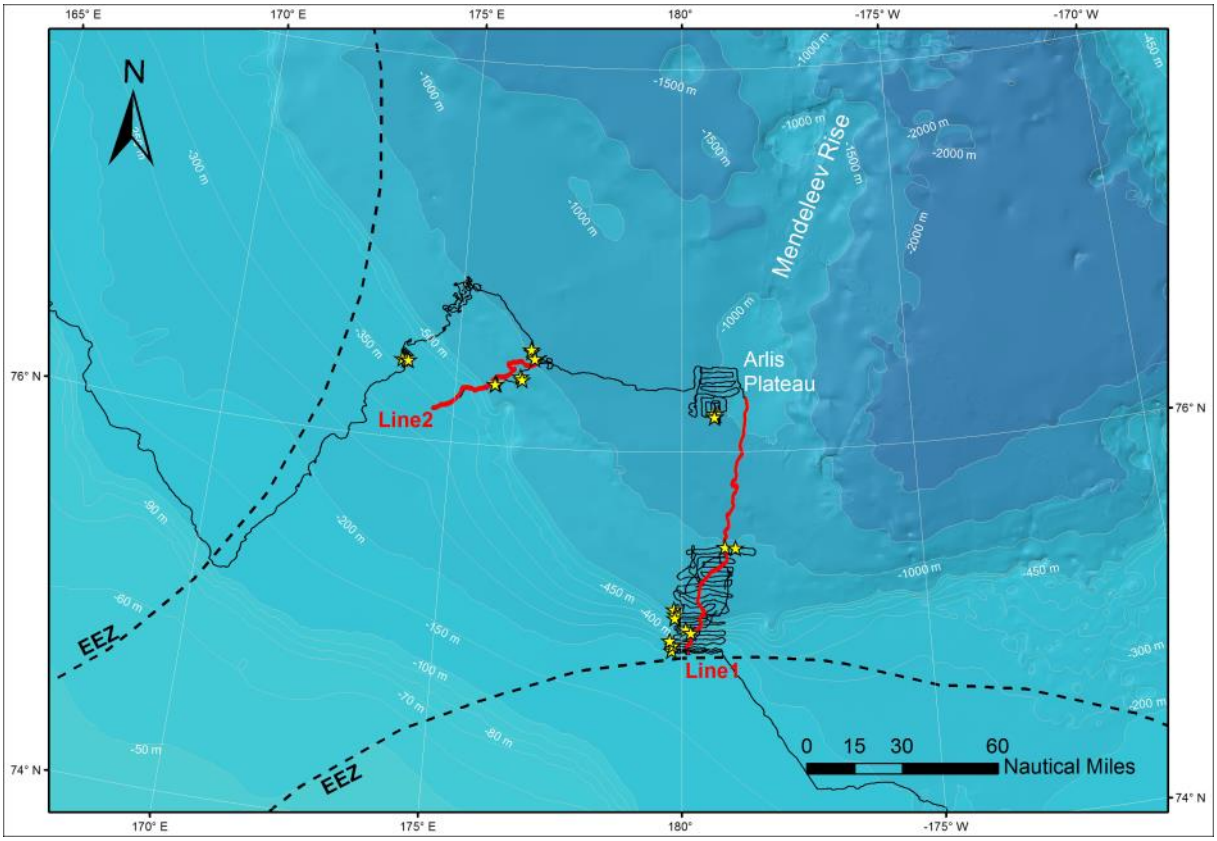

***Figure GM-38**: Map showing seismic lines 1 and 2. Their full names are SWERUS-L2-SEIS_Line1 and SWERUS-L2-SEIS_Line2. Coring sites are shown with yellow stars. All seismic lines were acquired outside of the Russian Exclusive Economic Zone (EEZ), which is outlined on the map.*

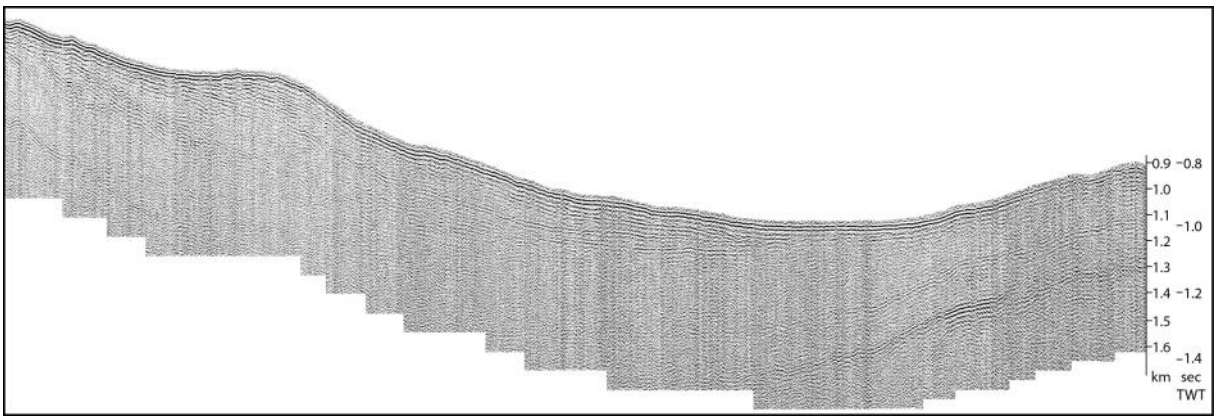

***Figure GM-39**: Seismic line 1 (SWERUS-L2-SEIS_Line1) filtered around 50 Hz.A hardware problem with the seismic registration system (mall functioning SCSI-card) prevented registration of more than 1.2 sec of each shot.The entire profile is 170 km long.*

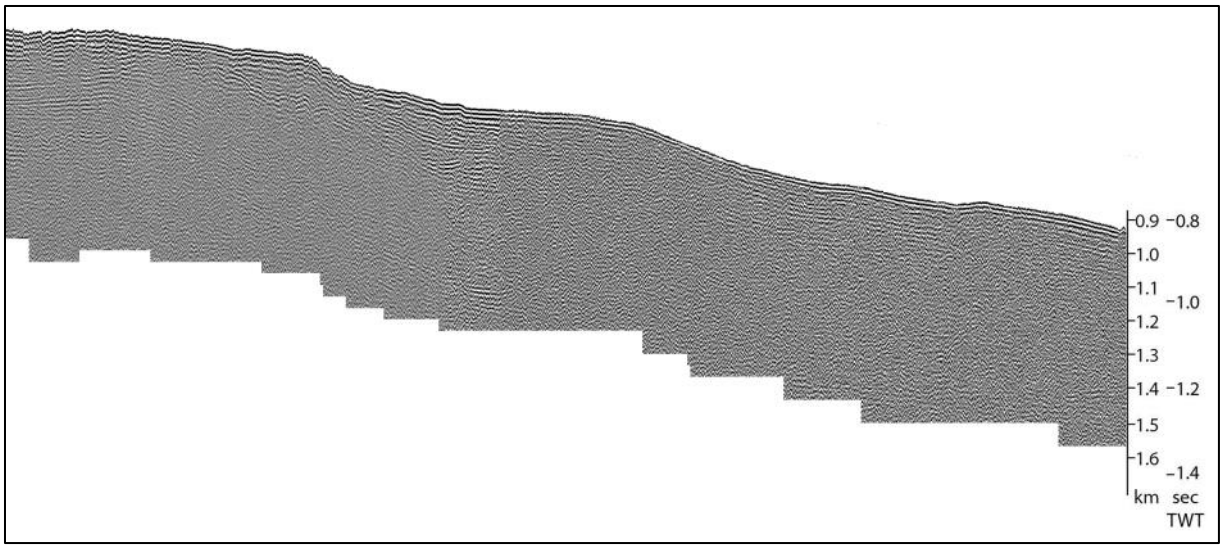

***Figure GM-40**: Seismic line 2(SWERUS-L2-SEIS_Line2) filtered around 50 Hz. A hardware problem with the seismic registration system (mall functioning SCSI-card) prevented registration of more than 1.2 sec of each shot. The entire profile is 74 km long.*

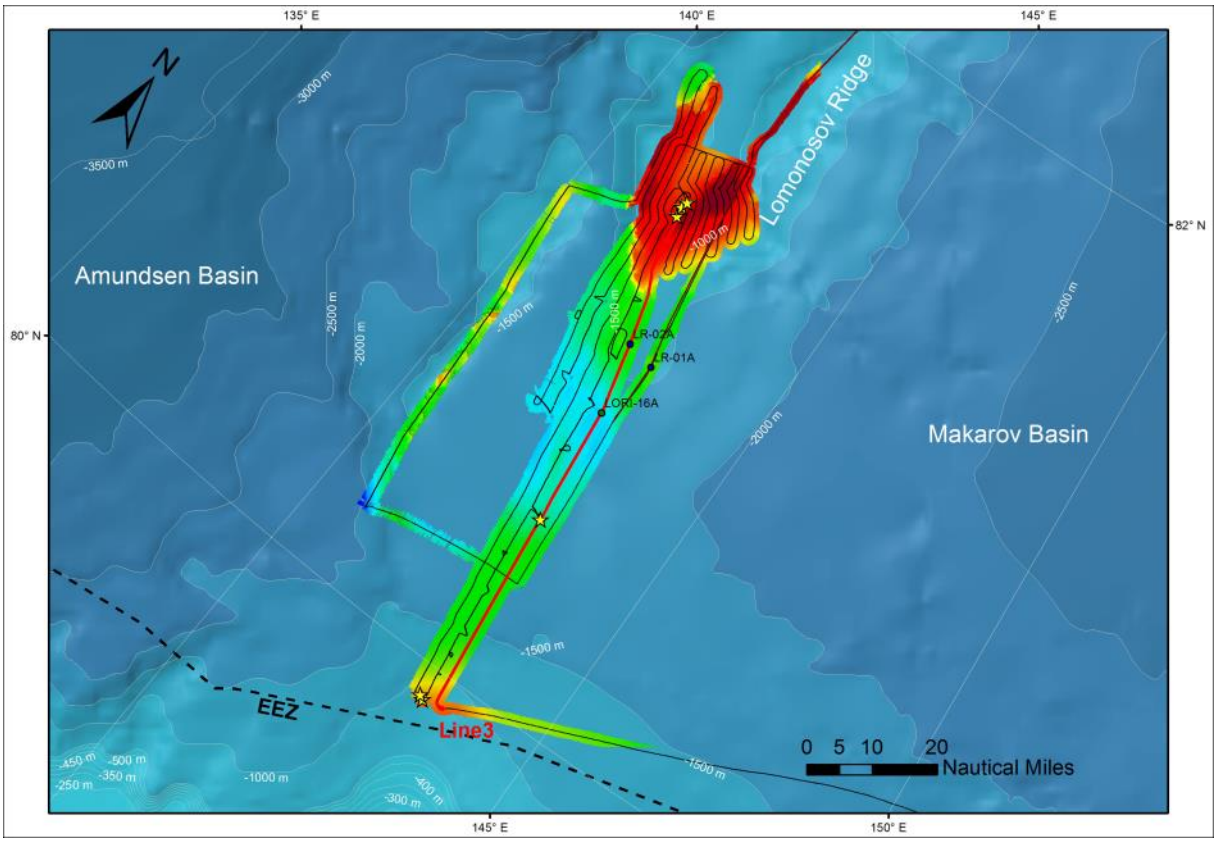

***Figure GM-41**: Map showing seismic line 3. The full name isSWERUS-L2-SEIS_Line3. Coring sites are shown with yellow stars. All seismic lines were acquired outside of the Russian Exclusive Economic Zone (EEZ), which is outlined on the map. The multibeam coverage in this area is shown with a rainbow color map. The locations of sites proposed to be drilled within the IODP program are shown (IODP proposal 708 by Stein et al.).The data through these sites (LR-01A; LR-02A; LORI-16A) will be submitted to the IODP site survey database.*

Along seismic profile 3 (Figs. GM-41 and 42), a number of narrow frequency bands were tested in order to obtain the best possible records. Settings focused around 150-200 Hz brought out the shallow layers higher resolution, whereas lower settings around 50-75 Hz brought out the deep reflectors at lower resolution (Fig. GM-42). However, this filter setting does not permit penetration to deep bedrock reflectors below the sediment drape on the Lomonosov Ridge.

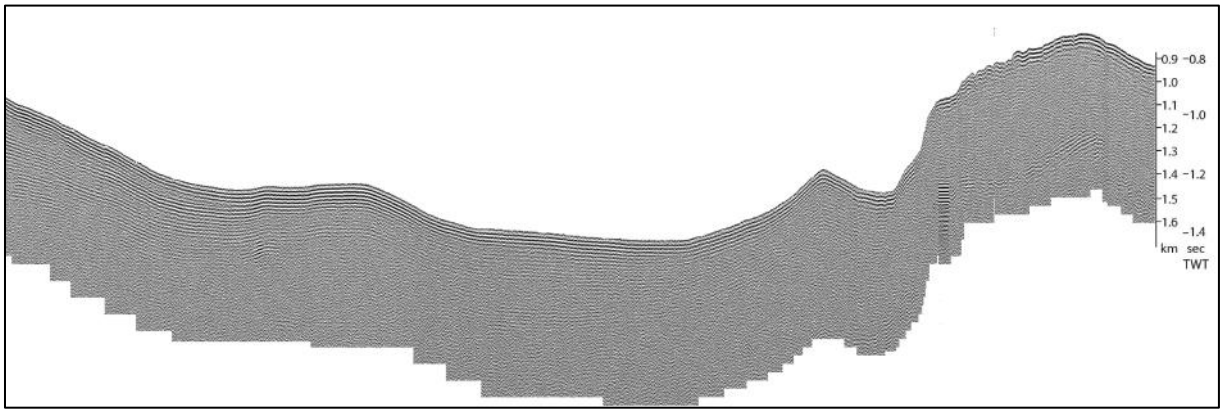

***Figure GM-42**: Seismic line 3 (SWERUS-L2-SEIS_Line3) filtered around 50 Hz. A hardware problem with the seismic registration system (mall functioning SCSI-card) prevented registration of more than 1.2 sec of each shot.*

Line 5 was shot through a pockmark area on the central Lomonosov Ridge (Figure GM-43).This line consist of several consecutive shorter segments including crossings.

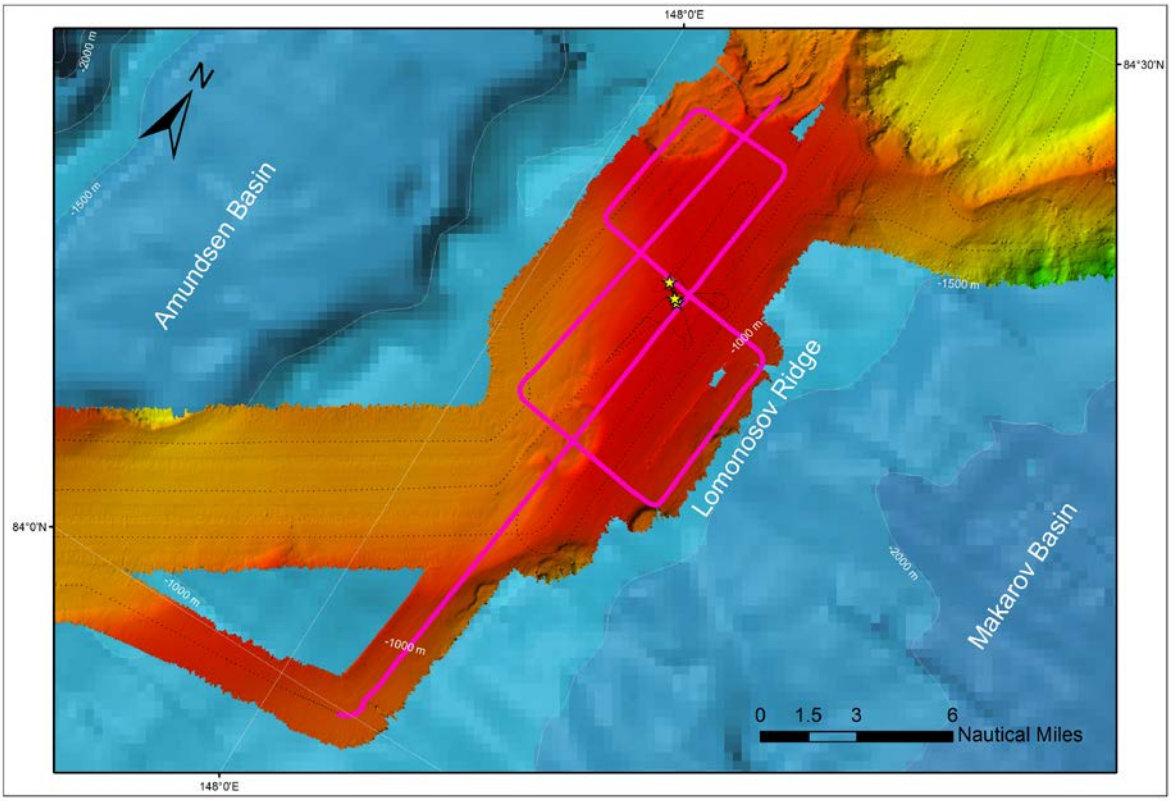

***Figure GM-43**: Map showing seismic line 4 (purple line). The full name is SWERUS-L2-SEIS_Line4. Coring sites are shown with yellow stars.*

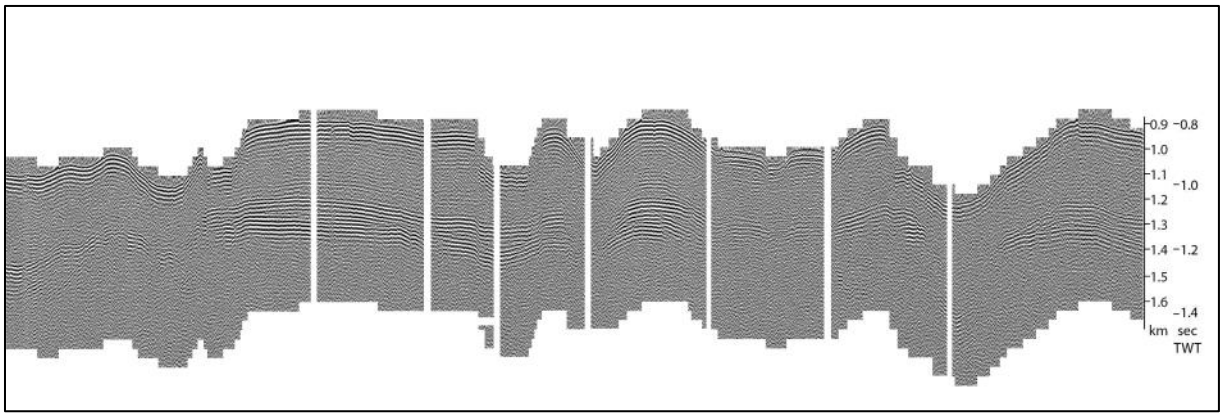

***Figure GM-44**: Seismic line 4 (SWERUS-L2-SEIS_Line4) filtered around 50 Hz. This line consist of several shorter segment acquired through a pockmark are on the central Lomonosov Ridge. A hardware problem with the seismic registration system (mall functioning SCSI-card) prevented registration of more than 1.2 sec of each shot.*

Electro magnetic

The analysis of selected typical curves of apparent resistivity and pre-award modelling of the typical geoelectrical cross-section for Herald Canyon was made onboard *IB Oden*. The preliminary shipboard result of this analysis is shown in Figure GM-45. Two types of Ro (t) curves can be distinguished. Type 1 (A) is characterized by that the apparent resistivity monotonically decreases with depth while type 2 shows an increase after some time (B). Assuming that anomalies of the high resistivity zones are related with a frozen ground, it is possible to construct a rough preliminary permafrost map of Herald Canyon. Further post-cruise analyses and modeling will shed more light on the permafrost setting of this area. A specific emphasis will be made to estimate the depth of the permafrost layer. The initial shipboard modelling of depth to high-resistivity layer was executed using the software EM1D (Pushkarev P. Ju. The Moscow State University).

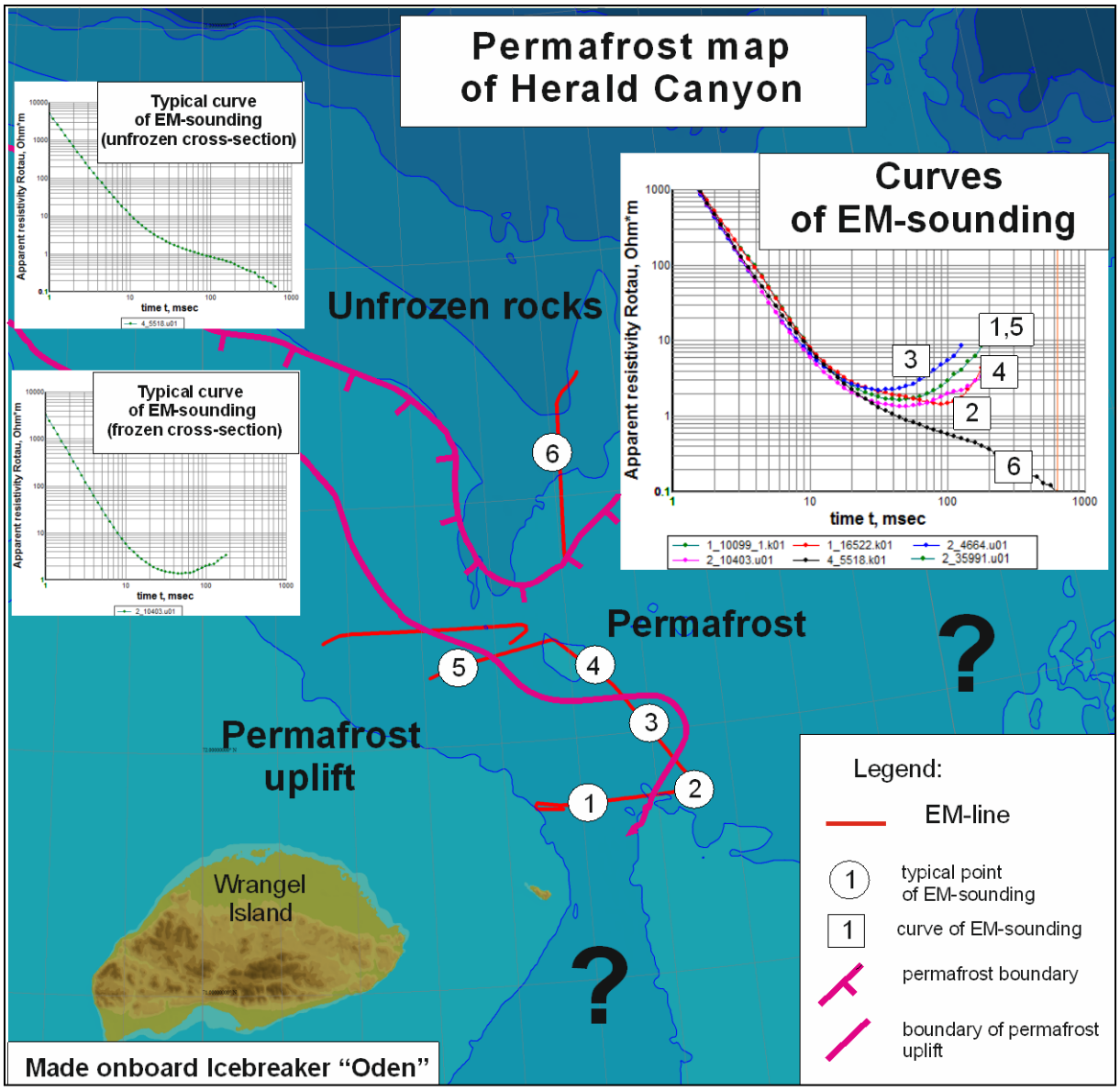

Figure GM-45: Preliminary results from analyses of a set of selected electromagnetic soundings.

WP WC (Water Column Mapping)

Data Structure and Organization

EK80 data were written directly on a 10.9 TB, Netgear NAS device provided by the University of New Hampshire and located in the Apparatrum. Data were organized by Survey Box (e.g. 1 through 5) plus transits. Within each survey box directory data were divided into directories representing surveys within the EEZ and outside the EEZ, and then directories for each day of data collection. The individual files are labelled ODEN-D2014MMDD-Thhmmss.raw with each file representing approximately 4 - 8 minutes of data collection and being approximately 500MB in size (Fig. WC-14). A duplicate copy of all EK80 data was made by Russian colleagues.

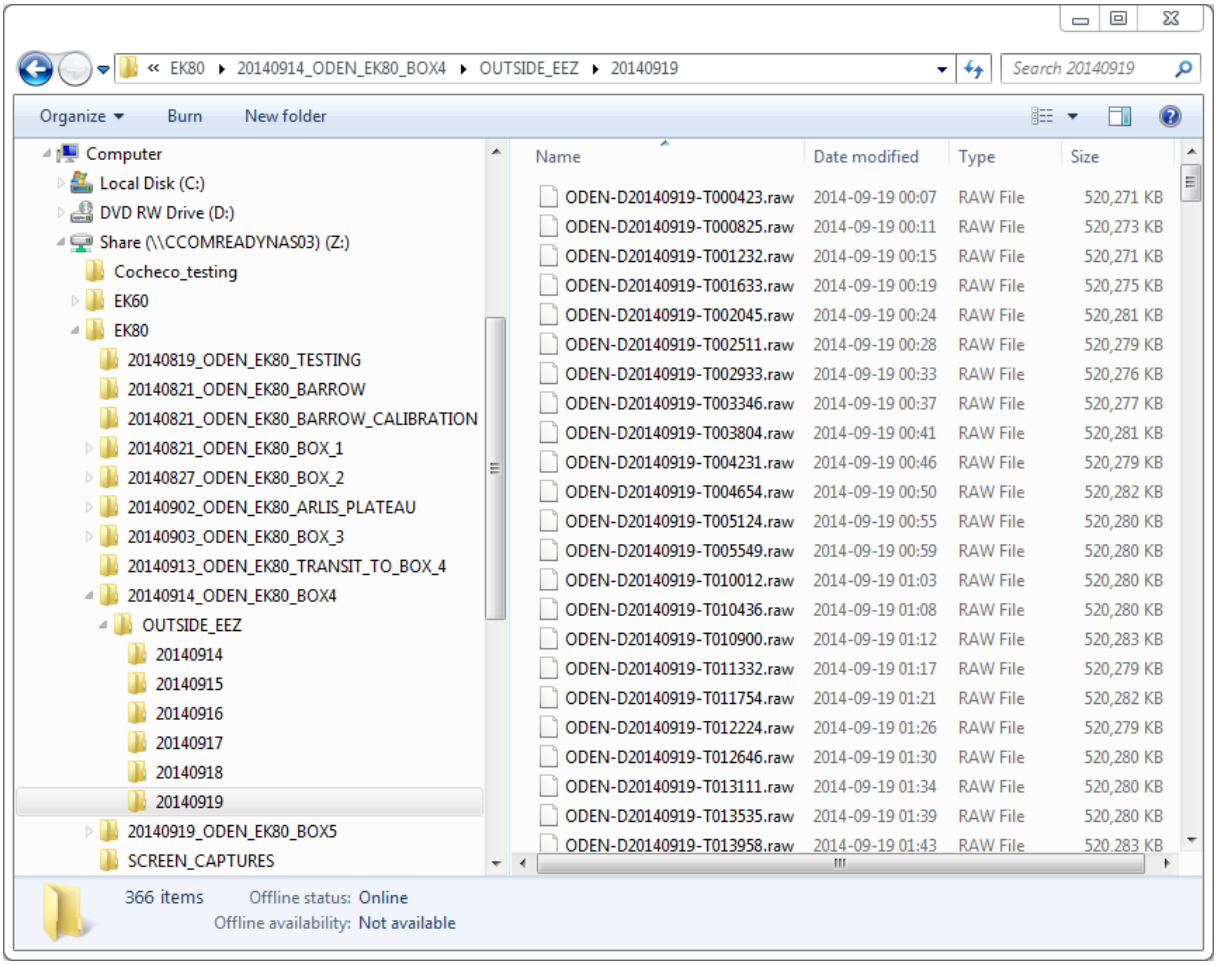

Figure WC-14: *Example of data file structure for collection of EM80 data*

WP WC Midwater Data Results

EK80 data were collected for the entire cruise from departure off Barrow to the securing of the systems approaching Tromso. A total of ca 7 Terabytes of EK80 data were recorded. These data provided the primary source of identification of seeps and other midwater targets. On Leg 2, approximately 34 individual seeps were identified in the EK80 data (some were multiple vents) almost all of them in the vicinity of Herald Canyon in Survey Box 1. Seeps in this region ranged in water depth from 50 to 88 m. Several other seeps were identified in slightly deeper water (100 – 118m) on the shelf end of Slope Transect 3 in Survey Box 3. For each of the identified seeps the processing stream described above was performed. Examples will be presented below.

The first example is of a single, isolated plume found in about 85 m of water. Figure 15 (left) shows the clear representation of this seep in the EK80 data. Above the plume a number of scatterers can be seen between the top of the plume and the sea surface. It is most likely that these are biological scatterers (attracted by the plume activity?) but may also be small bubble packets. Further analysis will be done to resolve this. Using the EK80 as a guide, the equivalent time is shown in the water column data from the EM122 (Fig. WC-15 middle). Note that the EM122 caught the bottom of the seep while the EK80 only saw the seep when it entered its 11 degree beam (approximately 11m wide at 80 m depth). Thus, in this case, the EM122 can provide a much more accurate location for the source of the seep than the EK80. The manual extraction of target data in the QPS software is a tedious and subjective process. To address this issue Tom Weber at UNH has written Matlab code to normalize background levels and automatically extract midwater targets. An example of the normalized extraction for this same target is presented in Figure WC-15 (right). Note that this is presented for a single ping. The normalization software will do this extraction for the entire time series of pings (the stacked pings) and thus extract the 3-D distribution of the target.

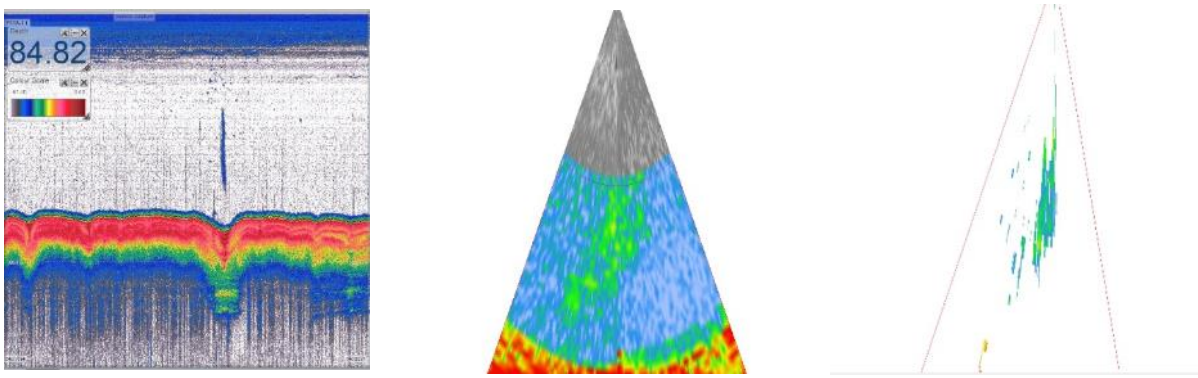

Figure WC-15: *EK80 observation of single seep in 84 m of water (left). Same seep as seen by EM122 (middle). Same target automatically extracted targets through normalization process. Note that the EM122 and normalization display represent a single ping. The seep is actually seen in several pings along the track.*

To establish the geomorphological and geological context the extracted seep was combined with the EM122 bathymetry and the SBP120 high-resolution subbottom profiler data (Fig. WC-16). In this example the seep is located directly in an iceberg scour which appears to have pierced a subsurface zone of gas (Fig. WC-16 – lower).

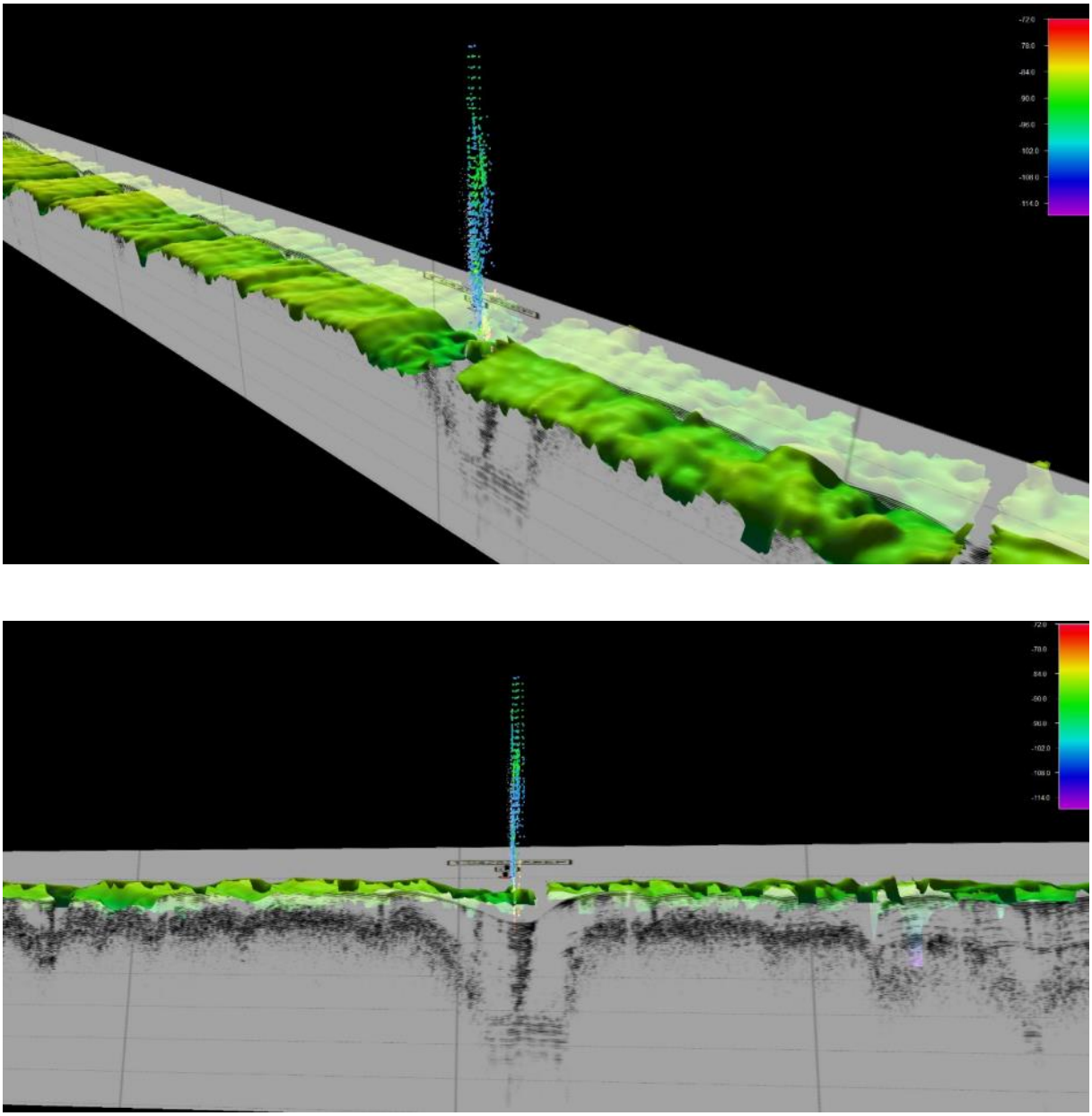

Figure WC-16: *Seep extracted from EM122 data georeferenced with EM122 bathymetry and SBP120 high-resolution subbottom profile. Color bar on right represents seafloor depths. Bubbles are identified to approximately 35m below the sea surface.*

The second example is of a line that appears as many small seeps in the EK80 record (Fig. 17). While these seeps appeared quite small on the EK80, the EM122 water column imagery showed at least one of these seeps (Fig. WC-17 left panel) to be the largest and strongest target seen with the EM122 on Leg 2 (Fig. WC-18). This difference demonstrates the fact that the two systems complement each other. The EK80 offers the opportunity to make calibrated measurements of target strength (and perhaps flux) but its field of view is limited to its approximately 11 degree beam width. Thus if the transducer does not pass within approximately 11 m of the target in 80 m of water, it will be missed. Also as bubbles move up through the water column the field of view narrows (5.5 m at 40 m depth, etc.) resulting in more opportunity to miss targets. The EM122 on the other hand with its 120 - 130 degree opening angle, ensonifies a swath of approximately four times the water depth – thus capturing targets across a swath of more than 300 m on the seafloor in 80 m of water. A georeferenced image of the seeps along the line described above along with the seafloor bathymetry

and the high-resolution subbottom image is presented in Fig. WC-19. In contrast to the first example, here the seeps do not seem to be associated with iceberg scours. Two of the seeps (those on the left side) appear to be associated with broad gas blanking zones that approach the seafloor while the third (which is the large one shown in Figure WC-18) sits above stratified sediments.

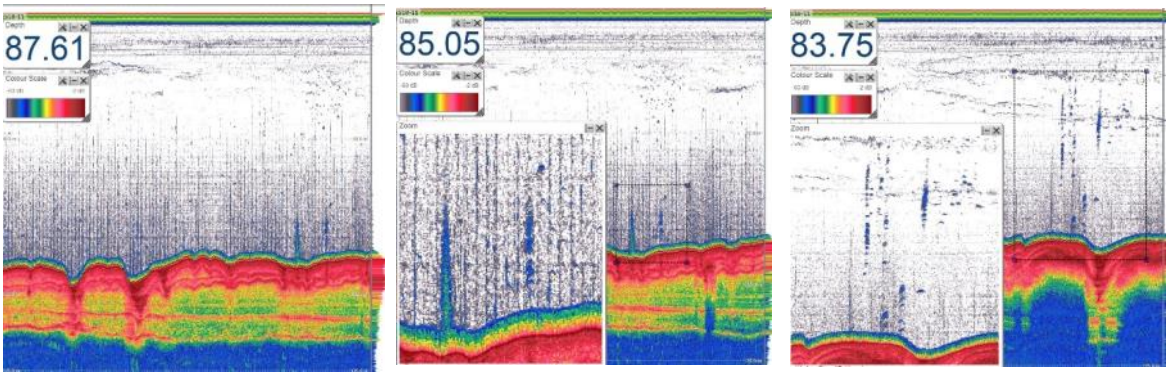

Figure WC-17: *Numerous small seeps as seen by EK80 along a single line. Insets in middle and right images are zoomed view of seeps.*

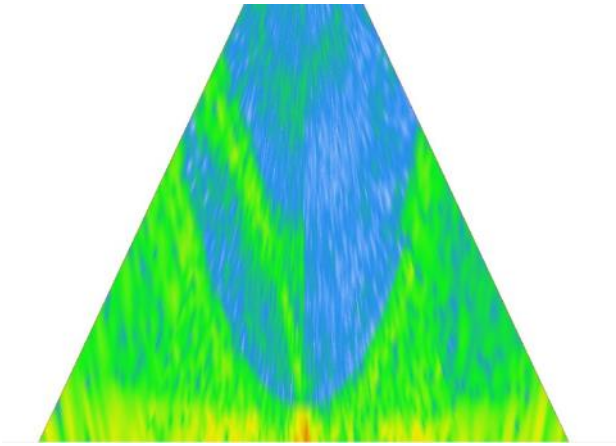

Figure WC-18: *EM122 water column data of seep displayed in Figure 17 left panel.*

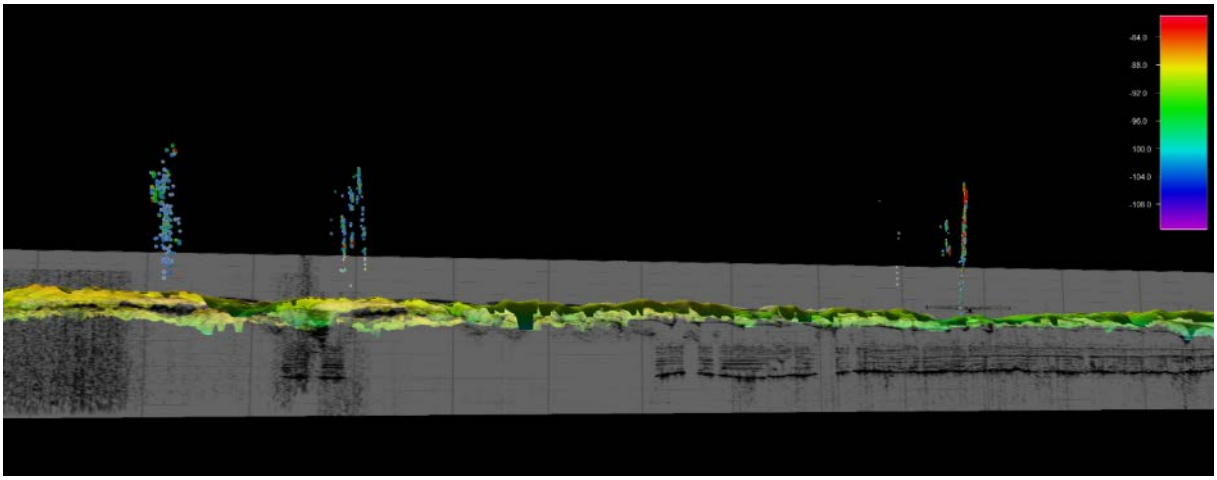

Figure WC-19: *Seeps shown in Figure WC-17 extracted from EM122 data georeferenced with EM122 bathymetry and SBP120 high-resolution subbottom profile. Color bar on right represents seafloor depths.*

The final example is of a single seep that is clearly related to a subsurface feature. Here the seep has a much less coherent appearance than some of the others – perhaps indicating intermittent rather than steady release of gas. While this seep is very clear in the EK80 image, it is much more difficult to locate in the multibeam (Fig. WC-20). Georeferencing of the extracted seep with the seafloor and subsurface morphology (Fig. WC-21) reveals the coincidence of the seep with a clear subsurface gas structure. The multibeam bathymetry shows a depression at the location of the seep but this depression is not apparent on either the EK80 or SBP120 and is thus most likely the result of "punch-through" (detection of the bottom deeper than the actual seafloor) of the multibeam sonar in the soft sediments disturbed by the gas expulsion.

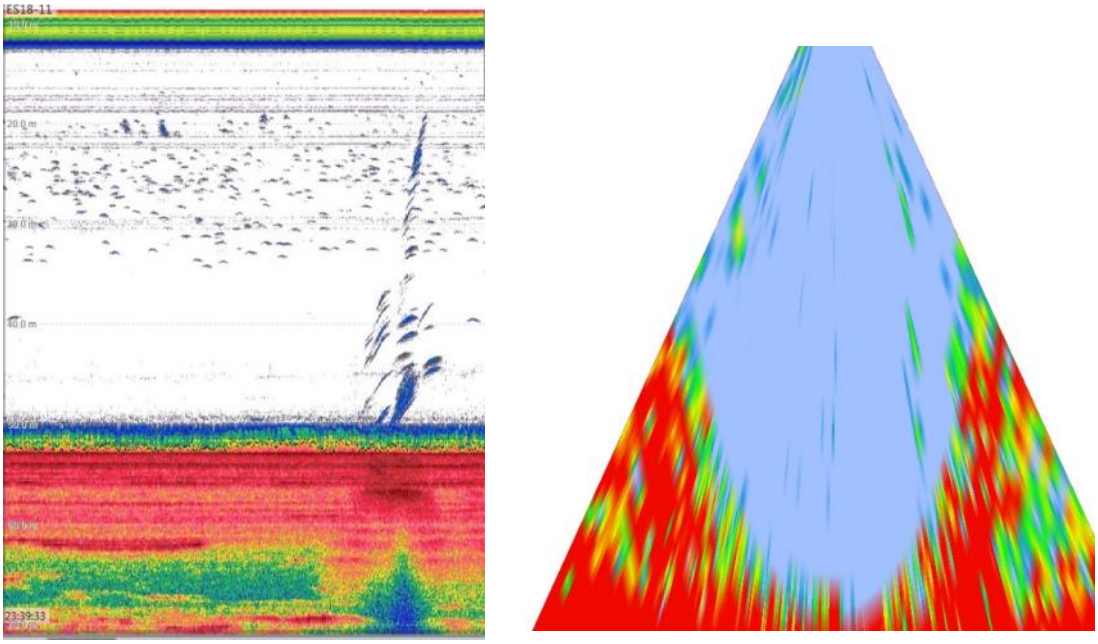

Figure WC-20: *EK80 observation of single seep in 52 m of water (left). Same seep as seen by EM122 (right side of right panel).*

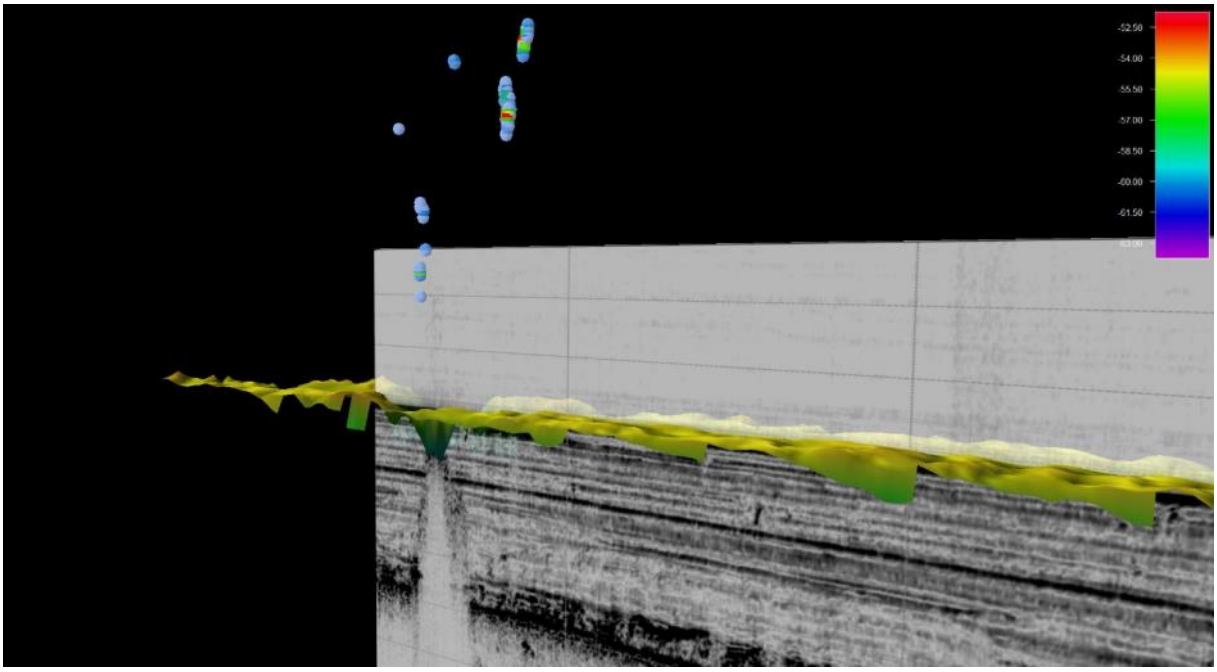

Figure WC-21: *Seep shown in Figure WC-20 extracted from EM122 data georeferenced with EM122 bathymetry and SBP120 high-resolution subbottom profile. Color bar on right represents seafloor depths.*

WP SC (Sediment Coring)

An overview of all retrieved sediment cores is presented in Table SC-1 for cores taken from within the Russian EEZ and in Table SC-2 for cores retrieved in international waters. These overviews show station number, core identification, latitude and longitude in decimal degrees, water depth, date and time of retrieval. Appendix SC-1 contains sub-bottom profiles for the piston and gravity cores sites and some selected multicore sites. The maps in figures SC-11 to SC-18 show the coring locations in Boxes 1-5. The overview map in the beginning of this cruise report shows the location of Boxes 1-5. Detailed information about each individual sediment core is summarized in Appendix SC-2 (cores retrieved from within the Russian EEZ) and Appendix SC-3 (cores retrieved in international waters).

Table SC-1: *Sediment cores taken from within the Russian EEZ.*

Summary of SWERUS Leg 2 sediment cores retrieved from within the Russian EEZ						
Coring Station	**Core ID**	**Latitude from time (UTC)**	**Longitude from time (UTC)**	**WD (m)**	**Date (UTC)**	**Time (UTC)**
Entrance from US EEZ into Russian EEZ: 2014-08-22, 19:09, 168°59'W, 71°35'N						
SWERUS-L2-1	SWERUS-L2-1-KL1	72.337483	-176.439009	73	140824	11:00
SWERUS-L2-2	SWERUS-L2-2-MC1	72.431673	-175.341468	56	140824	23:05
SWERUS-L2-2	SWERUS-L2-2-PC1	72.516580	-175.319605	72	140825	02:05
SWERUS-L2-2	SWERUS-L2-2-TWC1	72.516580	-175.319605	72	140825	02:05
SWERUS-L2-2	SWERUS-L2-2-KL1	72.566766	-175.265120	71	140825	03:54
SWERUS-L2-3	SWERUS-L2-3-MC1	72.377100	-175.786046	90	140825	07:02
SWERUS-L2-4	SWERUS-L2-4-PC1	72.838669	-175.727122	120	140826	08:04
SWERUS-L2-4	SWERUS-L2-4-TWC1	72.838669	-175.727122	120	140826	08:04
SWERUS-L2-4	SWERUS-L2-4-MC1	72.860940	-175.711060	124	140826	09:41
SWERUS-L2-5	SWERUS-L2-5-GC1	72.869910	-176.207350	116	140826	12:59
Exit from Russian EEZ, Western Chukchi Slope: 2014-08-27, 19:59, 179°8'W, 74°56'N						
Entrance into Russian EEZ, East Siberian Shelf: 2014-09-07, 03:12, 170°19'E, 75°14'N						
SWERUS-L2-19	SWERUS-L2-19-GC1	77.090994	162.617593	104	140908	01:01
SWERUS-L2-20	SWERUS-L2-20-GC1	77.359052	163.033304	115	140908	04:31
SWERUS-L2-21	SWERUS-L2-21-MC1	77.582359	163.293537	159	140908	06:43
SWERUS-L2-21	SWERUS-L2-21-MC2	77.579254	163.308346	153	140908	07:22
SWERUS-L2-22	SWERUS-L2-22-GC1	78.228240	164.387534	368	140908	20:05
SWERUS-L2-22	SWERUS-L2-22-MC1	78.223877	164.426767	367	140908	20:59
SWERUS-L2-22	SWERUS-L2-22-PC1	78.222926	164.461842	364	140908	21:55
SWERUS-L2-22	SWERUS-L2-22-TWC1	78.222926	164.461842	364	140908	21:55
SWERUS-L2-23	SWERUS-L2-23-GC1	78.660932	165.015603	508	140909	04:48
SWERUS-L2-23	SWERUS-L2-23-MC1	78.664367	165.032732	522	140909	05:29
SWERUS-L2-24	SWERUS-L2-24-GC1	78.796922	165.366530	964	140909	13:44
SWERUS-L2-24	SWERUS-L2-24-MC1	78.800030	165.382182	982	140909	14:34
SWERUS-L2-25	SWERUS-L2-25-MC1	79.226288	152.675619	101	140911	03:40
SWERUS-L2-26	SWERUS-L2-26-MC1	79.742133	154.388979	378	140911	21:52
SWERUS-L2-26	SWERUS-L2-26-PC1	79.749284	154.400991	395	140911	22:40
SWERUS-L2-26	SWERUS-L2-26-TWC1	79.749284	154.400991	395	140911	22:40
SWERUS-L2-27	SWERUS-L2-27-MC1	79.664634	154.126259	276	140912	01:29
SWERUS-L2-28	SWERUS-L2-28-MC1	79.919544	154.353544	1145	140912	06:44
SWERUS-L2-28	SWERUS-L2-28-GC1	79.924453	154.395755	1143	140912	07:32
Exit from Russian EEZ, East Siberian Shelf: 2014-09-12, 15:00, 154°30'E, 80°25'N						

Table SC-2: *Sediment cores taken in international waters.*

Summary of SWERUS Leg 2 sediment cores retrieved in international waters						
Coring Station	**Core ID**	**Latitude from time (UTC)**	**Longitude from time (UTC)**	**WD (m)**	**Date (UTC)**	**Time (UTC)**
SWERUS-L2-6	SWERUS-L2-6-GC1	74.965096	179.790905	353,1	140827	23:56
SWERUS-L2-7	SWERUS-L2-7-GC1	74.993181	179.819559	391,5	140828	05:05
SWERUS-L2-8	SWERUS-L2-8-GC1	75.179820	179.837674	555,2	140828	21:02
SWERUS-L2-8	SWERUS-L2-8-MC1	75.153192	179.873082	524	140828	22:46
SWERUS-L2-8	SWERUS-L2-8-PC1	75.135093	179.851639	515	140828	23:39
SWERUS-L2-8	SWERUS-L2-8-TWC1	75.135093	179.851639	515	140828	23:39
SWERUS-L2-9	SWERUS-L2-9-GC1	75.076126	-179.926110	475	140830	23:28
SWERUS-L2-9	SWERUS-L2-9-MC1	75.056727	-179.820416	446	140831	02:05
SWERUS-L2-10	SWERUS-L2-10-GC1	75.503513	-179.099796	1000	140831	08:07
SWERUS-L2-11	SWERUS-L2-11-GC1	75.498605	-178.880571	1018	140831	09:53
SWERUS-L2-12	SWERUS-L2-12-PC1	75.015920	179.752775	384	140831	22:54
SWERUS-L2-12	SWERUS-L2-12-TWC1	75.015920	179.752775	384	140831	22:54
SWERUS-L2-13	SWERUS-L2-13-GC1	76.199546	-179.262114	1109	140902	23:15
SWERUS-L2-13	SWERUS-L2-13-MC1	76.186327	-179.278362	1118	140903	01:22
SWERUS-L2-13	SWERUS-L2-13-PC1	76.180605	-179.289132	1119	140903	02:31
SWERUS-L2-13	SWERUS-L2-13-TWC1	76.180605	-179.289132	1119	140903	02:31
SWERUS-L2-14	SWERUS-L2-14-GC1	76.368032	176.432491	737	140904	04:10
SWERUS-L2-14	SWERUS-L2-14-MC1	76.352887	176.461110	733	140904	05:35
SWERUS-L2-15	SWERUS-L2-15-GC1	76.323278	175.898134	504	140904	08:15
SWERUS-L2-15	SWERUS-L2-15-MC1	76.320285	175.880574	501	140904	09:25
SWERUS-L2-16	SWERUS-L2-16-GC1	76.502192	176.648144	991	140904	21:51
SWERUS-L2-16	SWERUS-L2-16-MC1	76.512015	176.631991	1023	140904	22:58
SWERUS-L2-17	SWERUS-L2-17-PC1	76.464618	176.723823	977	140905	01:23
SWERUS-L2-17	SWERUS-L2-17-TWC1	76.464618	176.723823	977	140905	01:23
SWERUS-L2-18	SWERUS-L2-18-GC1	76.411590	173.788235	351	140906	07:03
SWERUS-L2-18	SWERUS-L2-18-MC1	76.409130	173.879144	349	140906	08:01
SWERUS-L2-18	SWERUS-L2-18-GC2	76.407537	173.919637	340	140906	08:28
SWERUS-L2-29	SWERUS-L2-29-GC1	81.299356	141.782550	824	140914	02:58
SWERUS-L2-29	SWERUS-L2-29-PC1	81.325804	141.749169	899	140914	04:30
SWERUS-L2-29	SWERUS-L2-29-TWC1	81.325804	141.749169	899	140914	04:30
SWERUS-L2-29	SWERUS-L2-29-MC1	81.342771	141.775463	910	140914	05:27
SWERUS-L2-30	SWERUS-L2-30-SGC1	80.466985	143.028528	1665	140915	00:37
SWERUS-L2-31	SWERUS-L2-31-PC1	79.914841	143.233458	1120	140915	14:56
SWERUS-L2-31	SWERUS-L2-31-TWC1	79.914841	143.233458	1120	140915	14:56
SWERUS-L2-31	SWERUS-L2-31-MC1	79.920391	143.164750	1157	140915	16:42
SWERUS-L2-32	SWERUS-L2-32-GC1	85.132313	151.569013	834	140920	22:38
SWERUS-L2-32	SWERUS-L2-32-MC1	85.141183	151.590145	837	140920	23:27
SWERUS-L2-32	SWERUS-L2-32-GC2	85.152613	151.664309	828	140921	00:49
SWERUS-L2-33	SWERUS-L2-33-GC1	84.274873	148.735319	886	140922	01:56
SWERUS-L2-33	SWERUS-L2-33-PC1	84.282038	148.646753	888	140922	03:07
SWERUS-L2-33	SWERUS-L2-33-TWC1	84.282038	148.646753	888	140922	03:07
SWERUS-L2-34	SWERUS-L2-34-MC1	84.276050	148.713423	886	140922	06:31

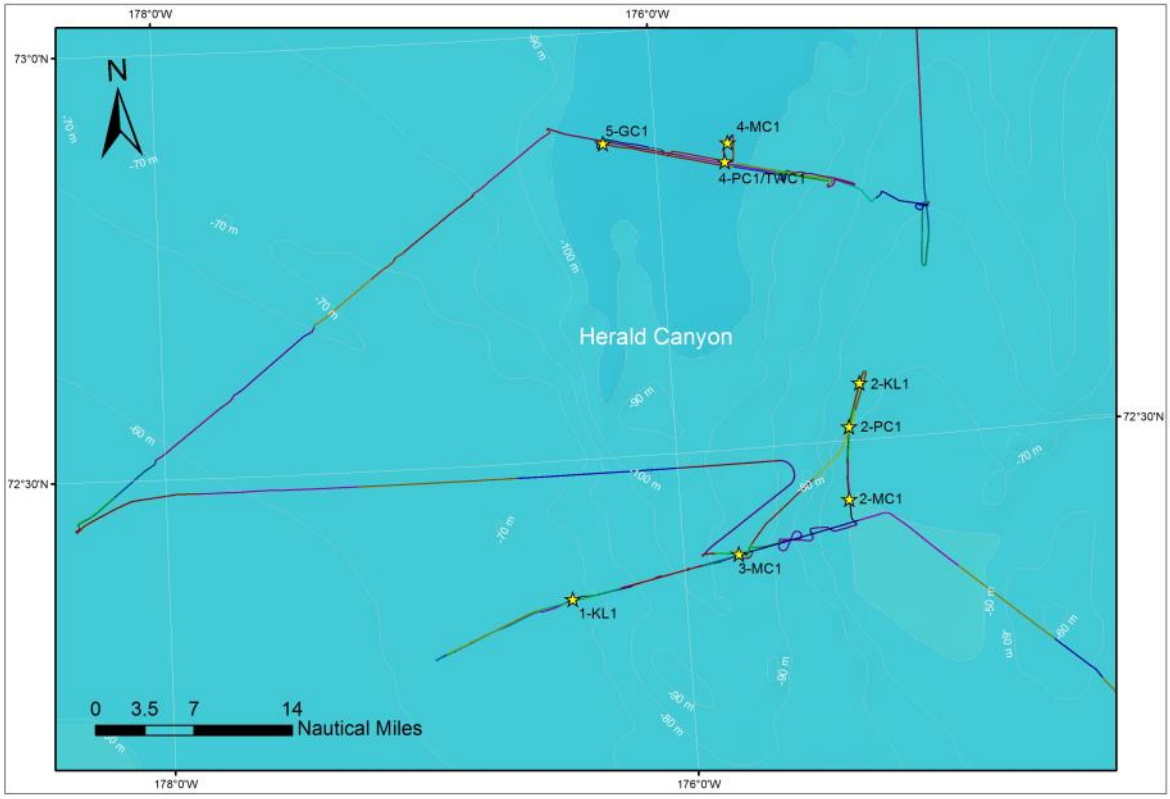

Figure SC-11: *Sediment cores retrieved in Box 1, Herald Canyon.*

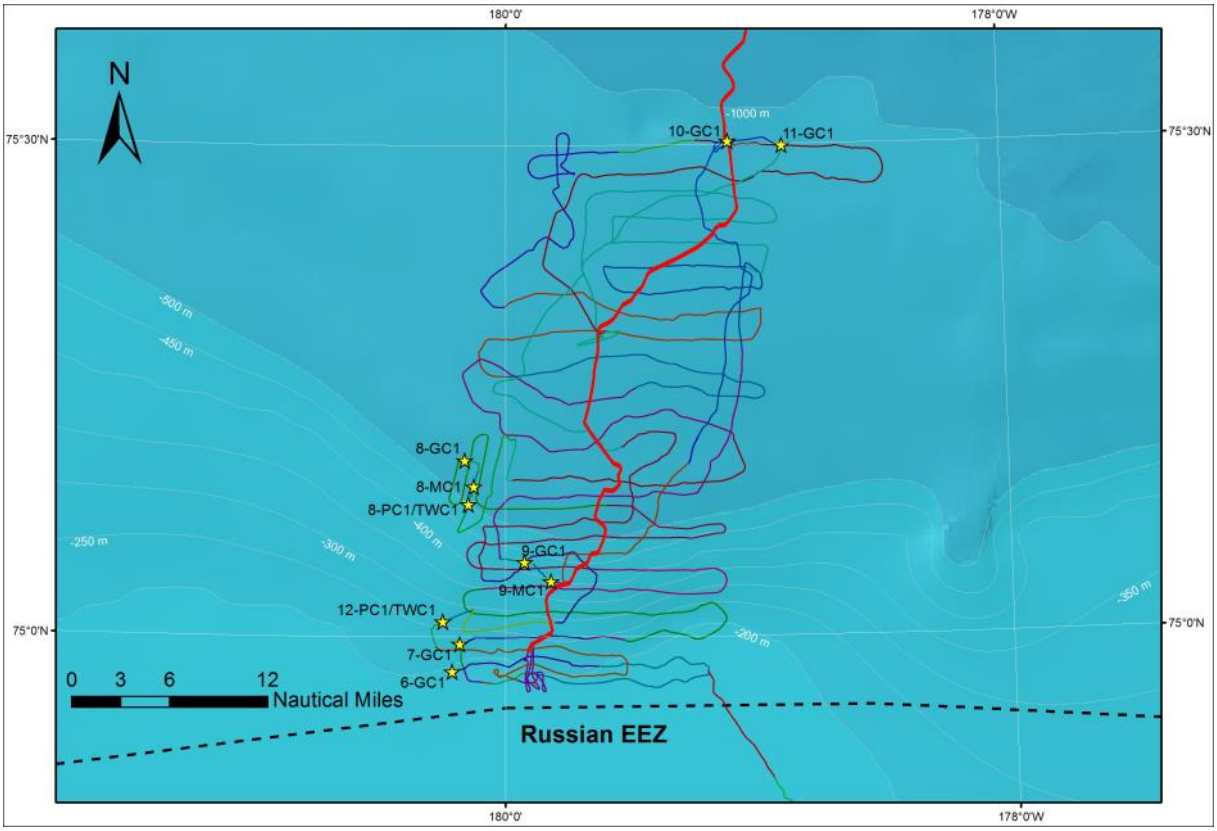

Figure SC-12: *Sediment cores retrieved in Box 2, continental slope north of Herald Canyon.*

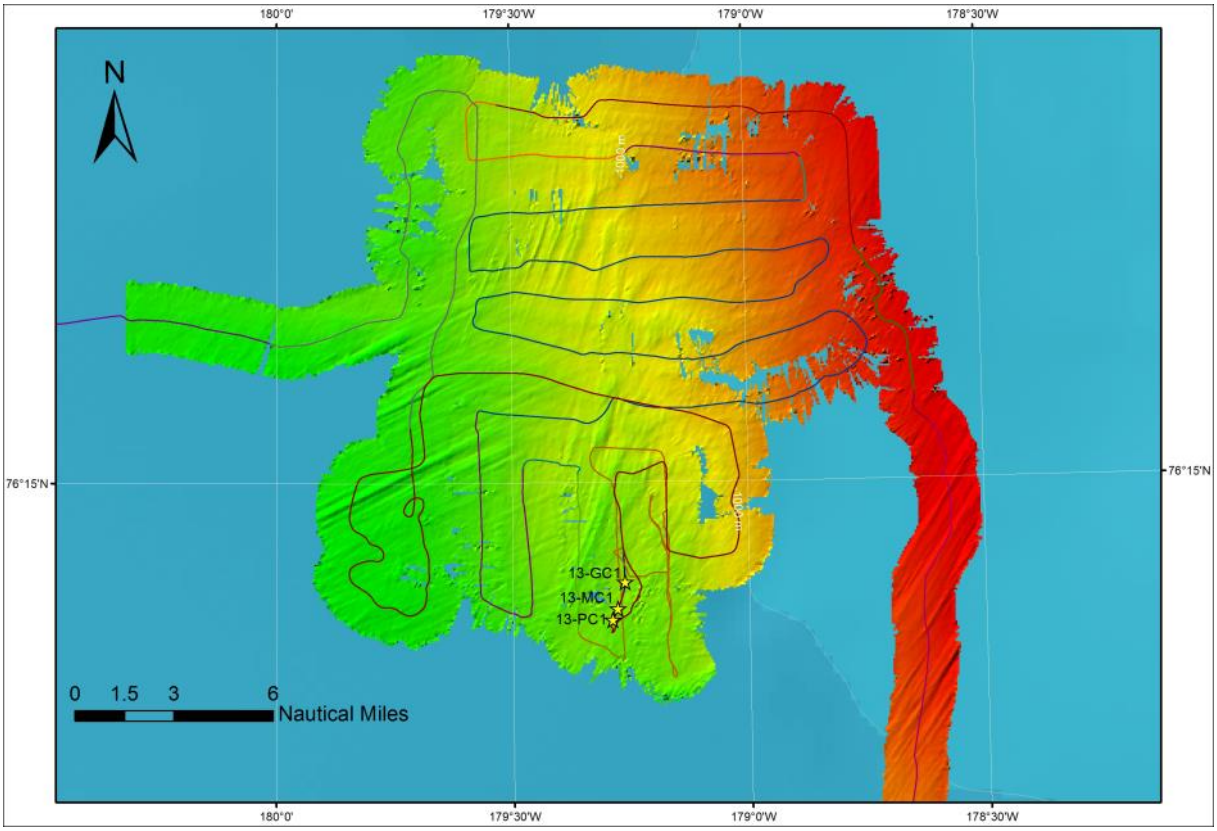

Figure SC-13: *Sediment cores retrieved in Box 2, the Arlis Plateau.*

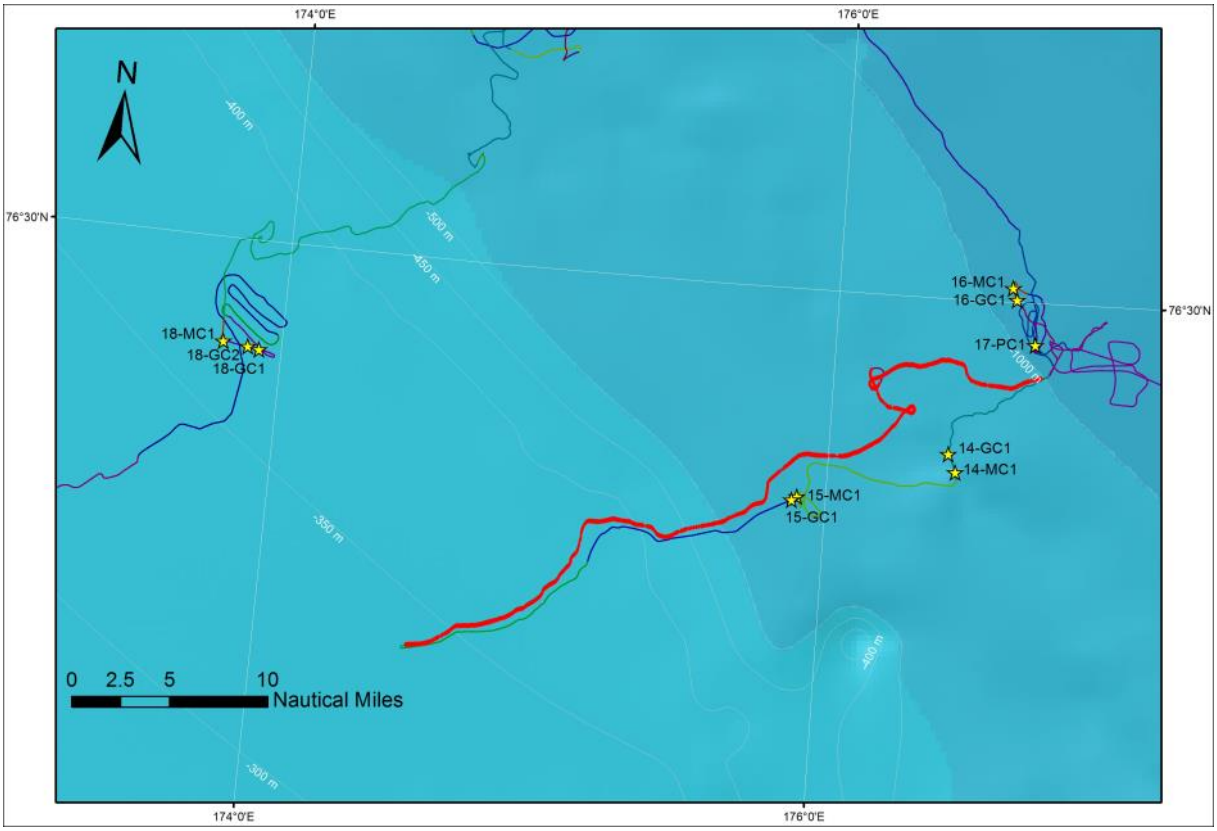

Figure SC-14: *Sediment cores retrieved in Box 3, transect 1 and 2 of the East Siberian Sea slope.*

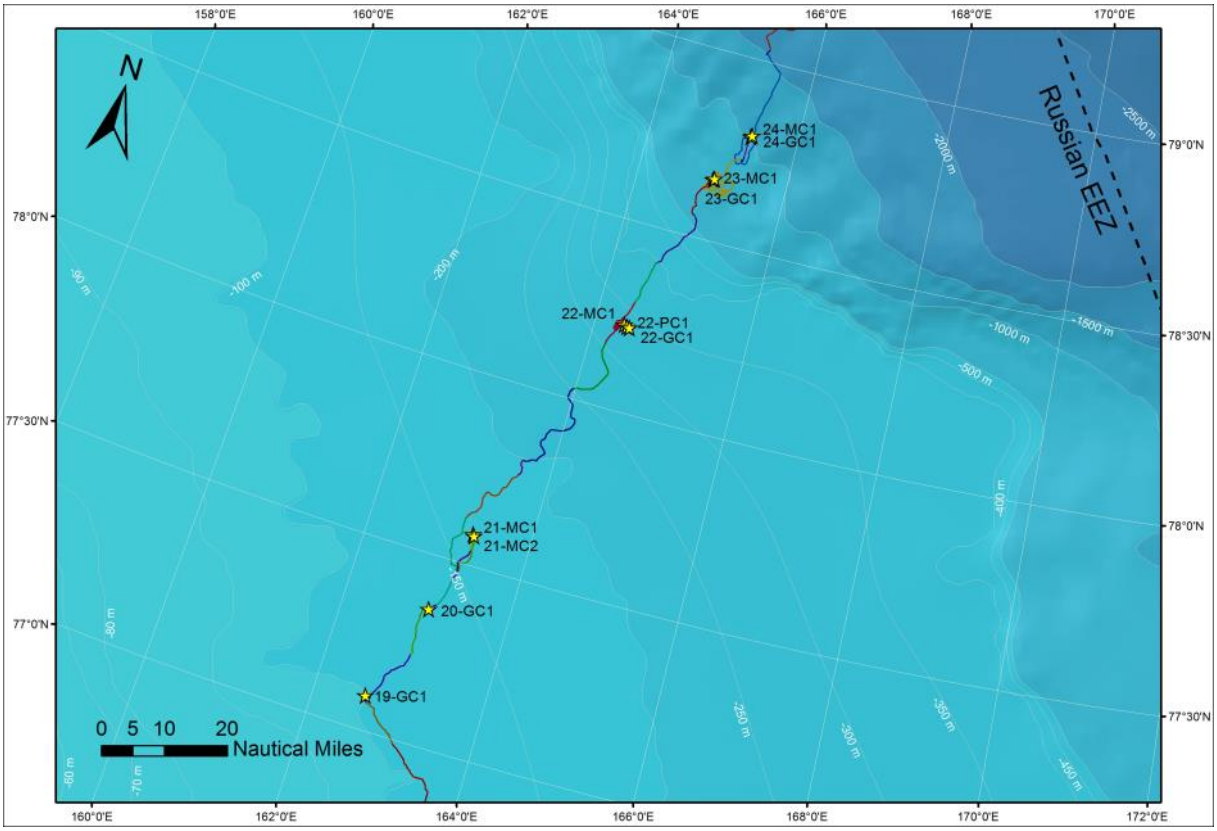

Figure SC-15: *Sediment cores retrieved in Box 3, transect 3 of the East Siberian Sea slope.*

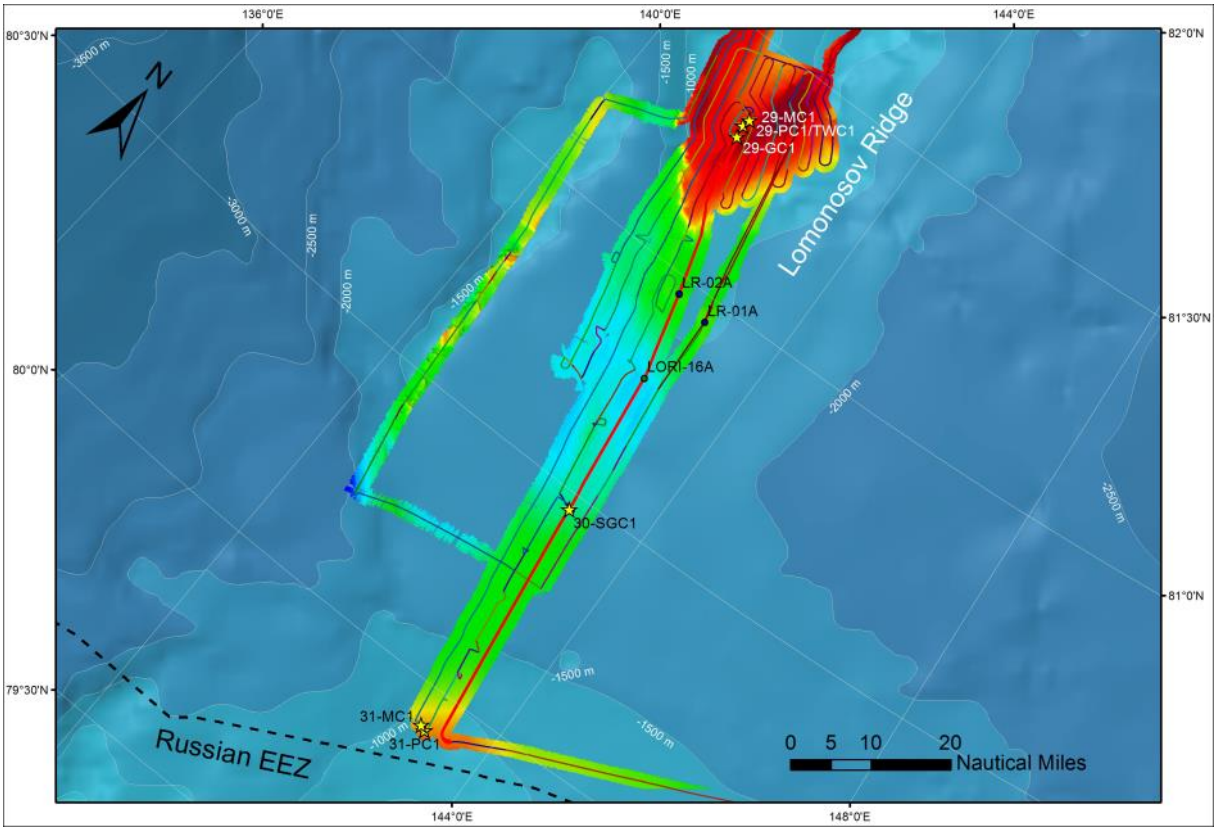

Figure SC-16: *Sediment cores retrieved in Box 4, southern Lomonosov Ridge.*

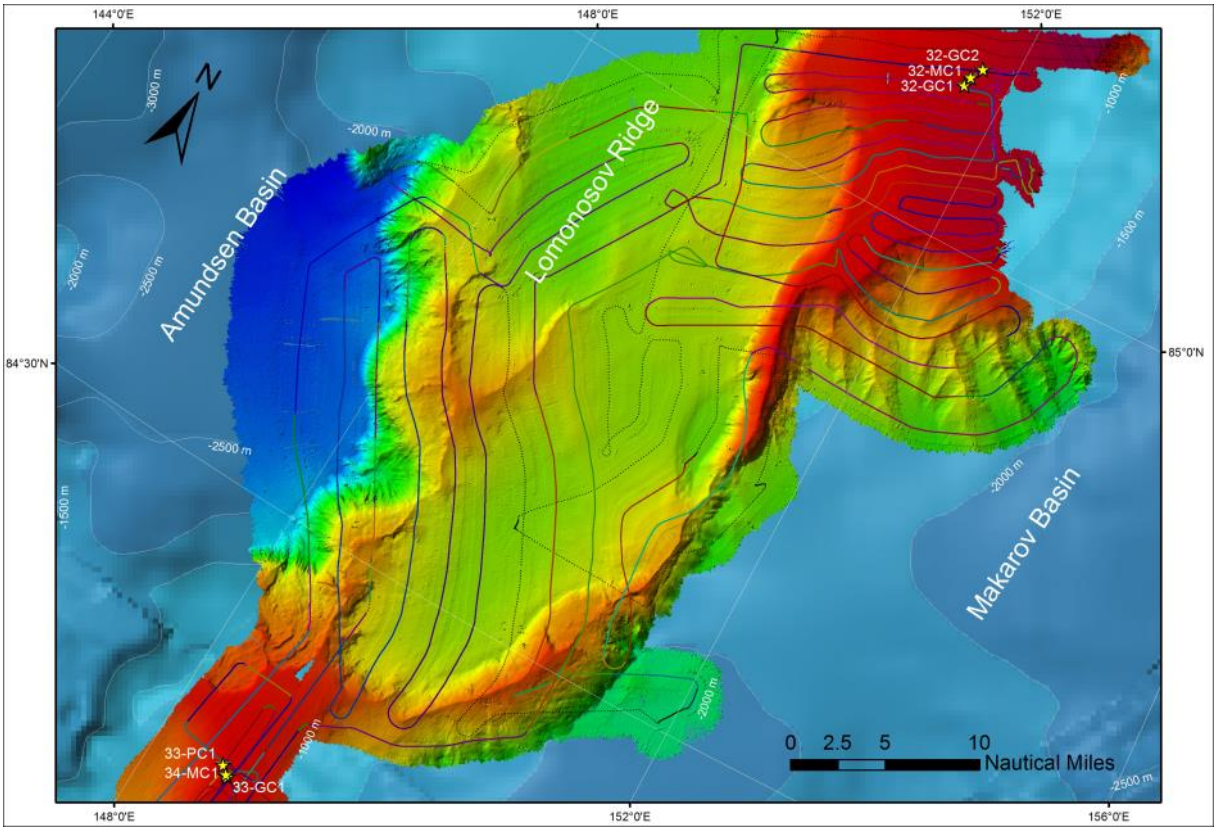

Figure SC-17: *Sediment cores retrieved in Box 5, central Lomonosov Ridge.*

Sediment core recovery

Ten piston cores were successfully taken, all rigged for 9 m. These ranged in length from 3.12 m to 8.43 m, with an average recovery of 6.12 m (68 %). The first five gravity cores were rigged for 3 m, yielding an average recovery of 2.56 m (85 %). The following 18 gravity cores were rigged for 6 m, including one smaller diameter core, yielding an average recovery of 3.26 m (54 %). Several of the six meter gravity cores were targeted on presumed stiffer sediments, which partly explains the modest recovery. The core quality is superb in both the piston and gravity cores, with a complete lack of flow-in structures or other disturbances. Twenty-one multicores were retrieved (Tables SC-1, SC-2), yielding an average recovery of 23 cm. The distribution of the eight tubes in each multicore is shown in WP MB. Two Kasten Lot (Kasten Corer) rigged for 3 m were taken during the first two days of coring operations during Leg 2 of SWERUS-C3 (Table SC-1). When successful, this coring device generate large quantities of sediment, but the low recovery (17 %) and less good core quality made us abandon this coring device for the remaining part of Leg 2.

WP SP (Sediment Physical Properties)

MSCL results.

The high-resolution MSCL physical property measurements for each core were combined with digital line scan images in the software *Strater* and are presented in Appendix PP-2. Digital images of the individual core sections were also compiled in *Strater*, and presented as digital photo compilations in Appendix PP-3. Cores that were not opened shipboard contain no associated images in these files. Trigger weight cores were not logged on the MSCL.

One gravity core (SWERUS-L2-9-GC1) was not logged because of high-resolution methane sampling that was performed when it was first recovered. The archive half of split core remains largely undisturbed, and can be logged onshore at Stockholm University.

In most cases, compressional wave velocity measurements worked well on the expedition. However, because the core logging occurred after the Rhizone sampling for pore water, there are intervals throughout many cores that remain affected by the reduction in the water content. SWERUS-L2-28-GC1 was sampled heavily for pore water (6 cm resolution, and >10 mL acquired from each location). Core logging data from this core should be used with caution.

Overall, the MSCL results from all of the working areas provided excellent data to construct preliminary stratigraphic correlations (Figure PP- 6).

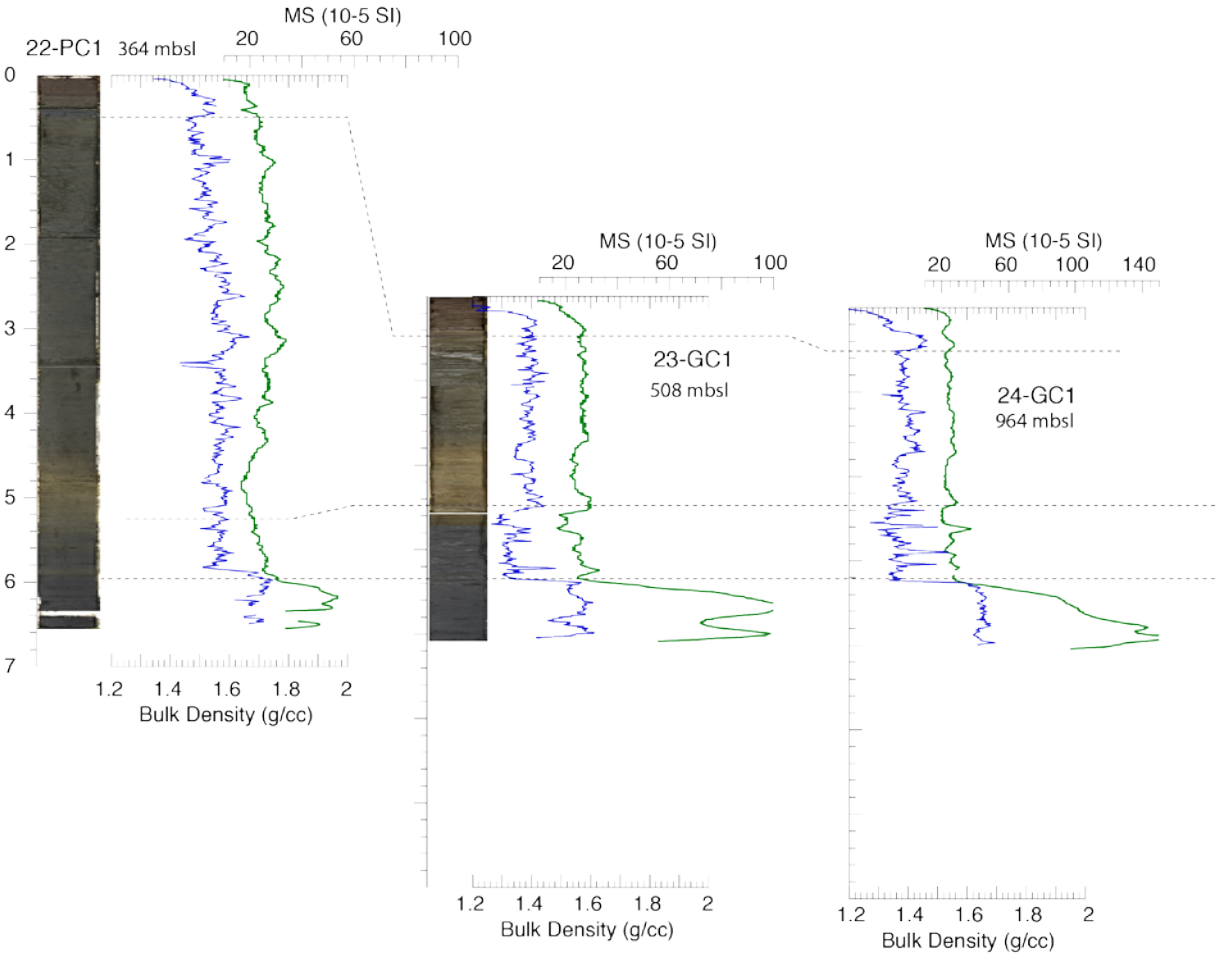

Figure PP-6: *Example of MSCL based correlation of 3 cores forming a downslope transect from 364 to 964 mbsl.*

In-situ temperature measurements

The combination of the DST magnetic and the temperature sensors provided an efficient way to derive in-situ temperatures and track movements of the core barrel through the water column and while embedded in the sediments. The orientation tool data could be downloaded and read within minutes of the core landing on deck, and in a few instances provided important information on establishing whether the core penetrated the sediments or fell horizontally on the seafloor (Figure PP-7).

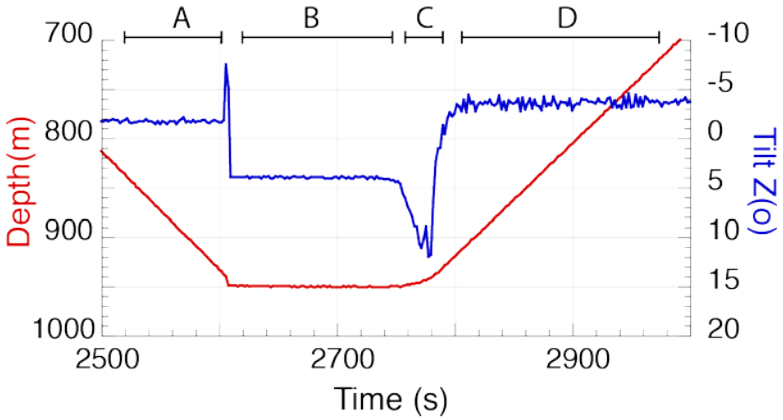

Figure PP-7: *Example of depth and tilt data from the DSC magnetic tool during a deployment of the piston core. A. As core barrel is lowered through the water column, the sensor is oriented at -2^{o} from vertical. B. The core barrel reached the seafloor, and the piston core is triggered. It sits within the seafloor for 160 s at an angle of 5^{o} from the vertical plane. C. During the slow pull out, the piston core is dragged towards the horizontal plane. This is likely due to the drift of the ship while the core was embedded in the seafloor. D. The core returns to a more vertical orientation during its ascent through the water column.*

In-situ temperature measurements were made at 33 gravity and piston coring stations. Further processing and analysis of the data is required to establish how many of these deployments provided reliable in-situ temperature estimates. At first glance, it seems that 60-80% of the deployments were successful (Figure PP-8). At some of the early measurement stations, located in shallow water and occupied during times of high winds, the sensors may not have been left in long enough to equilibrate to ambient conditions. At other stations, especially on the shallow slope, shelf, and in areas of glacial ice grounding, not enough of the sensors may have penetrated the seafloor to establish a gradient. Other possible obstacles to a successful deployment included movement of the core barrel while embedded in the sediments, or the failure of one or more of the probes.

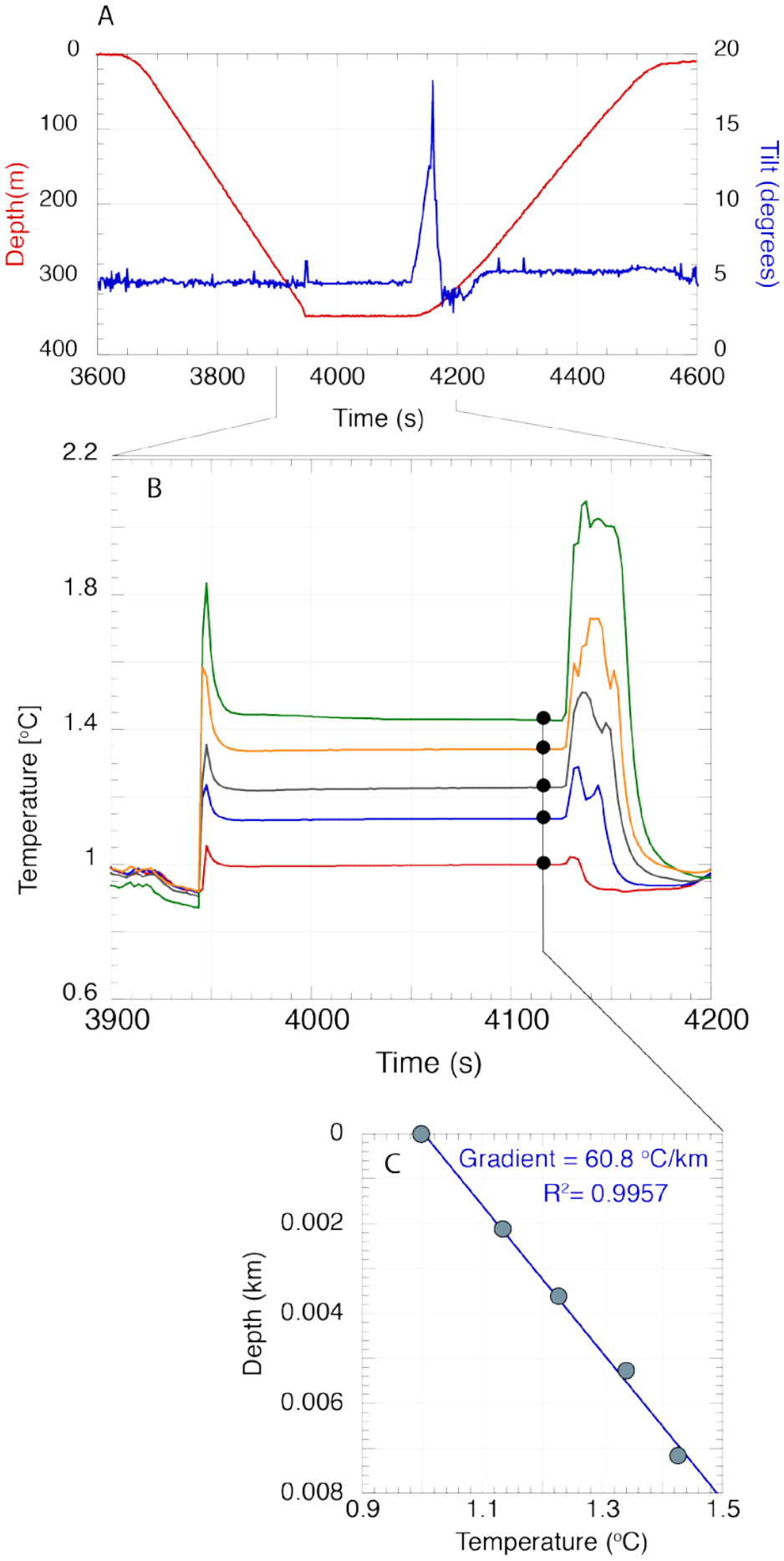
A
0
100
200
300
400
Depth(m)
20
15
10
5
0
Tilt (degrees)
3600
3800
4000
4200
4400
4600
Time (s)
B
2.2
1.8
1.4
1
0.6
Temperature [°C]
3900
4000
4100
4200
Time (s)
C
Gradient = 60.8 °C/km
R²= 0.9957
0
0.002
0.004
0.006
0.008
Depth (km)
0.9
1.1
1.3
1.5
Temperature (°C)

Figure PP-8: *A. Depth and Tilt data from the DSC magnetic tool during the deployment of a piston core. The piston core is triggered and enters the seafloor at 3945 ss after logging began. It is removed from the seafloor 4120 ss after logging began. B. The initial penetration of the core barrel causes a large amount of frictional heating of the temperature sensors. The sensor just above the nose cone experiences the largest frictional heating pulse. As the core barrel sits in the sediments this heating pulse decays, and the sensors begin to read the ambient in-situ temperature conditions. C: Equilibrated temperatures, generally reached after 100 s, are used to provide an initial estimate of the geothermal gradient at this location.*

Thermal constants measurements on sediments

The thermal constants measurements were performed as soon as the core sections were split. A total of 330 1-sided measurements were performed on 25 cores, generally at a 30 cm downcore resolution. Shipboard conditions were not always ideal to perform the measurements. Vibrations caused by icebreaking resulted in large temperature drifts and affected the measurement reliability. Whenever the temperature drift was considered too high (usually higher than 3-5 mK), the measurement was repeated.

The thermal data collected from the 25 cores show a clear relationship between the thermal constants: thermal diffusivity is higher when thermal conductivity increases, while specific heat capacity tends to decrease when thermal conductivity increases (Figure PP-9). Averages for thermal constants measured on Leg 2 are 1.090 W/mK, 0.3319 mm^2/s and 3.319 MJ/m^3K, respectively (Figure PP-10).

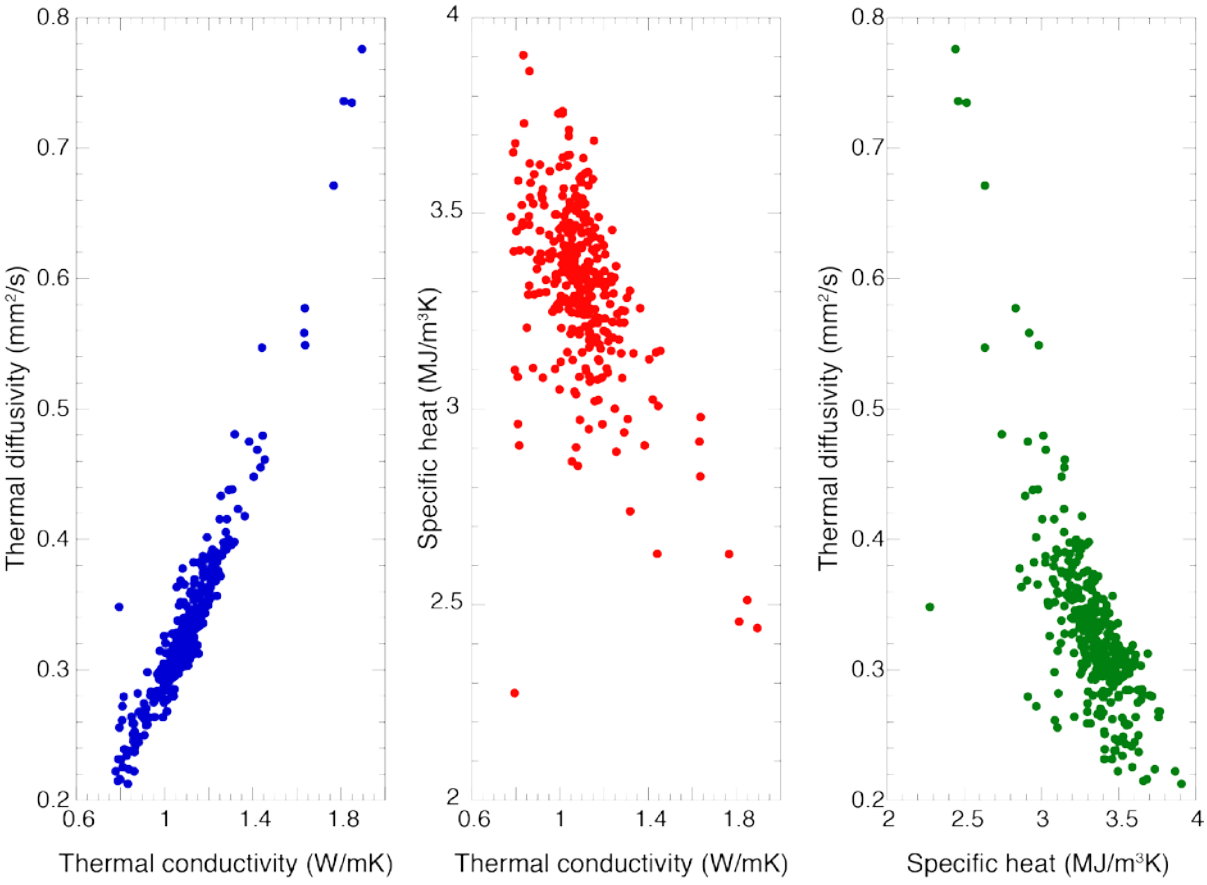

Figure PP-9: *Thermal constants results obtained during Leg 2 of SWERUS-C3. Left: thermal conductivity; center: thermal diffusivity; right: specific heat capacity*

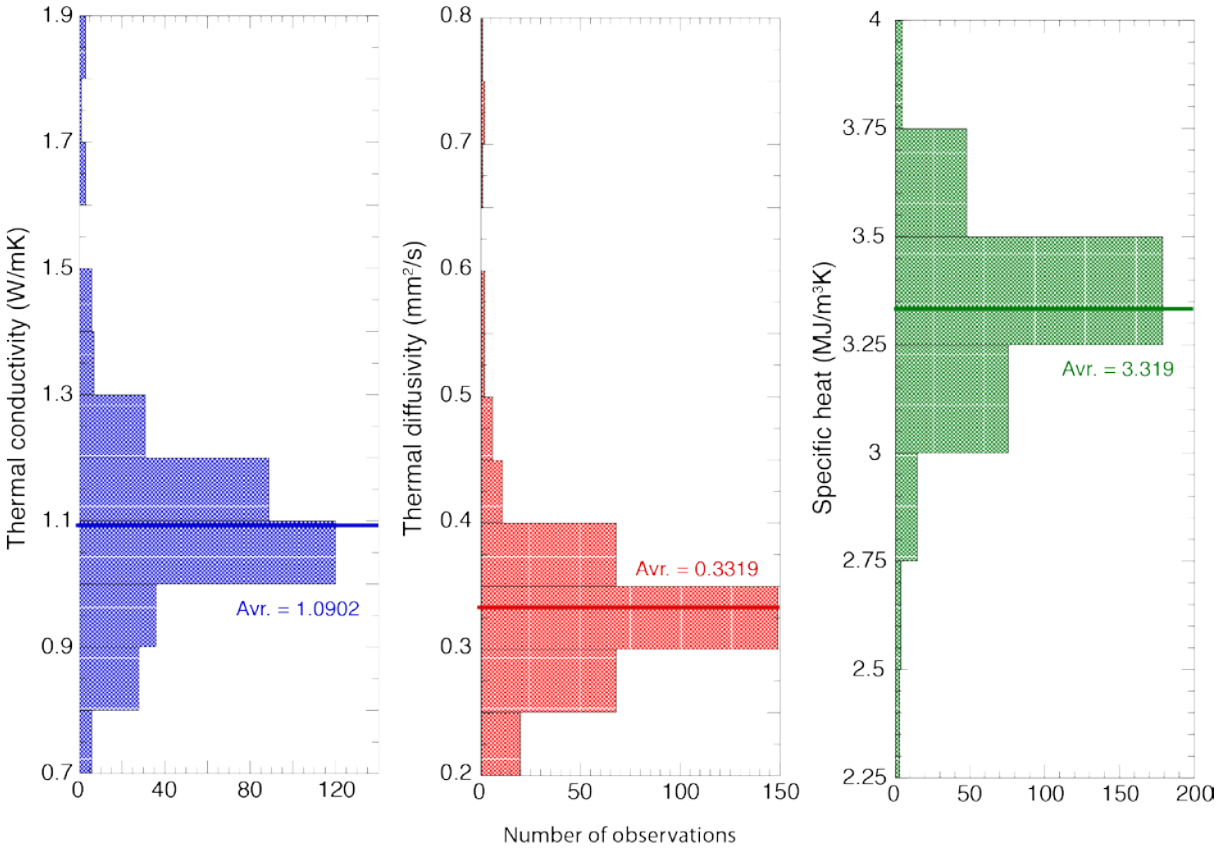

Figure PP-10: *Distribution of thermal constants values measured during Leg 2 of SWERUS-C3 and respective averages. Left: thermal conductivity; center: thermal diffusivity; right: specific heat capacity.*

Index property and shear strength measurements

Swell and icebreaking often made it impossible to use a scale to weigh the sediment samples for index property measurements. Therefore, water content was only obtained for 16 cores and grain density for only 4 cores. Grain density measurements on the remaining samples will be analysed at Stockholm University, and used in conjunction with the MSCL bulk density data to calculate porosity and water content.

The shear strength of sediments was calculated using the penetration values of the fall cone tests on the split cores. The fall cone tests were usually performed at the same downcore position as the thermal constants measurements. Whenever the penetration values tended to be low (≈5 mm), the test interval was reduced to 10 -15 cm, to better capture transitions into potentially overconsolidated sediments.

Predictable downcore trends existed in the index property, thermal constants, and shear strengths measurements. As sediments become more consolidated with increasing burial depth, the shear strength increases, water content decreases and the thermal conductivity increases (Figure PP-11). How these properties evolve at grater burial depths, and vary on a regional scale, will be a question addressed as part of the post-cruise research.

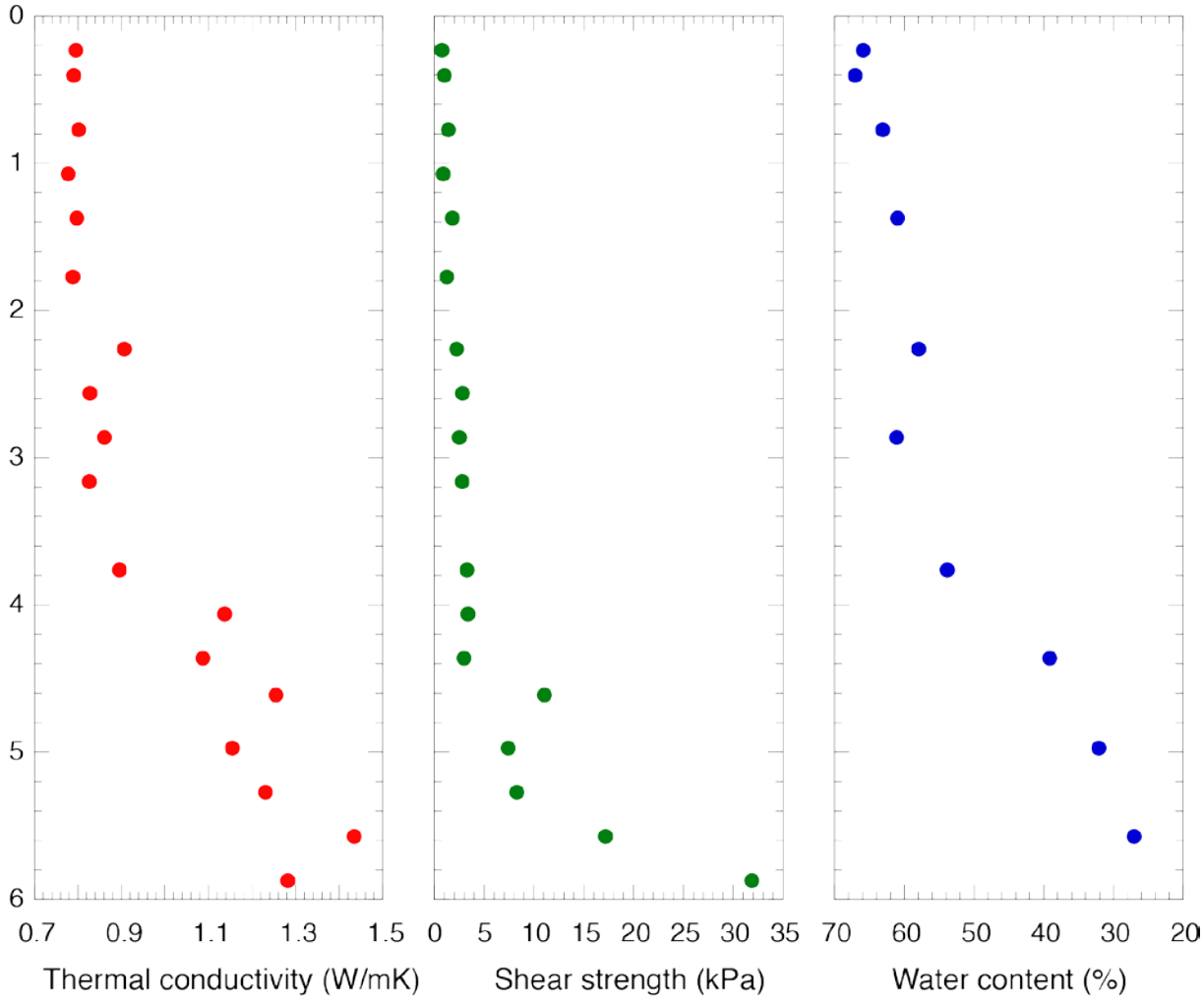

Figure PP-11: *Downcore profiles of thermal conductivity, shear strength and water content in a piston core recovered during Leg 2 of SWERUS.*

WP CP (Sediment Chemical Properties)

Poor water

All chemical properties analyses were controlled by the volume of water the rhizons were able to remove from the cores. Approximately 70% of the rhizons filled the sample syringe (10 mL). Most of the remainder yielded at least 7 mL. Priority was given to alkalinity, metals and sulfur, then hydrogen sulfide and sulfur isotopes. Only 200 samples were available for δ13C of DIC. Therefore, these samples were individually chosen by the work package leader. The remaining water was used for ammonia and phosphate. The aliquots of all samples is given in Table CP-2.

Sediments

Sediment samples for concentration analysis were taken at all multicoring stations (Fig. CP-6). One examples of vertical concentration profile in core SWERUS-L2-9-GC1 and 9-MC1 is shown along with methane concentration in water station # 9 in Figure CP-7.

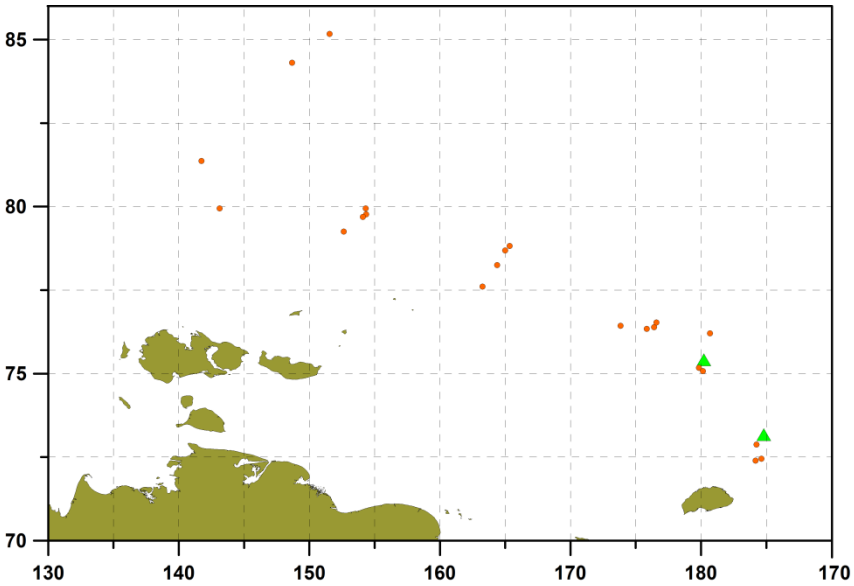

Figure CP-6: *Multicores are shown with orange dots and analyzed gravity cores with green triangles.*

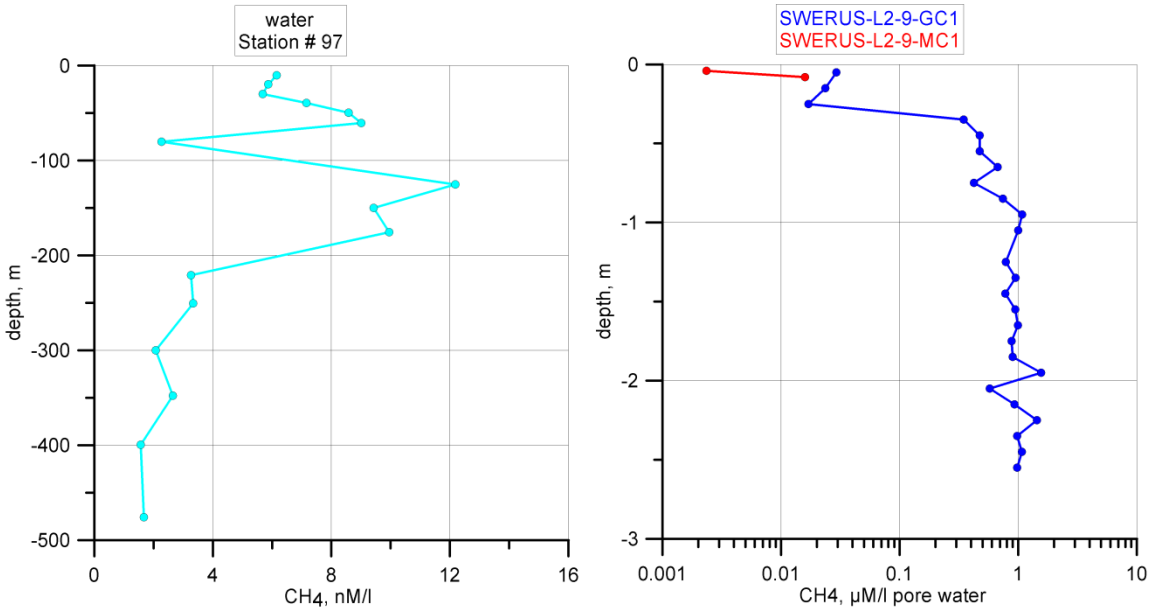

Figure CP-7: *Vertical concentration profile in cores SWERUS-L2-9-GC1 and 9-MC1 shown along with methane concentration in water station # 9.*

Table CP-2: *Master Sample List*

Sample Number	Sample ID	Metals & Sulfur	HS^- & S Isotope	DIC & C Isotope	Alkalinity	Phosphate	Ammonia	Russian EEZ
1	2MC - 4 +2	X	X	X	X	X	X	YES
2	2MC - 4 - 0	X	X		X	X	X	YES
3	2MC - 4 - 3	X	X		X	X	X	YES
4	2MC - 4 - 6	X	X		X	X	X	YES
5	2MC - 4 - 9	X	X		X	X	X	YES
6	2MC - 4 - 15	X	X		X	X	X	YES
7	2MC - 4 - 18	X	X		X			YES
8	2MC - 4 - 24	X	X		X	X		YES
9	2PC - Sec 1 - 10	X	X	X	X			YES
10	2PC - Sec 1 - 40	X	X		X	X		YES
11	2PC - Sec 1 - 70	X			X	X		YES
12	2PC - Sec 2 - 10	X	X		X	X		YES
13	2PC - Sec 2 - 40	X	X		X	X		YES
14	2PC - Sec 2 - 100	X	X		X	X		YES
15	2PC - Sec 2 - 130	X	X		X	X		YES
16	2PC - Sec 3 - 10	X	X		X			YES
17	2PC - Sec 3 - 40	X	X	X	X	X	X	YES
18	2PC - Sec 3 - 70	X	X		X	X	X	YES
19	2PC - Sec 3 - 100	X	X		X	X	X	YES
20	2PC - Sec 3 - 130	X	X	X	X	X	X	YES
21	2PC - Sec 4 - 10	X	X		X	X		YES
22	2PC - Sec 4 - 40	X			X		X	YES

23	2PC - Sec 4 - 70	X	X	X	X	X	X	YES
24	2PC - Sec 4 - 100	X	X		X	X	X	YES
25	2PC - Sec 4 - 130	X	X		X	X	X	YES
26	2PC - Sec 5 - 10	X	X		X	X	X	YES
27	2PC - Sec 5 - 40	X	X		X	X	X	YES
28	2PC - Sec 6 - 10	X	X		X	X	X	YES
29	2PC - Sec 6 - 40	X	X		X	X	X	YES
30	2PC - Sec 6 - 70	X	X		X	X	X	YES
31	2PC - Sec 6 - 130	X	X	X	X	X	X	YES
32	3MC - 4 +2	X	X		X		X	YES
33	3MC - 4 - 0	X	X	X	X	X		YES
34	3MC - 4 - 3	X	X		X	X	X	YES
35	3MC - 4 - 6	X	X		X	X	X	YES
36	3MC - 4 - 9	X	X		X	X		YES
37	3MC - 4 - 12	X	X		X	X		YES
38	3MC - 4 - 15	X	X		X	X		YES
39	3MC - 4 - 18	X	X			X	X	YES
40	3MC - 4 - 21	X	X		X	X		YES
41	4TWC-1 - 29.8	X						YES
42	4TWC-1 - 29.8	X						YES
43	4TWC-1 - 29.8	X						YES
44	Not Taken							YES
45	4MC - 4 +2	X	X		X	X	X	YES
46	4MC - 4 - 6	X	X	X	X		X	YES
47	4MC - 4 - 9	X	X		X			YES
48	4MC - 4 - 12	X	X		X	X	X	YES
49	4MC - 4 - 15	X	X		X	X	X	YES
50	4MC - 4 - 18	X	X		X		X	YES
51	4MC - 4 - 21	X	X		X	X	X	YES
52	4MC - 4 - 24	X	X		X			YES
53	4MC - 4 - 27	X	X		X	X		YES
54	4MC - 4 - 30	X	X		X	X		YES
55	4PC - Sec 1 - 5	X	X	X	X	X	X	YES
56	4PC - Sec 1 - 20	X	X		X	X	X	YES
57	4PC - Sec 1 - 40	X	X		X	X	X	YES
58	4PC - Sec 2 - 5	X	X		X	X	X	YES
59	4PC - Sec 2 - 34	X	X	X	X	X	X	YES
60	4PC - Sec 2 - 64	X	X		X	X	X	YES
61	4PC - Sec 2 - 94	X	X		X	X	X	YES
62	4PC - Sec 2 - 124	X	X		X	X	X	YES
63	4PC - Sec 3 - 6	X	X	X	X	X	X	YES
64	4PC - Sec 3 - 30	X	X		X	X	X	YES
65	4PC - Sec 3 - 60	X	X		X	X		YES
66	4PC - Sec 3 - 90	X	X		X	X	X	YES
67	4PC - Sec 3 - 120	X	X	X	X	X	X	YES

68	4PC - Sec 4 - 6	X	X		X			YES
69	4PC - Sec 4 - 35	X	X		X	X	X	YES
70	4PC - Sec 4 - 66	X	X		X			YES
71	4PC - Sec 4 - 97	X	X	X	X	X		YES
72	4PC - Sec 5 - 37	X	X		X			YES
73	4PC - Sec 5 - 90	X	X		X			YES
74	4PC - Sec 5 - 137	X	X		X			YES
75	8MC - 4 +2	X	X	X	X	X	X	No
76	8MC - 4 - 3	X	X		X	X	X	No
77	8MC - 4 - 9	X	X		X	X	X	No
78	8MC - 4 - 15	X	X		X	X	X	No
79	8PC - Sec 1 - 6	X	X	X	X	X	X	No
80	8PC - Sec 1 - 20	X	X		X	X	X	No
81	8PC - Sec 1 - 30	X	X		X	X	X	No
82	8PC - Sec 1 - 40	X	X		X	X	X	No
83	8PC - Sec 2 - 6	X	X		X	X	X	No
84	8PC - Sec 2 - 25	X	X	X	X	X	X	No
85	8PC - Sec 2 - 50	X	X		X	X	X	No
86	8PC - Sec 2 - 75	X	X	X	X	X	X	No
87	8PC - Sec 2 - 100	X	X		X	X	X	No
88	8PC - Sec 2 - 125	X	X	X	X	X	X	No
89	8PC - Sec 3 - 6	X	X		X	X	X	No
90	8PC - Sec 3 - 25	X	X	X	X	X	X	No
91	8PC - Sec 3 - 50	X	X		X	X	X	No
92	8PC - Sec 3 - 75	X	X	X	X	X	X	No
93	8PC - Sec 3 - 100	X	X		X	X	X	No
94	8PC - Sec 3 - 125	X	X	X	X	X		No
95	8PC - Sec 4 - 5	X	X		X	X	X	No
96	8PC - Sec 4 - 25	X	X	X	X	X	X	No
97	8PC - Sec 4 - 50	X	X		X	X		No
98	8PC - Sec 4 - 70	X	X		X	X	X	No
99	8PC - Sec 4 - 100	X	X	X	X	X	X	No
100	8PC - Sec 5 - 6	X	X					No
101	8PC - Sec 5 - 25	X	X		X	X	X	No
102	8PC - Sec 5 - 50	X	X	X		X		No
103	8PC - Sec 5 - 75	X	X	X	X	X	X	No
104	8PC - Sec 5 - 125	X	X	X	X	X	X	No
105	9MC - 4 +2	X	X	X	X	X		No
106	9MC - 4 - 6	X	X	X	X	X		No
107	9MC - 4 - 12	X	X	X	X	X		No
108	9MC - 4 - 17	X	X	X	X	X		No
109	9MC - 4 - 21	X	X	X	X			No
110	9MC - 4 - 27	X	X	X	X	X		No
111	10GC - Sec 1 - 24	X	X	X	X	X		No
112	10GC - Sec 1 - 44	X	X		X	X	X	No

113	10GC - Sec 1 - 59	X	X	X	X	X		No
114	10GC - Sec 1 - 78	X	X		X	X	X	No
115	10GC - Sec 2 - 6	X	X		X	X	X	No
116	10GC - Sec 2 - 40	X	X		X	X	X	No
117	10GC - Sec 2 - 60	X	X	X	X	X	X	No
118	10GC - Sec 2 - 80	X	X		X	X	X	No
119	10GC - Sec 2 - 100	X	X		X	X	X	No
120	10GC - Sec 2 - 115	X	X		X	X		No
121	10GC - Sec 2 - 130	X	X	X	X	X	X	No
122	10GC - Sec 3 - 6	X	X		X	X	X	No
123	10GC - Sec 3 - 20	X	X		X	X	X	No
124	10GC - Sec 3 - 40	X	X		X	X	X	No
125	10GC - Sec 3 - 60	X	X		X	X	X	No
126	10GC - Sec 3 - 80	X	X		X	X		No
127	10GC - Sec 3 - 100	X	X		X	X		No
128	10GC - Sec 3 - 115	X	X	X	X	X	X	No
129	10GC - Sec 3 - 130	X	X	X	X		X	No
130	12JPC - Sec 1 - 6	X	X	X	X	X		No
131	12JPC - Sec 1 - 20	X	X		X	X	X	No
132	12JPC - Sec 1 - 40	X	X	X	X	X		No
133	12JPC - Sec 1 - 60	X	X		X	X	X	No
134	12JPC - Sec 1 - 80	X	X		X	X	X	No
135	12JPC - Sec 1 - 92	X	X	X	X	X	X	No
136	12JPC - Sec 2 - 7	X	X		X	X	X	No
137	12JPC - Sec 2 - 20	X	X		X	X	X	No
138	12JPC - Sec 2 - 40	X	X	X	X	X	X	No
139	12JPC - Sec 2 - 60	X	X		X	X	X	No
140	12JPC - Sec 2 - 80	X	X		X	X	X	No
141	12JPC - Sec 2 - 100	X	X	X	X	X		No
142	12JPC - Sec 2 - 120	X	X		X	X	X	No
143	12JPC - Sec 2 - 130	X	X		X	X	X	No
144	12JPC - Sec 3 - 6	X	X	X	X	X	X	No
145	12JPC - Sec 3 - 20	X	X		X	X	X	No
146	12JPC - Sec 3 - 40	X	X		X	X	X	No
147	12JPC - Sec 3 - 60	X	X	X	X	X	X	No
148	12JPC - Sec 3 - 80	X	X		X	X	X	No
149	12JPC - Sec 3 - 100	X	X		X	X	X	No
150	12JPC - Sec 3 - 120	X	X		X			No
151	12JPC - Sec 3 - 130	X	X	X	X	X		No
152	12JPC - Sec 4 - 6	X	X		X	X	X	No
153	12JPC - Sec 4 - 20	X	X		X	X		No
154	12JPC - Sec 4 - 40	X	X	X	X	X		No
155	Not Taken							No
156	12JPC - Sec 4 - 80	X	X		X	X		No
157	12JPC - Sec 4 - 100	X	X		X	X		No

158	12JPC - Sec 4 - 120	X	X	X	X		X	No
159	12JPC - Sec 4 - 140	X	X		X	X		No
160	12JPC - Sec 5 - 6	X	X		X	X		No
161	12JPC - Sec 5 - 22	X	X	X	X		X	No
162	12JPC - Sec 5 - 42	X	X		X	X	X	No
163	12JPC - Sec 5 - 62	X	X		X			No
164	12JPC - Sec 5 - 82	X	X	X	X	X	X	No
165	12JPC - Sec 5 - 102	X	X		X	X		No
166	12JPC - Sec 6 - 6	X	X		X	X		No
167	12JPC - Sec 6 - 20	X	X	X	X	X		No
168	Not Taken							No
169	12JPC - Sec 6 - 60	X	X		X	X		No
170	12JPC - Sec 6 - 80	X	X		X		X	No
171	12JPC - Sec 6 - 100	X	X		X			No
172	12JPC - Sec 6 - 120	X	X		X	X		No
173	12JPC - Sec 6 - 130	X	X	X	X		X	No
174	13MC - 4 - +2	X	X	X	X		X	No
175	13MC - 4 - 3	X	X		X		X	No
176	13MC - 4 - 9	X	X		X		X	No
177	13MC - 4 - 15	X	X		X		X	No
178	14MC - 4 - +2	X	X		X		X	No
179	14MC - 4 - 0	X	X	X	X		X	No
180	14MC - 4 - 6	X	X		X		X	No
181	14MC - 4 - 12	X	X		X		X	No
182	14MC - 4 - 18				X			No
183	14GC - Sec 1 - 6	X	X	X	X	X	X	No
184	14GC - Sec 1 - 36	X	X	X	X	X	X	No
185	14GC - Sec 1 - 60	X	X	X	X	X	X	No
186	14GC - Sec 2 - 6	X	X	X	X	X	X	No
187	14GC - Sec 2 - 37	X	X		X	X	X	No
188	14GC - Sec 2 - 67	X	X	X	X	X	X	No
189	14GC - Sec 2 - 97	X	X		X	X	X	No
190	14GC - Sec 2 - 113	X	X	X	X	X	X	No
191	14GC - Sec 2 - 130	X	X		X	X	X	No
192	14GC - Sec 2 - 130	X	X		X	X	X	No
193	14GC - Sec 3 - 6	X	X		X	X	X	No
194	14GC - Sec 3 - 6	X	X		X			No
195	14GC - Sec 3 - 36	X	X	X	X	X	X	No
196	14GC - Sec 3 - 66	X	X		X	X	X	No
197	14GC - Sec 3 - 96	X	X		X	X	X	No
198	14GC - Sec 3 - 127	X	X	X	X	X	X	No
199	16MC - 4 - +2	X	X		X	X	X	No
200	16MC - 4 - 0	X	X		X	X	X	No
201	16MC - 4 - -3	X	X	X	X	X	X	No
202	17PC - Sec 1 - 6	X	X	X	X	X	X	No

203	17PC - Sec 1 - 37	X	X		X	X		No
204	17PC - Sec 1 - 37	X	X					No
205	17PC - Sec 2 - 6	X	X		X	X	X	No
206	17PC - Sec 2 - 37	X	X		X			No
207	17PC - Sec 2 - 37	X	X					No
208	17PC - Sec 2 - 67	X	X	X	X	X	X	No
209	17PC - Sec 2 - 97	X	X		X	X	X	No
210	17PC - Sec 2 - 130	X	X		X			No
211	17PC - Sec 2 - 130	X	X					No
212	17PC - Sec 3 - 6	X	X		X		X	No
213	17PC - Sec 3 - 36	X	X		X			No
214	17PC - Sec 3 - 66	X	X		X			No
215	17PC - Sec 3 - 66	X	X					No
216	17PC - Sec 3 - 96	X	X	X	X	X	X	No
217	17PC - Sec 3 - 130	X	X		X	X	X	No
218	17PC - Sec 4 - 6	X	X		X			No
219	17PC - Sec 4 - 36	X	X		X			No
220	17PC - Sec 4 - 36	X	X					No
221	17PC - Sec 4 - 66	X	X		X	X	X	No
222	17PC - Sec 4 - 96	X	X	X	X		X	No
223	17PC - Sec 4 - 111	X	X		X	X	X	No
224	17PC - Sec 5 - 6	X	X		X	X	X	No
225	17PC - Sec 5 - 36	X	X		X			No
226	17PC - Sec 5 - 36	X	X					No
227	17PC - Sec 5 - 66	X	X		X	X	X	No
228	17PC - Sec 5 - 130	X	X	X	X	X	X	No
229	18MC - 4 - +2	X	X	X	X	X	X	No
230	18MC - 4 - 4	X	X	X	X	X	X	No
231	18MC - 4 - 10	X	X		X			No
232	18MC - 4 - 16	X	X		X			No
233	18MC - 4 - 18	X			X			No
234	18MC - 4 - 32	X	X	X	X	X	X	No
235	18GC - Sec 1 - 14	X	X	X	X	X	X	No
236	18GC - Sec 2 - 6	X	X	X	X	X	X	No
237	18GC - Sec 2 - 37	X	X		X	X	X	No
238	18GC - Sec 2 - 67	X	X		X	X	X	No
239	18GC - Sec 2 - 97	X	X		X	X	X	No
240	18GC - Sec 2 - 121	X	X		X	X	X	No
241	18GC - Sec 2 - 143	X	X		X			No
242	18GC - CC - 10				X			No
243	21MC - 4 - +2	X	X		X		X	Yes
244	21MC - 4 - 4	X	X	X	X	X	X	Yes
245	21MC - 4 - 10	X	X		X			Yes
246	21MC - 4 - 16	X			X			Yes
247	21MC - 4 - 22	X			X			Yes

248	22MC - 4 - 3	X	X	X	X		X	Yes
249	22MC - 4 - 11	X			X	X		Yes
250	22MC - 4 - 21	X			X			Yes
251	22MC - 4 - 30	X	X	X	X		X	Yes
252	22TWC - 6	X	X	X	X		X	Yes
253	22PC - Sec 2 - 6	X	X	X	X	X	X	Yes
254	22PC - Sec 2 - 36	X	X	X	X	X	X	Yes
255	22PC - Sec 2 - 67	X	X		X		X	Yes
256	22PC - Sec 2 - 97	X	X		X	X	X	Yes
257	22PC - Sec 2 - 132	X	X	X	X	X	X	Yes
258	22PC - Sec 3 - 6	X	X		X	X	X	Yes
259	22PC - Sec 3 - 36	X	X		X	X	X	Yes
260	22PC - Sec 3 - 67	X	X	X	X	X	X	Yes
261	22PC - Sec 3 - 97	X	X	X	X	X	X	Yes
262	22PC - Sec 3 - 131	X	X		X	X	X	Yes
263	22PC - Sec 4 - 6	X	X	X	X	X	X	Yes
264	22PC - Sec 4 - 36	X	X	X	X	X	X	Yes
265	22PC - Sec 4 - 67	X	X		X	X	X	Yes
266	22PC - Sec 4 - 97	X	X	X	X	X	X	Yes
267	22PC - Sec 4 - 131	X	X	X	X		X	Yes
268	22PC - Sec 5 - 6	X	X		X		X	Yes
269	22PC - Sec 5 - 37	X	X	X	X	X	X	Yes
270	22PC - Sec 5 - 67	X	X		X		X	Yes
271	22PC - Sec 5 - 97	X	X	X	X	X	X	Yes
272	22PC - Sec 5 - 131	X	X		X		X	Yes
273	23MC - 4 - 2	X	X	X	X		X	Yes
274	23MC - 4 - 16	X			X			Yes
275	23MC - 4 - 30	X	X		X			Yes
276	24GC - Sec 1 - 6	X	X	X	X		X	Yes
277	24GC - Sec 1 - 36	X	X	X	X		X	Yes
278	24GC - Sec 1 - 59	X	X	X	X	X	X	Yes
279	24GC - Sec 1 - 83	X	X	X	X		X	Yes
280	24GC - Sec 2 - 7	X	X	X	X		X	Yes
281	24GC - Sec 2 - 37	X	X	X	X	X	X	Yes
282	24GC - Sec 2 - 67	X	X	X	X		X	Yes
283	24GC - Sec 2 - 97	X	X	X	X	X	X	Yes
284	24GC - Sec 2 - 130	X	X	X	X	X	X	Yes
285	24GC - Sec 3 - 7	X	X	X	X		X	Yes
286	24GC - Sec 3 - 37	X	X	X	X	X	X	Yes
287	24GC - Sec 3 - 67	X		X	X		X	Yes
288	24GC - Sec 3 - 97	X	X	X	X		X	Yes
289	24GC - Sec 3 - 130	X		X	X		X	Yes
290	24MC - 4 - 3	X		X	X		X	Yes
291	24MC - 4 - 6	X			X		X	Yes
292	24MC - 4 - 16	X		X	X		X	Yes

293	24MC - 4 - 30	X			X		X	Yes
294	25MC - 4 - 1	X		X	X	X	X	Yes
295	25MC - 4 - 4	X			X	X	X	Yes
296	25MC - 4 - 10	X			X		X	Yes
297	25MC - 4 - 16	X			X		X	Yes
298	25MC - 4 - 19				X	X	X	Yes
299	25MC - 4 - 23	X			X	X	X	Yes
300	26MC - 4 - 3.5	X	X	X	X	X	X	Yes
301	26MC - 4 - 10	X	X		X	X	X	Yes
302	26MC - 4 - 15.5	X	X		X		X	Yes
303	26MC - 4 - 21.5	X	X		X		X	Yes
304	26MC - 4 - 28	X	X		X		X	Yes
305	26MC - 4 - 36	X	X		X		X	Yes
306	27MC - 4 - 3	X	X	X	X	X	X	Yes
307	27MC - 4 - 6	X	X		X		X	Yes
308	27MC - 4 - 12	X	X		X		X	Yes
309	27MC - 4 - 18	X	X		X	X	X	Yes
310	27MC - 4 - 24	X	X		X		X	Yes
311	28MC - 4 - 0	X	X		X	X	X	Yes
312	28MC - 4 - 3	X	X		X		X	Yes
313	28MC - 4 - 9	X	X		X		X	Yes
314	28MC - 4 - 15	X	X		X		X	Yes
315	28MC - 4 - 21	X	X		X		X	Yes
316	28MC - 4 - 25	X	X		X		X	Yes
317	28GC - Sec 1 - 7 #1	X	X		X	X	X	Yes
318	28GC - Sec 1 - 7 #2	X	X		X	X	X	Yes
319	28GC - Sec 1 - 7 #3				X		X	Yes
320	28GC - Sec 1 - 35 #1	X	X		X	X	X	Yes
321	28GC - Sec 1 - 35 #2	X	X		X	X	X	Yes
322	28GC - Sec 2 - 28 #1	X	X		X	X	X	Yes
323	28GC - Sec 2 - 28 #2	X	X		X	X	X	Yes
324	28GC - Sec 2 - 56 #1	X	X		X	X	X	Yes
325	28GC - Sec 2 - 56 #2						X	Yes
326	28GC - Sec 2 - 85 #1	X	X		X	X	X	Yes
327	28GC - Sec 2 - 85 #2				X	X	X	Yes
328	28GC - Sec 2 - 113 #1	X	X		X	X	X	Yes
329	28GC - Sec 2 - 113 #2				X	X	X	Yes
330	28GC - Sec 2 - 139 #1	X	X		X	X	X	Yes
331	28GC - Sec 2 - 139 #2	X	X		X		X	Yes
332	28GC - Sec 3 - 28 #1	X	X		X	X	X	Yes
333	28GC - Sec 3 - 28 #2				X	X	X	Yes
334	28GC - Sec 3 - 56 #1	X	X		X	X	X	Yes
335	28GC - Sec 3 - 56 #2	X	X		X		X	Yes
336	28GC - Sec 3 - 85 #1	X	X		X	X	X	Yes
337	28GC - Sec 3 - 85 #2				X	X	X	Yes

338	28GC - Sec 3 - 113 #1	X	X		X	X	X	Yes
339	28GC - Sec 3 - 113 #2	X	X		X		X	Yes
340	28GC - Sec 3 - 139 #1	X	X		X	X	X	Yes
341	28GC - Sec 3 - 139 #2	X	X		X		X	Yes
342	28GC - Sec 4 - 25	X	X		X	X	X	Yes
343	28GC - Sec 4 - 49	X	X		X	X	X	Yes
344	28GC - Sec 4 - 79	X	X		X	X	X	Yes
345	28GC - Sec 4 - 98	X	X		X	X	X	Yes
346	28GC - Sec 4 - 104	X	X		X	X	X	Yes
347	28GC - Sec 4 - 123 #1	X	X		X	X	X	Yes
348	28GC - Sec 4 - 123 #2	X	X		X		X	Yes
349	28GC - Sec 1 - 14 #1	X	X		X	X	X	Yes
350	28GC - Sec 1 - 14 #2	X	X		X	X	X	Yes
351	28GC - Sec 1 - 14 #3	X	X		X	X	X	Yes
352	28GC - Sec 2 - 7 #1	X	X		X	X	X	Yes
353	28GC - Sec 2 - 7 #2	X			X		X	Yes
354	28GC - Sec 2 - 35 #1	X	X		X	X	X	Yes
355	28GC - Sec 2 - 35 #2	X			X		X	Yes
356	28GC - Sec 2 - 64	X	X		X	X	X	Yes
357	28GC - Sec 2 - 78	X	X		X	X	X	Yes
358	28GC - Sec 2 - 92 #1	X	X		X	X	X	Yes
359	28GC - Sec 2 - 92 #2	X			X		X	Yes
360	28GC - Sec 2 - 120 #1	X	X		X	X	X	Yes
361	28GC - Sec 2 - 120 #2	X			X		X	Yes
362	28GC - Sec 3 - 7 #1	X	X		X	X	X	Yes
363	28GC - Sec 3 - 7 #2	X	X		X	X	X	Yes
364	28GC - Sec 3 - 35 #1	X	X		X	X	X	Yes
365	28GC - Sec 3 - 35 #2	X			X		X	Yes
366	28GC - Sec 3 - 64 #1	X	X		X		X	Yes
367	28GC - Sec 3 - 64 #2	X			X		X	Yes
368	28GC - Sec 3 - 92	X			X		X	Yes
369	28GC - Sec 3 - 120 #1	X	X		X	X	X	Yes
370	28GC - Sec 3 - 120 #2	X	X		X		X	Yes
371	28GC - Sec 4 - 7 #1	X	X		X	X	X	Yes
372	28GC - Sec 4 - 7 #2	X			X		X	Yes
373	28GC - Sec 4 - 37	X	X		X	X	X	Yes
374	28GC - Sec 4 - 55	X	X		X		X	Yes
375	28GC - Sec 4 - 80	X	X		X	X	X	Yes
376	28GC - Sec 4 - 104	X	X		X		X	Yes
377	28GC - Sec 4 - 128	X	X		X	X	X	Yes
378	29GC - Sec 2 - 7	X	X	X	X		X	No
379	29GC - Sec 2 - 37	X	X		X	X	X	No
380	29GC - Sec 2 - 67	X	X		X		X	No
381	29GC - Sec 2 - 97	X	X		X	X	X	No
382	29GC - Sec 2 - 122	X	X		X		X	No

383	29GC - Sec 3 - 7	X	X	X	X		X	No
384	29GC - Sec 3 - 37	X	X		X	X	X	No
385	29GC - Sec 3 - 67	X	X		X		X	No
386	29GC - Sec 3 - 97	X	X		X	X	X	No
387	29GC - Sec 3 - 127	X	X		X		X	No
388	29GC - Sec 4 - 6	X	X	X	X		X	No
389	29GC - Sec 4 - 30	X	X		X	X	X	No
390	29GC - Sec 4 - 60	X	X		X		X	No
391	29GC - Sec 4 - 90	X	X		X	X	X	No
392	29GC - Sec 4 - 125	X	X	X	X		X	No
393	29MC - 4 - 3	X	X	X	X		X	No
394	29MC - 4 - 9	X	X		X		X	No
395	29MC - 4 - 21	X	X		X		X	No
396	31MC - 4 - 3	X	X	X	X	X	X	No
397	31MC - 4 - 6	X	X		X	X	X	No
398	31MC - 4 - 28.5	X	X		X	X	X	No
399	31MC - 4 - 37	X	X		X	X	X	No
400	31PC - Sec 1 - 23	X	X	X	X	X	X	No
401	31PC - Sec 1 - 37	X	X	X	X	X	X	No
402	31PC - Sec 2 - 6	X	X	X	X	X	X	No
403	31PC - Sec 2 - 36	X	X	X	X	X	X	No
404	31PC - Sec 2 - 66	X	X	X	X	X	X	No
405	31PC - Sec 2 - 97	X	X	X	X	X	X	No
406	31PC - Sec 2 - 127	X	X	X	X	X	X	No
407	31PC - Sec 3 - 6	X	X	X	X	X	X	No
408	31PC - Sec 3 - 37	X	X	X	X	X	X	No
409	31PC - Sec 3 - 67	X	X	X	X	X	X	No
410	31PC - Sec 3 - 97	X	X	X	X	X	X	No
411	31PC - Sec 3 - 127	X	X	X	X	X	X	No
412	31PC - Sec 4 - 6	X	X	X	X	X	X	No
413	31PC - Sec 4 - 37	X	X	X	X		X	No
414	31PC - Sec 4 - 67	X	X	X	X	X	X	No
415	31PC - Sec 4 - 98	X	X	X	X		X	No
416	31PC - Sec 4 - 131	X	X	X	X	X	X	No
417	31PC - Sec 5 - 6	X	X	X	X	X	X	No
418	31PC - Sec 5 - 37	X	X	X	X		X	No
419	31PC - Sec 5 - 67	X	X	X	X	X	X	No
420	31PC - Sec 5 - 97	X	X	X	X		X	No
421	31PC - Sec 6 - 6	X	X	X	X	X	X	No
422	31PC - Sec 6 - 36	X	X	X	X		X	No
423	31PC - Sec 6 - 67	X	X	X	X		X	No
424	31PC - Sec 6 - 97	X	X	X	X	X	X	No
425	31PC - Sec 6 - 131	X	X	X	X	X	X	No
426	28GC - Sec 1 - 21 #1	X	X		X	X	X	Yes
427	28GC - Sec 1 - 21 #2	X	X		X	X	X	Yes

428	28GC - Sec 1 - 21 #3	X	X		X	X	X	Yes
429	28GC - Sec 2 - 14 #1	X	X		X	X	X	Yes
430	28GC - Sec 2 - 14 #2	X				X	X	Yes
431	28GC - Sec 2 - 42	X			X	X	X	Yes
432	28GC - Sec 2 - 71 #1	X	X		X	X	X	Yes
433	28GC - Sec 2 - 71 #2	X			X	X	X	Yes
434	28GC - Sec 2 - 99 #1	X	X		X	X	X	Yes
435	28GC - Sec 2 - 99 #2	X			X	X	X	Yes
436	28GC - Sec 2 - 127 #1	X	X		X	X	X	Yes
437	28GC - Sec 2 - 127 #2	X	X		X	X	X	Yes
438	28GC - Sec 3 - 14 #1	X	X		X	X	X	Yes
439	28GC - Sec 3 - 14 #2	X	X		X	X	X	Yes
440	28GC - Sec 3 - 42 #1	X	X		X	X	X	Yes
441	28GC - Sec 3 - 42 #2	X	X		X	X	X	Yes
442	28GC - Sec 3 - 70 #1	X	X		X	X	X	Yes
443	28GC - Sec 3 - 70 #2	X			X	X	X	Yes
444	28GC - Sec 3 - 99 #1	X	X		X	X	X	Yes
445	28GC - Sec 3 - 99 #2	X			X	X	X	Yes
446	28GC - Sec 3 - 128 #1	X	X		X	X	X	Yes
447	28GC - Sec 3 - 128 #2	X	X		X	X	X	Yes
448	28GC - Sec 4 - 12	X	X		X	X	X	Yes
449	28GC - Sec 4 - 37	X	X		X	X	X	Yes
450	28GC - Sec 4 - 61	X			X	X	X	Yes
451	28GC - Sec 4 - 85 #1	X	X		X	X	X	Yes
452	28GC - Sec 4 - 85 #2	X			X	X	X	Yes
453	28GC - Sec 4 - 110	X	X		X	X	X	Yes
454	28GC - Sec 4 - 116	X			X	X	X	Yes
455	28GC - Sec 4 - 135	X	X		X	X	X	Yes
456	32MC - 4 - 1.5	X	X	X	X	X	X	No
457	32MC - 4 - 4	X	X	X	X		X	No
458	32MC - 4 - 10	X	X	X	X		X	No
459	32MC - 4 - 16	X	X		X			No
460	32MC - 4 - 22	X	X	X	X		X	No
461	32MC - 4 - 28	X	X	X	X		X	No
462	32MC - 4 - 32	X			X			No
463	33MC - 4 - +2	X	X	X	X		X	No
464	33MC - 4 - +2	X	X	X	X		X	No
465	33MC - 4 - 3.5	X	X	X	X	X	X	No
466	33MC - 4 - 6	X	X	X	X		X	No
467	33MC - 4 - 9	X	X	X	X	X	X	No
468	33MC - 4 - 12	X	X	X	X		X	No
469	33MC - 4 - 15	X	X	X	X		X	No
470	33GC - Sec 1 - 6	X	X	X	X	X	X	No
471	33GC - Sec 1 - 30	X	X	X	X		X	No
472	33GC - Sec 2 - 6	X	X	X	X		X	No

473	33GC - Sec 2 - 37	X	X	X	X	X	X	No
474	33GC - Sec 2 - 67	X	X	X	X	X	X	No
475	33GC - Sec 2 - 97	X	X	X	X		X	No
476	33GC - Sec 2 - 121	X	X	X	X		X	No
477	33GC - Sec 3 - 6	X	X	X	X	X	X	No
478	33GC - Sec 3 - 36	X	X	X	X		X	No
479	33GC - Sec 3 - 67	X	X	X	X		X	No
480	33GC - Sec 3 - 97	X	X	X	X	X	X	No
481	33GC - Sec 3 - 120	X			X		X	No
482	33PC - Sec 1 - 6	X	X	X	X	X	X	No
483	33PC - Sec 2 - 6	X	X	X	X		X	No
484	33PC - Sec 2 - 36	X	X	X	X	X	X	No
485	33PC - Sec 2 - 67	X	X	X	X		X	No
486	33PC - Sec 2 - 98	X	X	X	X	X	X	No
487	33PC - Sec 2 - 121	X	X	X	X		X	No
488	33PC - Sec 3 - 6	X	X	X	X		X	No
489	33PC - Sec 3 - 36	X	X	X	X	X	X	No
490	33PC - Sec 3 - 67	X	X	X	X		X	No
491	33PC - Sec 3 - 91	X	X	X	X	X	X	No
492	33PC - Sec 3 - 121	X	X	X	X	X	X	No
493	33PC - Sec 4 - 6	X	X	X	X		X	No
494	33PC - Sec 4 - 36	X	X	X	X	X	X	No
495	33PC - Sec 4 - 66	X	X	X	X		X	No
496	33PC - Sec 4 - 85	X	X	X	X	X	X	No
497	33PC - Sec 4 - 107	X	X	X	X		X	No
498	33PC - Sec 5 - 6	X	X	X	X		X	No
499	33PC - Sec 5 - 36	X	X	X	X	X	X	No
500	33PC - Sec 5 - 66	X	X	X	X		X	No
501	33PC - Sec 5 - 97	X	X	X	X	X	X	No
502	33PC - Sec 5 - 120	X	X	X	X		X	No
503	28GC - Sec 1 - 28	X	X		X	X	X	Yes
504	28GC - Sec 1 - 28	X	X		X	X	X	Yes
505	28GC - Sec 2 - 21	X	X		X	X	X	Yes
506	28GC - Sec 2 - 21	X			X	X	X	Yes
507	28GC - Sec 2 - 50	X	X		X	X	X	Yes
508	28GC - Sec 2 - 50	X			X	X	X	Yes
509	28GC - Sec 2 - 78	X			X	X	X	Yes
510	28GC - Sec 2 - 106	X	X		X	X	X	Yes
511	28GC - Sec 2 - 106	X			X	X	X	Yes
512	28GC - Sec 2 - 135	X	X		X	X	X	Yes
513	28GC - Sec 2 - 135	X			X	X	X	Yes
514	28GC - Sec 3 - 21	X	X		X	X	X	Yes
515	28GC - Sec 3 - 21	X			X	X	X	Yes
516	28GC - Sec 3 - 49	X	X		X	X	X	Yes
517	28GC - Sec 3 - 49	X			X	X	X	Yes

518	28GC - Sec 3 - 77	X	X		X	X	X	Yes
519	28GC - Sec 3 - 77	X			X	X	X	Yes
520	28GC - Sec 3 - 106	X	X		X	X	X	Yes
521	28GC - Sec 3 - 134	X	X		X	X	X	Yes
522	28GC - Sec 4 - 18	X			X	X	X	Yes
523	28GC - Sec 4 - 43	X	X		X	X	X	Yes
524	28GC - Sec 4 - 67	X	X		X	X	X	Yes
525	28GC - Sec 4 - 92	X	X		X	X	X	Yes
526	28GC - Sec 4 - 92	X			X	X	X	Yes
527	28GC - Sec 4 - 123	X	X		X	X	X	Yes
528	28GC - Sec 4 - 139	X	X		X	X	X	Yes
529	28GC - Sec 4 - 139	X			X	X	X	Yes
530	Seawater Standard	X	X		X	X	X	--
531	Field Blank	X	X					--

WP MB (Micropaleontology and Biostratigraphy)

Distribution of multicore tubes

A multicorer was used to acquire undisturbed samples across the water-sediment interface from 23 coring stations. This coring device is described in this cruise report under WP SC. The recovery in the 60 cm long multicore tubes was 23 cm. In most deployments, all eight multicore tubes were retrieved. These were assigned to different investigators and investigations (Table MB-2).

Table MB-2: *Distribution of multi core sediment tubes among investigators*

Tube	Investigator	Analysis
1	Alexandr Gukov	Macrobenthos; sieved onboard using 1 mm mesh
2	Alexandr Gukov	Macrobenthos; sieved onboard using 1 mm mesh
3	Alexandr Gukov	Macrobenthos; sieved onboard using 1 mm mesh
4	Natalia Barrientos	Benthic foraminifera geochemistry; stored in freezer container
	Tom Cronin, Laura Gemery	Ostracodes; stored in freezer
	Clint Miller	Rhizone pore water sampling onboard
5	Natalia Barrientos	Benthic foraminifera geochemistry; stored in freezer container
	Tom Cronin, Laura Gemery	Ostracodes; stored in freezer container
6	Martin Jakobsson	Biosilica; stored in freezer container
7	Tommaso Tesi	Organic matter; stored in freezer container
8	Denis Kosmach	Methane content in sediment; immediate sampling

Shipboard sampling of gravity-/kasten-/ and piston-cores

The working halves of the sediment cores were sampled using 5 and/or 10 cm^3 plastic scoops. On average, three samples from each 1.5 m long section (intervals 15-17 cm, 75-77 cm and 135-137 cm) were processed onboard to assess microfossil preservation and to target intervals with preserved microfossils. These samples were washed with ship water through a 63 µm sieve using a light-diffusive pressure stream. The washing disaggregated the soft sediment samples and collected the coarse fraction, which was rinsed and decanted from the sieve using 18.2 mΩ Milli-Q water from a squirt bottle on to labeled filter paper, then dried in the oven at ≤50°C during a minimum of five hours. After drying, the samples were transferred into 15 ml snap-cap glass vials. An overview of samples taken for micropaleontology, IP25 and geotechnical/physical properties are shown in Tables MB-3 and MB-4.

Table MB-3: *Summary of samples taken onboard (page 1/2).*

Core	Backman	*size*	Barrientos	*cc*	Cronin and Gemery	*cc*	IP25	*cc*
SWERUS-L2-1-KL1	-	-	41	*50/100*	-	-	39	*10/30*
SWERUS-L2-2-KL1	-	-	12	*30*	-	-	12	*10*
SWERUS-L2-2-PC1	21	*t-pick*	83	*20*	39	*20*	83	*5*
SWERUS-L2-4-PC1	12	*t-pick*	62	*20*	29	*20*	62	*5*
SWERUS-L2-4-TWC1	-	-	5	*20*	2	*20*	5	*5*
SWERUS-L2-5-GC1	5	*t-pick*	18	*20*	7	*20*	13	*5*
SWERUS-L2-7-GC1	9	*t-pick*	29	*20*	14	*29*	29	*5*
SWERUS-L2-8-PC1	11	*t-pick*	64	*20*	30	*20*	63	*5*
SWERUS-L2-9-GC1	6	*t-pick*	28	*20*	13	*20*	27	*5*
SWERUS-L2-10-GC1	10	*t-pick*	43	*20*	20	*20*	41	*5*
SWERUS-L2-11-GC1	8	*t-pick*	16	*20*	18	*20*	37	*5*
SWERUS-L2-12-PC1	12	*t-pick*	-	-	41	*20*	84	*5*
SWERUS-L2-13-PC1	16	*t-pick*	89	*20*	32	*20*	77	*5*
SWERUS-L2-13-TWC1	-	-	5	*5/20*	-	-	4	*5*
SWERUS-L2-14-GC1	8	*t-pick*	40	*20*	18	*20*	38	*5*
SWERUS-L2-15-GC1	6	*t-pick*	26	*20*	12	*20*	26	*5*
SWERUS-L2-16-GC1	9	*t-pick*	39	*20*	16	*20*	33	*5*
SWERUS-L2-17-PC1	6	*t-pick*	54	*20*	29	*20*	63	*5*
SWERUS-L2-17-TWC1	-	-	4	*5*	-	-	3	*5*
SWERUS-L2-18-GC1	1	*t-pick*	19	*20*	10	*20*	19	*5*
SWERUS-L2-20-GC1	-	-	4	*20*	4	*20*	7	*5*
SWERUS-L2-22-PC1	-	-	63	*5/20*	30	*20*	65	*5*
SWERUS-L2-22-TWC1	-	-	10	*5/20*	-	*20*	5	*5*
SWERUS-L2-23-GC1	-	-	43	*20*	19	*20*	41	*5*
SWERUS-L2-24-GC1	-	-	42	*20*	18	*20*	40	*5*
SWERUS-L2-26-PC1	-	-	25	*20*	12	*20*	25	*5*
SWERUS-L2-28-GC1	-	-	57	*20*	29	*20*	53	*5*
SWERUS-L2-29-GC1	-	-	50	*20*	20	*20*	46	*5*
SWERUS-L2-31-PC1	-	-	81	*5/20*	37	*20*	81	*5*
SWERUS-L2-31-TWC1	-	-	5	*20*	2	*20*	5	*5*
SWERUS-L2-32-GC2	-	-	27	*20*	12	*20*	26	*5*
SWERUS-L2-33-GC1	-	-	-	-	-	-	-	-
SWERUS-L2-33-GC1	-	-	-	-	-	-	-	-
SWERUS-L2-33-PC1	-	-	59	*20*	30	*20*	65	*5*
SWERUS-L2-33-TWC1	-	-	4	*20*	1	*20*	3	*5*

Continuation of Table MB-3.

Core	O'Regan	*cc*	pH experim.	*cc*	Geotechnical whole rounds
SWERUS-L2-1-KL1	-	-	-	-	(station-type-section, cm)
SWERUS-L2-2-KL1	-	-	-	-	-
SWERUS-L2-2-PC1	12	*20*	-	-	-
SWERUS-L2-4-PC1	10	*20*	-	-	5-PC1-5, 139-150 cm
SWERUS-L2-4-TWC1	1	*20*	-	-	-
SWERUS-L2-5-GC1	3	*20*	-	-	5-GC1-CC, 0-10 cm + 18-25 cm
SWERUS-L2-7-GC1	4	*20*	-	-	-
SWERUS-L2-8-PC1	8	*20*	-	-	8-PC1-5, 140-150 cm
SWERUS-L2-9-GC1	4	*20*	-	-	-
SWERUS-L2-10-GC1	6	*20*	-	-	10-GC1-3, 143-153 cm
SWERUS-L2-11-GC1	5	*20*	-	-	11-GC1-3, 143-153 cm
SWERUS-L2-12-PC1	12	*20*	-	-	-
SWERUS-L2-13-PC1	10	*20*	-	-	-
SWERUS-L2-13-TWC1	-	-	-	-	-
SWERUS-L2-14-GC1	6	*20*	4	*5*	-
SWERUS-L2-15-GC1	4	*20*	-	-	15-GC1-2, 135-150 cm
SWERUS-L2-16-GC1	5	*20*	2	*5*	16-GC1-3, 135-151 cm
SWERUS-L2-17-PC1	11	*20*	2	*5*	-
SWERUS-L2-17-TWC1	-	-	-	-	-
SWERUS-L2-18-GC1	3	*20*	-	-	-
SWERUS-L2-20-GC1	-	-	-	-	20-GC1-1, 42-52 cm
SWERUS-L2-22-PC1	9	*20*	-	-	-
SWERUS-L2-22-TWC1	-	*20*	-	-	-
SWERUS-L2-23-GC1	6	*20*	-	-	-
SWERUS-L2-24-GC1	-	-	-	-	24-GC1-3, 135-150 cm
SWERUS-L2-26-PC1	-	-	-	-	-
SWERUS-L2-28-GC1	-	-	-	-	-
SWERUS-L2-29-GC1	-	-	-	-	-
SWERUS-L2-31-PC1	-	-	-	-	-
SWERUS-L2-31-TWC1	-	-	-	-	-
SWERUS-L2-32-GC2	-	-	-	-	-
SWERUS-L2-33-GC1	-	-	-	-	33-GC1-2, 136-151 cm
SWERUS-L2-33-GC1	-	-	-	-	33-GC1-3, 135-150 cm
SWERUS-L2-33-PC1	-	-	-	-	-
SWERUS-L2-33-TWC1	-	-	-	-	-

Lithostratigraphy

After logging in the multi sensor core logger and splitting the cores into Archive and Work halves, the lithostratigraphy of the Working half of each core was described through visual inspection. Core

descriptions are presented in Appendix MB-1. Emphasis was placed on sediment color using the standard Munsell color scheme, texture, grain size, structures (laminations, lenses etc.), the nature of contacts between lithologic units (ie., sharp, gradational), and identification of specific features such as ice-rafted dropstones and macro-invertebrate remains (ie., mollusc shells). No attempt was made onboard to apply lithostratigraphic schemes used by various authors on sediments from central Arctic Ocean areas. Efforts are planned to integrate the visual descriptions with the physical property and micropaleontological data for improved correlation with sediments from other regions.

Calcareous nannofossils

Calcareous nannofossils are remains of tiny phytoplankton organisms (1-30 µm) that evolved in marine environments during the late Triassic. They can be divided in nannoliths, calcareous elements that have an unknown origin, for example discoasters, and coccoliths, elements produced by haptophyte single-celled algae (coccolithophorids). Coccolithophorids are autotrophic organism containing chloroplasts for photosynthesis and represent an important group of phytoplankton in being a major contributor to deep sea calcareous sediments. Coccolithophorids occur in astronomical numbers in the ice free ocean areas of the low to high middle latitudes, often reaching several tens of millions of specimens per gram sediment. Members of this group are much less abundant in Arctic Ocean sediments, as they do not thrive and reproduce under thick sea ice covers. They do occur in central Arctic Ocean sediments, however, over the nearest few glacial/interglacial cycles, and then chiefly during interglacial and/or interstadial conditions. When occurring, they provide useful biostratigraphic information. The general lack of calcareous nannofossils in sediments older than MIS 7 is considered to reflect preservational problems rather of calcite in the Arctic Ocean sediment. They are brought in via Atlantic waters, and Pacific waters during times when the shallow Bering Strait has been an open seaway. The stratigraphic and geographic distribution of calcareous nannofossils in the SWERUS Leg 2 sediments will be pursued as shore-based studies.

Foraminifera

Arctic sediments contain three groups of foraminifera (*Protista*) that have been used in paleoceanography and biostratigraphy. The general occurrence of foraminifera in SWERUS cores is given in Table MB-4 based on preliminary examination of the >63 µm size fraction (future studies of <63 µm foraminifera may be carried out).

The first group includes planktic foraminifera, which are planktonic in habitat and live at or below the Arctic surface layers, including within and below sea ice. Planktic foraminiferal assemblages and shell chemistry (mainly oxygen and carbon isotopes and magnesium/calcium ratios) have been used extensively in studies of Arctic sediment cores. In SWERUS Leg 2 sediments, the predominant planktic foraminiferal species found in most cores taken on the continental slope and Arctic submarine ridges was *Neogloboquadrina pachyderma* sinistral (left coiling of chambers). Planktic foraminifera are rare to absent in cores from the continental shelves. Some specimens of *N. pachyderma* dextral (right coiling, also called *N. incompta*) were also encountered but no quantitative faunal analyses were conducted onboard. *N. pachyderma* is typically the dominant species in Quaternary deposits of the Arctic Ocean. *N. pachyderma* shells will be used for radiocarbon analyses in several cores.

The second major foraminiferal group includes benthic calcareous ($CaCO_3$) foraminifera, which has been used extensively in the Arctic Ocean to reconstruct paleoenvironmental conditions, changes in water masses and ocean circulation, sea level, sea-ice cover, biological productivity, and salinity. Benthic foraminifera were found in most cores from continental shelf and slope regions and submarine ridges. Although no quantitative analyses of benthic assemblages was performed onboard, it should be noted that the dominant taxa in cores from the continental shelves were *Elphidium*, *Haynesina*, *Buccella*, *Nonionella*, *Cassidulina reniforme*, and various miliolid genera (*Quinqueloculina*, *Triloculina*, *Pyrgo*). Cores from continental slope regions located in the path of Atlantic Water contained common *Islandiella teretis* and related forms considered distinct species by some foraminiferal experts (i.e., *I. norcrossi, Cassidulina neoteretis*). At deeper sites (>700 m), the deeper water species *Oridorsalis tener* (*O. unbonatus* of some authors) was found. This species has biostratigraphic importance as it is a dominant species in assemblages younger than Marine Isotope Stage 5 at many sites in the western Arctic. The age significance and applicability of the shell chemistry of *I. teretis* and *O. tener* to paleoceanography in SWERUS cores will be addressed in future studies. The important deep-sea species *Cibicidoides wuellerstorfi* (assigned to the genus *Fontbotia* by some authors) was found in low numbers in three cores.

The third group of foraminifera includes a variety of agglutinated species characteristic of the continental shelf and slope. In contrast to calcareous species, which secrete their shells from ocean water, agglutinated foraminifera build their tests out of sediment material usually cemented together. Some commonly encountered genera included *Cyclammina, Cyclogyra, Recurvoides, Trochammina*, among many others. In some samples that contain rich agglutinated foraminiferal assemblages, it is possible there has been post-depositional, selective dissolution of the calcareous species. Foraminiferal dissolution, a major issue in terms of shell preservation in Arctic sediments, is being addressed in studies of sediment pH and foraminiferal preservation in selected cores.

Table MB-4: *Distribution of foraminifers in samples processed onboard.*

Station-Core type-Section, cm	WD (m)	*Neogloboquadrina pachyderma*	*Oridorsalis tener*	*Islandiella teretis*	*Cassidulina reniforme*	*Elphidium* spp.	*Cibicidoides wuellerstorfi*	*Quinqueloculina arctica*	*Pyrgo* spp.	*Miliolinella* spp.	*Nonionella* spp.	*Buccella* spp.	Agglutinated foraminifera
2-PC1-1, 15-17 cm	72					X					X	X	X
2-PC1-1, 75-77 cm	72					X					X	X	X
2-PC1-2, 15-17 cm	72					X					X	X	X
2-PC1-2, 75-77 cm	72					X					X	X	X
2-PC1-2, 135-137 cm	72					X					X	X	X
2-PC1-3, 15-17 cm	72					X					X	X	X

2-PC1-3, 75-77 cm	72				X			X	X	X
2-PC1-3, 135-137 cm	72				X			X	X	X
2-PC1-4, 15-17 cm	72				X			X	X	X
2-PC1-4, 75-77 cm	72				X					
2-PC1-4, 135-137 cm	72				X					
2-PC1-5, 15-17 cm	72				X					
2-PC1-5, 75-77 cm	72				X			X	X	X
2-PC1-6, 15-17 cm	72				X			X	X	X
2-PC1-6, 75-77 cm	72				X					
2-PC1-6, 135-137 cm	72									
2-KL1, 0-2 cm	71			X	X			X	X	X
4-PC1-1, 15-17 cm	120		X	X	X		X		X	X
4-PC1-2, 15-17 cm	120		X	X	X		X		X	X
4-PC1-2, 75-77 cm	120		X	X	X		X		X	X
4-PC1-2, 135-137 cm	120		X	X	X		X		X	X
4-PC1-3, 15-17 cm	120		X	X	X		X		X	X
4-PC1-3, 75-77 cm	120		X	X	X		X		X	X
4-PC1-3, 135-137 cm	120		X	X	X		X		X	X
4-PC1-4, 15-17 cm	120		X	X	X		X		X	X
4-PC1-4, 75-77 cm	120		X	X	X		X		X	X
4-PC1-5, 15-17 cm	120		X	X	X		X		X	X
4-PC1-5 75-77 cm	120		X	X	X		X		X	X
4-PC1-5, 135-137 cm	120									
5-GC1-1, 15-17 cm	116				X			X		X
5-GC1-1, 75-77 cm	116				X			X		X
5-GC1-CC, 29-30 cm	116				X					X
6-GC1-CC	353				X					X
7-GC1-1, 15-17 cm	392									
7-GC1-1, 75-77 cm	392		X							
7-GC1-1, 135-137 cm	392	X		X						X
7-GC1-2, 15-17 cm	392	X								
7-GC1-2, 75-77 cm	392									X
8-PC1-1, 10-12 cm	515				X					X
8-PC1-1, 30-32 cm	515		X							X
8-PC1-1, 50-52 cm	515									
8-PC1-2, 100-102 cm	515									X
8-PC1-2, 130-132 cm	515									
8-PC1-3, 70-72 cm	515									
8-PC1-4, 20-22 cm	515									
8-PC1-4, 80-82 cm	515									
8-PC1-5, 50-52 cm	515									X

8-PC1-5, 70-72 cm	515			
8-PC1-5, 130-132 cm	515			X
8-GC-CC	555			X
9-GC1-1, 5-7 cm	475			X
9-GC1-1,15-17 cm	475			
9-GC1-1, 35-37 cm	475			
9-GC1-1, 75-77 cm	475			X
9-GC1-2,15-17 cm	475			
9-GC1-2,35-37 cm	475			
9-GC1-2, 40-42 cm	475			X
9-GC1-2, 75-77 cm	475			
9-GC1-2, 135-137 cm	475			
10-GC1-1, 15-17 cm	1000	X		X
10-GC1-1, 15-17 cm	1000			
10-GC1-1, 35-37 cm	1000			
10-GC1-1, 75-77 cm	1000			X
10-GC1-2, 15-17 cm	1000			
10-GC1-2, 75-77 cm	1000			
10-GC1-2, 135-137 cm	1000			
10-GC1-3, 15-17 cm	1000			
10-GC1-3, 75-77 cm	1000			
10-GC1-3, 95-97 cm	1000			
10-GC1-3, 115-117 cm	1000			X
10-GC1-3, 135-137 cm	1000			
10-GC1-CC, 8-10 cm	1000			
10-GC1-CC, 15-17 cm	1000			
10-GC1-CC, 18-20 cm	1000			
11-GC1-1, 15-17 cm	1018			X
11-GC1-1, 75-77 cm	1018			
11-GC1-2, 15-17 cm	1018			
11-GC1-2, 75-77 cm	1018			
11-GC1-2, 135-137 cm	1018			
11-GC1-3, 15-17 cm	1018			
11-GC1-3, 75-77 cm	1018			
11-GC1-3, 135-137 cm	1018			
12-PC1-1, 0-2 cm	384			X
12-PC1-1, 15-17 cm	384			X
12-PC1-1, 75-77 cm	384			
12-PC1-3, 75-77 cm	384			
12-PC1-4, 75-77 cm	384			
12-PC1-5, 75-77 cm	384			

12-PC1-6, 75-77 cm	384								
12-PC1-CC, 5-7 cm	384								
13-PC1-1, 15-17 cm	1119	X	X	X		X			X
13-PC1-2, 15-17 cm	1119								
13-PC1-2, 75-77 cm	1119	X							X
13-PC1-2, 135-137 cm	1119	X							X
13-PC1-3, 0-2 cm	1119								
13-PC1-3, 10-12 cm	1119								
13-PC1-3, 20-22 cm	1119	X							
13-PC1-3, 30-32 cm	1119	X		X					X
13-PC1-3, 40-42 cm	1119								X
13-PC1-3, 50-52 cm	1119	X			X				X
13-PC1-3, 60-61 cm	1119	X							
13-PC1-3, 65-66 cm	1119	X	X	X					X
13-PC1-3, 70-71 cm	1119	X	X		X	X			X
13-PC1-3, 75-76 cm	1119	X	X		X				X
13-PC1-3, 80-81 cm	1119								X
13-PC1-3, 85-86 cm	1119								X
13-PC1-3, 90-91 cm	1119								X
13-PC1-3, 95-96 cm	1119								X
13-PC1-3, 100-101 cm	1119								X
13-PC1-3, 105-106 cm	1119								
13-PC1-3, 110-111 cm	1119								
13-PC1-3, 115-116 cm	1119								
13-PC1-3, 120-121 cm	1119								
13-PC1-3, 125-126 cm	1119								
13-PC1-3, 130-131 cm	1119								
13-PC1-3, 140-142 cm	1119								
13-PC1-4, 15-17 cm	1119								
13-PC1-4, 75-77 cm	1119								
13-PC1-4, 135-137 cm	1119								
13-PC1-5, 15-17 cm	1119								
13-PC1-5, 75-77 cm	1119								
13-PC1-6, 15-17 cm	1119								
13-PC1-6, 75-77 cm	1119								
13-PC1-6, 135-137 cm	1119								
13-GC1-CC	1109	X							X
14-GC1-1, 5-6 cm	737								X
14-GC1-1, 15-17 cm	737	X							X
14-GC1-1, 75-77 cm	737	X							
14-GC1-2, 5-6 cm	737	X							

14-GC1-2, 15-17 cm	737	X								X
14-GC1-2, 75-77 cm	737	X	X							
14-GC1-2, 135-137 cm	737	X								X
14-GC1-2, 138-139 cm	737									X
14-GC1-3, 15-17 cm	737									
14-GC1-3, 75-77 cm	737									
14-GC1-3, 78-79 cm	737									
14-GC1-3, 135-137 cm	737	X								X
15-GC1-1, 15-17 cm	504	X								X
15-GC1-1, 75-77 cm	504									X
15-GC1-2, 15-17 cm	504									X
15-GC1-2, 35-37 cm	504									X
15-GC1-2, 55-57 cm	504									X
15-GC1-2, 75-77 cm	504									
16-GC1-1, 14-15 cm	991	X	X	X	X	X	X	X		X
16-GC1-1, 15-17 cm	991	X	X	X	X	X	X	X		X
16-GC1-2, 15-17 cm	991	X								X
16-GC1-2, 75-77 cm	991									X
16-GC1-2, 130-131 cm	991									
16-GC1-2, 135-137 cm	991									X
16-GC1-3, 15-17 cm	991	X								
16-GC1-3, 75-77 cm	991									
17-PC1-1, 0-1 cm	997	X					X			X
17-PC1-1, 15-17 cm	997	X			X			X		X
17-PC1-2, 15-17 cm	997	X								X
17-PC1-2, 75-77 cm	997	X	X	X						
17-PC1-2, 135-137 cm	997									X
18-GC1-1, 15-17 cm	351	X		X	X			X		X
18-GC1-1, 75-77 cm	351	X		X	X			X		X
18-GC1-2, 15-17 cm	351	X								X
18-GC1-2, 75-77 cm	351									X
18-GC1-2, 135-137 cm	351	X								X
18-GC1-CC, 15-17 cm	351	X								X
18-GC2-CC	340	X								X
20-GC1-CC	115	X		X	X	X			X	X
22-GC1-CC	368	X								X
22-PC1-1, 15-17 cm	364	X	X	X	X					X
23-GC1, ~100cm	508	X	X							X
24-GC1-1, 15-17 cm	964	X	X							X
29-TWC1-CC	899	X	X	X		X		X		X
29-GC1-1, 15-17 cm	824	X	X	X	X	X		X		X

29-GC1-CC	899	X	X	X	X	X		X
31-PC1, 15-17 cm	1120	X						X
32-GC1-1, 15-17 cm	834	X		X		X		X
32-GC2-1, 15-17 cm	828	X		X		X		
32-GC2-1, 75-77 cm	828							
32-GC2-2, 15-17 cm	828	X		X		X		
32-GC2-2, 75-77 cm	828							
32-GC2-2, 135-137 cm	828							
33-TWC, 15-17 cm	888	X		X		X	X	X
33-TWC-CC	888	X		X		X	X	X
33-PC1-1, 15-17 cm	888	X		X		X	X	X
33-PC1-2, 15-17 cm	888							

Ostracodes

Ostracodes are small *Crustacea* many of which secrete calcium carbonate ($CaCO_3$) bivalved shells commonly preserved in marine sediments. Most Arctic ostracodes species are constituents of benthic meiofaunal communities and, as such, are often used in conjunction with benthic foraminifera to reconstruct paleoenvironmental changes in ocean circulation, bottom temperature, salinity and other factors. One species, *Acetabulastoma arcticum*, lives as an epipelagic parasite on the sub-sea ice dwelling amphipod *Gammarus*, and it is used in sediment studies as a proxy for past changes in perennial sea ice cover.

Preliminary analyses of surface sediment and fossil ostracodes from SWERUS sediment cores yielded more than 25 species, each with distinct habitat preferences. We identified species that today dominate shallow, nearshore inner continental shelves, continental slopes and central Arctic ridges. Several species that are key indicators of lower salinity in nearshore brackish environments signify periods of lower global sea level. Other species recovered in SWERUS cores are indicators of distinct Arctic Ocean water masses (such as Atlantic Water), perennial sea ice cover, and elevated biological productivity. Shells of shallow water species found in central Arctic Ocean sediments often indicate shelf to basin transport by sea ice.

In addition to their application to paleoenvironmental reconstruction based on species' ecology, several ostracodes have been used in paleoceanographic reconstruction based on the chemical composition of their shells. Ostracode shell chemistry applications include stable isotopes (oxygen, carbon), minor element composition (magnesium/calcium, strontium/calcium ratios), and potentially boron isotopes. They can also be used for radiocarbon dating if shells are abundant. Shore-based shell chemistry studies are planned in conjunction with assemblage analyses and foraminiferal studies.

An overview of the stratigraphic distribution of ostracode taxa observed in SWERUS Leg 2 sediments is presented in Table MB-5.

Macrobenthos

At each of the 22 multicoring stations completed during Leg 2, three multicore tubes were assigned for macrobenthos analysis. The sediment from these three multi cores was mixed in an integral sample that represents a seafloor surface of 210 cm^2. The sediment was washed through 1mm sieves using sea water. Large echinodermats, bivalve and crustacean specimens (2-10 cm) were found at

the following coring stations (prefix SWERUS-L2 is omitted): 1-MC1, 2-MC1, 4-MC1, 8-MC1, 14-MC1, 15-MC1, 21-MC1, 22-MC1, 23-MC1, 24-MC1 and 25-MC1. The benthic organisms were soaked in 70% ethanol for conservation of their soft parts. They will be used for isotope analysis and to estimate macrobenthos abundance, diversity and biomass of macrobenthos in bottom biocenis (g/m^2) using the methods described in Gukov (1989). Filming of the bottom surface at some of the multicoring stations supported the analyses of the bottom habitat (Figs. MB-1). Figure MB-2 shows one example of a polychaets (worm) found in 34-MC1 retrieved from the Lomonosov Ridge.

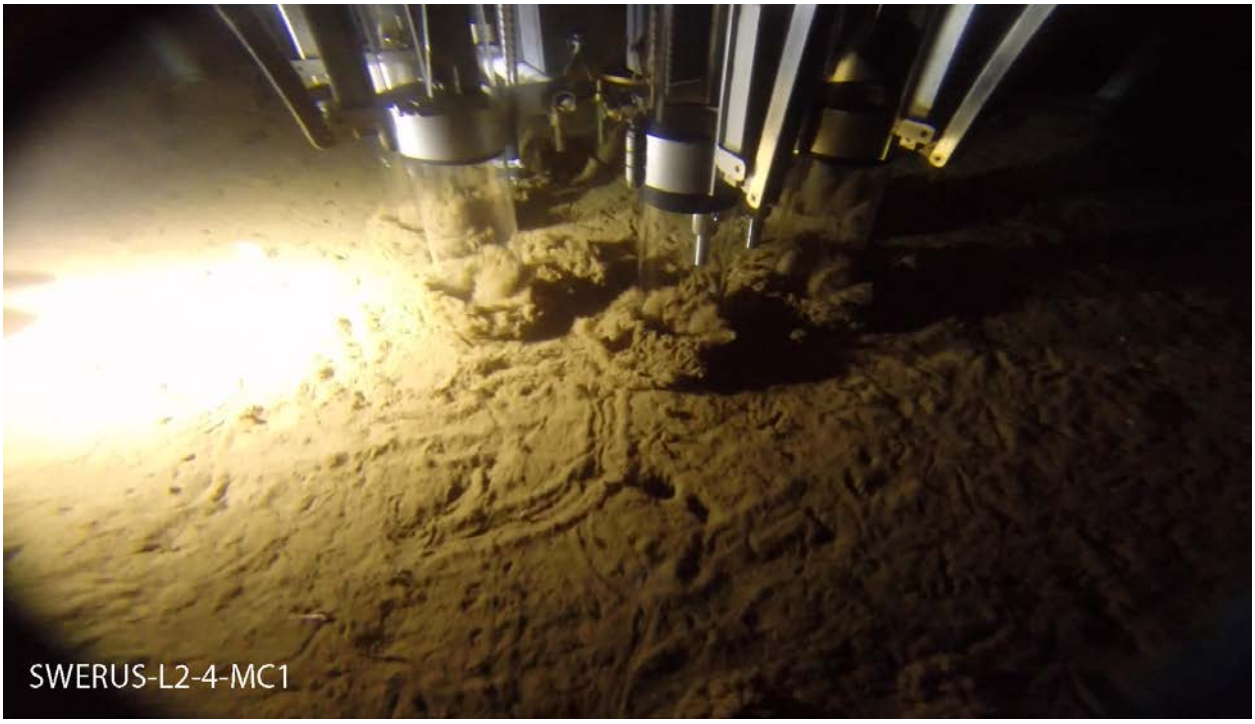

Figure MB-1: *Snapshot from filming the multicorer impact at station SWERUS-L2-MC1. Note the crawl marks from bottom living organisms.*

Figure MB-2: *Polychaets that formed the housing from particles and shells fragments including foraminifera. This was found in multicorer 34-MC1 on the Lomonosov Ridge.*

Table MB-5: Preliminary ostracode identifications SWERUS Leg 2 (L. Gemery & T. M. Cronin). Note: Species listed for each core do not necessarily occur in the same samples or stratigraphic units. Note: Cores not listed did not yield ostracodes in preliminary inspections.

General region	Core ID	Latitude	Longitude	Water Depth (m)	Comment	Acanthocythereis dunelmensis	Acetabulastoma arcticum	Argilloecia spp.	Bythocythere sp.	Bythoceratina scaberrima	Cluthia cluthae	Cytheromopha macchensneyi	Cytheropteron arcuatum	Cytheropteron biconvexa	Cytheropteron champlainium	Cytheropteron elaeni	Cytheropteron sulense	Cytheropteron suzdalskyi	Cytheropteron spp.	Elofsonella concinna	Heterocyprideis sorbayana	Jonesia acuminata	Kotoracythere arctoborealis	Krithe glacialis	Krithe minima	Munseyella arctica	Normanicythere leioderma	Palmenella limacola	Paracytherois sp.	Paracyprideis pseudopunctillata	Paradoxastoma	Pedicythere neofluitans	Polycope spp.	Propontocypris	Rabilimus mirabilis	Robertsonites tuberculatus	Sarsicytheridea bradii	Sarsicytheridea puntillata	Semicytherura complanata	Semicytherura mainensis	Sainocythere	Other
Herald Trough	**SWERUS-L2-1-KL1**	72.337483	-176.439009	73.4							X												X																			
Herald Trough	**SWERUS-L2-2-MC1**	72.4317	-175.3415	55.7		X																																			
Herald Trough	**SWERUS-L2-2-PC1**	72.51658	-175.319605	71.7	detailed shipboard study	X		x			x				x	x		x		x	x	x	x				x	x		x	x				x	x		x	x		
Herald Trough	**SWERUS-L2-2-KL1**	72.5668	-175.2651	71.4		X												X																							
Herald Trough	**SWERUS-L2-3-MC1**	72.3771	-175.7880	89.6		X													X																						
Herald Trough	**SWERUS-L2-4-PC1**	72.8387	-175.7271	120		X						X	X	X			X		X			X	X							X					X			X	X		
Herald Trough	**SWERUS-L2-5-GC1**	72.8699	-176.2074	116																																	X					
S Mendeleev Ridge [slope]	**SWERUS-L2-6-GC1**	74.9651	179.7909	353																																		X				
E Siberian Sea Slope	**SWERUS-L2-16-GC1**	76.502192	176.648144	991															X					X																		
E Siberian Sea Slope	**SWERUS-L2-17-PC1**	76.464618	176.723823	977															X					X										X								
E Siberian Sea Slope	**SWERUS-L2-17-TWC1**	76.464618	176.723823	977																																						
E Siberian Sea Slope	**SWERUS-L2-18-GC1**	76.41159	173.7862	351																																						
E Siberian Sea Slope	**SWERUS-L2-20-GC1**	77.359052	163.033304	115															X		X															X			X	X		
E Siberian Sea Slope	**SWERUS-L2-22-PC1**	78.222926	164.461842	364																															X		X					
E Siberian Sea Slope	**SWERUS-L2-23-GC1**	78.660932	165.015603	508					X	X									X					X									X		X						X	
E Siberian Sea Slope	**SWERUS-L2-24-GC1**	78.796922	165.36653	964															X					X										X								
S Lomonosov Ridge	**SWERUS-L2-29-GC1**	81.299356	141.78255	824	More spp present		X												X					X									X								
S Lomonosov Ridge	**SWERUS-L2-31-PC1**	79.914841	143.233458	1120	More spp present														X					X											X							
S Lomonosov Ridge	**SWERUS-L2-31-MC1**	79.920391	143.16475	1157	More spp present														X					X																		
Lomonosov Ridge	**SWERUS-L2-32-GC2**	85.152613	151.664309	828	More spp present														X					X	X				X						X							X
Lomonosov Ridge	**SWERUS-L2-33-PC1**	84.282038	148.646753	888	More spp present														X					X																		X
Lomonosov Ridge	**SWERUS-L2-33-TWC1**	84.282038	148.646753	888	More spp present														X					X																		

Radiocarbon sampling

Twenty samples containing specimens of shells of different mollusk species, or the planktic foraminifera species *Neogloboquadrina pachyderma*, or mixed benthic foraminifera species were picked for radiocarbon analysis (Table MB-6). The taxonomy of the mollusk shells was provided by Alexander Gukov. Sample ID refer to: SWERUS-Leg 2-Station number-Core type+number of this type at single stations-Section number, cm depths. sp.=indentified at the genus level. CC=Core Catcher.

Table MB-6: *Samples selected for radiocarbon (^{14}C) dating.*

Sample ID	Shell type
SWERUS-L2-2-KL1, 0 - 2 cm	One shell: *Astarte crenata*?
SWERUS-L2-2-PC1-1, 134-136 cm	One shell: *Macoma* sp.
SWERUS-L2-2-PC1-4, 50-52 cm	Shell fragments: *Portlandia fraterna*?
SWERUS-L2-2-PC1-5, 40-42 cm	Shell fragments: *Yoldia* sp.
SWERUS-L2-2-PC1-5, 100-101 cm	Three shells: *Yoldia amigdalea hyperborea, Astarte borealis* and *Macoma calcarea*
SWERUS-L2-2-PC1-5, 100-102 cm	Shell fragments: unidentifiable bivalve species
SWERUS-L2-2-PC1-6, 23-24 cm	One shell: *Macoma* sp.
SWERUS-L2-2-PC1-6, 86-87 cm	One shell: *Macoma* sp.
SWERUS-L2-4-PC1-1, 15-17 cm	Two shells: *Nuculana pernula*
SWERUS-L2-4-PC1-2, 141-142 cm	Shell fragments: *Yoldia amigdalea hyperborea*
SWERUS-L2-4-PC1-5, 10-12 cm	Shell fragments: *Yoldia amigdalea hyperborea*
SWERUS-L2-13-PC1-3, 65-66 cm	Planktic foraminifera shells: *Neogloboquadrina pachyderma*
SWERUS-L2-13-PC1-3, 70-71 cm	Planktic foraminifera shells: *Neogloboquadrina pachyderma*
SWERUS-L2-20-GC1-CC, 2-4 cm	Benthic foraminifera shells: *Elphidium* spp.
SWERUS-L2-20-GC1-CC, 20-22 cm	Shell fragments: *Arctinula groenlandica*
SWERUS-L2-20-GC1-CC, 27-29 cm	One shell fragment: *Macoma* sp.?
SWERUS-L2-20-GC1-CC	Shell fragments: *Portlandia fraterna*?
SWERUS-L2-29-TWC-CC	Planktic foraminifera shells: *Neogloboquadrina pachyderma*
SWERUS-L2-29-TWC-CC	Shell fragments: *Yoldia* sp.
SWERUS-L2-29-PC1-CC	Planktic foraminifera shells: *Neogloboquadrina pachyderma*

pH measurements

There is some concern that calcareous microfossils may dissolve in the sediment over time due to changes in pH and thus bias micropaleontological studies. A preliminary study of pH changes in a few selected SWERUS Leg 2 sediment cores was pursued to address this issue. Two different approaches were used. In five whole round cores, 9 mm holes were drilled through the liner and 2-5 pH electrodes inserted for measurements every 10 minutes over 19-72 hours. In some of these cores, pore water was also sampled for alkalinity measurement. In seven split cores, pH was measured once, at depths subsequently sampled, processed and examined for microfossils. This will be repeated in a month or two, with new measurements and sampling at the same depths, to assess the microfossil preservation. An overview of the measurements is presented in Table MB-7.

Table MB-7. *Overview of shipboard measurements of sediment pH change over time.*

Sample ID	Initial pH	Final pH	Duration	Date (init. pH)	Foram sample	Comment
4-TWC1, 9 cm	7.44	7.30	24 h	2014-08-25	-	Whole round, horizontal
4-TWC1, 25 cm	7.61	7.36	24 h	2014-08-25	-	Whole round, horizontal
4-TWC1, 41 cm	7.62	7.44	24 h	2014-08-25	-	Whole round, horizontal
13-TWC1, 7 cm	7.42	7.19	24 h	2014-09-02	-	Whole round, horizontal
13-TWC1, 7 cm	7.29	7.11	24 h	2014-09-02	-	Whole round, horizontal
13-TWC1, 7 cm	7.16	6.98	24 h	2014-09-02	-	Whole round, horizontal
14-GC1-1, 5.5 cm	7.25	-	-	2014-09-06	Yes	Split core
14-GC1-2, 5.5 cm	7.05	-	-	2014-09-06	Yes	Split core
14-GC1-2, 138.5 cm	7.11	-	-	2014-09-06	Yes	Split core
14-GC1-3, 78.5 cm	6.98	-	-	2014-09-06	Yes	Split core
16-GC1-1, 14.5 cm	7.44	-	-	2014-09-07	Yes	Split core
17-PC1-1, 0.5 cm	7.36	-	-	2014-09-08	Yes	Split core
17-PC1-2, 130.5 cm	7.14	-	-	2014-09-08	Yes	Split core
17-TWC1, 6.5 cm	7.44	7.31	72 h	2014-09-04	-	Whole round, vertical
17-TWC1, 19 cm	7.29	7.18	72 h	2014-09-04	-	Whole round vertical
22-TWC1, 20.5 cm	7.08	7.03	19 h	2014-09-08	Yes	Whole round, horizontal
22-TWC1, 39.5 cm	6.94	6.85	19 h	2014-09-08	Yes	Whole round, horizontal
26-TWC1, 2 cm	7.12	-	-	2014-09-20	Yes	Split core
26-TWC1, 11 cm	7.02	-	-	2014-09-20	Yes	Split core
26-TWC1, 21 cm	6.96	-	-	2014-09-20	Yes	Split core
26-TWC1, 31 cm	6.84	-	-	2014-09-20	Yes	Split core
26-TWC1, 41 cm	6.95	-	-	2014-09-20	Yes	Split core
31-TWC1, 6 cm	7.03	-	-	2014-09-19	Yes	Split core
31-TWC1, 11 cm	6.91	-	-	2014-09-19	Yes	Split core
31-TWC1, 21 cm	6.90	-	-	2014-09-19	Yes	Split core
31-TWC1, 31 cm	7.01	-	-	2014-09-19	Yes	Split core
31-TWC1, 41 cm	7.23	-	-	2014-09-19	Yes	Split core
33-PC1-1, 20 cm	7.79	7.60	24 h	2014-09-21	-	Whole round, horizontal
33-PC1-2, 20 cm	7.71	7.33	24 h	2014-09-21	-	Whole round, horizontal
33-PC1-3, 20 cm	6.44	7.39	24 h	2014-09-21	-	Whole round, horizontal (pH unstable)
33-PC1-4, 20 cm	7.39	7.14	24 h	2014-09-21	-	Whole round, horizontal
33-PC1-5, 20 cm	7.19	7.01	24 h	2014-09-21	-	Whole round, horizontal
33-PC1-1, 2 cm	7.58	-	-	2014-09-23	Yes	Split core

33-PC1-1, 11 cm	7.59	-	-	2014-09-23	Yes	Split core
33-PC1-1, 21 cm	7.55	-	-	2014-09-23	Yes	Split core
33-PC1-1, 31 cm	7.52	-	-	2014-09-23	Yes	Split core
33-PC1-2, 2 cm	7.45	-	-	2014-09-23	Yes	Split core
33-PC1-3, 21 cm	7.30	-	-	2014-09-23	Yes	Split core
33-PC1-4, 21 cm	7.12	-	-	2014-09-23	Yes	Split core
33-PC1-5, 21 cm	6.96	-	-	2014-09-23	Yes	Split core
33-TWC1, 4 cm	7.44	-	-	2014-09-23	Yes	Split core
33-TWC1, 11 cm	7.56	-	-	2014-09-23	Yes	Split core
33-TWC1, 21 cm	7.56	-	-	2014-09-23	Yes	Split core
33-TWC1, 31 cm	7.53	-	-	2014-09-23	Yes	Split core

WP CO (Chemical Oceanography)

All data of this WP were separated into data acquired within the Russian Exclusive Economic Zone and outside. This was done in order to be able to fulfil conditions outline in the Russian research permit. Stations were water was collected are shown in figure CO1, and the constituents determined or collected for later determination ashore are given in appendix CO1.

In total water from 52 stations were collected (see Figure CO1 for locations) and a total of more than 800 samples were analysed for many of the constituents of this WP.

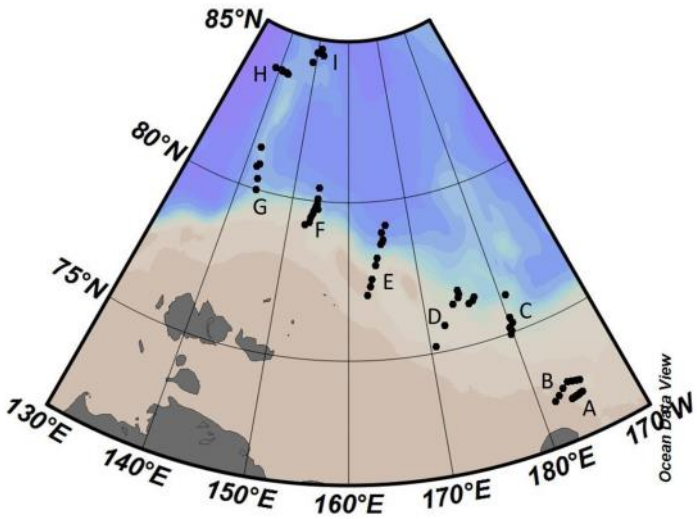

Figure CO1. Map with stations at which water samples were collected. Noted are sections of stations for which specific data are illustrated.

Inorganic carbon, oxygen, and nutrients (DIC, TA, pH,O_2, N, P, Si)

The interaction between the shelf and the deep basin is clearly seen in the sections at the shelf break. In the section G the only specific chemical signature deriving from the shelf is elevated silicate concentrations in the surface waters (Fig. CO2 a), likely a reminiscence of runoff that has mixed into the upper water column. The oxygen (here represented by Apparent Oxygen Utilization, AOU) and fCO_2 property illustrate that photosynthesis is negligible in the surface water but that there is a small sub-surface signature of organic matter decay at around 50 m depth (Fig. CO2, b,c). On the contrary there are strong signals of shelf basin exchange at the section D (Fig. CO2, d-f). Starting at the bottom of the shelf and going down to some 200 meters depth there are clear signature of organic matter decay, i.e. high AOU, SiO_2 and fCO_2. This signal weakens when moving away from the shelf, pointing to mixing with surrounding waters when spreading into the deep parts

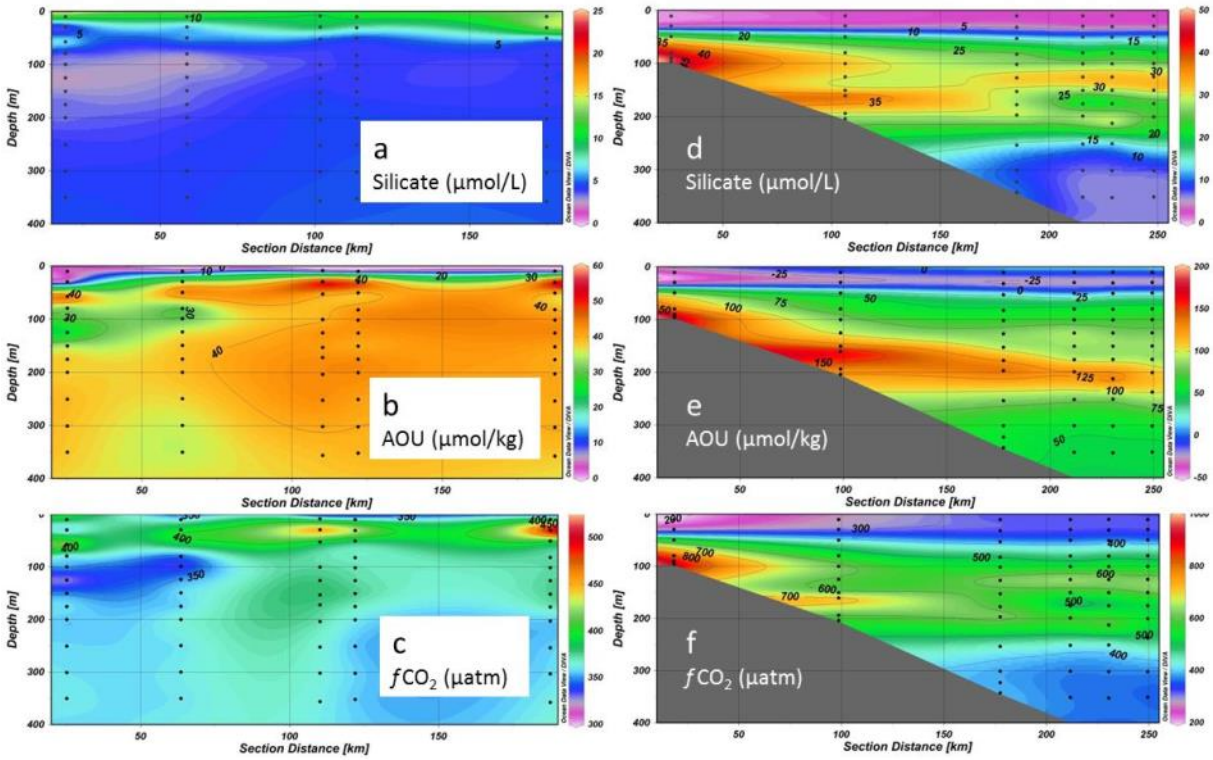

Figure CO2. Sections of silicate concentration (a & d), Apparent Oxygen Utilization (b & e), and fugacity of carbon dioxide (c & f) across G (left) and D (right).

The surface water distribution along the stations of leg two reveal elevated silicate concentrations (above 10 µmol/L) north of the New Siberian Islands and over the Lomonosov Ridge (Fig. CO3) and low levels (less than 5 µmol/L) to the east. Oxygen concentrations are very close to equilibrium with the atmosphere except for at the south eastern stations where oversaturation is seen. This point to recent primary production in the latter region, but minimal primary production or decay of organic matter in the rest of the investigated area. Considering minimal biological activity over the Lomonosov Ridge, the elevated silicate concentration likely reflect input from river runoff, mainly the Lena river, that has been transported out into this region by the wind. Such a feature can be one of the explanations for the limited sea ice cover in the area.

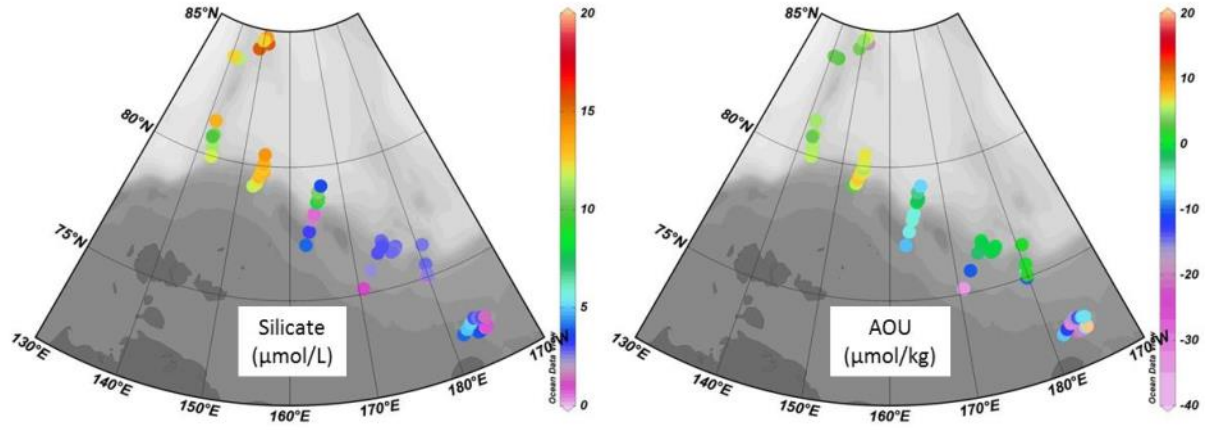

Figure CO3. Surface water concentration of silicate and Apparent Oxygen Utilization (AOU) at the individual stations.

Methane (CH_4, concentrations and isotopes)

Water samples for methane determination were taken at all stations where water was collected by the Niskin bottles (Fig. CO1, Appendix CO1).

Methane distribution in Herald Canyon (Fig. CO4).

High CH_4 concentrations were observed in the Herald Canyon at about 100 m depth. Concentrations decreases from the bottom towards the surface, clearly indicating a sediment source. Also at some stations (st. # 79, 81, 89, 91) of transect B there are bottom maxima of the methane - 70 nmol/L. However, at stations # 83, 85, 87 there is no maxima at the bottom but at e.g. st. #85 there is a local concentration maxima of CH_4at about 100 m, showing a horizontal input from another area.

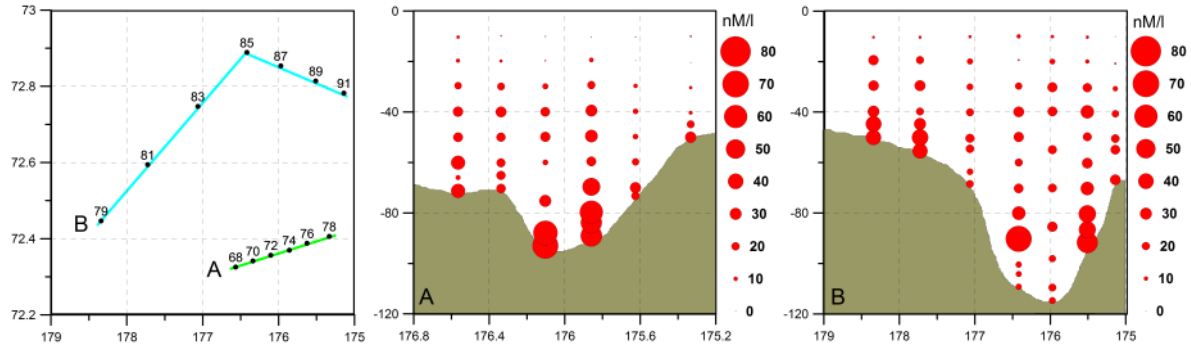

Figure CO4. Methane distribution in Herald canyon – transects A, B (box 1)

Methane distribution at the continental slope (Fig. CO5).

Methane concentrations vary substantially by depth at the continental slope. Transects plots at locations C, D, E and F show a similar major source i.e. from the sediments in the shelf area. The maximum CH_4 concentration is in the range of 16-18 nmol/L at a depth of about 100 m and has been transported from the continental slope out into the Arctic Ocean in the same way as the nutrients, (see Fig. CO2). The methane distributions in deeper waters show very low concentration with minor sediment sources.

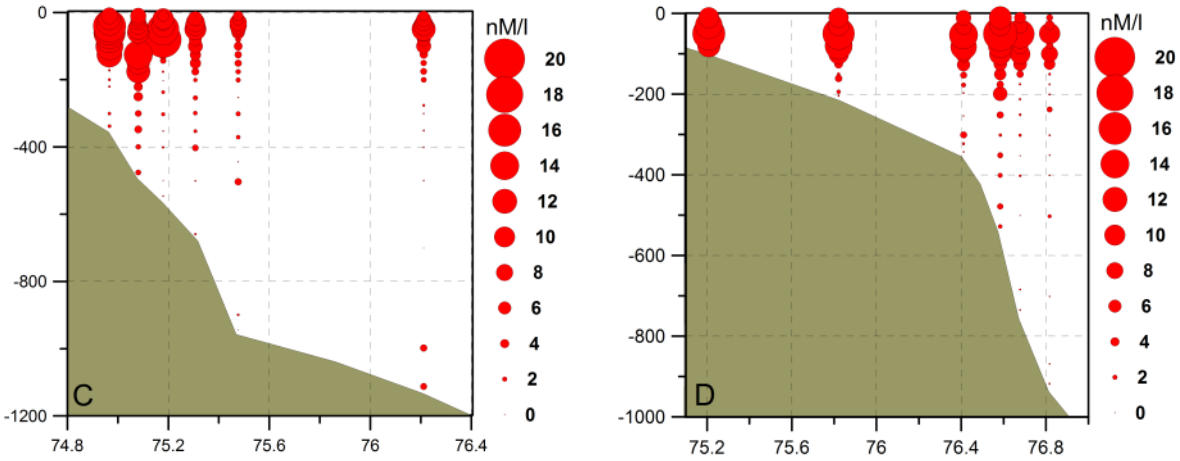

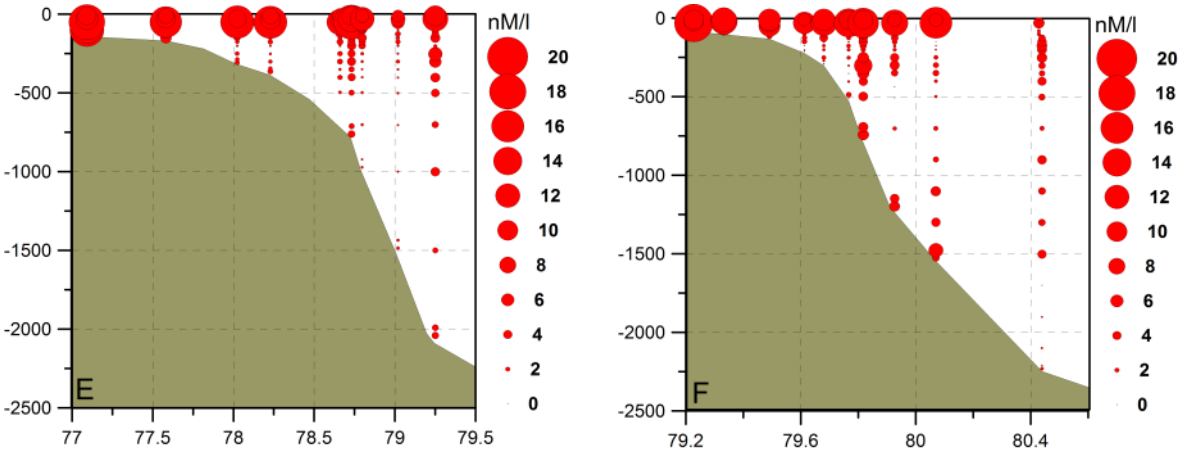

Figure CO5. Methane concentration distribution along the transects C, D, E, and F across the continental slope

Methane distribution along (section G) and at the Lomonosov Ridge slope between 84^0-85^0 N (Fig. CO6).

The CH_4 concentration at the southern end of the Lomonsov Ridge is oversaturated along the bottom as well as around 100 m depth (section G of Fig. CO6). Further to the north (sections H and I) very low CH_4 concentration are seen in deep water masses. However, in the pycnocline some localized elevated concentrations of 6-8 nmol/L are seen.

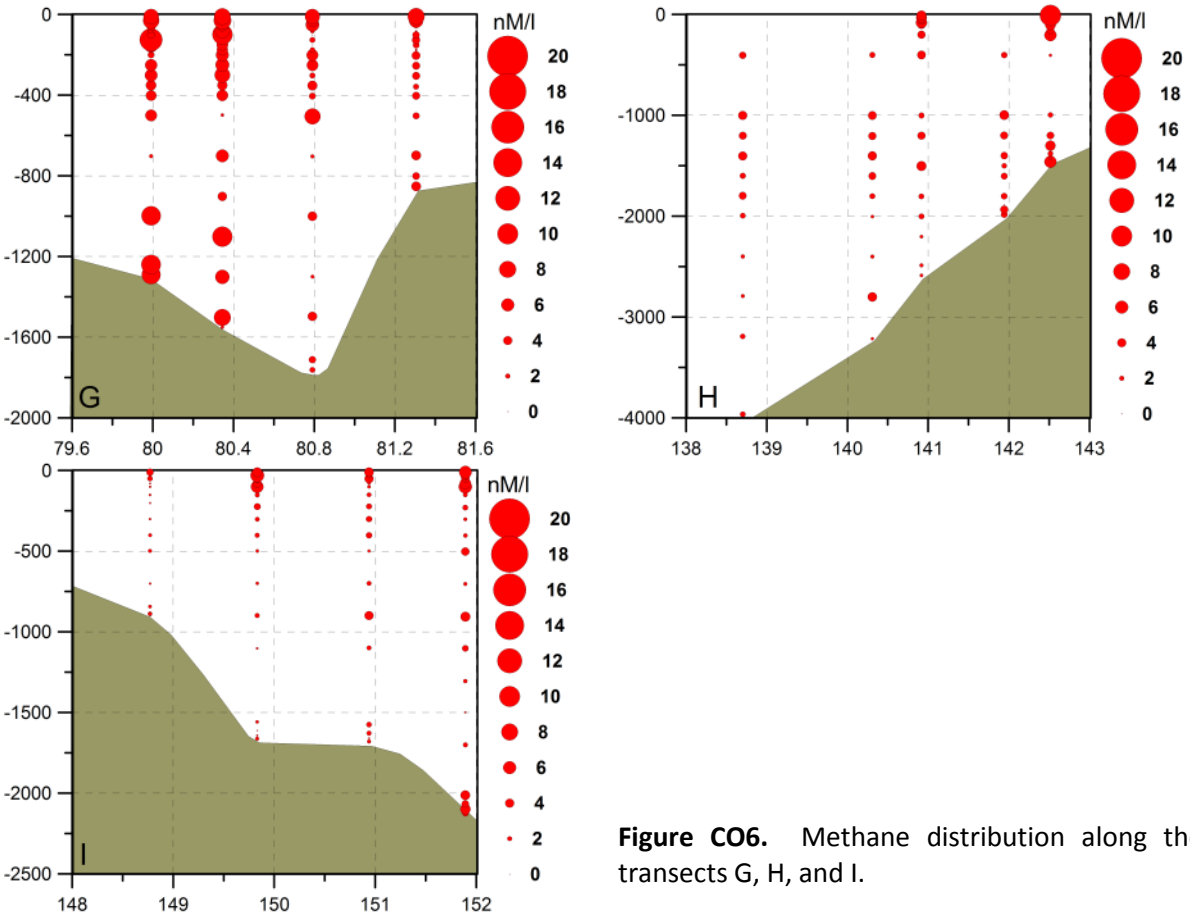

Figure CO6. Methane distribution along the transects G, H, and I.

Stored samples for stable isotope analysis of CH_4 in the water column.

Water samples for CH_4stable isotope determination were taken every second station where water was collected by the Niskin bottles (Appendix CO1). A selection of these samples can be analyzed at the end of 2014 but the general time frame is 8-24 months for isotope analysis, considering the quantity of samples.

Transient tracers (^3H, He, SF_6, CFC-12)

During Leg 2 108 samples both for helium and tritium were collected at 28 stations (Appendix CO1). Besides that additionally 8 samples were collected for only helium on 4 stations (Appendix CO1). A selection of these samples can be analyzed at the end of 2014 but the general time frame is 8-24 months for isotope analysis, considering the quantity of samples.

The preliminary transient tracer concentrations of CFC-12 and SF6 along the southern section of the Lomonosov Ridge are illustrated in Fig. CO7. Transient tracers are used to investigate ocean ventilation processes and provide an estimate of the mean age and anthropogenic carbon content of water parcels. Data calibration and processing will be carried out as part of a collaboration between the GEOMAR Helmholtz Centre for Ocean Research in Kiel (Germany) and the University of Gothenburg (Sweden).

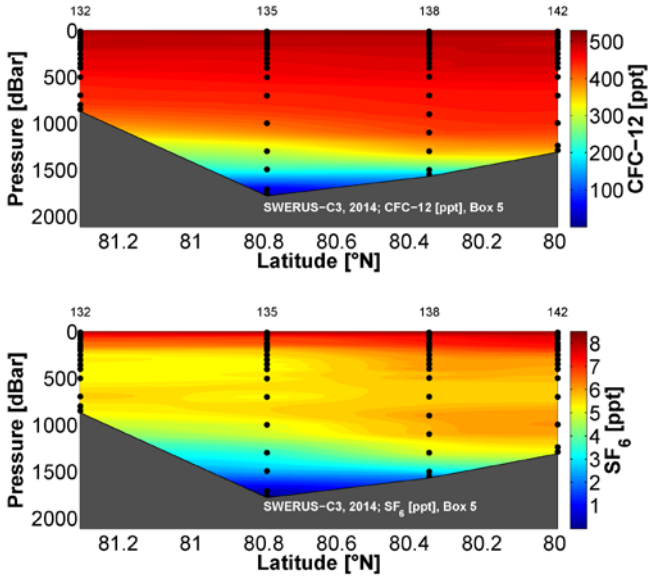

Figure CO7. Preliminary CFC-12 (top) and SF_6 concentrations (bottom) in ppt along the southern part of the Lomonosov Ridge (un-calibrated).

WP PO (Physical Oceanography)

All CTD and ADCP data were separated into data acquired within the Russian Exclusive Economic Zone and outside. This was done in order to be able to fulfill conditions outline in the Russian research permit. For times and positions of the CTD stations see figure PO2 and Table PO1.

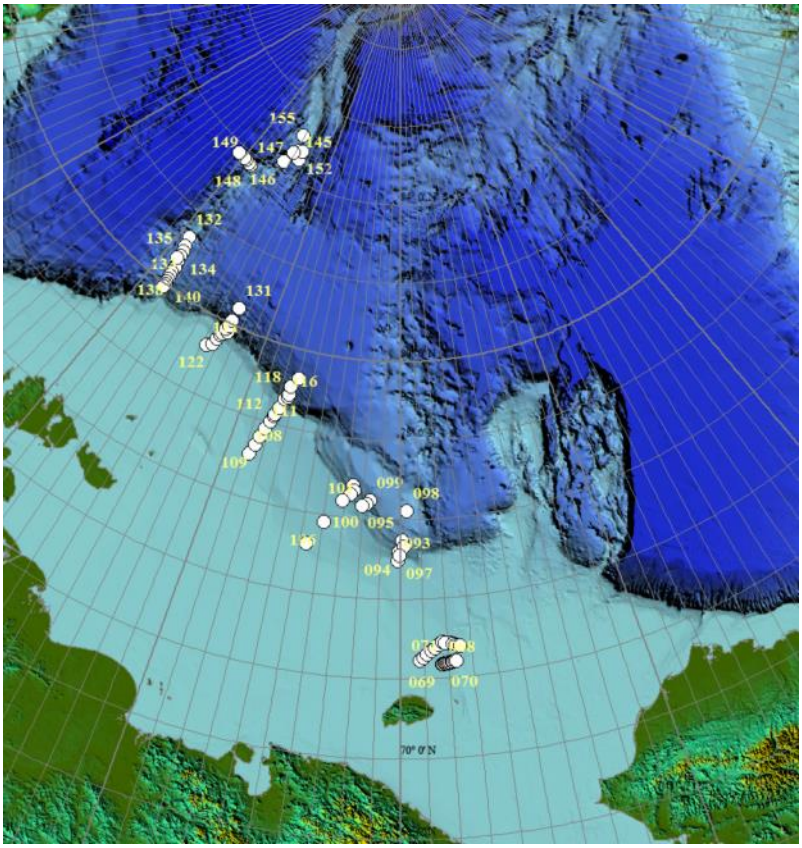

***Figure PO-2**: Map showing the positions of the physical oceanography stations during Leg2.*

Station no	Date	Time (UTC)	Lat dec	Lon dec	Sounder Depth (m)	Max CTD pressure (dbar)	Ru EEZ
68	20140824	09.52	72.3258	-176.5653	74	71	Y
69	20140824	11.34	72.3385	-176.4297	72	70	Y
70	20140824	12.42	72.3417	-176.3380	73	71	Y
71	20140824	13.48	72.3487	-176.2070	79	77	Y
72	20140824	14.38	72.3567	-176.1030	99	93	Y
73	20140824	15.46	72.3630	-175.9875	108	100	Y
74	20140824	16.40	72.3697	-175.8593	91	89	Y
75	20140824	18.16	72.3790	-175.7437	82	80	Y
76	20140824	18.59	72.3878	-175.6253	83	79	Y
77	20140824	20.30	72.3955	-175.5002	74	72	Y
78	20140824	21.54	72.4062	-175.3330	54	50	Y
79	20140825	19.08	72.4468	-178.3408	58	56	Y
80	20140825	20.30	72.5210	-178.0368	62	60	Y
81	20140825	21.45	72.5942	-177.7255	67	65	Y
82	20140825	23.08	72.6730	-177.3933	68	66	Y
83	20140826	00.25	72.7472	-177.0640	71	69	Y
84	20140826	01.52	72.8178	-176.7405	95	95	Y
85	20140826	03.14	72.8888	-176.4183	111	109	Y
86	20140826	08.42	72.8482	-175.7287	113	111	Y
87	20140826	11.30	72.8535	-175.9720	127	115	Y
88	20140826	13.20	72.8713	-176.2022	113	111	Y
89	20140826	15.54	72.8138	-175.5098	94	92	Y
90	20140826	17.26	72.8023	-175.3243	84	80	Y
91	20140826	18.23	72.7822	-175.1385	69	67	Y
92	20140826	19.31	72.7685	-174.9480	97	65	Y

93	20140827	23.14	74.9667	179.7550	340	338	N
94	20140828	21.27	75.1793	179.8648	551	547	N
95	20140829	20.58	75.4765	-179.7643	947	944	N
96	20140830	06.51	75.3070	-179.6217	662	660	N
97	20140830	21.38	75.0808	179.9745	479	477	N
98	20140902	21.24	76.2110	-179.2652	1115	1112	N
99	20140904	01.03	76.4683	176.7767	1103	1100	N
100	20140904	04.27	76.3647	176.4375	737	734	N
101	20140904	08.30	76.3220	175.8947	507	505	N
102	20140905	19.26	76.8172	174.7953	921	918	N
103	20140905	22.29	76.6778	174.9255	738	735	N
104	20140906	02.19	76.5840	174.6430	530	528	N
105	20140906	07.20	76.4112	173.8157	345	343	N
106	20140906	19.02	75.8212	172.1650	207	205	N
107	20140907	02.09	75.2083	170.6537	98	96	N
108	20140908	00.37	77.0922	162.6140	102	100	Y
109	20140908	04.11	77.3613	163.0167	112	110	Y
110	20140908	06.58	77.5812	163.2773	157	155	Y
111	20140908	12.40	77.8095	163.6203	234	232	Y
112	20140908	15.29	78.0235	163.9737	309	307	Y
113	20140908	17.34	78.1687	164.2142	358	356	Y
114	20140908	18.54	78.2283	164.3040	368	363	Y
115	20140909	01.11	78.4080	164.5720	395	393	Y
116	20140909	04.03	78.6600	164.9920	498	496	Y
117	20140909	10.09	78.7317	165.3075	163	761	Y
118	20140909	12.14	78.7972	165.3732	974	972	Y
119	20140909	18.44	79.0190	165.3047	1488	1485	Y
120	20140910	02.09	79.2505	166.0460	2043	2040	Y
121	20140911	03.53	79.2273	152.6882	102	100	Y
122	20140911	05.35	79.3322	153.3107	93	91	Y
123	20140911	07.08	79.4910	153.5602	121	119	Y
124	20140911	08.33	79.6125	153.7695	214	212	Y
125	20140911	09.41	79.6800	153.9210	292	290	Y
126	20140911	17.38	79.7497	154.5592	419	421	Y
127	20140911	18.38	79.7665	154.5912	515	512	Y
128	20140912	03.12	79.8172	154.1692	744	742	Y
129	20140912	07.54	79.9265	154.4170	1200	1198	Y
130	20140912	11.23	80.0698	154.4200	1529	1527	y
131	20140912	16.35	80.4390	154.4987	2234	2231	N
132	20140914	03.20	81.3048	141.7645	855	852	N
133	20140914	08.58	81.0580	142.0773	1502	1499	N
134	20140914	11.50	80.9153	142.3277	1587	1584	N
135	20140914	16.00	80.7912	142.4752	1765	1763	N
136	20140914	19.19	80.6427	142.6280	1721	1718	N
137	20140914	22.25	80.4805	142.8208	1705	1702	N
138	20140915	03.08	80.3448	142.8565	1553	1550	N
139	20140915	05.42	80.2470	142.9905	1537	1534	N
140	20140915	07.56	80.1287	143.0963	1501	1495	N
141	20140915	09.57	80.0537	143.1325	1414	1411	N
142	20140915	12.06	79.9917	143.1842	1293	1290	N
143	20140915	15.29	79.9163	143.2140	1136	1133	N
144	20140917	06.39	80.7015	142.1060	1764	1758	N
145	20140920	03.59	84.5063	151.8915	2129	2126	N
146	20140922	04.11	84.2745	148.7712	894	893	N
147	20140922	13.22	83.7332	142.5147	1487	1482	N
148	20140922	15.55	83.7357	141.9418	1987	1985	N
149	20140922	18.44	83.7553	140.9170	2602	2595	N
150	20140922	21.43	83.7752	140.3085	3221	3216	N
151	20140923	01.38	83.7848	138.7028	3970	3966	N
152	20140924	22.45	84.7190	150.9383	1685	1680	N

153	20140925	02.32	84.7325	151.6358	1705	1701	N
154	20140925	06.00	84.5948	149.8318	1636	1663	N
155	20140925	12.51	85.0870	149.6403	1763	1761	N

***Table PO1**: Positions for all CTD stations during SWERUS-C3 Leg 2. Note: Station 131 included two casts of which cast no 2 (the deep one) is presented here..*

Comparison between XBT and CTD measured temperatures

On two CTD stations XBT profilers were launched to allow for a comparison of the temperature measurements. Analyses of the two sets of measurements suggest that the XBT profilers have an error in the estimated depth. A better agreement between the two records is obtained by the simple remapping of the XBT-measured depth as

$$Z_{ctd} = 0.96\, Z_{xbt}.$$

Thus, the XBT appears to overestimate its depth during the descent. The two comparisons also suggest that the XBT:s have a warm bias. However, the bias seems to vary. At CTD station 147, subtraction -0.09 C gives a reasonable fit, whereas at station 95 the bias is less and subtraction -0.03 C gives a reasonable fit. The cable to the XBT launcher was cut and shortened between the two stations, which may cause the change in temperature bias.

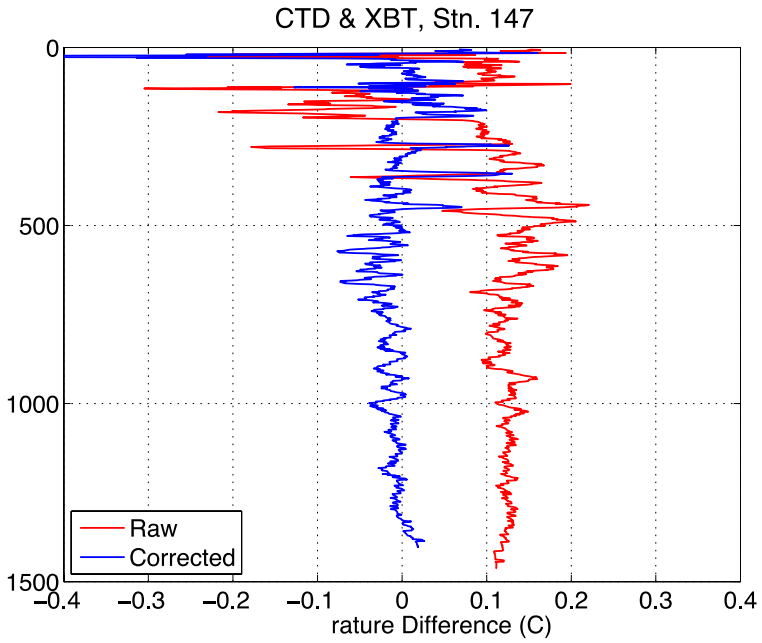

***Figure PO-3**: Difference in measured temperature between XBT (T5_00105) and CTD at station 147 (red curve). The blue curve shows the difference after depth correction and subtraction of constant temperature bias.*

Results from the Keyhole area

Two sections were taken in the keyhole outside the Russian economic zone. In addition, three stations were taken to connect with a section taken during leg one. The sections comprised by the stations 93-98 and 102-107 share several features. On both sections, the hydrographic structure rises towards the continental slope, causing the Atlantic Water layer to reach up towards the shelf edge. It is not clear whether this is a permanent feature, or if it reflects a transient response to wind forcing.

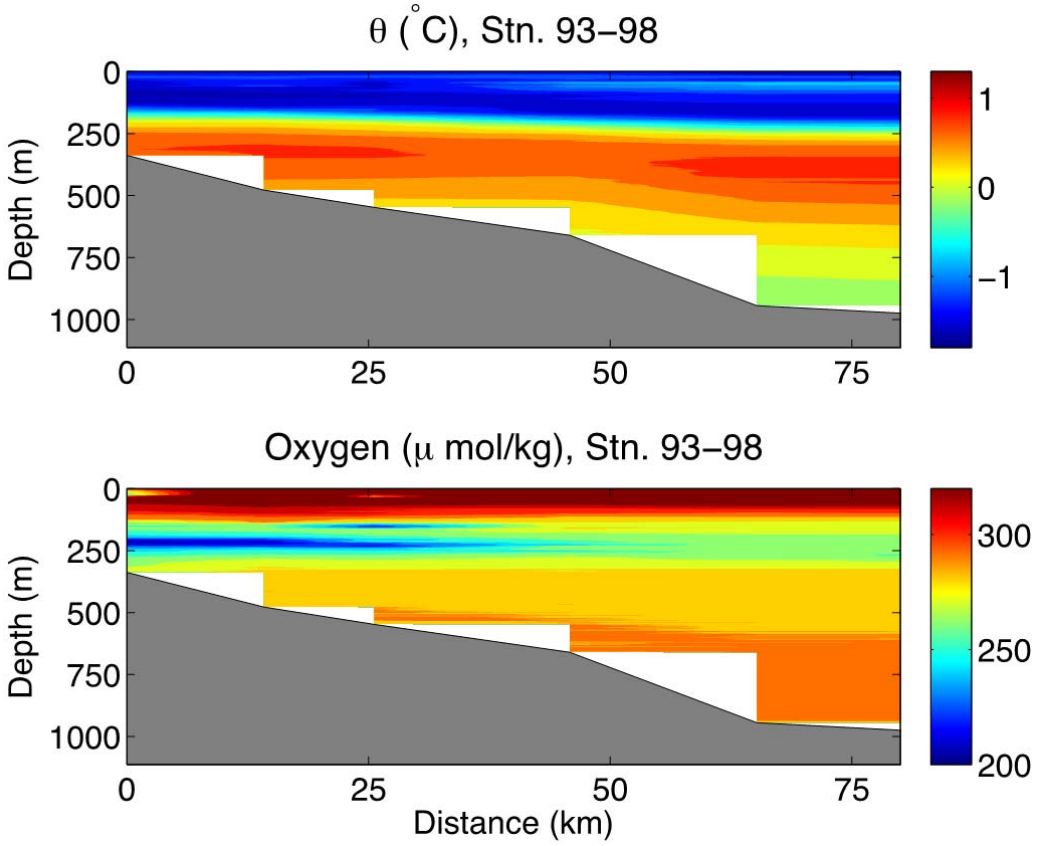

Figure PO-4*: The Keyhole section, stations 93-98. Upper/lower panel potential temperature/oxygen. The latitude increases towards the right. The station 98, over the Arlis Plateau, is located outside the figure to the right.*

Another noteworthy feature is an oxygen minimum in the upper part of the Atlantic layer. This minimum extends seaward over the slope, but becomes gradually less pronounced. Analyzes of the oxygen as a function of the potential density at the stations suggest that the oxygen minimum is propagated seaward, from the shelfbreak, by mixing essentially acting along isopycnal (see Fig. PO-5). The outer station 95 (the station on the Arlis Plateau 98 differs in structure and is excluded in the figure) may be viewed as representing the ambient conditions.

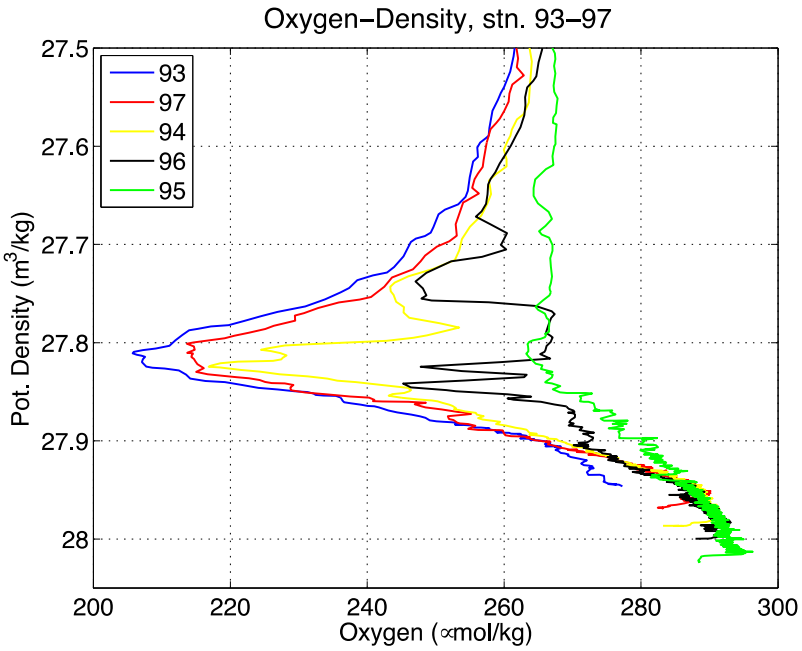

Figure PO-5 *Oxygen as a function of potential density for the stations 93-97; note that the station numbers do not increase uniformly away from the shelf.*

Results from Box 4; the southern Lomonosov Ridge

The stations 132 to 143 were taken along the Lomonosov Ridge between the continental slope and a local bathymetric high near 81 N. There was no sea-ice in box 4 during the period that the CTD work was carried out. The transect was located just east of sill with a depth of nearly 1700 m separating the Amudsen and Makarov Basins. The transect revealed slightly warmer Atlantic Water in the south and slightly colder Atlantic Water with conspicuous layers with nearly homogeneous temperature and salinity to the north. However, additional XBT casts reveal the presence of warmer Atlantic Water around the flanks of the northern part of the section. Accordingly, there seems to be a relatively high spatial variability within the Atlantic layer in the region, which may reflect eddies and flows steered around local bathymetric features. The temperature field across the sections shows the presence of eddies. Also, the salinity field in the upper 100 m reveals fronts with a surface salinity maximum near the middle of the section. Relative to zero flow at the bottom, the geostrophic surface velocities reach amplitudes of about 10 cm/s.

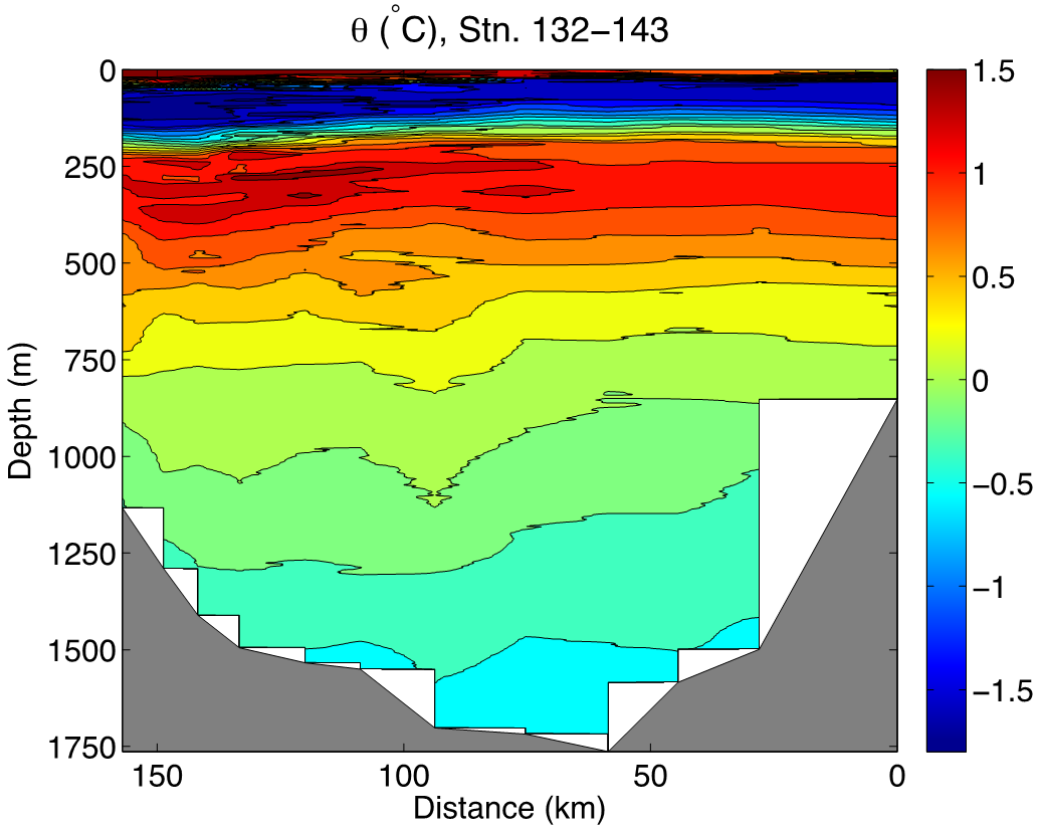

Figure PO-6*: Potential temperature in the section comprised by the stations 132-143 in Box 4. North is to the right in the figure*

Below 1000 m the temperature structure tends to rise towards the north. Near the bottom of the stations that were deeper than 1500 m, the temperature and the salinity increased. This shows the presence of Markarov Basin Water in the sill area and is indicative of a flow towards the Amudsen basin when the section was occupied. The CTD records suggest that there were thin (10-30 m) bottom boundary layer with well-mixed salinity and potential temperature. These bottom boundary layers were deeper on the stations on the northern flank stations. In fact, well-mixed bottom boundary layers were essentially absent on the southern flank stations. This may indicate that the deep flow towards the Amudsen Basin was occurring chiefly on the northern flank of the gap when the stations were taken.

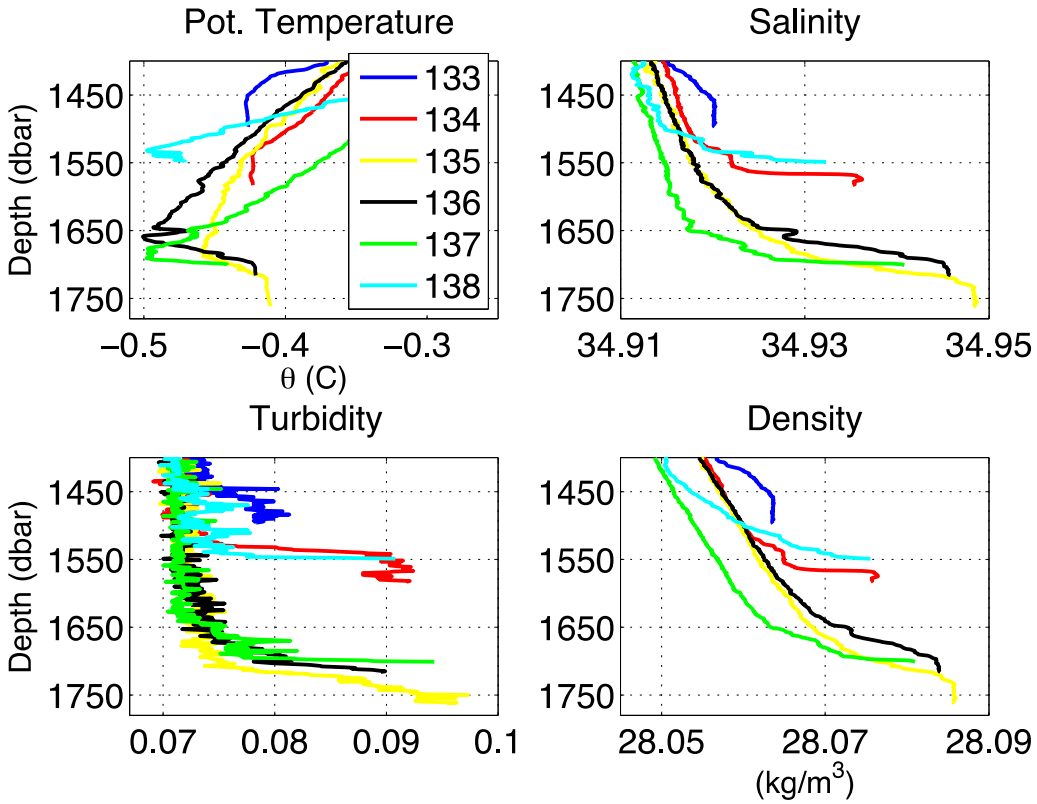

***Figure PO-7**: Near bottom properties at the stations 133-138 in Box 4.*

WP BLM (Boundary Layer Meteorology)

The data collected will allow the analysis of the structure of the atmospheric boundary layer, clouds, and surface energy budget over the Arctic Ocean, including regions of open water, sea ice, and the marginal ice zone. The variety of measurements made will allow an improved understanding of the processes producing the complex interactions in these regions. Figure BLM-12 shows an example of

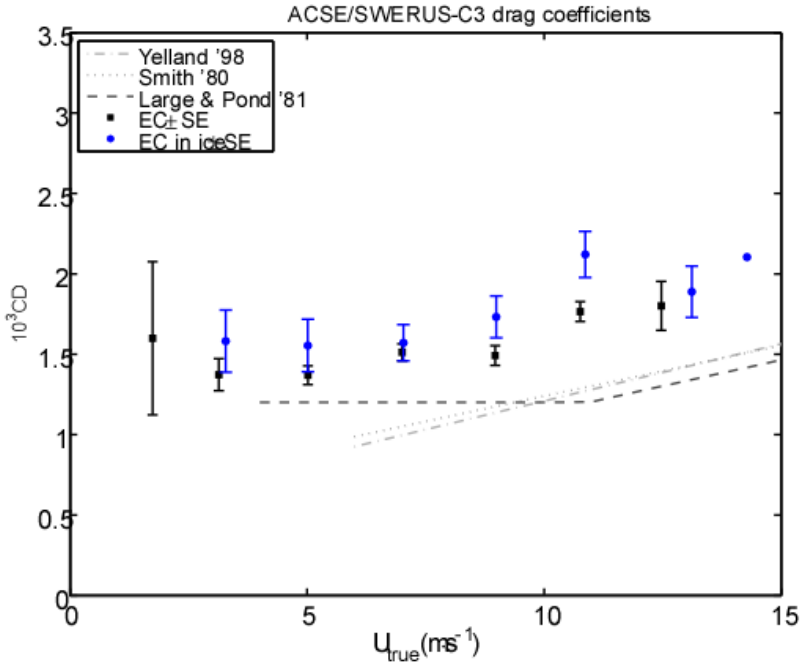

Figure BLM-12: *Preliminary eddy covariance drag coefficient (CD) as a function of the wind speed as measured from the Metek sonic anemometer. Points are bin averaged, with error bars representing one standard deviation. Blue show those points from within the pack ice and black from open water outside the pack ice. The various dashed lines show relationships described by previous studies. The data has not been corrected for ship airflow distortion, though it has gone through basic quality control. The expected increase with wind speed is seen, as is the increase within the ice compared to open water.*

preliminary results from the Metek sonic anemometer, where bin-averaged surface drag coefficients are plotted as a function of wind speed for within and outside the pack ice. The drag coefficient increases with wind speed as expected, while it is also larger within the pack ice compared to over open water. This is likely due to the large number of vertical roughness elements represented by the edges of the various ice floes when ice concentrations are near 40-60%, as suggested by Andreas et al (2010). In this case, the freezing-point surplus temperature of the 8-m water was used to define the in-ice/out-of-ice categories, rather than a sea-ice concentration.

Post-cruise analyses will also combine measurements from many of the sensors to provide a physical understanding of the active processes. As an example, Figures BLM-13 through BLM-17 show data from various instruments during the latter part of Leg 2 when the Oden was making measurements between 84 - 85 deg N within a large "bay" formed by the sea ice (see Fig. BLM-2b). These data will provide detailed understanding of the likely complex interactions of synoptic scale, mesoscale, and microphysical atmospheric processes producing structures seen in these figures, and resulting in a surface energy budget producing the freeze-up of the Arctic Ocean in the vicinity of multi-year sea ice. The upper-level rawinsonde (Fig. BLM-13) and windprofiler (Fig. BLM-15) data reveal some of the large-scale synoptic evolution, while the lowest 500 m likely include changes from mesoscale interactions with the nearby ice edge. The vertical potential temperature gradient (Fig. BLM-13a) shows predominantly near-neutral conditions in the lowest 400 m, consistent with the fairly turbulent conditions (Fig. BLM-6c) with strong winds through the boundary layer (Fig. BLM-17). The

period of colder temperatures seen in the rawinsonde data occurred at the northern end of the "bay", while the coldest air in the lowest 500 m occurred when airflow came directly from the ice to over the Oden, as shown by the various wind measurements (Figs. BLM-13b, BLM-15, BLM-17). A low-level jet (Fig. BLM-15) occurs in the off-ice flow at the upper portions of this cold air (Fig. BLM-13a) just below the clouds (Fig. BLM-13b, BLM-14), and likely represents a feature formed by the mesoscale thermal gradients in this region. The cloud radar (Fig. BLM-14) and lidar data (Fig. BLM-16) show some of the macro and

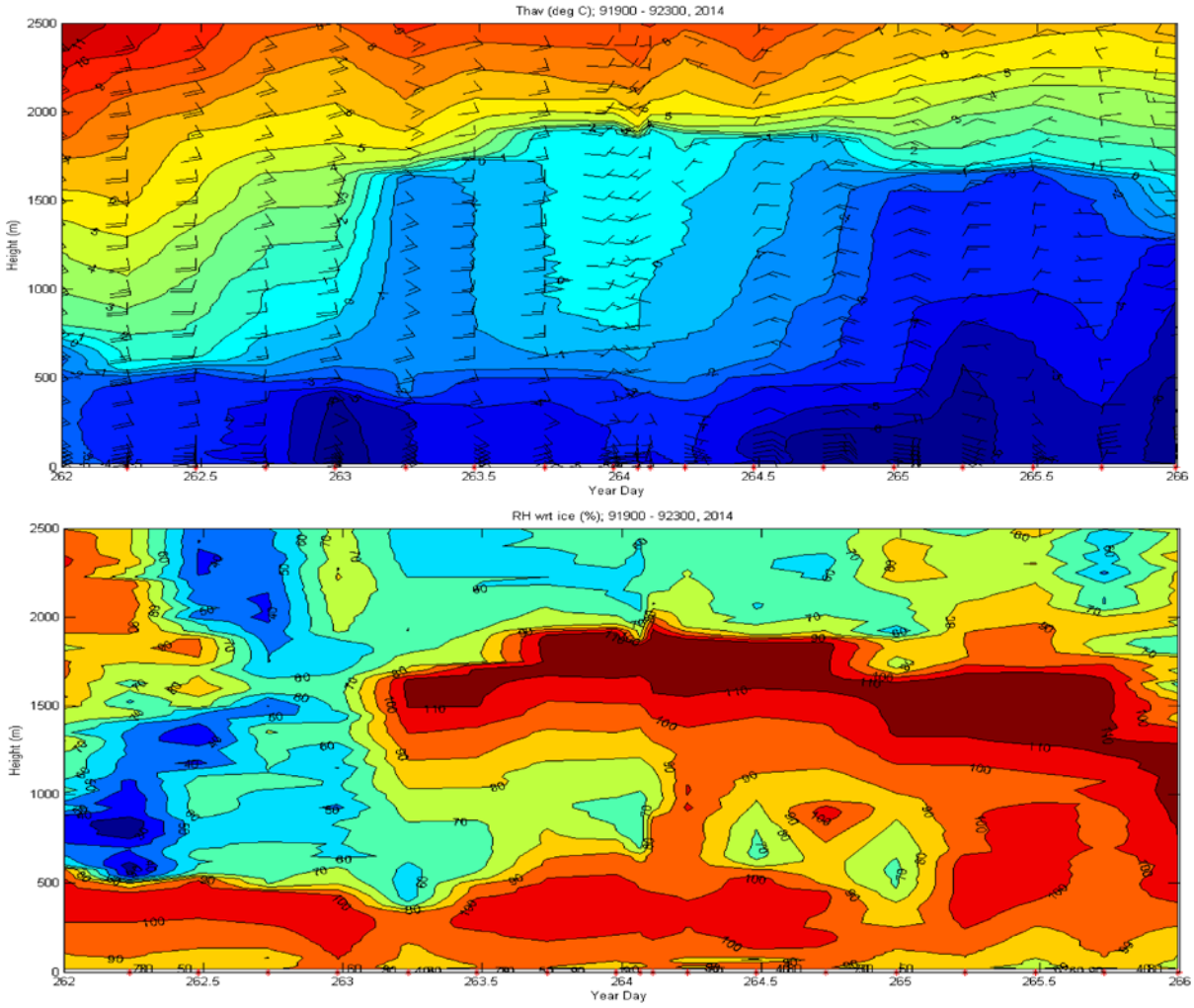

Figure BLM-13: *Time-height cross-section of virtual potential temperature (deg C) and wind barbs (top) and relative humidity with respect to ice (%, bottom) in the lowest 2500 m from the rawinsondes launched from the R/V Oden during YD262-265 (Sep. 19-22, 2014).*

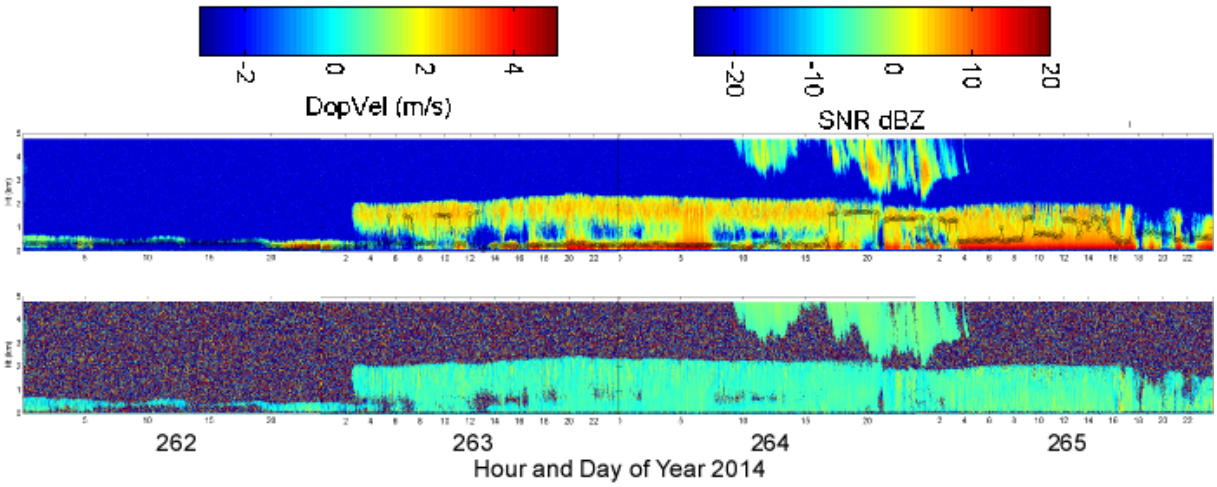

Figure BLM-14: W-band cloud radar signal-to-noise ratio and ceilometer cloud base height (open circles) (top) and W-band vertical velocity (bottom) for Sep. 19-22 (YD262-265). The lowest 5 km of the atmosphere is shown. The weak downward vertical velocities of < 1.5 m/s indicate snow or ice crystals.

microphysical aspects of these clouds that impacted the available solar and longwave radiation. The lidar data shows that the upper part of the low-level clouds was dominated by spherical particles, most likely supercooled liquid water, which strongly modulate radiative fluxes. Combined turbulent surface sensible and latent heat fluxes were positive (0 - +70 W m^{-2}), especially over the open water (Fig. BLM6c,d), contributing to the cooling of the ocean surface and the observed formation of sea ice. The radiation terms of the surface energy budget (not shown) are determined from measurements at the top of the 7th deck of the Oden (Fig. BLM3b), while changes to the ocean surface are documented by the surface temperature measurements and video imagery. The microwave radiometers provide additional temporal information on the boundary-layer heat and moisture evolution. The turbulence sensors also provide a direct measurement of the momentum flux (Fig. BLM6b), which are linked to the surface waves over the open ocean that may have had an impact on the observed ice formation, and waverider buoy deployments will show some of the wave spectra characteristics.

Clearly, the analyses to be done on this data set obtained during ACSE/SWERUS must combine the large variety of measurements and will require coordinated work in order to provide a clearer picture of the various processes involved in this complex physical system.

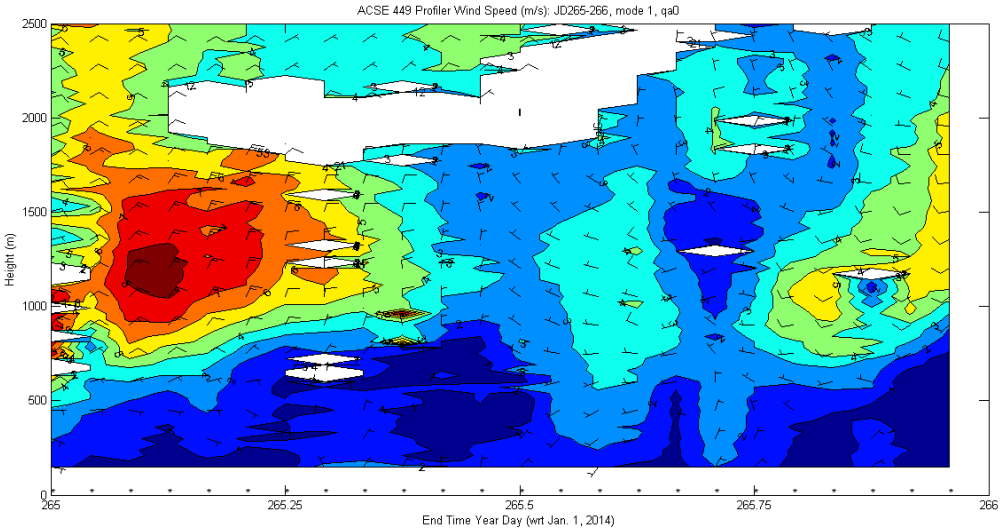

Figure BLM-15: *Time-height section of isotachs and wind barbs derived from the 449 MHz wind profiler data for Sep. 19-22 (YD262-265). A low-level jet centered at about 1100 m is present in the off-ice NE winds on Sep.22*

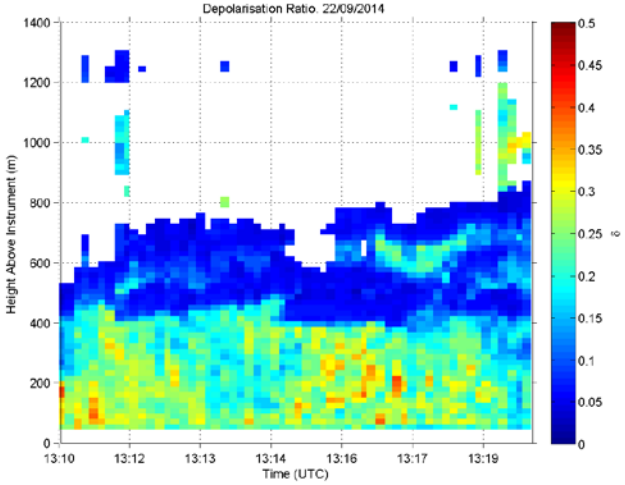

Figure BLM-16: *Example of a time-height cross-section of the lidar depolarization ratio [ratio=B_cross/ (B_cross+B_parra)] near 13 UTC on Sep. 22 (YD 265). The low values indicate spherical particles, likely liquid drops at the tops of these lower clouds. The larger ratios below suggest the primary presence of ice crystals.*

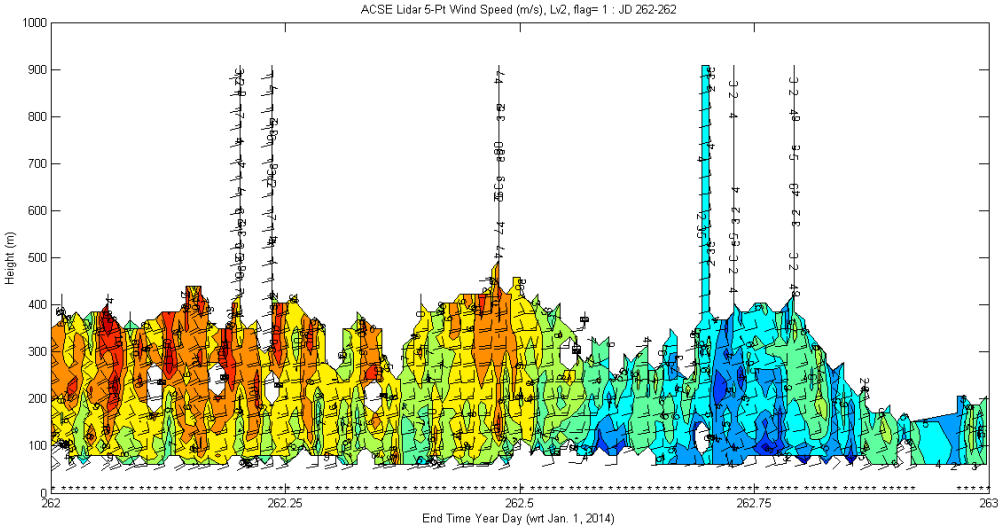

Figure BLM-17: *Time-height cross-section of boundary-layer winds derived from the 5-beam lidar scan every 10 minutes during YD262 (Sep. 19). Shown are isotachs (m/s), with wind direction available from the wind barbs. Moderate 10 m/s SSE winds occur at the top of the boundary layer early in the day, which turned to due south by midday. The winds weakened later in the day, with some turning back towards the southeast. The stars at the bottom show the times when a good profile is encountered. This data is preliminary, as it has not been corrected for the ship's tilt at the exact time of each beam measurement.*

References

Calder, B.R., and Mayer, L.A., 2003, Automatic processing of high-rate, high-density multibeam echosounder data. *Geochemistry Geophysics Geosystems*, v. 4, p. 1-22.

Chierici, M., Fransson, A., and Anderson, L.G. (1999), Influence of acidity of the indicator m-cresol purple on the pH of a seawater sample: correction factors evaluated from a chemical speciation model. *Marine Chemistry, 65*, 281-290.

Gukov, A. Yu., 1989. Bottom biocoenoses of the Buor-Khaya Bay. *Oceanology, XXIV(2), 316 – 317.*

Haraldsson, C., Anderson, L. G., Hassellöv, M., Hulth, S., and Olsson, K. (1997), Rapid, high-precision potentiometric titration of alkalinity in ocean and sediment pore waters. *Deep-Sea Research I*, 44, 2031-2044.

Fofonoff, P. and Millard, R.C. Jr, 1983. Algorithms for computation of fundamental properties of seawater, 1983. _UNESCO Tech. Pap. *In Marine Science*, No. 44, 53 pp.

IOC, SCOR and IAPSO, 2010: The international thermodynamic equation of seawater - 2010: Calculation and use of thermodynamic properties. Intergovernmental Oceanographic Commission, Manuals and Guides No. 56, UNESCO (English), 196 pp. Available from http://www.TEOS-10.org

Jakobsson, M., Mayer, L., Coakley, B., Dowdeswell, J.A., Forbes, S., Fridman, B., Hodnesdal, H., Noormets, R., Pedersen, R., Rebesco, M., Schenke, H.W., Zarayskaya, Y., Accettella, D., Armstrong, A., Anderson, R.M., Bienhoff, P., Camerlenghi, A., Church, I., Edwards, M., Gardner, J.V., Hall, J.K., Hell, B., Hestvik, O., Kristoffersen, Y., Marcussen, C., Mohammad, R., Mosher, D., Nghiem, S.V., Pedrosa, M.T., Travaglini, P.G., Weatherall, P., 2012. The International Bathymetric Chart of the Arctic Ocean (IBCAO) Version 3.0. *Geophysical Research Letters*, 39, L12609.

Johnson, K. M., Sieburth, J. M., Williams, P. J., and Brändström, L. (1987), Coulometric total carbon dioxide analysis for marine studies: automation and calibration. *Marine Chemistry*, 117-133.

Shakhova, N., Semiletov, I., Salyuk, A., Yusupov, V., Kosmach, D., Gustafsson, Ö., 2010. Extensive Methane Venting to the Atmosphere from Sediments of the East Siberian Arctic Shelf. *Science,* 327, 1246-1250.

Stöven, T., and Tanhua, T. (2014), Ventilation of the Mediterranean Sea constrained by multiple transient tracer measurements, Ocean Sci., 10, 439–457, doi: 10.5194/os-10-439-201.

Westbrook, G.K., Thatcher, K.E., Rohling, E.J., Piotrowski, A.M., Pälike, H., Osborne, A.H., Nisbet, E.G., Minshull, T.A., Lanoisellé, M., James, R.H., Hühnerbach, V., Green, D., Fisher, R.E., Crocker, A.J., Chabert, A., Bolton, C., Beszczynska-Möller, A., Berndt, C., Aquilina, A., 2009. Escape of methane gas from the seabed along the West Spitsbergen continental margin. *Geophysical Research Letters,* 36, L15608.